Isolation and identification of SARS-CoV-2 antibodies from COVID-19 patient samples

Chang Liu

University of Oxford

Nuffield Department of Medicine

DPhil thesis

January 2024

Abstract

Severe acute respiratory syndrome coronavirus 2 (SARS-CoV-2), which is the causing agent for COVID-19, has led to over 7 million deaths since it was first detected in Wuhan, China in December 2019. Antibodies induced by both vaccination and infection are crucial for the immune protection against SARS-CoV-2, with some monoclonal antibodies (mAbs) therapeutically in use. Throughout the pandemic, we dedicated ourselves to isolate thousands of human monoclonal antibodies recognising the spike protein (S) from human peripheral blood mononuclear cells (PBMCs) of convalescent patients recovered from primary or breakthrough infections and characterised their neutralising abilities against eight SARS-CoV-2 live variants and more than 30 pseudo-viruses expressing variant S proteins. We also devised a competition data-driven method to map RBD binding sites of RBD-specific antibodies. To assess the immune escape abilities of variants of concern (VoC), we measured their neutralisation by a panel of plasma obtained from vaccinees or convalescent individuals infected by different variants. Using these data, we built a model to analyse the antigenic distance between variants to illustrate the emerging antigenic landscape of SARS-CoV-2. This provides important new insights for immunisation policy and sheds light on the construction of future variant vaccines.

Keywords: SARS-CoV-2, antibodies, immune escape, variants of concern (VoC), antigenic landscape.

Contents

Abstract *2*

Abbreviations *8*

Acknowledgements *8*

CHAPTER 1. Introduction *12*

1.1 SARS-CoV-2 and its variants **12**

1.1.1 Genome and life cycle of SARS-CoV-2 12

1.1.2 Occurrence and characterisation of SARS-CoV-2 variants 17

1.2 The humoral response and antibodies against SARS-CoV-2 infection **19**

1.2.1 Antibody generation 19

1.2.2 Antibodies generated by SARS-CoV-2 infection 21

1.3 SARS-CoV-2 vaccines **23**

1.3.1 Development of SARS-CoV-2 vaccines 23

1.3.2 Vaccine induced immunity 27

CHAPTER 2. Materials and methods *30*

2.1 Materials and reagents **30**

2.1.1 General materials and reagents 30

2.1.2 Human resources 31

2.1.3 Viral stocks 36

2.1.4 Bacterial strains and cell lines 37

2.2 Plasmid constructions **37**

2.2.1 Trimeric spike of SARS-CoV-2 37

2.2.2 NTD and RBD of spike 38

2.2.3 Plasmid construction for pseudotyped lentiviral particle production 38

2.2.4 ACE2 construction 41

2.3 Protein production and purification **41**

2.3.1 Protein production of Trimeric spike, NTD, RBD and ACE2 41

2.3.2 Protein purification of Trimeric spike, NTD, RBD and ACE2 42

2.4 Isolation and expression of mAbs 42

2.4.1 Human blood sample processing 42

2.4.1 Isolation of S-specific single B cells by fluorescence-activated cell sorting (FACS) 44

2.4.2 Cloning and expression of S-specific human antibodies 45

2.4.3 Human monoclonal antibody purification 50

2.5 Construction and expression of Fab 51

2.5.1 Construction of Fab expression plasmids 51

2.5.2 Fab production and purification 52

2.6 ELISA 52

2.6.1 ELISA for determination of plasma and antibody binding to recombinant proteins 52

2.6.2 ELISA for measuring IgG concentration in cell culture 53

2.6.3 ELISA for ACE2 inhibition assay 53

2.7 Live virus isolation from patient swabs and sequencing 54

2.7.1 Live virus isolation 54

2.7.2 Viral RNA extraction 54

2.7.3 Live virus S gene sequencing 54

2.8 FRNT assay 55

2.9 Pseudotyped lentiviral particles production and neutralisation test 56

2.9.1 Pseudotyped lentiviral particles production 56

2.9.2 Pseudoviral neutralisation assay 56

2.10 Data analyses 57

2.10.1 Flow cytometry analyses 57

2.10.2 Analysis of FRNT neutralisation 57

CHAPTER 3 Isolation and characterisation of early-pandemic SARS-CoV-2 antibodies . 58

3.1 Introduction 58

3.2 Results 58

3.2.1 Isolation and characterisation of mAbs 58

3.2.2 Neutralisation activity of early-pandemic SARS-CoV-2 mAbs 63

3.2.3 Structural analysis of potent early-pandemic mAbs 65
3.2.4 Public heavy-chain V-region usage 67
3.2.5 Light-chain switch can increase neutralisation titre 68
3.2.6 In vivo efficacy of potent early-pandemic mAbs 68
3.3 Discussion 71
CHAPTER 4 Immune evasion of SARS-CoV-2 variants Alpha, Beta, Gamma and Delta . 72
4.1 Introduction 72
4.2 Results 75
4.2.1 The effects of RBD mutations on ACE2 affinity 75
4.2.2 Immune escape of Alpha, Beta, Gamma and Delta from early-pandemic mAbs ... 76
4.2.3 Immune escape of Alpha, Beta and Gamma variants from commercial mAbs 79
4.2.4 Immune escape of Alpha, Beta and Gamma variants from convalescent plasma .. 80
4.2.5 Protection from Alpha, Beta, Gamma, and Delta by vaccine serum 82
4.2.6 The antigenic landscape of Alpha, Beta, Gamma and Delta 83
4.3 Discussion 84
CHAPTER 5 Generation and characterisation of Beta mAbs 87
5.1 Introduction 87
5.2 Results 87
5.2.1 mAb generation from Beta infected patient samples 87
5.2.2 Cross-reactivity of Beta mAbs 90
5.2.3 Antibody gene usage 92
5.2.4 Quantitative dissection of differences in mAb responses 94
5.2.5 Potent mAbs protect against Beta infection in mice model 95
5.2.6 Beta mAb epitope mapping using BLI 96
5.2.7 Two IgVH1-69 mAbs target a neutralising epitope conserved between SARS-CoV-1 and SARS-CoV-2 97
5.3 Discussion 100
CHAPTER 6 Potent cross-reactive antibodies following BA.1 breakthrough infection ... 102
6.1 Introduction 102
6.2 Results 103

6.2.1 RBD of BA.1 compared with early VoCs 103
6.2.2 Neutralisation of BA.1 by vaccinated or convalescent serum 105
6.2.3 Neutralisation of BA.1 by early pandemic, Beta, and therapeutic mAbs 107
6.2.4 Antigenic cartography of BA.1 112
6.2.5 Isolation of potent mAbs following BA.1 breakthrough infection 112
6.2.6 Broad neutralisation of VoC by potent BA.1 mAbs 115
6.2.7 Mapping of RBD-specific potent BA.1 mAbs by using BLI competition measurement 117
6.2.8 Quantitative dissection of the BA.1 mAb responses 118

6.3 Discussion 119

CHAPTER 7 Immune escape of SARS-CoV-2 Omicron sublineages 122

7.1 Introduction 122

7.2 Results 123

7.2.1 Emerging Omicron sub-lineages 123
7.2.2 Widespread escape from neutralisation by Omicron mAbs 124
7.2.3 Neutralisation of Omicron sub-lineages by therapeutic mAbs 127
7.2.4 Severe knockdown of serum neutralisation titres 130

7.3 Discussion 131

CHAPTER 8 Generation of potent antibodies from BA.2 breakthrough cases 133

8.1 Introduction 133

8.2 Results 134

8.2.1 Antibody isolation from BA.2 infected cases 134
8.2.2 Neutralisation of SARS-CoV-2 variants by BA.2 136
8.2.3 Epitope mapping of the BA.2 mAbs by BLI 136

8.3 Discussion 141

CHAPTER 9 Discussion and prospect 143

A.1. Primer sequences 146

A.2. Antibody expression vectors 157

A.3. Vector map pcDNA3.1(+) 157

A.4. pHLSec **158**

References ***162***

Publications during DPhil ***159***

Patents ***161***

Acknowledgements

This thesis would not have been possible without the help of many generous people. I am sincerely thankful to my supervisors Professor Gavin R. Screaton and Dr. Juthathip Mongkolsapaya for giving me the great opportunity to study in the University of Oxford, guiding me through my academic and personal life, and their input in the project and the writing of this thesis. They provided invaluable advice and guidance through my DPhil career. I am equally grateful to Dr. Wanwisa Dejnirattisai (Nui) and Dr. Piyada Supasa (Ray), who welcomed me to the group with open arms. Apart from teaching me all the important techniques, they contributed heavily in the work of antibody production, live virus isolation and neutralisation assays presented in this thesis. Together with Dr. Beibei Wang, they helped me with my research as well as daily life tremendously, and fought shoulder by shoulder with me through the difficult yet exciting years of pandemic lockdown. They are my teachers as well as my friends in both my career and my life.

Our research group have provided me with a host of friends and colleagues to help along the way. I would also like to thank Alison E. Cowper, our resourceful lab manager, for her effort to make our research life easy and smooth, and keep the lab disciplined. Dr. César López-Camacho and Dr. Jose Slon-Campos helped me with protein production and purification, and also lightened me up with their good humour and warm-heartedness, which were really important in a difficult time like a global pandemic. Dr. Rungtiwa Nutalai and Dr. Aekkachai Tuekprakhon are irreplaceable members of the group, who set up the pseudovirus construction and neutralisation assays in the lab, and I wouldn't have been able to achieve so much without their kind help and hard work. I have been having great working relationships with Dr. Aiste Dijokaite-Guraliuc, Dr. Muneeswaran Selvaraj, and Dr. Raksha Das since their arrival at the group, I benefited so much from their knowledge and diligence on research work, their help on antibody isolation, neutralisation assay, protein production and pseudovirus construction, and easing the workload for me to be able to finish the thesis. I hope we can sustain our relationships and together contribute more to the science community in the future.

I would like to offer my appreciation to our collaborators from Division of Structural Biology Prof. David I. Stuart, Dr. Elizabeth Fry, Dr. Jingshan Ren, Dr. Daming Zhou, Dr. Helen M.E. Duyvesteyn, and Dr. Helen M. Ginn, who helped to solve the structures and determine binding epitopes of the antibodies. Our project wouldn't have been able to start without the help of our collaborators from University of Oxford and University of Sheffield Dr. Alexander J. Mentzer, Prof. Paul Kleneman, Prof. Andrew J. Pollard, Prof. Teresa Lambe, Prof. Philip Goulder, Prof. Susanna J. Dunachie, Dr. Barbara Kronsteiner, Dr. Lizzie Stafford, Prof. Thushan de Silva, and Prof. Tao Dong who provided us with precious clinical samples. Thank you to Prof. Derrick Crook, Dr. Bede Constantinides, and Hermione Webster, who sequenced and provided us with patient swabs to isolate live SARS-CoV-2 viruses for the project, and to Prof. Michael S. Diamond and Dr. Rita E. Chen of Washington University School of Medicine, USA for their help on testing the activity of the antibodies against SARS-CoV-2 in mouse model.

I am grateful to Prof. Tao Dong and the Chinese Academy of Medical Sciences Oxford Institute (COI) for not only giving me the great opportunity and financial support to study and live at the University of Oxford, but also providing me with conferences and networks to communicate and exchange ideas with brilliant peers. All my achievements were built on their kindness and generosity.

Thank you to my warm-hearted housemate, Harry Tian Hu and Cristiano Peron, with whom I lived over three years, for taking on much of the domestic work and helping me with my daily life. We lived together through happiness and crises, and your kindness and warmth made me a home in Oxford.

Finally, I would like to thank family for supporting me in my study abroad. Many things happened in the four years' time and I'm more than grateful to my parents and my wife for taking care of my young son in my absence due to the restriction on travelling during the pandemic and my busy schedule, and letting me be fully absorbed in my study and research. To my son, I am reminded by you every day of the unrelenting power of change as you grow.

Abbreviations

3CLpro	3C-like protease
ACE2	Angiotensin-converting enzyme 2
Ad5	Adenovirus type-5
APC	Antigen-presenting cell
BLI	Biolayer interferometry
CMC	Carboxymethyl cellulose
COVID-19	Coronavirus disease 2019
CPD	Codon paired deoptimisation
CPE	Cytopathic effect
DMEM	Dulbecco's Modified Eagle medium
EDTA	Ethylenediaminetetraacetic acid
EF	Extrafollicular
FACS	Fluorescence-activated cell sorting
FBS	Fetal bovine serum
FiO2	Fraction of inspired O2
FP	Fusion peptide
FRNT	Focus reduction neutralisation assay
GC	Germinal centre
GCP	Good Clinical Practice
HCoV	Human coronavirus
HR	Heptad repeat
IC50	Half-maximal inhibitory concentration
ICH	International Conference on Harmonization
IFN-γ	Interferon-gamma
Ig	Immunoglobulin
IL-2	Interleukin 2
IL-2R	Interleukin 2 receptor
M	Membrane

mAb	Monoclonal antibody
MERS-CoV	Middle east respiratory syndrome coronavirus
N	Nucleocapsid
NSP	Non-structural protein
NTD	Amino-terminal domain
ORF	Open reading frame
PaO_2	Partial pressure O_2
PBMC	Human peripheral blood mononuclear cell
PBS	Phosphate buffered saline
PEI	Polyethylenimine
PFU	Plaque-forming unit
PLpro	Papain-like protease
RBD	Receptor binding domain
RBM	Receptor binding motif
RdRp.	RNA-dependent RNA polymerase
REC	Research ethics committee
RT-PCR	Reverse transcriptase polymerase chain reaction
S	Spike protein
SARS-CoV	Severe acute respiratory syndrome coronavirus
SARS-CoV-2	Severe acute respiratory syndrome coronavirus 2
SH	Stem helix
TCR	T-cell receptor
Tfh cell	Follicular helper T cell
Th1	Type 1 T helper
TMPRSS2	Transmembrane protease serine 2
TNF-α	Tumour necrosis factor-alpha
VH	Heavy chain variable region
VLP	Viral like particle
VoC	Variant of concern

CHAPTER 1. Introduction

1.1 SARS-CoV-2 and its variants

1.1.1 Genome and life cycle of SARS-CoV-2

Since the initial emergence of severe acute respiratory syndrome coronavirus 2 (SARS-CoV-2) in Wuhan in December 2019, it has caused more than 772 million COVID-19 cases and more than 7 million deaths as of July 2023[1]. SARS-CoV-2 is an enveloped, positive-sense, single-stranded RNA virus, which belongs to the genus Beta coronavirus. Apart from SARS-CoV-2, this genus also includes severe acute respiratory syndrome coronavirus (SARS-CoV), which was the causative agent of the 2002-2004 SARS epidemic and shares 79% nucleotide sequence identity with SARS-CoV-2[2], and human coronavirus (HCoV)-OC43, HCoV-HKU1, and Middle East respiratory syndrome coronavirus (MERS-CoV). Another two coronaviruses, 229E and NL63, have also been found to infect humans, which both belong to Alphacoronavirus.

Coronaviruses are characterised by high genetic recombination and mutation rates, which is the reason of their diversity[3]. The RNA-dependent RNA polymerase (RdRp) of SARS-CoV-2 has been shown to be the fastest among known viruses with the cost of low fidelity[4]. Although SARS-CoV-2 and indeed all known coronaviruses have a proofreading activity to increase replication fidelity and maintain genomic stability[5], the massive number of infections and sequencings throughout the pandemic and the recombination resulted by co-infection have caused identification of numerous variants. In the seven human coronaviruses mentioned above, 229E, OC43, NL63, and HKU1 cause mild respiratory illness with the symptom of common cold[6]. By contrast, SARS, MERS[7] and SARS-CoV-2 can cause severe human respiratory diseases with high mortality.

The size of the SARS-CoV-2 genome is about 30kb, containing 14 open reading frames (ORFs) and encoding 29 viral proteins. There are two overlapping polyproteins, pp1a and pp1ab[8], encoded at the 5' end of the SARS-CoV-2 genome, occupying around two thirds of the genome. A -1 frameshift between ORF1a and ORF1b renders to the difference in translation.

The two polyproteins are digested by two viral proteases, a papain-like protease (PL^{pro}) and a 3C-like protease ($3CL^{pro}$), to generate 16 non-structural proteins (NSPs), which are essential for viral replication and transcription (Figure 1.1). The structural proteins of the virus are encoded by the four ORFs at the 3' terminus of the genome, which are nucleocapsid (N), spike (S) protein, membrane (M) protein, and envelope (E) protein. These structural proteins are very important for virion assembly and are also involved in the suppression of the host immune responses. A group of accessory genes are located between the structural genes, they encode ORF3a, ORF3b, ORF6, ORF7a, ORF7b, ORF8b, ORF9b and ORF14, and are involved in the regulation of viral infection but not necessarily incorporated into the virion, except for ORF3a and ORF7a (Figure 1.1).

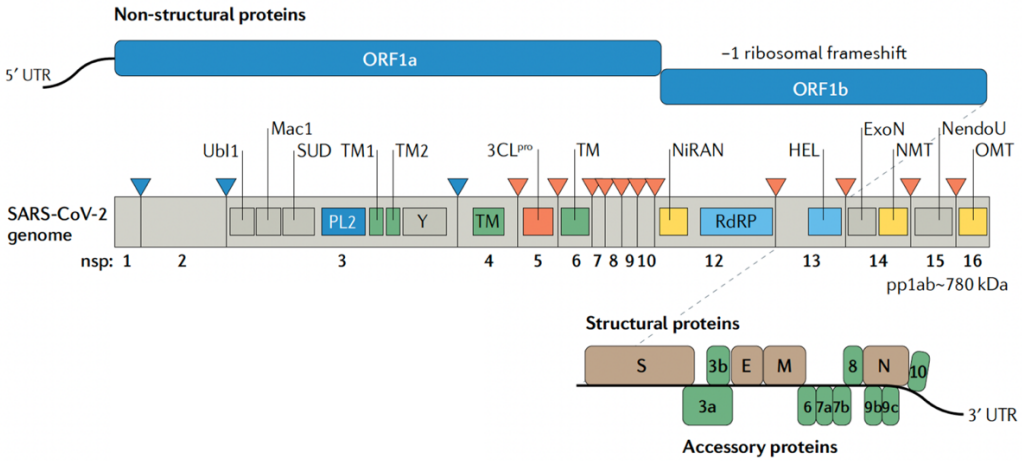

Figure 1.1 SARS-CoV-2 genome organisation, with functional domains shown in rectangles. Taken from Yang *et al., Nat Rev Microbilo*, Nov 2021[9]. Licence number: 5696430445134.

The S protein is a homotrimer that protrudes from the virion and shapes the viral surface like a solar corona. S is a glycosylated protein and anchored in the viral membrane, where it binds to the host receptor angiotensin-converting enzyme 2 (ACE2)[10,11]. It is also the most targeted protein by neutralising antibodies[12]. The S protein comprises ~1,200 residues which can be cleaved by furin-like protease into two subunits, S1 and S2 (Figure 1.2A, B). The S1 subunit of the SARS-CoV-2 S protein wraps around a threefold axis, covering the S2 subunit underneath. The S1 subunit folds into four domains in its prefusion conformation: the amino-terminal domain (NTD), the receptor binding domain (RBD), and two carboxy-terminal domains SD1 and SD2 (Figure 1.2A, B). The RBD can switch between two conformational states: the closed 'down' state and the open 'up' state[13](Figure 1.2C). The receptor-binding regions on the RBD are shielded in the 'down' state, while the RBD undergoes a

conformational switch to an 'up' state to expose its receptor-binding regions to recognise the ACE2[10,11]. S2 contains four conserved regions: a fusion peptide, two heptad repeats (HR1 and HR2) and a transmembrane region.

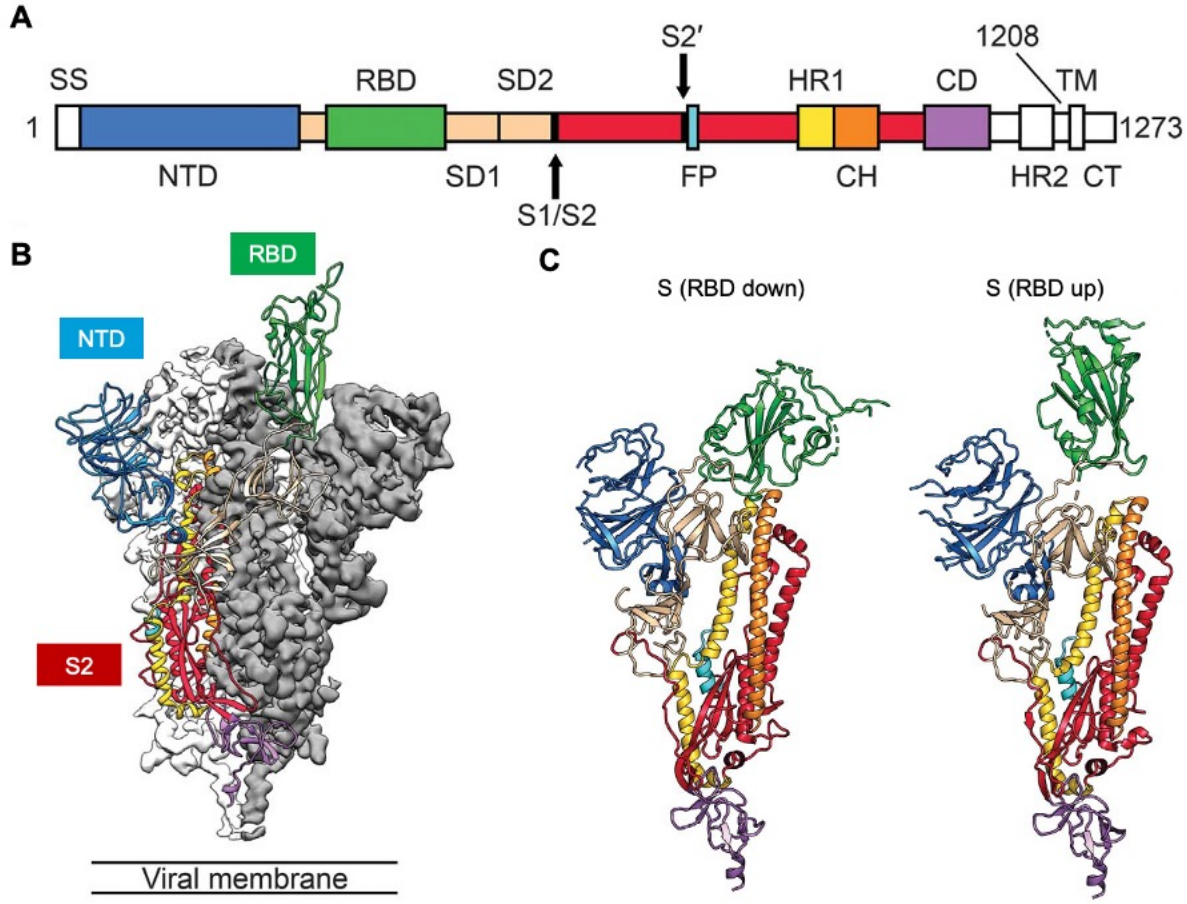

Figure 1.2 Structures of the SARS-CoV-2 spike protein in the prefusion conformation. (A) Trimeric SARS-CoV-2 spike protein is shown in ribbons coloured by domain. SS, signal sequence; S2', S2' protease cleavage site; FP, fusion peptide; HR1, heptad repeat 1; CH, central helix; CD, connector domain; HR2, heptad repeat 2; TM, transmembrane domain; CT, cytoplasmic tail. Arrows represent protease cleavage sites. (B) Side view of the prefusion structure of the SARS-CoV-2 spike protein with a. single RBD in the up conformation. (C) Single protomer of SARS-CoV-2 spike protein with the RBD in down (left) and up (right) conformation. Taken from Wrapp *et al., Science*, March 2020[13]. An open access article.

The life cycle of SARS-CoV-2 is initialised by the binding of the S protein, which is located on the outer surface of the virion, to the host receptor ACE2[10,11], to attach to the cell membrane. Subsequently, the S protein undergoes a conformational transition enabled through two proteolytic cleavage steps following ACE2 engagement. The attachment of S protein and ACE2 is followed by viral and host cell membrane fusion and the release of viral genomic RNA into the cells. Type II transmembrane protease serine 2 (TMPRSS2), which expresses in

respiratory epithelial cells as well as in epithelial cells in gastrointestinal track and prostate, is found to be involved in priming of S protein in SARS-CoV-2[14]. When there is insufficient type II transmembrane protease serine 2 (TMPRSS2) expressed by the target cell, or if a virus-ACE2 complex does not encounter TMPRSS2, virus is internalized by clathrin-mediated endocytosis into the endolysosomes, in which S2' cleavage is performed by cathepsins under an acidic environment. When TMPRSS2 is presented, S2' cleavage occurs at the cell surface. In both pathways, the cleavage of the S2' site exposes the fusion peptide (FP) and dissociation of S1 from S2, which induces dramatic conformational changes in the S2 subunit, pushing the fusion peptide forward into the target membrane, initiating membrane fusion. Fusion between viral and cellular membranes forms a fusion pore through which viral RNA is released into the cytoplasm of host cell for uncoating and replication (Figure 1.3A)[15]. It was reported that there was a shift from TMPRSS2-dependent cell surface entry pathway to TMPRSS2-independent endosomal entry pathway following the emergence of Omicron variants due to the less efficient spike cleavage at S1/S2, which led to altered pathogenesis[16].

After viral RNA entry, ORF1a and ORF1ab is translated by the host ribosome. The viral polyproteins are cleaved into NSPs by viral protease and self-assemble into the replication and transcription complexes. Subgenomic viral mRNAs (after capping) act as templates for viral protein translation. Progeny virions are assembled in the endoplasmic reticulum and Golgi body. After virion assembly, the virions are released out of host cells (Figure 1.3B).

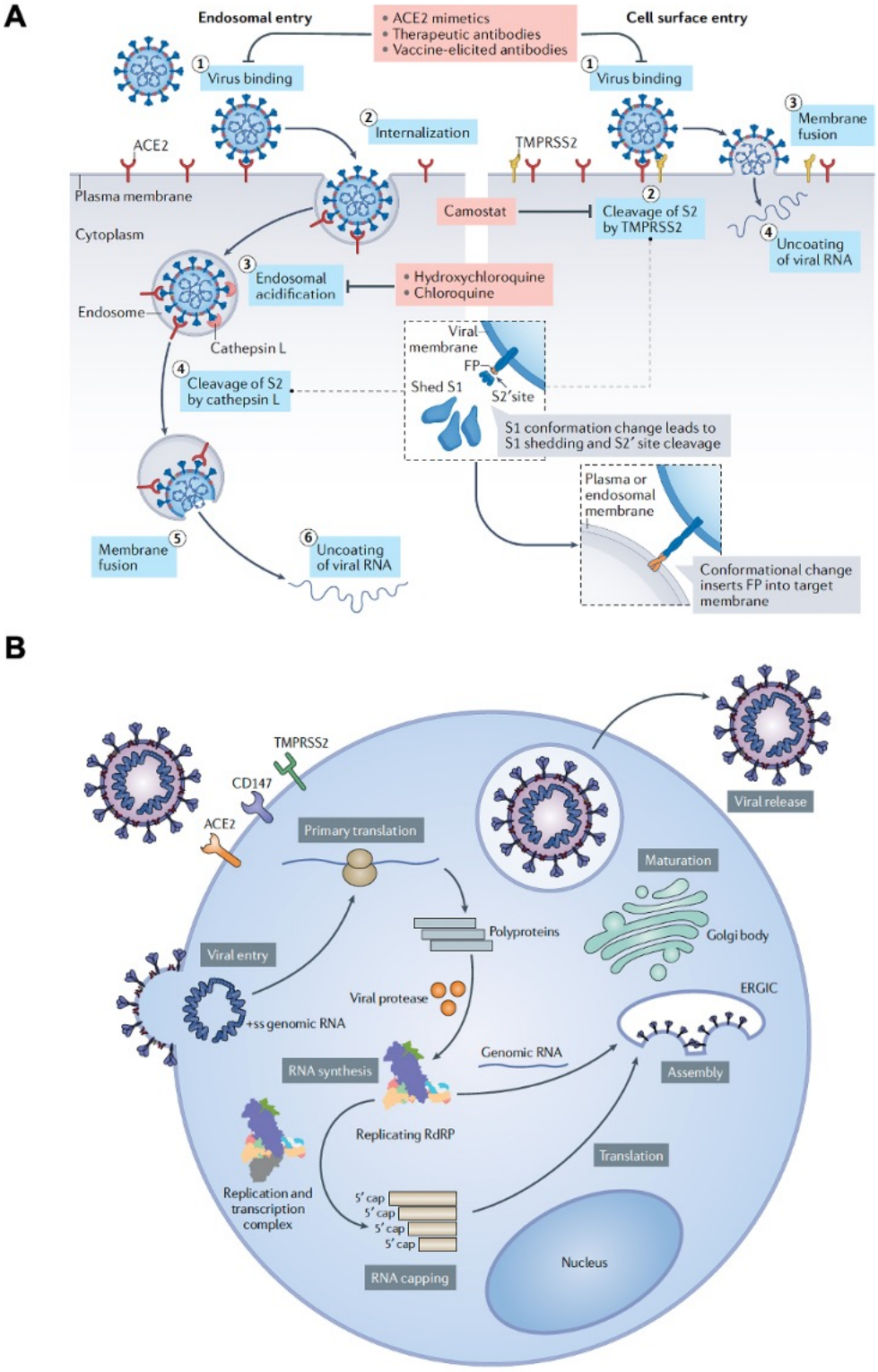

Figure 1.3 The entry and life cycle of SARS-CoV-2. (A) SARS-CoV-2 has two distinct entry pathways. Endosome entry is used when the target cell expresses insufficient TMPRSS2, and cell surface entry is used when virus-ACE2 complex encounters TMPRSS2. Taken from Jackson *et al. Nat Rev Mol Cell Biol*, Jan 2022[15]. Licence number: 5696430824271. (B) The life cycle of SARS-CoV-2, including viral entry, replication and transcription, assembly and release. Taken from Yang *et al., Nat Rev Microbilo*, Nov 2021[9]. Licence number: 5696430445134.

1.1.2 Occurrence and characterisation of SARS-CoV-2 variants

After the emergence of SARS-CoV-2 in late 2019, until July 2020, for the first eight months the virus seemed to have only limited evolution. This was partially due to the limited transmission globally in the early stage of the pandemic, while spread of the virus was still not ubiquitous, and in the later stage as a result of a combination of lacking medical interventions and sample sequencing in the world. Additionally, with the knowledge of the proofreading capacity of the coronavirus polymerase enzyme[17], it resulted at the time in the expectations that SARS-CoV-2 would evolve slowly, and that variants would not be a big risk in the further control of the pandemic. The most noticeable mutation occurred in this period was the D614G substitution in the spike protein of SARS-CoV-2[18], and the first eight months of the pandemic was characterised as limited viral diversity and evolution.

Eight months after the pandemic, the first divergent SARS-CoV-2 lineage was detected and transmitting rapidly in the United Kingdom, carrying a large number of mutations in the spike region with a RBD region mutation N501Y [19] (Figure 1.4). This lineage was Pango classified as B.1.1.7 and named as VoC Alpha by the World Health Organization (WHO). Weeks after the detection of Alpha, there were two rapidly expanding variants reported in South Africa and Brazil, and named thereafter as VoC Beta (Pango lineage B.1.351) and Gamma (Pango lineage P.1), respectively. Each of these variants harbours a large number of substitutes in their genome, and more significantly in their spike proteins with more than 10 mutations in each spike (Figure 1.4), although the RBD mutations in the two VoCs are almost identical (K417N/T, E484K, and N501Y)[20,21]. These mutations enhance transmissibility and contribute to immune escape properties[22,23]. In May 2021, Delta variant (Pango lineage B.1.617.2) was reported in India, although the circulation of the variant was months before[24]. The RBD region of Delta spike contains two different mutations comparing with Alpha, Beta and Gamma, which are L452R and T478K (Figure 1.4). The Delta variant rapidly replaced previous VoCs and led to a drastic surge in the case number around the world[25].

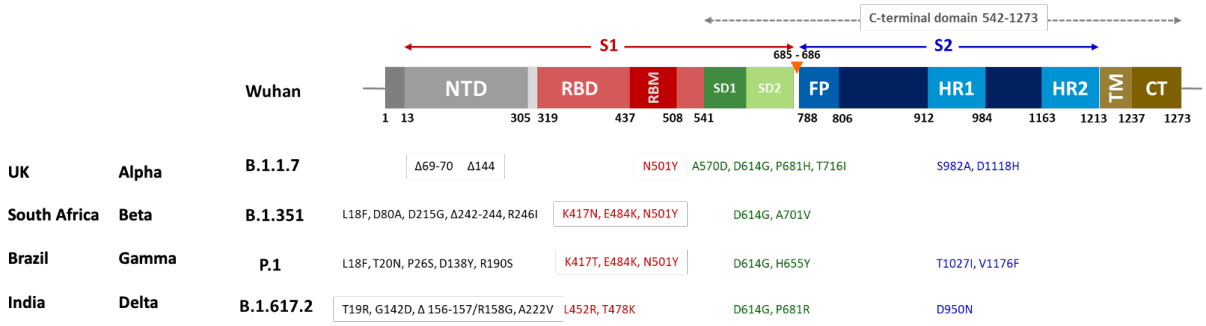

Figure 1.4. Amino acid substitutions in spike proteins of Alpha, Beta, Gamma, and Delta VOCs compared with original SARS-CoV-2.

The detection of BA.1 (Pango lineage B.1.1.529) in November 2021 in South Africa and Botswana, which was designated by WHO as VoC Omicron, was a big shock to scientific community. It contains 30 substitutions, six deletions and three insertions within its spike, far exceeded the number of mutations observed in previous variants[26]. BA.1 generated a new wave of infection and overtook Delta to become the dominant variant globally. In February 2022, two sublineages of Omicron, BA.1.1 and BA.2, were identified, and BA.2 became the dominant lineage in several countries after BA.1[27]. The ancestral recombination of BA.1 and BA.2 also resulted in the emergence of the BA.3 lineage[26]. Since the emerge of BA.2, a number of Omicron sublineages evolved from BA.2 with increased antibody evasion capacity and transmissibility have emerged and caused regional and global outbreaks, including BA.2.12.1, BA.4/5, BA.4.6, BA.2.75, BA.2.75.2, BA.2.3.20, BA.2.10.4, BJ.1, BF.7, BS.1, BN.1, BN.1.2.1, BQ.1, BQ.1.1, CK.1, CA.3.1, CH.1.1, and DS.1[28]. In October 2022, a recombination variant of BJ.1 and BA.2.75 sublineages was detected in multiple countries and termed by WHO as XBB[29]. XBB derived a series of sublineages after its emergence, including XBB.1, XBB.1.5, XBB.1.5.10, and XBB.1.16[30,31], and the variants are still evolving into more sublineages (Table 1.1).

Table 1.1 Mutations in RBD for Omicron sublineages. Indicated mutations are those additional mutations relative to the sequence of BA.2.

Variant	Mutations in RBD area																					
BA.2	G339D			T376A	D405N	R408S									E484A			Q493R				
Victoria																						
BA.1	G339D							G446S							E484A			Q493R		G496S		
BA.1.1	G339D	R346K						G446S							E484A			Q493R		G496S		
BA.2.12.1	G339D			T376A	D405N	R408S				L452Q					E484A			Q493R				
BA.4/5	G339D			T376A	D405N	R408S				L452R					E484A	F486V		R493Q				
BA.4.6	G339D	R346T		T376A	D405N	R408S				L452R					E484A	F486V		R493Q				
BA.2.75	G339H			T376A	D405N	R408S		G446S				N460K			E484A			R493Q				
BA.2.10.4	G339D			T376A	D405N	R408S		G446S							E484A	F486P		R493Q	S494P			
BJ.1	G339H	R346T		T376A	D405N	R408S		V445P	G446S					V483A	E484A		F490V	R493Q				
BA.2.75.2	G339H	R346T		T376A	D405N	R408S		G446S				N460K			E484A	F486S		R493Q				
BF.7	G339D	R346T		T376A	D405N	R408S				L452R					E484A	F486V		R493Q				
BS.1	G339D	R346T		T376A	D405N	R408S				L452R		N460K	G476S		E484A			Q493R				
BA.2.3.20	G339D			T376A	D405N	R408S	K444R		N450D	L452M		N460K			E484R			R493Q				
BN.1	G339H	R346T	K356T	T376A	D405N	R408S		G446S				N460K			E484A		F490S	R493Q				
BQ.1	G339D			T376A	D405N	R408S	K444T			L452R		N460K			E484A	F486V		R493Q				
BQ.1.1	G339D	R346T		T376A	D405N	R408S	K444T			L452R		N460K			E484A	F486V		R493Q				
XBB	G339H	R346T		L368I	T376A	D405N	R408S	V445P	G446S			N460K			E484A	F486S	F490S	R493Q				
XBB.1	G339H	R346T		L368I	T376A	D405N	R408S	V445P	G446S			N460K			E484A	F486S	F490S	R493Q				
XBB.1.5	G339H	R346T		L368I	T376A	D405N	R408S	V445P	G446S			N460K			E484A	F486P	F490S	R493Q				

1.2 The humoral response and antibodies against SARS-CoV-2 infection

1.2.1 Antibody generation

One of the most important aspects of adaptive immunity against viral infection is the antibody response. It can be roughly separated into two phases following viral infection or vaccination based on the predominant isotypes and the level of somatic hypermutations of the generated antibodies. The first phase is the extrafollicular (EF) phase. In this phase, a few days after infection, B cells are activated by antigens and differentiate into plasma cells within foci outside of the follicle[32], rapidly producing antibodies with lower level of somatic hypermutations but still having efficient affinities and capable of neutralising the virus[33]. The induced EF plasma cells are mainly IgM isotype after immunisation, but they can switch to IgG or IgA isotype especially in viral infection responses, and they are relatively short-lived.

The second phase is the germinal centre (GC) phase. This phase takes days to a week to start but is able to last for months. Antigen-specific B cells go through somatic hypermutation and affinity-based selection, generate mainly isotype-switched, high-affinity and long-lived plasma cells, located in the bone marrow. In fact, both EF phase and GC phase can produce antigen-specific memory B cells that last for a long time after primary infection[34] (Figure 1.5).

In the case of SARS-CoV-2 infection, seroconversion is always finished within two weeks post-symptom onset, and IgM and IgG antibodies, which mainly target the spike and nucleocapsid proteins, are produced[35-37]. Interestingly, high neutralising titres in serum against SARS-CoV-2 are not always correlated with better disease outcomes. Rather, they are often found in severe cases of COVID-19 primary infection than those with mild or without symptoms[38-40]. The high level of antibodies in severe cases is likely generated from EF responses due to the high viral load at the early stage of severe infection. SARS-CoV-2 neutralising antibody levels in serum peak in the first few weeks post infection or vaccination, and decline subsequently, which may result in reduced protection leading to re-infection by newly emerged variants[41-44]. In people who have been infected by SARS-CoV-2 previously, vaccine booster shots can generate broader neutralising antibodies than those without infection history[45]. Another factor that may generate cross-reactive antibodies against SARS-CoV-2 after infection is the previous exposure to other coronaviruses[46,47].

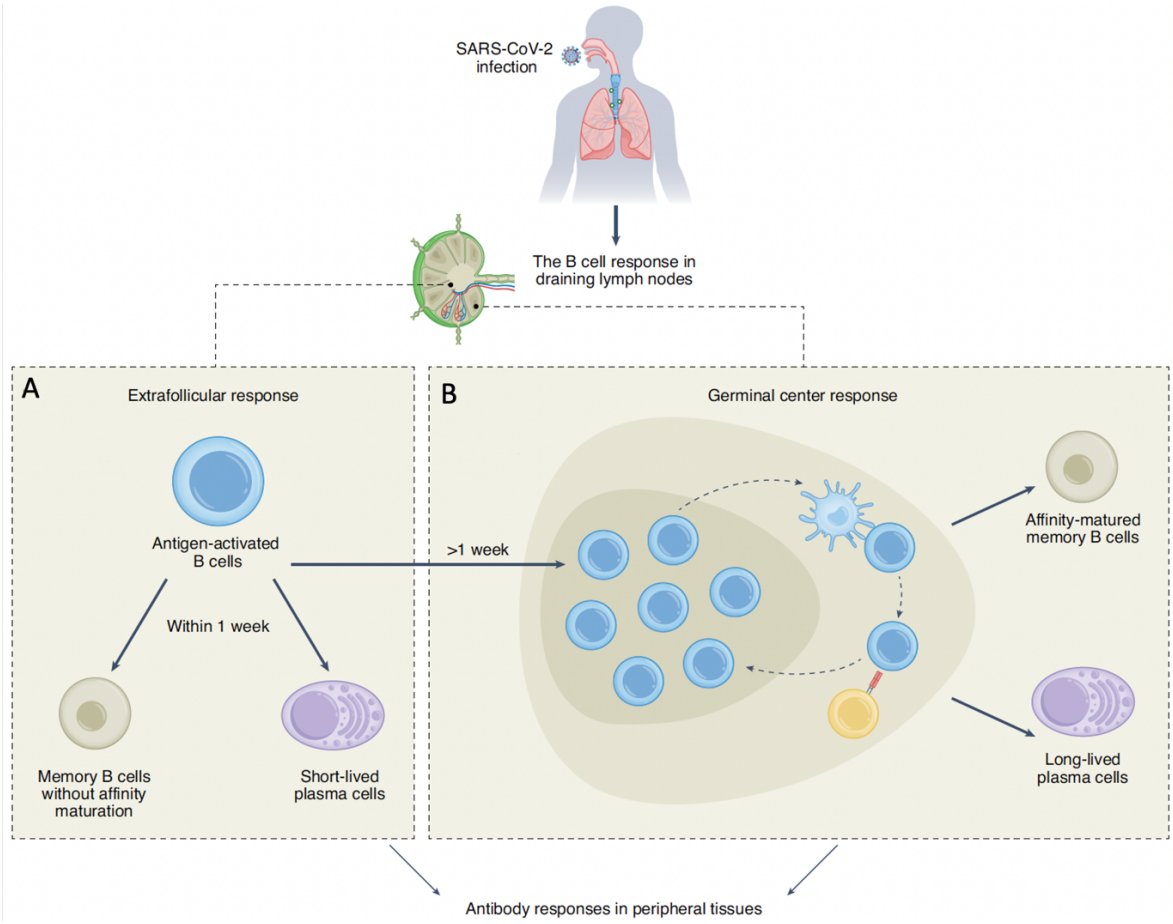

Figure 1.5 The B cell and antibody response against SARS-CoV-2 infection. (A) The rapid extrafollicular (EF) response against SARS-CoV-2 infection. (B) The germinal centre (GC) reaction at later stage of SARS-CoV-2 infection. Taken from *Qi et al., Nat Immunol*, July 2022[48]. Licence number: 5704300362094.

1.2.2 Antibodies generated by SARS-CoV-2 infection

1.2.2.1 Mucosal antibodies in SARS-CoV-2 infection

Although neutralising antibodies in blood or tissues help to control the spread of the virus in the body, mucosal antibodies like secretory IgA may play an important role in preventing the airway transmission of SARS-CoV-2. The distribution of the IgA, along with the potent neutralising activity of dimeric secretory IgA, contribute to the protection of SARS-CoV-2 transmission. In fact, virus-specific IgA is detected in infected patient saliva, as well as in nasal fluids in seronegative healthcare workers[49,50]. Significant levels of SARS-CoV-2 antibodies, including neutralising IgA, is still detectable in nasal fluids months after infection[51,52].

1.2.2.2 Cross-reactive antibodies

There are 79% and 50% of genome sequence identity between SARS-CoV-2 and SARS-CoV and SARS-CoV-2 and MERS-CoV, respectively, including in the RBD regions in S[2,53]. The similarity between SARS-CoV-2 and other human coronavirus is lower, but it is still possible to generate cross-reactive antibodies. In theory, SARS-CoV-2 infection could recall the antibodies generated during previous coronavirus infection, particularly IgG and IgA[54]. It has been reported previously that SARS-CoV antibodies isolated from SARS infected patients could cross-react with human coronavirus 229E and OC43[55], and antibodies cross-react to SARS-CoV and SARS-CoV-2 have also been found[56-58]. SARS-CoV-2 spike binding antibodies have also been detected in blood of healthy population taken before COVID-19 pandemic, which is likely to be cross-reactive antibodies generated through the prior infection by the human coronavirus which causes common cold[59]. A study in Canada detected antibodies that could cross-react to SARS-CoV-2 spike and spikes from human coronavirus HKU1, NL63, and 229E, but not OC43[60]. Another study in sub-Saharan Africa reveals the existence of serological cross-reactivity to SARS-CoV-2 spike and nucleocapsid due to the previous infection by NL63 and 229E[61]. These cross-reactive antibodies are likely against the S2 domain of spike protein, which is highly conserved, rather than the S1 domain which goes under much stronger selective pressure exerted by the immune system[46,47,62]. An intriguing observation is

that people who have seroreactivity to OC43 spike don't have detectable cross-neutralising antibodies against SARS-CoV-2[63].

1.2.2.3 Auto-reactive antibodies

During viral infection, it is possible to generate auto-reactive antibodies due to the inflammation, cell-death-related autoantigen release, and molecular mimicry[64,65]. SARS-CoV-2 infection can cause an increase in autoantibodies targeting a broad set of autoantigens, ranging from complement proteins, cytokines, chemokines to surface proteins[66]. Autoantibodies targeting type I interferons have been uncovered in some COVID-19 cases and are associated with critical disease[67,68]. There are also a series of reports revealing a wide range of autoimmune conditions after SARS-CoV-2 infection, including Guillain-Barre syndrome[69,70], systemic lupus erythematosus[71], and cold agglutinin syndrome[72].

1.2.2.4 anti-spike neutralising antibodies

Spike on the viral surface of SARS-CoV-2 is the major target of neutralising antibodies in the immune response following infection. Among all anti-spike antibodies, RBD is the predominant target for neutralising antibodies. The mechanism of anti-RBD antibodies neutralising the virus is mainly by blocking the binding between S and its receptor on the host cell surface, ACE2, and then further disrupt the membrane fusion[12]. Another way of anti-RBD antibodies neutralisation involves competing with ACE2 for RBD binding through receptor mimicry and inducing rapid and premature shedding of S1 from the trimeric spike[73]. After the first round of primary infection by the early-pandemic SARS-CoV-2 strains during the pandemic, it is noticed by researchers that the neutralising anti-RBD antibodies isolated from infected patients preferentially use heavy chain germline variable (V_H) genes IGHV3-53/3-66[74] and IGHV1-58[75] with limited levels of somatic hypermutation and relatively short complementarity-determining region CDR3.

Anti-NTD antibodies are also capable of neutralising SARS-CoV-2 viruses through a different mechanism. Unlike anti-RBD antibodies, they do not block the binding of S with ACE2, rather by interfering the conformational changes required for attachment to the receptor or membrane fusion[76]. They also play an important role in Fc-mediated effector functions both

in vitro and *in vivo*[77]. It has been widely reported that neutralising NTD antibodies targeting a 'NTD supersite', which is composed by N1 (aa 14-26), N3 (aa 141-156), and N5 (aa 246-260) loops in NTD that are surrounded by glycan and positively charged[76,78]. Many mutations found in circulating variants are around these areas, especially insertions and deletions, for example Δ69-70, ΔY144, Δ157-158, and Δ242-244 are commonly found among variants[22,23,79-82]. The occurrence of multiple deletions in NTD is different to RBD which is dominated by substitutions, possibly because of the plasticity of NTD and the moderate impact of NTD to the receptor binding. Due to the small binding area of the supersite and the abundance of mutations in NTD, it is easy to comprehend that NTD neutralising antibodies are conformation-sensitive and mostly don't have broadly neutralising ability.

1.2.2.5 anti-NTD enhancing antibodies

Antibody-dependent enhancement was first discovered in Dengue virus infection[83] and has been widely reported in Flavivirus now[84]. Whether the ADE of SARS-CoV-2 is involved in the clinical outcome of the disease is still debatable, but there are reports revealing that some anti-NTD antibodies have the ability to enhance the infection of SARS-CoV-2 *in vitro* independent of Fc-receptor. The mechanism of enhancement is that some NTD-antibodies can induce RBD to change into the open state by binding to a specific site of NTD, and mutation of four amino acids, W64, H66, V213, and R214, significantly impact the binding of enhancing NTD-antibodies[85]. But there is no enhancement observed in vivo through monkeys and mice experiment by enhancing NTD-antibodies[86].

1.3 SARS-CoV-2 vaccines

1.3.1 Development of SARS-CoV-2 vaccines

According to the WHO data released on 30 March 2023, 183 vaccines are in clinical development, and 199 vaccines are in pre-clinical development. The platforms used by these vaccines are mainly protein subunit (32% of the total), RNA (24%), viral vector (replicating and non-replicating, 14%), inactivated virus (12%), DNA (9%) and viral like particle (VLP, 4%) (https://www.who.int/publications/m/item/draft-landscape-of-covid-19-candidate-vaccines). As of 2 December 2022, there are 12 vaccines have been granted for emergency use

by WHO, including 3 protein subunit vaccines (COVOVAX, Novavax Nuvaxovid, SKYCovione), 2 RNA vaccines (Moderna Spikevax, Pfizer/BioNTech Comirnaty), 4 non-replicating viral vector (CanSino Convidecia, Janssen Jcovden, Oxford/AztraZeneca Vaxzevria, Covishield), and 3 inactivated vaccines (Covaxin, Sinopharm Covilo, Sinovac CoronaVac).

1.3.1.1 Protein subunit vaccines

Protein subunit COVID-19 vaccines are often recombinant S protein or RBD protein expressed using different protein-expression system, such as mammalian cells or insect cells. The Novavax subunit vaccine, Nuvaxovid (NVX-CoV2373) used a full-length recombinant S protein with a pre-fusion conformation containing a mutation in the furin cleavage site, and it was produced by Sf9 insect cell expression system. The S protein with a prefusion conformation is easily converted to the post-fusion conformation, but by introducing mutations on two residues, K986P and V987P, the prefusion conformation can be stabilised (S-2P)[87,88]. There is also a report of vaccine developed using RBD manufactured in insect cells[89].

Except for neutralising antibodies, protein vaccines can also induce Th1 cell responses[90]. However, the expression efficiency of S is relatively low comparing with RBD, although RBD lacks other domains on the S which also can induce neutralising antibodies[91].

1.3.1.2 mRNA vaccines

mRNA vaccines are vaccines made by encapsulating mRNA with vectors, usually lipid nanoparticles (LNP), but lipoplexes, polymer nanoparticles, cationic polypeptides, and polysaccharide particles are also used[92,93]. For mRNA-1273 vaccine, the optimised mRNA encoding SARS-CoV-2 S-2P protein with stable pre-fusion conformation was synthesised and purified by oligo-dT affinity purification, and then encapsulated in LNP[94]. Another mRNA vaccine, BNT162b2, also uses a similar mRNA encoding S-2P[87,95], while BNT162b1 utilises the mRNA encoding RBD and fuses C terminus with the trimer domain of T4 fibrin. A good delivery system can not only protect mRNA from degradation, but also effectively transfer mRNA into cells and induce a strong immune response, hence improving the efficacy of the vaccine.

The mechanism of the mRNA vaccines is transmitting the genetic information of the antigen into host cells by LNP and the translation process happens inside the host cells[91]. It can induce

strong B cell responses and Th1 cell responses, while producing long-lived plasma cells and memory cells[96,97]. The disadvantage of mRNA vaccines is the instability of RNA and the requirement of a higher storage condition, such as cold chain transportation and low temperature storage.

1.3.1.3 DNA vaccines

DNA vaccines are similar to mRNA vaccines which are produced by recombinant plasmids encoding viral antigens, and genes of viral antigens are transcript and translated inside host cells[87]. A COVID-19 DNA vaccine, INO-4800, was synthesised based on a previously reported MERS-CoV vaccine[98]. Another DNA vaccine was constructed by linking the DNA encoding SARS-CoV-2 S protein, which was optimised based on human codons, into the pWRG vector that had been used to generate a hantavirus vaccine previously[99].

DNA vaccines are more stable over a long time than RNA vaccines[100] and can be prepared in big scales by Escherichia coli. However, DNA vaccines have lower immunogenicity compared with RNA vaccines and different injection methods can influence the vaccine's efficacy[91].

1.3.1.4 Inactivated virus vaccines

Inactivated virus vaccines are generated by using chemical reagents to inactivate the *in vitro* cultured virus[101]. The viral particle would be intact after treatment by chemical reagents[87]. An inactivated vaccine was generated by in vitro culturing of a SARS-CoV-2 strain from patient swabs in Vero cells. From three isolated strains, the one with the strongest replication ability was selected and subcultured for seven generations. Then the seventh generation of the virus, BJ-P-0207, was inactivated using β-propiolactone[102].

A benefit for using inactivated virus vaccine is that it uses full viral particle as an immunogen, hence it can elicit antibodies targeting a wider range of antigens comparing with vaccines produced based on SARS-CoV-2 S protein or RBD. However, the efficacy of inactivated vaccines is lower than the vaccines built by some other platforms.

1.3.1.5 Viral vector vaccines

Viral vector vaccines are engineeringly replication-attenuated virus carrying genetic information of viral proteins which would be translated inside host cells after immune transduction following vaccine administration[101]. A human adenovirus type-5 (Ad5) virus based vaccine was generated by introducing a codon optimised S protein gene of SARS-CoV-2 ancestral strain into a human Ad5 virus with E1 and E3 gene deletion to produce a vector expressing S protein[103]. A platform based on engineered chimpanzee Ad25 vector was also used to prepare SARS-CoV-2 vaccine ChAdOx1 nCoV-19 vaccine[104]. SputnikV vaccine was also generated by using Recombinant vectors based on a combination of human Ad5 and Ad26 viruses[105]. Except for adenovirus, there is also a COVID-19 vaccine produced by using vesicular stomatitis virus, which induces a stronger humoral immune response via intranasal and intramuscular routes[106].

One of the advantages of viral vector vaccines is its safety in manufacturing process, as no live viruses are involved[91]. In addition, viral vector vaccines are able to induce Th1 cell responses[107,108]. But one of the issues for viral vector vaccines is the pre-existing immunity in populations, which may reduce the immunogenicity of the vaccines. Besides, how to minimise the generation of immunity towards vectors after repeated administration of viral vector vaccines is also worth pondering[109].

1.3.1.6 VLP vaccines

VLP vaccines are non-infectious particles which have viral structural proteins and viral polypeptides on the surface[110]. A SARS-CoV-2 vaccine was constructed by forming a covalent iso-peptide bonds between RBD and a protein nanoparticle to obtain an RBD-Spy VLP[111]. Another VLP vaccine was constructed by using full-length S proteins which includes R667G, R668S, R670S, K971P, and V972P mutations to stabilise the proteins based on a plant expression system[112].

Because of not containing viral genomes, VLP vaccines are relatively safe, and some plant-based vaccines can even be administrated orally. If multiple RBD from different SARS-CoV-2 variants are displayed on the protein particles, it may be able to elicit cross-neutralising mAbs. However, the manufacturing process of VLP vaccines is complicated and there is no relevant clinical data available.

1.3.1.7 Live-attenuated vaccines

Live attenuated vaccines are designed based on the virulence-reduced viruses or viruses produced by reverse genetics to be used as antigens[87]. The processes of generating live attenuated vaccines include codon paired deoptimisation (CPD) and virulence gene knockout[91,113,114]. Currently, there are reported SARS-CoV-2 live attenuated vaccines produced by CPD method in which amino acid 283 and the furin cleavage site of the S protein were deleted to reduce the virulence of the virus but its replication ability still remained[115,116].

The advantage of CPD-made live attenuated virus is that most of the viral structure and epitopes can still be kept intact and extensively induce innate, humoral and cellular immune responses in vaccinees[115]. Live attenuated vaccines can also induce mucosal immune response by nasal administration to protect the upper respiratory tract[91]. However, the reduced virulence of live attenuated vaccines has the opportunity to revert during replication and proliferation in the host after administration.

1.3.2 Vaccine induced immunity

The vaccines described above can be categorised into three classes based on their antigen types. Class 1 are vaccines based on viral proteins produced in vitro, including protein subunit vaccines, inactivated vaccines, and VLP vaccines. Class 2 are vaccines based on antigens generated in vivo, including mRNA vaccines, DNA vaccines and viral-vector vaccines. Class 3 are live-attenuated vaccines. These vaccines can induce humoral responses in recipients to produce protective neutralising antibodies. In addition, some vaccines can induce T cell responses which also effectively protect recipients against SARS-CoV-2 virus infection. Memory cells also can be induced by vaccines to provide long-term protection against COVID-19.

1.3.2.1 Vaccine induced Th1 cell response

Th1 cell responses can be induced by administration of several COVID-19 vaccines, including ChAdOx1 nCoV-19 (viral vector vaccine), mRNA-1273 (mRNA vaccine), and BNT162 (mRNA vaccines)[117-119]. $CD4^+$ T cells in peripheral lymphoid organs can differentiate into Th1 cells after recognising the T cell receptor (TCR) and AP-MHC class II complex. Type 1 T helper (Th1) cells secret multiple cytokines including interleukin 2 (IL-2) which binds to IL-2 receptors (IL-2R) and promotes T-cell proliferation and $CD8^+$ T-cell activation. After activation, $CD8^+$ T cells differentiate into CTLs to boost cellular immunity. Th1 cells secrete

tumour necrosis factor-alpha (TNF-α) as well as interferon-gamma (IFN-γ), with the latter inducing the differentiation of $CD4^+$ T cells and increasing the immune responses. After the antigen is cleared, the cell responses will be reduced due to the lack of stimulating signal. However, the antigen-specific memory T cells will be generated and responsible for long-term protection[120].

1.3.2.2 Vaccine induced humoral and germinal centre response

It is reported that some mRNA vaccines can induced follicular helper T cells (Tfh cells) and then activate SARS-CoV-2 specific germinal-centre B cell (GC B-cell) responses[96,121] as discussed previously (Section 1.2.1). After the first dose of BNT162b2 vaccine, a strong SARS-CoV-2 S protein GC B-cell response was detected in lymph node fine-needle aspirates from the vaccinees, and the response was enhanced after the second dose of the vaccine[96]. Memory B cells will also be formed from GC B cells.

1.3.2.3 Vaccine induced memory cell responses

Both T cells and B cells can generate memory cells for long-term protection after vaccination. Unlike primary T cell response, memory T cells do not need the activation of antigen-presenting cells (APC) and induce stronger immune responses. Memory B cells can also be activated rapidly to produce neutralising antibodies against the same antigen. Both mRNA vaccines BNT162b2 and mRNA-1273 could induce memory B cell response to generate higher-level production of antibodies[97]. In addition, patients recovered from SARS-CoV-2 infection can also generate detectable level of memory B cells and vaccination induces the memory B cell response[122].

1.4 Aim of this study

Since the emergence of SARS-CoV-2 in December 2019, it has caused huge losses to human lives and economy. Hence it is vital to find an effective treatment for the viral infection and to

understand the evolution of the virus. By isolating antibodies from different variants of SARS-CoV-2 infected convalescent patient PBMCs, and by characterising their neutralising abilities and binding epitopes, we were aiming to find broadly neutralising antibodies targeting conserved epitopes. Also using serum acquired from infected patients to neutralise different variants, we could build an antigenic distance map of these variants to help to reveal the selective pressure given by vaccination and infection on the evolution of SARS-CoV-2 and shed light on the selection of future vaccine candidates.

CHAPTER 2. Materials and methods

2.1 Materials and reagents

2.1.1 General materials and reagents

2.1.1.1 Antibodies

Human anti-NP mAb 206 was isolated and reported by Dejnirattisai et al[123]; Regeneron mAbs (REGN10933 and REGN10987) and AstraZeneca mAbs (AZD1061, AZD8895, and AZD7442) were obtained from AstraZeneca; Vir mAbs (S309), Lily mAbs (LY-CoV555, LY-CoV16, and LY-CoV1404), and Adagio mAbs (ADG10, ADG20, and ADG30) were obtained from Adagio; mouse mAb StrepMAB-Classic (Cat#2-1507-001) StrepMAB Classic-DY549 (Cat#2-1566-050) were purchased from IBA Lifesciences; mouse anti-human IgG mAb (Cat#I9559), ALP-conjugated anti-human IgG (Cat#A9544), peroxidase-conjugated goat anti-human IgG (Cat#A0170), and anti-human IgG Fc specific-FITC (Cat#F9512) were purchased from Sigma-Aldrich. Anti-human CD3-FITC (Cat# 555332), anti-human CD14-FITC (Cat#555397), anti-human CD56-FITC (Cat#562794), anti-human CD16-FITC (Cat#555406), anti-human IgM-FITC (Cat#555782), Anti-Human CD19-BUV395 (Cat#563549), and Anti-Human IgG-BV786 (Cat#564230) were purchased from BD. Anti-human IgA-FITC (Cat#F0188) and Anti-human IgD-FITC (Cat#F0189) were purchased from Dako.

2.1.1.2 Reagents

Phosphate buffered saline (PBS) (Cat#P2272), Dulbecco's Modified Eagle Medium (high glucose, Cat#5796), Dulbecco's Modified Eagle Medium (low glucose, Cat#6046), L-Glutamine-Penicillin-Streptomycin (Cat#G1146), Ampicillin (Cat#PHR2838), Agarose (Cat#A2929), Carboxymethyl cellulose (Cat#C4888), Triton X-100 (Cat#8787), Polyethylenimine (branched, Cat#408727) and Sodium Chloride (NaCl, Cat#S9888) were purchased from Sigma-Aldrich; FreeStyle™ 293 Expression Medium (Cat#12338018), GlutaMAX™ Supplement (Cat#35050061), Opti-MEM™ (Cat#11058021), TypLE™ Express Enzyme (Cat#12604013), Fetal Bovine Serum (Cat#12676029) and L-Glutamine 200 mM (100×) (Cat#2036885) were purchased from Gibco; UltraDOMA PF Protein-free Medium (Cat#12-727F) was purchased from Lonza; Strep-TactinXT (Cat#2-1206-025) was purchased from IBA Lifesciences; LB broth (Cat#51577–51656), SYBR™ Safe DNA Gel Stain

(Cat#S33102), and Phusion™ High-Fidelity DNA Polymerase (Cat#F530S) were purchased from Fisher Scientific UK. Kanamycin (Cat#K22000) and Tris-base (Cat#T60040) were purchased from Melford. Bright-Glo™ Luciferase Assay System (Cat#E2620) and RNase inhibitor (Cat#N2611) were bought from Promega. HIV1 p24 ELISA Kit (Cat#ab218268) was purchased from Abcam. HotStarTaq DNA Ploymerase (Cat#203205), OneStep RT-PCR kit (Cat#210212), QIAprep Spin Miniprep Kit (Cat#27106), and QIAquick PCR & Gel Cleanup kit (Cat#28704) were purchased from QIAGEN.

2.1.2 Human resources

2.1.2.1 Early pandemic strains infected patient and blood samples

Patients were recruited from the John Radcliffe Hospital in Oxford, UK, between March and May 2020 by identification of patients hospitalised during the SARS-CoV-2 pandemic and recruited into the Sepsis Immunomics project [Oxford research ethics committee (REC) C, reference:19/SC/0296] ISARIC/WHO Clinical Characterization Protocol for Severe Emerging Infections [Oxford REC C, reference 13/SC/0149].Time between onset of symptoms and sampling were known for all patients and if labelled as convalescent patients were sampled at least 28 days from the start of their symptoms. Written informed consent was obtained from all patients. All patients were confirmed to have tested positive for SARS-CoV-2 using the reverse transcriptase polymerase chain reaction (RT-PCR) from an upper respiratory tract (nose/throat) swab tested in accredited laboratories. The degree of severity was identified as a mild, severe or critical infection according to recommendations from the World Health Organization. Severe infection was defined for COVID-19 confirmed patients with one of the following conditions: respiratory distress with RR > 30/min; blood oxygen saturation < 93%; arterial oxygen partial pressure (PaO_2) / fraction of inspired O_2 (FiO_2) < 300 mmHg; and critical infection was defined as respiratory failure requiring mechanical ventilation or shock; or other organ failures requiring admission to ICU. Comparator samples from healthcare workers or epidemiologically detected early clusters with confirmed SARS-CoV-2 infection who all had mild non-hospitalised disease were collected under the Gastro-intestinal illness in Oxford: COVID sub study [Sheffield REC, reference: 16/YH/0247] (Table 2.1).

Blood samples were collected and separated into plasma by centrifugation at 500 g for 10 mins. Plasma was removed from the uppermost layer and stored at 80 ℃. The PBMC layer

was then gently suspended in the remaining plasma and RPMI media, and then isolated by Ficoll-Hypaque gradient centrifugation. All PBMC samples were stored in liquid nitrogen until use.

2.1.2.2 Serum from Pfizer vaccinated individuals

Pfizer vaccine serum was obtained 7-17 days following the second dose of vaccine which was administered 3 weeks after the first dose (participants were to the best of their knowledge seronegative at entry).

The study was approved by the Oxford Translational Gastrointestinal Unit GI Biobank Study 16/YH/0247 [REC at Yorkshire & The Humber – Sheffield]. The study was conducted according to the principles of the Declaration of Helsinki (2008) and the International Conference on Harmonization (ICH) Good Clinical Practice (GCP) guidelines. Written informed consent was obtained for all patients enrolled in the study. Vaccinees were Health Care Workers, based at Oxford University Hospitals NHS Foundation Trust, not known to have prior infection with SARS-C0V-2. Each received two doses of COVID-19 mRNA Vaccine BNT162b2, 30 mg, administered intramuscularly after dilution as a series of two doses (0.3 ml each) 18-28 days apart. The mean age of vaccinees was 43 years (range 25-63), 11 male and 14 female (Table 2.2).

2.1.2.3 Serum from AstraZeneca-Oxford vaccinated individuals

Full details of the randomized controlled trial of ChAdOx1 nCoV-19 (AZD1222), were previously published (PMID: 33220855/PMID: 32702298). These studies were registered at ISRCTN (15281137 and 89951424) and ClinicalTrials.gov (NCT04324606 and NCT04400838). Written informed consent was obtained from all participants, and the trial is being done in accordance with the principles of the Declaration of Helsinki and Good Clinical Practice. The studies were sponsored by the University of Oxford (Oxford, UK) and approval obtained from a national ethics committee (South Central Berkshire Research Ethics Committee, reference 20/SC/0145 and 20/SC/0179) and a regulatory agency in the United Kingdom (the Medicines and Healthcare Products Regulatory Agency). An independent DSMB reviewed all interim safety reports. A copy of the protocols was included in previous publications (PMID: 33220855/PMID: 32702298).

Data from vaccinated volunteers who received two vaccinations are included in this paper. Vaccine doses were either 531010 viral particles (standard dose; SD/SD cohort n = 21) or half dose as their first dose (low dose) and a standard dose as their second dose (LD/SD cohort n = 4). The interval between first and second doses was in the range of 8-14 weeks. Blood samples were collected, and serum separated on the day of vaccination and on pre-specified days after vaccination e.g., 14 and 28 days after boost (Table 2.2).

2.1.2.4 Serum from Alpha infected individuals

Plasma and peripheral blood mononuclear cells were collected from individual with SARS-CoV2 Alpha confirmed through a test positive for SARS-CoV-2 using RT-PCR from an upper respiratory tract (nose/throat) swab tested in accredited laboratories. Patients were recruited through a variety of studies including Sepsis Immunomics [Oxford REC C, reference:19/SC/0296]), ISARIC/WHO Clinical Characterization Protocol for Severe Emerging Infections [Oxford REC C, reference 13/SC/0149] and the Gastro-intestinal illness in Oxford: COVID substudy [Sheffield REC, reference: 16/YH/0247]. In all cases it was known whether a patient was recruited into one or several studies and clinical information including severity of disease (mild, severe or critical infection according to recommendations from the World Health Organization) and times between symptom onset and sampling and age of participant was known (Table 2.1).

2.1.2.5 Sera from Beta, Gamma, and Delta infected cases

Beta and Delta samples from UK infected cases were collected under the 'Innate and adaptive immunity against SARS-CoV-2 in healthcare worker family and household members' protocol affiliated to the Gastro-intestinal illness in Oxford: COVID sub study discussed above and approved by the University of Oxford Central University Research Ethics Committee. All individuals had sequence confirmed Beta/Delta infection or PCR-confirmed symptomatic disease occurring whilst in isolation and in direct contact with Beta/Delta sequence-confirmed cases. Additional Beta infected serum (sequence confirmed) was obtained from South Africa. At the time of swab collection patients signed an informed consent to consent for the collection of data and serial blood samples. The study was approved by the Human Research Ethics

Committee of the University of the Witwatersrand (reference number 200313) and conducted in accordance with Good Clinical Practice guidelines (Table 2.1).

Gamma samples were provided by the International Reference Laboratory for Coronavirus at FIOCRUZ (WHO) as part of the national surveillance for coronavirus and had the approval of the FIOCRUZ ethical committee (CEP 4.128.241) to continuously receive and analyse samples of COVID-19 suspected cases for virological surveillance. Clinical samples were shared with Oxford University, UK under the MTA IOC FIOCRUZ 21-02 (Table 2.1).

Table 2.1 Information of Early pandemic, Alpha, Beta, Gamma, and Delta cases

	Early pandemic	Alpha	Beta	Gamma	Delta	Vaccine-V1 Delta	Delta-V1-Vaccine
Participants							
Female	1	1	4	6	7	5	4
Male	9	6	5	4	3	4	4
Median Age (Y)	60 (Range 53-69)	57 (Range 29-76)	47 (Range 16-64)	32 (Range 23-49)	26 (Range 12-36)	40 (Range 28-70)	41 (Range 31-54)

2.1.2.6 Sera from BA.1 infected cases

Following informed consent, individuals with omicron BA.1 were co-enrolled into the ISARIC/WHO Clinical Characterisation Protocol for Severe Emerging Infections [Oxford REC C, ref. 13/SC/0149] and the ‘‘Innate and adaptive immunity against SARS-CoV-2 in healthcare worker family and household members’’ protocol affiliated to the Gastro-intestinal illness in Oxford: COVID sub study [Sheffield REC, ref. 16/YH/0247] further approved by the University of Oxford Central University Research Ethics Committee. Diagnosis was confirmed through reporting of symptoms consistent with COVID-19 or a positive contact of a known Omicron case, and a test positive for SARS-CoV-2 using RT-PCR from an upper respiratory tract (nose/throat) swab tested in accredited laboratories and lineage sequence confirmed through national reference laboratories. A blood sample was taken following consent at least 10 days after PCR test confirmation. Clinical information including severity of disease (mild, severe or critical infection according to recommendations from the World Health Organisation) and times between symptom onset and sampling and age of participant was captured for all individuals at the time of sampling (Table 2.2).

2.1.2.7 Sera from BA.2 infected cases

Following informed consent, healthcare workers with BA.2 infection were co-enrolled under the Sheffield Biobank study (STHObs) (18/YH/0441). All individuals had PCR-confirmed symptomatic disease and sequence confirmed BA.2 infection through national UKHSA sequencing data. A blood sample was taken following consent at least 12 days after PCR test confirmation. Clinical information including vaccination history, times between symptom onset and sampling and age of participant was captured for all individuals at the time of sampling (Table 2.2).

2.1.2.8 Sera from BA.4/5 infected cases

Following informed consent, individuals with omicron BA.4 or BA.5 were co-enrolled into one or more of the following three studies: the ISARIC/WHO Clinical Characterisation Protocol for Severe Emerging Infections [Oxford REC C, ref. 13/SC/0149], the ‘‘Innate and adaptive immunity against SARS-CoV-2 in healthcare worker family and household members’’ protocol (approved by the University of Oxford Central University Research Ethics Committee), or the Gastro-intestinal illness in Oxford: COVID sub study [Sheffield REC, ref. 16/YH/0247]. Diagnosis was confirmed through reporting of symptoms consistent with COVID-19, hospital presentation, and a test positive for SARS-CoV-2 using RT-PCR from an upper respiratory tract (nose/throat) swab tested in accredited laboratories and lineage sequence confirmed through national reference laboratories in the United Kingdom. A blood sample was taken following consent at least 14 days after PCR test confirmation. Clinical information including severity of disease (mild, severe or critical infection according to recommendations from the WHO) and times between symptom onset and sampling and age of participant was captured for all individuals at the time of sampling (Table 2.2).

Table 2.2 Information of BA.1, BA.2, BA.4/5 infection and vaccination cases

	BA.1 infection	BA.2 infection	BA.4/5 infection	AZ V3+28	BNT162b2 V3+28
Participants					
Female	7	19	6	20	8
Male	7	4	5	21	10
Median Age (Y)	22 (Range 21-56)	41 (Range 22-57)	42 (Range 20-94)	37 (Range 25-53)	45 (Range 30-59)
Vaccine History					
First dose	2020 Dec-2021 Jul	2020 Dec-2021 March	2020 Dec-2021 June	2020 Apr-2020 May	2020 Dec-2021 Jan)
ChAdOx1	4	3	2	41	0
BNT162b2	9	20	8	0	18
J&J	1	0	0	0	0
Second dose	2021 Jan-2021 Sep	2021 March-2021 May	2021 Feb-2021 Aug	2020 Jul-2020 Aug	2021 Jan
ChAdOx1	4	3	2	41	0
BNT162b2	9	20	8	0	18
Third dose	2021 Sep-2022 Jan	2021 Sep-2021 Dec	2021 Oct-2021 Dec	2021 March	2021 Sep-2021 No
ChAdOx1	0	0	0	41	0
BNT162b2	11	22	4	0	18
Moderna	0	1	4	0	0
Infection History	BA.1 (2021 Dec)	BA.2 (2022 Feb-2022 Apr)	BA.4/5 (2022 June)	None	None
Pre-1st dose	0	0	1		
Pre-3rd dose	4	0	2		
Post-vaccine (1 dose)	1	0	0		
Post-vaccine (2 doses)	2	0	0		
Post-vaccine (3 doses)	7	23	8		
Average days after infection or last vaccination (D)	42 (Range 27-55)	28 (Range 12-43)	37 (Range 24-49)	28	28

2.1.3 Viral stocks

SARS-CoV-2/human/AUS/VIC01/2020[124], Alpha and Beta were provided by Public Health England, Gamma cultured from a throat swab from Brazil, Delta was a gift from Wendy Barclay and Thushan de Silva, from the UK G2P genotype to phenotype consortium.

BA.1 was grown from a positive throat swab (IRAS Project ID: 269573, Ethics Ref: 19/NW/0730). Sequencing of the Omicron BA.1 isolate shows the expected consensus S gene changes (A67V, D69-70, T95I, G142D/D143-145, D211/L212I, ins214EPE, G339D, S371L, S373P, S375F, K417N, N440K, G446S, S477N, T478K, E484A, Q493R, G496S, Q498R, N501Y, Y505H, T547K, D614G, H655Y, N679K, P681H, N764K, D796Y, N856K, Q954H, N969K, L981F), an intact furin cleavage site and a single additional mutation A701V.

Sequencing of the BA.1.1 isolate shows an additional mutation R346K and lack of mutation A701V compared with BA.1, and sequencing of BA.2 confirmed the expected changes in the S gene (T19I, D24–26, A27S, G142D, V213G, G339D, S371F, S373P, S375F, T376A, D405N, R408S, K417N, N440K, S477N, T478K, E484A, Q493R, Q498R, N501Y, Y505H, D614G, H655Y, N679K, P681H, N764K, D796Y, Q954H and N969K). BA.1, BA.1.1 and BA.2

isolates have been fully sequenced and the deposited reads have INSDC accession numbers ERR8959182, ERR9321875 and ERR9321876 respectively.

Viral titres were determined by a focus-forming assay on Vero cells. Victoria passage 5, Alpha passage 2, Beta passage 4, Gamma passage 1, Delta passage 3, BA.1 passage 2, BA.1.1 passage 2, and BA.2 passage 2 were sequenced to verify that they contained the expected spike protein sequence and no changes to the furin cleavage sites.

2.1.4 Bacterial strains and cell lines

Vero (ATCC CCL-81) cells and Vero-furin cells[125] were cultured at 37℃ in Dulbecco's Modified Eagle medium (DMEM) supplemented with 10% fetal bovine serum (FBS), 10 mM HEPES, and 100 U/ml of penicillin–streptomycin. Spike ectodomain, human mAbs and Fabs were expressed in HEK293T cells cultured in FreeStyle 293 Expression Medium (12338018, Thermo-Fisher) at 37 C with 5% CO_2.

For ACE2 and RBD, transient expression used Expi293F cells (Thermo Fisher, Cat# A14527) grown in Expi293 Expression Medium (Thermo Fisher, Cat# A1435103) in suspension with 8% CO_2 at 30 or 37℃ and shaking at 130 × g. His-tagged RBD for structural analysis was expressed in a stable HEK293S cell line cultured in DMEM (high glucose, Sigma) supplemented with 10% FBS (Invitrogen), 1 mM glutamine and 1 x non-essential amino acids at 37℃. Cells were transferred to roller bottles (Greiner) and cultured in DMEM supplemented with 2% FBS, 1 mM glutamine and 1x non-essential amino acids at 30℃ for 10 days for protein expression. For plaque assays Vero-furin cells[125] were cultured at 37℃ in DMEM supplemented with 10% FBS and 100 U/ml of penicillin–streptomycin.

2.2 Plasmid constructions

2.2.1 Trimeric spike of SARS-CoV-2

To construct the expression plasmid for trimeric S protein of original strain (Wuhan), the synthetic fragments coding for human codon-optimized Spike glycoprotein sequence from CoV-SARS2 (GenBank accession number MN908947; amino acids 1-1208) was cloned into expression plasmid pHLSec vector at the downstream of the chicken β-actin/rabbit β-globin hybrid promoter and followed by a T4 fibritin trimerization domain, an HRV 3C cleavage site,

an 8×His tag and a Twin-Strep-tag at the C terminus[13]. The furin cleavage site (aa 683-687) on the Spike is mutated from PRRAR to PGSAS, whereas residues 986 and 987 in the linker between two helices in S2 were mutated from KK to PP sequence to prevent the conversion to the post-fusion helical conformation.

To construct the expression plasmids for the trimeric S protein of Beta variant, nine pairs of primers were designed to introduce L18F, D80A, D215G, 242-244 deletion and R246I, K417N, E484K, N501Y, D614G, and A701V into S protein of Wuhan strain. The fragments with corresponding mutations were joint together by Gibson reaction[126] with pHLSec expression vector. The new construct was fully sequenced by sanger sequencing[127]. Expression plasmids for S proteins of other variants were constructed following the same method.

2.2.2 NTD and RBD of spike

To construct NTD of all VoCs, the gene encoding NTD of SARS-CoV-2 (amino acids 13-305 of the SARS-CoV-2 S protein) was amplified from the trimeric S protein expression plasmid of each variant with 6×His tag at the C terminal. The PCR product was cloned into the pHLSec expression vector using AgeI and XhoI restriction sites. All constructs were sequence confirmed by sanger sequencing[127].

To construct RBD of all VoCs, the gene encoding RBD of SARS-CoV-2 (amino acids 330-532 of the SARS-CoV-2 S protein) was amplified from each variant. The PCR product was inserted into the pOPINTTGneo expression vector incorporating a C-terminal 6×His tag. All constructs were sequence confirmed by sanger sequencing[57].

2.2.3 Plasmid construction for pseudotyped lentiviral particle production

A synthetic codon-optimised SARS-CoV-2 spike gene from Wuhan-Hu-1 (GenBank: MN908947) on pcDNA3.1 vector was used as the template to construct Pseudovirus product plasmids for all variants. To construct Victoria (S247R in S gene), primers with certain mutations were used to generate two insert fragments together with two primers of pcDNA3.1 vector, and the vector was also PCR amplified by another pair of primers. After PCR products purification, the two fragments were joint with the vector by Gibson assembly. Other variants

were constructed using the same method and the mutation list for all variants used in this project are shown in Table 2.3.

Table 2.3 Mutations in S proteins of Pseudovirus used in this study

variant name	Mutations in S
Victoria	S247R
Alpha	deletion 69-70 and 144, N501Y,A570D,D614G, P681H,T716I,S982A,D1118H
Beta	L18F, D80A, D215G, L242-244, R246I, K417N,E484K, N501Y, D614G, A701V
Gamma	L18F, T20N, P26S, D138Y, R190S, K417T, E484K, N501Y, D614G, H655Y, T1027I, V1176F
Delta	T19R, G142D, Δ156-157/R158G, A222V, L452R, T478K, D614G, P681R, D950N
BA.1	A67V, Δ69-70, T95I, G142D/Δ143-145, Δ211/L212I, ins214EPE, G339D, S371L, S373P, S375F, K417N, N440K,G446S, S477N, T478K, E484A, Q493R, G496S, Q498R, N501Y, Y505H, T547K, D614G, H655Y, N679K, P681H, N764K, D796Y, N856K, Q954H, N969K, L981F
BA.1.1	A67V, Δ69-70, T95I, G142D/Δ143-145, Δ211/L212I, ins214EPE, G339D, R346K, S371L, S373P, S375F, K417N, N440K,G446S, S477N, T478K, E484A, Q493R, G496S, Q498R, N501Y, Y505H, T547K, D614G, H655Y, N679K, P681H, N764K, D796Y, N856K, Q954H, N969K, L981F
BA.2	T19I, Δ24-26, A27S, G142D, V213G, G339D, S371F, S373P, S375F, T376A, D405N, R408S, K417N, N440K, S477N, T478K, E484A, Q493R, Q498R, N501Y, Y505H, D614G, H655Y, N679K, P681H, N764K, D796Y, Q954H, N969K
BA.2.12.1	T19I, Δ24-26, A27S, G142D, V213G, G339D, S371F, S373P, S375F, T376A, D405N, R408S, K417N, N440K, L452Q, S477N, T478K, E484A, Q493R, Q498R, N501Y, Y505H, D614G, H655Y, N679K, P681H, S704L, N764K, D796Y, Q954H, N969K
BA.2.75	T19I, Δ24-26, A27S, G142D, K147E, W152R, F157L, I210V, V213G, G257S, D339H, S371F, S373P, S375F, T376A, D405N, R408S, K417N, N440K, G446S, N460K, S477N, T478K, E484A, Q498R, N501Y, Y505H, D614G, H655Y, N679K, P681H, N764K, D796Y, Q954H, N969K
BA.2.75.2	T19I, Δ24-26, A27S, G142D, K147E, W152R, F157L, I210V, V213G, G257S, D339H, R346T, S371F, S373P, S375F, T376A, D405N, R408S, K417N, N440K, G446S, N460K, S477N, T478K, E484A, F486S, Q498R, N501Y, Y505H, D614G, H655Y, N679K, P681H, N764K, D796Y, Q954H, N969K, D1199N
BA.2.3.20	T19I, Δ24-26, A27S, G142D, M153T, N164K, V213G, H245N, G257D, G339D, S371F, S373P, S375F, T376A, D405N, R408S, K417N, N440K, K444R, N450D, L452M, N460K, S477N, T478K, A484R, Q498R, N501Y, Y505H, D614G, H655Y, N679K, P681H, N764K, D796Y, Q954H, N969K
BA.2.10.4	T19I, Δ24-26, A27S, W64R, Δ141-144, V213G, Δ243-244, G339D, S371F, S373P, S375F, T376A, D405N, R408S, K417N, N440K, G446S, S477N, T478K, E484A, F486P, S494P, Q498R, N501Y, Y505H, D614G, H655Y, N679K, P681H, N764K, D796Y, Q954H, N969K, P1143L
BA.4/5	T19I, Δ24-26, A27S, Δ69-70, G142D, V213G, G339D, S371F, S373P, S375F, T376A, D405N, R408S, K417N, N440K, L452R, S477N, T478K, E484A, F486V, Q498R, N501Y, Y505H, D614G, H655Y, N679K, P681H, N764K, D796Y, Q954H, N969K
BA.4.6	T19I, Δ24-26, A27S, Δ69-70, G142D, V213G, G339D, R346T, S371F, S373P, S375F, T376A, D405N, R408S, K417N, N440K, L452R, S477N, T478K, E484A, F486V, Q498R, N501Y, Y505H, D614G, H655Y, N658S, N679K, P681H, N764K, D796Y, Q954H, N969K
BA.5.9	T19I, Δ24-26, A27S, Δ69-70, G142D, V213G, G339D, R346I, S371F, S373P, S375F, T376A, D405N, R408S, K417N, N440K, L452R, S477N, T478K, E484A, F486V, Q498R, N501Y, Y505H, D614G, H655Y, N679K, P681H, N764K, D796Y, Q954H, N969K
BJ.1	T19I, Δ24-26, A27S, V83A, G142D, Δ145/H146Q, Q183E, G213E, G339H, R346T, L368I, S371F, S373P, S375F, T376A, D405N, R408S, K417N, N440K, V445P, G446S, S477N, T478K, V483A, E484A, F490V, Q493R, Q498R, N501Y, Y505H, D614G, H655Y, N679K, P681H, N764K, D796Y, Q954H, N969K, S1003I
BF.7	T19I, Δ24-26, A27S, Δ69-70, G142D, V213G, G339D, R346T, S371F, S373P, S375F, T376A, D405N, R408S, K417N, N440K, L452R, S477N, T478K, E484A, F486V, Q498R, N501Y, Y505H, D614G, H655Y, N679K, P681H, N764K, D796Y, Q954H, N969K
BS.1	T19I, Δ24-26, A27S, G142D, Δ144, V213G, G257V, G339D, R346T, S371F, S373P, S375F, T376A, D405N, R408S, K417N, N440K, L452R, G476S, N460K, S477N, T478K, E484A, Q493R, Q498R, N501Y, Y505H, D614G, S640F, H655Y, N679K, P681H, N764K, D796Y, Q954H, N969K
BN.1	T19I, Δ24-26, A27S, G142D, K147E, W152R, F157L, I210V, V213G, G257S, D339H, R346T, K356T, S371F, S373P, S375F, T376A, D405N, R408S, K417N, N440K, G446S, N460K, S477N, T478K, E484A, F490S, Q498R, N501Y, Y505H, D614G, H655Y, N679K, P681H, N764K, D796Y, Q954H, N969K
BN.1.2.1	T19I, Δ24-26, A27S, G142D, K147E, W152R, F157L, I210V, V213G, G257S, D339H, R346T, K356T, S371F, S373P, S375F, T376A, D405N, R408S, K417N, N440K, G446S, N460K, T470N, S477N, T478K, E484A, F490S, R493Q, Q498R, N501Y, Y505H, D614G, H655Y, N679K, P681H, N764K, D796Y, Q954H, N969K
BQ.1	T19I, Δ24-26, A27S, Δ69-70, G142D, V213G, G339D, S371F, S373P, S375F, T376A, D405N, R408S, K417N, N440K, K444T, L452R, N460K, S477N, T478K, E484A, F486V, Q498R, N501Y, Y505H, D614G, H655Y, N679K, P681H, N764K, D796Y, Q954H, N969K
BQ.1.1	T19I, Δ24-26, A27S, Δ69-70, G142D, V213G, G339D, R346T, S371F, S373P, S375F, T376A, D405N, R408S, K417N, N440K, K444T, L452R, N460K, S477N, T478K, E484A, F486V, Q498R, N501Y, Y505H, D614G, H655Y, N679K, P681H, N764K, D796Y, Q954H, N969K
BQ.1.1+A475V	T19I, Δ24-26, A27S, Δ69-70, G142D, V213G, G339D, R346T, S371F, S373P, S375F, T376A, D405N, R408S, K417N, N440K, K444T, L452R, N460K, A475V, S477N, T478K, E484A, F486V, Q498R, N501Y, Y505H, D614G, H655Y, N679K, P681H, N764K, D796Y, Q954H, N969K
CK.1	T19I, Δ24-26, A27S, Δ69-70, G142D, Δ144, V213G, G339D, S371F, S373P, S375F, T376A, D405N, R408S, K417N, N440K, K444N, L452R, N460K, S477N, T478K, E484A, F486V, Q498R, N501Y, Y505H, D614G, H655Y, N679K, P681H, N764K, D796Y, Q954H, N969K
CA.3.1	T19I, Δ24-26, A27S, G142D, K147E, W152R, F157L, I210V, V213G, G257S, D339H, R346T, S371F, S373P, S375F, T376A, D405N, R408S, K417N, N440K, K444M, G446S, L452R, N460K, S477N, T478K, E484A, F486S, Q498R, N501Y, Y505H, D614G, H655Y, N679K, P681H, N764K, D796Y, Q954H, N969K, D1199N
CH.1.1	T19I, Δ24-26, A27S, G142D, K147E, W152R, F157L, I210V, V213G, G257S, D339H, R346T, S371F, S373P, S375F, T376A, D405N, R408S, K417N, N440K, K444T, G446S, L452R, N460K, S477N, T478K, E484A, F486S, Q498R, N501Y, Y505H, D614G, H655Y, N679K, P681H, N764K, D796Y, Q954H, N969K
XBF	T19I, Δ24-26, A27S, G142D, K147E, W152R, F157L, I210V, V213G, G257S, D339H, R346T, S371F, S373P, S375F, T376A, D405N, R408S, K417N, N440K, G446S, N460K, S477N, T478K, E484A, F486P, F490S, Q498R, N501Y, Y505H, D614G, H655Y, N679K, P681H, N764K, D796Y, Q954H, N969K
DS.1	T19I, Δ24-26, A27S, G142D, K147E, W152R, F157L, I210V, V213G, G257S, G339H, R346T, K356T, S371F, S373P, S375F, T376A, R403K, D405N, R408S, K417N, N440K, G446S, N460K, S477N, T478K, E484A, F486S, F490S, Q498R, N501Y, Y505H, D614G, H655Y, N679K, P681H, N764K, D796Y, Q954H, N969K
XBB	T19I, Δ24-26, A27S, V83A, G142D, Δ144, H146Q, Q183E, V213E, G339H, R346T, L368I, S371F, S373P, S375F, T376A, D405N, R408S, K417N, N440K, V445P, G446S, N460K, S477N, T478K, E484A, F486S, F490S, R493Q*, Q498R, N501Y, Y505H, D614G, H655Y, N679K, P681H, N764K, D796Y, Q954H, N969K
XBB.1	T19I, Δ24-26, A27S, V83A, G142D, Δ144, H146Q, Q183E, V213E, G252V, G339H, R346T, L368I, S371F, S373P, S375F, T376A, D405N, R408S, K417N, N440K, V445P, G446S, N460K, S477N, T478K, E484A, F486S, F490S, R493Q*, Q498R, N501Y, Y505H, D614G, H655Y, N679K, P681H, N764K, D796Y, Q954H, N969K
XBB.1.5	T19I, Δ24-26, A27S, V83A, G142D, Δ144, H146Q, Q183E, V213E, G252V, G339H, R346T, L368I, S371F, S373P, S375F, T376A, D405N, R408S, K417N, N440K, V445P, G446S, N460K, S477N, T478K, E484A, F486P, F490S, Q498R, N501Y, Y505H, D614G, H655Y, N679K, P681H, N764K, D796Y, Q954H, N969K
XBB.1.5.10	T19I, Δ24-26, A27S, V83A, G142D, Δ144, H146Q, Q183E, V213E, G252V, G339H, R346T, L368I, S371F, S373P, S375F, T376A, D405N, R408S, K417N, N440K, V445P, F456L, G446S, N460K, S477N, T478K, E484A, F486P, F490S, Q498R, N501Y, Y505H, D614G, H655Y, N679K, P681H, N764K, D796Y, Q954H, N969K
XBB.1.16	T19I, Δ24-26, A27S, V83A, G142D, Δ144, H146Q, E180V, Q183E, V213E, G252V, G339H, R346T, L368I, S371F, S373P, S375F, T376A, D405N, R408S, K417N, N440K, V445P, G446S, N460K, S477N, T478R, E484A, F486P, F490S, Q498R, N501Y, Y505H, D614G, H655Y, N679K, P681H, N764K, D796Y, Q954H, N969K

2.2.4 ACE2 construction

The gene encoding amino acids 19-615 of the human ACE2 was amplified from an image clone (Sourcebiosciences, clone ID5297380). The amplified fragment was inserted into the vector pOPINTTGneo incorporating a C-terminal 6×His tag or the vector pOPINTTGneoGc incorporating a C-terminal hIgG1Fc-6×His tag[57].

2.3 Protein production and purification

2.3.1 Protein production of Trimeric spike, NTD, RBD and ACE2

HEK293T (ATCC CRL-11268) cells were used for protein production. Cells were cultured in DMEM, low glucose media (Sigma-Aldrich, #D6046) supplemented with 10% FBS (GIBCO, #12676029) (D10) at 37℃ with 5% CO_2. Protein expression vectors encoding genes of Trimeric spike, NTD, RBD or ACE2 were used to do transient transfection by using polyethylenimine (PEI) (Polysciences, #23966-2).

2.3.1.1 Split 293T cells for transfection

HEK 293T cells are semi-attached cells. The growth medium for cells is D10. To split 293T cells from flask, all old medium was discarded and washed by 10 ml PBS. After discarding PBS, 10 ml 2.5 mM ethylenediaminetetraacetic acid (EDTA) is added and incubate at RT for 1 min to detach cells. Then discard EDTA, tap the flask to loosen cells. Add 10 ml medium into flask and wash down all cells. Cells are collected into a tube, pipette up and down to separate all cells into single cell. Cell number is counted and split 293T cells into 24-well plates two days before transfection in D10 medium with 2.0×10^5 cells/0.5 ml/well. Cells are mixed well, and 500 µl of cells is split into each well of 24 well plates. Plates are cultured at a 37℃ incubator with CO_2 for 48 h.

2.3.1.2 PEI transfection

Change medium of 293T cell culture to fresh D10 before transfection and incubate for 1 hr. For a 15-cm plate, 2 ml DMEM medium, 25 µl of protein expression plasmid, and 100 µL PEI are mixed by flicking the tube. The mixture is left at room temp for 15 min before adding to

cells in drop wise. Transfected cells are left for 6-18 hours before washing with PBS once and changing to protein free medium Ultra-DOMA. After 4-5 days of incubation, supernatant is harvested for further purification.

2.3.2 Protein purification of Trimeric spike, NTD, RBD and ACE2

2.3.2.1 Purification of Trimeric spike by Twin-Strep tag

To purify Trimeric spike protein, supernatant of cell culture 7 days after transfection is collected, centrifuged at 3,000 × g for 15min, and filtered by 0.45 μm filter system. 2 ml of Strep-Tactin Superflow high-capacity beads is added into a gravity flow column with 1 ml of column bed volume. Equilibrate the strep-Tactin column with 2 ml of wash Buffer W, and filtered supernatant is loaded to the column. After the supernatant is fully loaded onto the column, the column is washed 5 times with 1 ml Buffer W before protein is eluted by adding 6 times of 0.5 ml Buffer E. The purified Trimeric spike protein is further polished using a Superdex 75 HiLoad 16/60 gel filtration column (GE Healthcare).

2.3.2.2 Purification of NTD, RBD an ACE2 by 6×His tag

To purify NTD, RBD, or ACE2 protein, supernatant of cell culture 7 days after transfection is collected, centrifuged at 3,000×g for 15min, and filtered by 0.45 μm filter system. The supernatant is dialysed and purified with a 5 ml HisTrap nickel column (GE Healthcare), and the purified protein is further purified by using a Superdex 75 HiLoad 16/60 gel filtration column (GE Healthcare).

2.4 Isolation and expression of mAbs

2.4.1 Human blood sample processing

2.4.1.1 Heparinized whole blood

Prepare tubes containing Na heparin 1 in 500 of total volume of whole blood to be taken i.e. 50 ml whole blood + 100 μl Na heparin. Draw venous blood and transfer to Na heparin containing tube and gently invert mix.

2.4.1.2 Heparinized plasma collection

The rest of heparinized whole blood is collected to a 250 ml tube for further PBMCs isolation and spin at 2,000 × g for 10 min at room temperature. Heparinized plasma is collected into a new 50 ml tube and aliquot 200 µl/tube to be kept at -80℃.

2.4.1.3 Isolation of PBMC

Whole blood is diluted 1:1 with RPMI1640. For 1 sample, top up RPMI1640 to 180 ml. Mix well. 15 ml of lymphoprep is added into 50 ml filter tubes and centrifuged at 1,500 × g for 5 min. Gently overlay diluted blood on top of lymphoprep with the pipette, and spin at 800 × g (2, 000 × g) for 20 min at room temperature, brake off slowly. The interface layer (white band) containing mainly PBMC is removed into two 50 ml tubes, which is washed with 50ml of RPMI1640 and spin at 2,000 × g for 10 min followed by washing with 50ml of RPMI1640 and spining at 1,200 × g for 10 min. Cells are resuspended with 10 ml of RPMI, then top up the tube to 50 ml, and spin at 1,500 × g for 5 min. Cells are resuspended again to 50 ml of RPMI1640 and cell numbers are determined. Resuspended cells are spin at 1, 500 × g for 5min, and then resuspended in freezing buffer. PBMCs are frozen for subsequent use at density 3 × 10^6 cells/ml/vial in D10 in freezing boxes at -80 ℃ overnight before transferring into liquid nitrogen.

2.4.1.4 RNA extraction from PBMC

Prepare 4 tubes of PBMC cells for each sample with 1×10^5 cells per tube and top up each tube with 1 ml of PBS. Pellet the appropriate number of cells by centrifuging for 5 min at 300 × g in a centrifuge tube. Carefully remove all supernatant by aspiration and disrupt the cells by adding 350 µl buffer RLT followed by homogenizing the lysate by vortexing for 1 min. 350 µl of 70% ethanol is added to the homogenized lysate and mixed well by pipetting. Transfer up to 700 µl of the sample, including any precipitate that may have formed, to a RNeasy spin column placed in a 2 ml collection tube. Close the lid gently, and centrifuge for 15 s at ≥8, 000 × g. Discard the flow-through and load other tubes into the same RNeasy spin column. Discard the flow-through after each centrifugation. Add 700 µl Buffer RW1 to the RNeasy spin column, then close the lid gently, and centrifuge for 15 s at ≥8,000 × g (≥ 10,000 × g) to wash the spin

column membrane. Add 500 µl Buffer RPE to the RNeasy spin columnand centrifuge for 15 s at ≥8,000 × g (≥ 10,000 × g) to wash the spin column membrane. 500 µl Buffer RPE is added to the RNeasy spin column and centrifuge for 2 min at ≥8,000 × g (≥ 10,000 × g) to wash the spin column membrane. After wash, RNeasy spin column is placed in a new 2 ml collection tube and discard the old collection tube with the flow-through. Centrifuge at full speed for 1 min. Place the RNeasy spin column in a new 1.5 ml collection tube and elute RNA by adding 30 µl RNase-free water directly to the spin column membrane before centrifuging for 1 min at ≥8, 000 × g to elute the RNA.

2.4.1 Isolation of S-specific single B cells by fluorescence-activated cell sorting (FACS)

2.4.1.1 PBMC staining

Thaw PBMCs by warming it up quickly in a water bath at 37℃ until floating ice is visible. Cells are transferred into a 50 ml Falcon tube with 9 ml of cold RPMI1640 + 10% FBS (R10) in drop-wised manner. Centrifuge the cell suspensions at 1,500 × g for 5 min at 4℃. Discard the supernatant and add 10 ml of R10 to resuspend the cells before centrifuging at 1,500 × g for 5 min at 4℃. Cells are resuspended in 5 ml of FBS and incubate at 37 ℃ for 30 min. Cell suspension is filtered through 40µm cell strainer into 50ml tubes in order to get rid of the dead cell clumps. Count cells with trypan blue and then wash cells with PBS by spinning down at 1, 500 × g for 5min. Cells are resuspended in 5 ml of PBS and cell number is determined again. Spin down cells at 1,500× g, 5min.

To prepare stock of Live/Dead Dye (LIVE/DEAD™ Fixable Aqua Dead Cell Stain Kit; L34957), 50 µl of DMSO is added to the vial of reactive dye to dissolve all the dye. Aliquot the solution of reactive Live/Dead Dye to EP tubes, 5µl/tube, and keep them in -20℃.

The working solution of Live/Dead Dye is prepared by diluting the stock 40-fold into PBS. Add 200ul working solution of Live/Dead Dye into each sample, incubate for 15min at room temperature. The samples are protected from light.

Wash the Live/Dead stained PBMC with 2 ml of FACS staining buffer (PBS + 2mM EDTA + 0.5% BSA) twice to quencher the free dye, centrifuge 1,500× g for 5min, then discard the supernatant. After wash, 100 µl of 20 ug/ml purified Trimeric spike protein in FACS staining

buffer is added into each PBMC sample. Incubate the PBMCs at 4 ℃ for 30 min, then wash twice with 2 ml of FACS staining buffer. Surface markers are stained (Table 2.3.1) and anti-Strep tag in 150 µl FACS staining buffer. Cells are washed twice with 2 ml of FACS staining buffer, and resuspended FACS staining buffer at concentration of 1×10^7 cells/ml. To prevent the blockage of the sorter, pass through cell suspension using cell strainer.

Table 2.3.1 PBMC staining panel for FACS sorting

	Fluorochrome	**Wavelength**	**Vol (µl)/100ul**
Live/Dead Fixable Aqua Dead Cell Stain Kit (Life Technologies, L34957)	Aqua	405-525/50	16ul (1:40 of stock)
20 µg/ml spike protein for 1 Rx = 100 µl/sample			
Purified soluble Trimeric Spike-Strep tag	-	-	100 µl/sample of 20 µg/ml
For 1 Rx = 150 µl/sample		**1x**	
anti-Human CD3-FITC (BD, 555332)	FITC	488-530/30	7.5
anti-Human CD14-FITC (BD, 555397)			7.5
anti-Human CD56-FITC (BD, 562794)			1.5
anti-Human CD16-FITC (BD, 555406)			7.5
anti-Human IgM-FITC (BD, 555782)			7.5
anti-Human IgA-FITC (Dako, F0188)			1.5
anti-Human IgD-FITC (Dako, F0189)			1.5
anti-Human CD19-BUV395 (BD, 563549)	BUV395	355-379/28	1.5
anti-Human IgG-BV786 (BD, 564230)	BV786	405-780/60	3
StrepMAB-Classic-DY549 (iba, 2-1566-050)	DY549	561-582/15	1.5
Total (µl)			**40.5**
FACS staining buffer (µl)			**109.5**

2.4.1.2 FACS sorting

BD FACSAriaTM Fusion Cell Sorter is used for IgG^+ S^+ memory B cell sorting from PBMC samples. The gating strategies for sorting are shown in each chapter.

2.4.2 Cloning and expression of S-specific human antibodies

2.4.2.1 Reverse-transcript PCR (RT-PCR)

QIAGEN OneStep RT-PCR Kit (Qiagen, 210210) is used for RT-PCR reaction. Reverse-transcript PCR reaction system is as follow:

RT-PCR	**1X**
FW primer 5' RT mix	1
RV primer 3' RT mix	1
dNTP Mix, 10 mM each (40 mM final)	1
QIAGEN OneStep RT-PCR Buffer,5x	5
Rnase free water	6.5
enzyme mix	0.5
aliquot	15
Sample	10
Total	**25**

The PCR cycle is as follow:

RT-PCR cycle		
50°C	30 min	
95°C	15 min	
94°C	30 sec	
58°C	30 sec	50 cycles
72°C	1 min	
72°C	10 min	
4°C	Hold	

2.4.2.2 Nested-PCR

Nested-PCR for amplifying heavy chains, kappa chains, and lambda chains are performed separately by using different sets of primers, and HotStartTaq DNA Polymerase kit (Qiagen, 203205) is used for PCR reaction The PCR reaction systems are as follow:

Heavy Chain:

	1×
FW primer	
Fin_AgeI VH mix	0.5
RV primer	
Rin_126KasI_IgCH mix(1) or Rin_SalI JH (2)	0.5
25 mM dNTPs mix	0.25
PCR Buffer, 10x*	2
HotStarTaq DNA polymerrase	0.1
Rnase free water	15.1
aliquot	18.5
Sample	1.5
Total	**20**

Kappa Chain:

	1×
FW primer	
Lambda: Fin_AgeI VL mix	0.5
RV primer	
Lambda: Rin_XhoI CL	0.5
25 mM dNTPs mix	0.25
PCR Buffer, 10x*	2
HotStarTaq DNA polymerase	0.1
Rnase free water	15.1
aliquot	18.5
Sample	1.5
Total	**20**

Lambda Chain:

	1×
FW primer	
Kappa: Fin_AgeI VK mix	0.5
RV primer	
Kappa: Rin_BsiWI_JK mix	0.5
25 mM dNTPs mix	0.25
PCR Buffer, 10x*	2
HotStarTaq DNA polymerase	0.1
Rnase free water	15.1
aliquot	18.5
Sample	1.5
Total	**20**

The PCR reaction cycle is as follow:

95°C	15 min	
94°C	30 sec	
58°C	30 sec	50 cycles
72°C	45 sec	
72°C	10 min	
4°C	Hold	

1% agarose gel is prepared for running the Nested-PCR products, 3 µl PCR product each. Results are analysed and positive wells are labelled in a spreadsheet.

2.4.2.2 Gibson and transfection

1) Preparing 5 × ISO buffer

PEG-8000	3	g
1M Tris-HCl pH 7.5	6	ml
1M $MgCl_2$	300	µl
100mM dNTPmix	480	µl
1M DTT	600	µl
0.25M NAD	240	µl
Nuclease free Water	4.08	ml
Total	= 12	ml

Aliquot 500 ul in 2ml Eppendorf and stored at -20℃ for up to 1 year.

2) Preparing 1.33 × AMM buffer

5 X ISO buffer	500	µl
10U/ml T5 exonuclease	1	µl
2U/ml Phusion	31.25	µl
40U/ml Taq Ligase	250	µl
Nuclease free Water	1,092.75	µl

Aliquot 15 µl and stored at -20℃ for up to 2 years.

3) Preparing expression vectors

For heavy chain vector:

10 µg Heavy chain vector

1 µl AgeI-HF

10µl Cutsmart buffer

up to 100 ul by SDW

Digest for 37°C overnight (can check complete cut at this step by run on gel)

1.5µl SalI-HF/ 2.5 µl KasI

Digest for 37°C overnight

For kappa chain:

10 µg Kappa vector

1µl AgeI-HF

10µl Cutsmart buffer

Digest for 37°C overnight (can check complete cut at this step by run on gel)

Add 2 µl BsiWI-HF

Digest for 37°C overnight

For Lambda chain:

10 ug Lambda vector

1µl AgeI-HF

10µl Cutsmart B

Digest for 37°C overnight (can check complete cut at this step by run on gel)

1 ul XhoI

Digest for 37°C overnight

Heat inactivates digested plasmids at 65°C for 20 min, then leave on ice for 5 min. Plasmids are dephosphorylated by adding 1 µl of CIP into reaction system, incubate at 37° for 1 hour. Heat inactivates the reaction at 65°C 20 min, the leave it on ice.

4) Digested plasmids are recovered using QIAquick Gel Extraction Kit (Qiagen, 28706). Briefly, DNA fragment is excised from the agarose gel with a clean, sharp scalpel. The gel slice is put in a colourless tube and weigh it. 3 volumes of Buffer QG is added to 1 volume of gel (100mg≈100µl). Incubate at 50 ℃ for 10 min until the gel has completely dissolved. 1 volume of isopropanol is added to the sample and mix, then apply the sample to the QIAquick spin column and spin for 1 min at 11,000 × g. 0.5 ml of Buffer QG is added to QIAquick column and centrifuge for 1 min, and then the column is washed by 0.75 ml of Buffer PE. Discard the flow-through and centrifuge the QIAquick column for an additional 1 min at 11,000 × g, then the column is placed into a clean 1.5 ml microcentrifuge tube to elute DNA by adding 50 µl of Buffer EB (10 mM Tris-Cl, pH 8.5) or water (pH7.0-8.5) to the column. Let the column stand at room temperature for 1 min, and then centrifuge for 1 min at 11,000 ×g.

5) Positive Nested-PCR wells are picked out and Gibson reaction is set up by mixing 1.5 µl of Nested-PCR product, 2.5 µl of 33.3 µg/ml enzyme cut vector and 12 µl of 1.33 × AMM. Incubate in a PCR machine at 50℃ for 1-3 hrs.

6) Gibson products are transformed into DH5α competent cells (produced in-house) by mixing 2.5 µl of Gibson product with 60 µl of DH5α competent cells. Stand the mixture on ice for 30 min, and then heat shock at 42℃ for 45 seconds, following incubating on ice for another 2 min. After that, 1 ml of sterile L-Broth medium is added into the tube and incubate at 37℃ for 1 h with shaking at 180 × g. Pellet the DH5α cells by spinning at 10,000 × g for 2 min and resuspend the pellet with 100 µl of L-Broth. Resuspended cells are plate on a LB Agar plate with 100 µg/ml of Ampicillin. Let cells grow over night at 37 ℃ to form single colonies.

7) 2-3 single colonies are picked from each LB Agar plate to culture in 10 ml of L-Broth over night at 37 ℃ with shaking. Plasmid in each culture is extracted with QIAGEN Plasmid Mini Kit (QIAGEN, 12125). All plasmids are confirmed by Sanger sequencing.

8) Split 293T cells and PEL transfection

HEK293T cells are prepared for transfection as described previously. PEI transfection is conducted by mixing 60 µl DMEM medium, 6.5 µl H Gibson product, 6.5 µl λ/κ Gibson product, and 3µl PEI (1 µg/µL) in a sterile 96-well plate. For a 15-cm plate, 2 ml DMEM medium,15 µg HC plasmid, 15 µg λ/κ chain plasmid, and 100 µl PEI (Polyethylenimine,1 µg/µl) are mixed by flicking the tube. The mixture is left at room temp for 15 min before adding to cells in drop wise. Transfected cells are left for 6-18 hours before washing with PBS once and changing to protein free medium Ultra-DOMA. After 4-5 days of incubation, supernatant is harvested for further purification.

2.4.3 Human monoclonal antibody purification

2.4.3.1 Antibody purification

Columns and tubes for antibody purification are washed with 1M NaOH followed with a wash by 50 ml Milli-Q H_2O, then by 50 ml PBS for 3 times, check if the pH of the flow through is 7. Columns are packed with 1 - 1.5ml protein A/G beads (capacity: 20mg of IgG/1ml beads). Beads are washed with 50 ml filtered PBS for 3 times, then samples are loaded at 4℃ overnight (collect flow through). Beads are washed with 50 ml filtered PBS for 3 times, make sure no unbound protein left in the columns. Bound IgG is eluted with 1 ml of 0.1 M Glycine pH 2.7 into 9 ml of neutralisation buffer Tris-HCl pH 8 in drop-wised manner and is mixed immediately. Protein concentration is measured by spectro-photometry (OD280). Top up column with 0.1 M Glycine to wash away all proteins from beads, and then wash beads with 50 ml PBS for 3 times, followed by 50 ml filtered 0.1%NaN_3/PBS and store the beads in 0.1% NaN_3/PBS.

2.4.3.2 Antibody buffer exchange

Amicon Ultra-15; Ultracel 10k (Millipore; Cat. UFC901096) is washed with 5 ml PBS for 3 times by quickly shaking the tube to get rid of the glycerol coated over the membrane. Ultracel is filled with PBS and spin at 3000 × g for 5 mins. Discard all PBS, all fractions containing protein (OD280 > 0.009) are pooled in the tube and top up with PBS to 15ml. Centrifuge the Ultracel at 3000 × g for around 20 mins to make the volume down to 1ml. Top up the column with 14ml PBS, and repeat this step for 3 times. Protein concentration is measured by spectro-photometry (OD280), and purified antibodies are filtered through a 0.22um Syringe-Driven Filter Unit (Millipore; Cat. SLGV004SL). The concentration of the purified antibody is determined, the antibody is aliquot and freezed at -80 ℃.

2.5 Construction and expression of Fab

2.5.1 Construction of Fab expression plasmids

Heavy chain plasmids of specific antibodies were used as templates to amplify the variable region and CH1 expression gene by using Fab expression primers, the PCR system is as follow:

5 × HF buffer	10 µl
10mM dNTP	1 µl
RIn_CH1_SC_G1_TB (10mM)	2.5 µl
FIn_dbST_Hvec (10mM)	2.5 µl
SO water	33.3 µl
Phusion	0.5 µl
Heavy chain expression plasmid	0.2 µl
Total	50 µl

And another PCR system is set up for amplifying Twin-strep tag:

5 × HF buffer	10 µl
10mM dNTP	1 µl
Fin_CH1_SC G1_TB	2.5 µl
RIn_dbST_Hvec	2.5 µl
SO water	33.3 µl
Phusion	0.5 µl
dbstrep-tag oligo	0.2 µl
Total	50 µl

The PCR program is as follow:

98℃	1 min	
98℃	10 sec	
60℃	30 sec	40 cycles
72℃	3 min for vector, 30 sec for Twin-strep-tag	
72℃	30 sec	

After PCR, cool down the system, add 0.5-1 µl Dpn I in each tube, then incubate at 37℃ for 30 min. This process is to digest templates.

PCR products of vector run on 0.7% DNA gel at 120v for 30 min. PCR products are purified using QIAquick Gel Extraction Kit (Qiagen, 28706) following its instruction.

Gibson reaction is set up by mixing 100 ng of Fab and vector product, 100 ng of Twin-strep tag, 15 µl of 1.33 × AMM and Nuclease-free H_2O to make up a 20 µl reaction system. Incubate in a PCR machine at 50℃ for 1-3 hrs. Gibson products are transformed and sequenced the same way as in the monoclonal antibody plasmid construction.

2.5.2 Fab production and purification

Successfully constructed Fab plasmids are co-transfected with their corresponding light chain plasmids into 293T cells by PEI. Cells are incubated at 37℃ with 5% CO_2 for 5 days, and supernatant of cell culture is collected, filtered and Fab is purified by Twin-strep tag.

2.6 ELISA

2.6.1 ELISA for determination of plasma and antibody binding to recombinant proteins

To test on Trimeric Spike proteins, MAXISORP immunoplates (NUNC, 442404) are coated with 0.125 µg of StrepMAB-Classic (iba, 2-1507-001) overnight at 4 ℃, blocked with 2% skimmed milk in PBS for testing plasma, or 2% BSA in PBS for testing mAbs 1 hour at room temperature, followed by incubating plates with 50 µl of 5 µg/ml Twin-Strep tagged Trimeric Spike protein for 1 hour at 37 ℃. 50 µl of serially diluted plasma or mAbs was added into the plates, and after 1 hour of incubation at 37℃ and wash with PBST (PBS + 1 ml/L of Tween-20), 50 µl of 1:10,000 diluted ALP-conjugated anti-human IgG (Sigma, A9544) is added into

the plates. The reaction is developed by the addition of PNPP substrate for 1 hour and stopped with 0.2 M NaOH. The absorbance is measured at 405nm.

To measure RBD or NTD, 50 µl of 5 µg/ml of purified RBD and NTD is used to coat MAXISORP immunoplates overnight at 4 ℃. Plates are blocked with with 2% skimmed milk in PBS for testing plasma, or 2% BSA in PBS for testing mAbs 1 hour at room temperature, followed by incubating plates with 50 µl of serially diluted plasma or mAbs. After 1 hour of incubation at 37℃ and wash with PBST (PBS + 1 ml/L of Tween-20), 50 µl of 1:10,000 diluted ALP-conjugated anti-human IgG (Sigma, A9544) is added into the plates. The reaction is developed by the addition of PNPP substrate for 1 hour and stopped with 0.2 M NaOH. The absorbance is measured at 405nm.

2.6.2 ELISA for measuring IgG concentration in cell culture

50 µl of 1:10,000 diluted anti-human IgG (Sigma, I5885) is used to coat MAXISORP immunoplates overnight at 4 ℃. Plates are blocked with 2% BS in PBS for 1 hour at room temperature. Serial diluted mAb generation supernatant and 2-fold diluted standard human IgG (starting from 1 µg/ml) are added into the plates and incubate at 37℃ for 1 hour, followed by 50 µl of 1:10,000 diluted ALP-conjugated anti-human IgG (Sigma, A9544). The reaction is developed by the addition of PNPP substrate for 1 hour and stopped with 0.2 M NaOH. The absorbance is measured at 405nm. IgG concentration in cell culture is determined by comparing OD405 of diluted supernatant samples with OD405 of standard IgG.

2.6.3 ELISA for ACE2 inhibition assay

5 µg/ml of purified ACE2-His protein is used to coat MAXISORP immunoplates overnight at 4 ℃, and then blocked by 2% BSA in PBS. Meanwhile, 2.5 µg/ml of purified Trimeric S-twin-Strep is mixed with serially diluted mAbs. Antibody-S protein mixtures are incubated at 37 ℃ for 1 hour. After incubation, the mixtures are transferred into the ACE2-coated plates and incubated for 1 hour at 37 ℃. After wash with PBST, StrepMAB-Classic (iba, 2-1507-001) is diluted to 0.2 µg/ml by 2% BSA and used as primary antibody followed by Goat anti-mouse IgG-AP (Invitrogen, A16093) at 1:2,000 dilution. The reaction is developed by adding PNPP substrate and stopped with NaOH. The absorbance is measured at 405 nm. The ACE2/Spike

binding inhibition is calculated by comparing to the antibody-free control well. IC50 was determined using the Probit program from the SPSS package[128].

2.7 Live virus isolation from patient swabs and sequencing

2.7.1 Live virus isolation

VeroE6/ TMPRSS2 cells were maintained in DMEM high glucose supplemented with 1% fetal bovine serum, 2mM Glutamax, 100 IU/ml penicillin-streptomycin and 2.5ug/ml amphotericin B, at 37 C in the presence of 5% CO_2 before inoculation with 200ul of swab fluid. Cells were further maintained at 37℃ with daily observations for cytopathic effect (CPE). Virus containing supernatant were clarified at 80% CPE by centrifugation at 3,000 × g. at 4 C before being stored at 80℃ in single-use aliquots. Viral titers were determined by a focus-forming assay on Vero CCL-81 cells.

2.7.2 Viral RNA extraction

RNA of SARS-CoV-2 live virus is extracted using QIAamp Viral RNA Kit (QIAGEN, Cat#52904) following the instruction of the kit. Briefly, carrier RNA is prepared by adding 310 µl Buffer AVE to 310 µg lyophilized carrier RNA to make the final concentration of 1 µg/µl. The dissolved carrier RNA is stored at -80 ℃. 560 µl of Buffer AVL with 5.6 µl of prepared carrier RNA are mixed with 140 µl of virus culture. After 10 min incubation at room temperature, 560 µl of ethanol (96-100%) is added and mixed. The mixed solution is applied to the QIAamp Mini column and centrifuged at 6,000 × g for 1 min. Collection tubes are changed after each centrifuging step. Columns are washed by 500 µl Buffer AW1 with centrifugation of 6,000 × g for 1 min, followed by 500 µl Buffer AW2 with centrifugation of 20,000 × g for 3 min. After wash, the columns are centrifuged at full speed for 1 min. RNA is eluted with 60 µl Buffer AVE by centrifuging at 6,000 × g for 1 min.

2.7.3 Live virus S gene sequencing

To sequence live virus S gene, 1.5 µl of 10 mM dNTPs, 1.5 µl of 10 µM R_RT_SASR2_AUS_1 primer, and 12 µl of extracted viral RNA are mixed, incubated at 65 ℃ for 5 min, followed by 4 ℃ for 3 min. After incubation, 3 µl of 10 × RT buffer of Superscript III first-strand synthesis enzyme kit (Invitrogen, Cat#18080-051), 6 µl of 25 mM $MgCl_2$, 3 µl of 0.1M DTT, 1.5 µl of 40U/µl RNase OUT, and 1.5 µl of 200U/µl SuperScriptIII RT are added into the mixture and

incubate at 50 ℃ for 90 min, then 85 ℃ for 5 min before cooled down to 4 ℃ to synthesise cDNA. 1.2 µl of RNase H is added into the system and incubated at 37 ℃ for 20 min to digest the viral RNA. After digestion, 1 µl of synthesised cDNA is added into a mixture of 41.6 µl of Nuclease-free H_2O, 5 µl of 10 × Buffer 1 of AccuPrime™ Taq DNA Polymerase kit (Invitrogen, Cat#12346-086), 1 µl of 10 µM F Primer, 1 µl of 10 µM R Primer, and 0.4 µl of Accuprime Taq DNA Polymerase as PCR template to amplify the S gene. The PCR cycle is as follow:

94°C 15 sec
1 Cycle
94°C 15 sec
56°C 30 sec
68°C 4 mins (1 min/ Kb)
45 Cycles
68°C 8 mins
1 Cycle
4°C ∞.

3 µl of PCR product is used to run 0.8% agarose gel before PCR purification by QIAquick spin column (QIAGEN, Cat#28104) following instruction of the kit. Briefly, 500 µl of PB buffer is mixed with the PCR product, and loaded onto a QIAquick spin column before centrifuged at 10,000 × g for 1 min. The column is washed with 700 µl of PE buffer by centrifuging at 10,000 × g for 1 min, followed by another centrifugation. The PCR product is eluted with 30 µl of Nuclease-free H_2O and the concentration is determined by nanodrop. PCR product is diluted to 30 µg/µl and sequenced by sequencing primers shown in appendix A.1.

2.8 FRNT assay

The neutralisation potential of mAbs or serum samples from infected patients or vaccinees is measured by comparing the reduction in the number of the infected foci with a negative control well without antibody or serum.

Serially diluted mAbs or serum is mixed with SARS-CoV-2 strains and incubated for 1 hour at 37 ℃. Then the mixtures are transferred to 96-well, cell culture-treated, flat-bottom microplates containing confluent Vero cell monolayers in duplicate and incubate for a further

2 hours followed by the addition of 1.5% semi-solid carboxymethyl cellulose (CMC) overlay medium to each well to limit virus diffusion. 20-24 hours later, a focus forming assay is then performed by fixing Vero cells with 4% Formaldehyde, permeabilising with 2% Triton X-100 in PBS, then staining Vero cells with a mouse anti-NP mAb (in-house) followed by peroxidase-conjugated goat anti-mouse IgG (Sigma, A0170). Finally, the foci (infected cells) approximately 100 per well in the absence of antibodies, are visualised by adding TrueBlue Peroxidase Substrate. Virus-infected cell foci are counted on the classic AID EliSpot reader using AID ELISpot software. The percentage of focus reduction is calculated and IC50 is determined using the probit program from the SPSS package[123].

2.9 Pseudotyped lentiviral particles production and neutralisation test

2.9.1 Pseudotyped lentiviral particles production

HEK293T/17 cells (ATCC CRL-11268) are co-transfected with three essential plasmids: plasmid (pCDNA 3.1 expressing SARS-CoV-2 S protein, lentiviral vector expressing firefly luciferase reporter protein (pCSFLW), and the scond generation of lentiviral packaging plasmid (p8.91) expressing gag, pol, and rev proteins at the ratio of 1:1.5:1 µg, respectively, in 200 µl opti-MEM (GIBCO, 11058021). The DNA cocktails are then supplemented with the equal volume of opti-MEM containing 35 µl of 1 mg/ml PEI. After 20 min incubation, the plasmid DNA-PEI complexes are added into a T75 cm^2 culture flask containing approximately 50% confluency of HEK293T/17 cells. The medium is changed twice, one hour prior to transfection and 18-24 hours post transfection. The culture supernatant containing pseudotyped lentiviral particles are harvested at 72 hours post-transfection by centrifugation and kept at -80℃. HIV-gag protein in the harvested psedoviral culture supernatant is measured by RETROtek HIV-1 p24 Antigen-ELISA kit (Zeptometrix, 0801002)[80].

2.9.2 Pseudoviral neutralisation assay

Pseudotyped lentiviral particles expressing SRS-CoV-2 S protein are diluted to 90 ng/ml of HIV-gag protein by DMEM + 1% FBS (D1) and incubated with serially diluted mAbs or plasma in white opaque 96-well plates at 37 ℃, 5% CO_2 for 1 hour. The stable HEK293T/17 cells expressing human ACE2 are then added to the mixture at 1.5×10^4 cells/well. Plates are spun at 200 × g for 1 min and further incubated for another 48 hours.

Culture supernatants are removed and 50 µl of 1:2 Bright-GloTM Luciferase assay system (Promega, E2620) in PBS is added to each well. The reaction is incubated at room temperature for 5 min and the firefly luciferase activity is measured using CLARIOstar (BMG Labtech). The percentage of neutralisation of mAbs or plasma samples against pseudotyped lentiviruses is calculated relative to the mAb-free control[80].

2.10 Data analyses

2.10.1 Flow cytometry analyses

Flow cytometry was performed on BD FACSAriaTM Fusion Cell Sorter X20 and the program used during sorting was DIVA. Flowjo was used for data analysis after sorting.

2.10.2 Analysis of FRNT neutralisation

Neutralisation of mAbs and serum samples was measured by FRNT. The percentage of focus reduction was calculated and IC50 (FRNT50) was determined using the probit program from the SPSS package. The Wilcoxon matched-pairs signed rank test was used for the analysis and two-tailed P values were calculated on geometric mean values.

CHAPTER 3 Isolation and characterisation of early-pandemic SARS-CoV-2 antibodies

3.1 Introduction

After the release of the sequence of SARS-CoV-2 in early January 2020, it has led to an unprecedented international scientific response[8]. Vaccines were developed based on S protein in a short period of time and a great number of monoclonal antibodies against S protein were isolated.

S from SARS-CoV-2 uses ACE2 as the cell surface receptor. S has two subunits, S1 that mediates binding of receptor and S2 that is responsible for viral and host cell membrane fusion. S1 contains the NTD and RBD, and RBD contains the interacting surface for ACE2 binding[13,129]. RBD has two different conformations, "up" and "down", and there are mAbs recognise one or both of the conformations. Previous research has revealed that most potent mAbs bind to the ACE2 interacting surface on the RBD to block the binding between RBD and ACE2[130,131]. Some anti-RBD antibodies have been used therapeutically.

Here we report an isolation of 377 human mAbs from PBMC obtained from convalescent patients infected by early pandemic SARS-CoV-2 using two different sorting methods, with 80 RBD-specific mAbs. We devised a generally applicable method combining biophysical competition measurements with a relatively small number of antibody-antigen structure determinations to locate the binding sites for all 80 anti-RBD mAbs, which dissects RBD into five binding regions. We find novel binding modes for some potently inhibitory antibodies and demonstrate that strongly neutralizing mAbs protect, prophylactically or therapeutically, in animal models.

3.2 Results

3.2.1 Isolation and characterisation of mAbs

We studied a cohort of 42 patients who had proven SARS-CoV-2 infection diagnosed by RT-PCR before May 2020 (Table 3.1).

Table 3.1 Summary of SARS-CoV-2 infected patients enrolled in the study.

Participants	
Female	17
Male	25
Average Age (y)	55.4 (IQR 47-61)
Days post-symptom onset	45.5 (IQR 40-53)
Disease severity	
Asymptomatic	1 (2.4%)
Mild	28 (66.6%)
Severe	12 (28.6%)
Critical	1 (2.4%)

Patients were recruited using the ISARIC protocol following informed consent and recalled following convalescence (31-62 days). ELISAs were performed on serum samples against purified full-length trimeric S protein (Wuhan) and RBD (aa 330-532) (Figure 3.1).

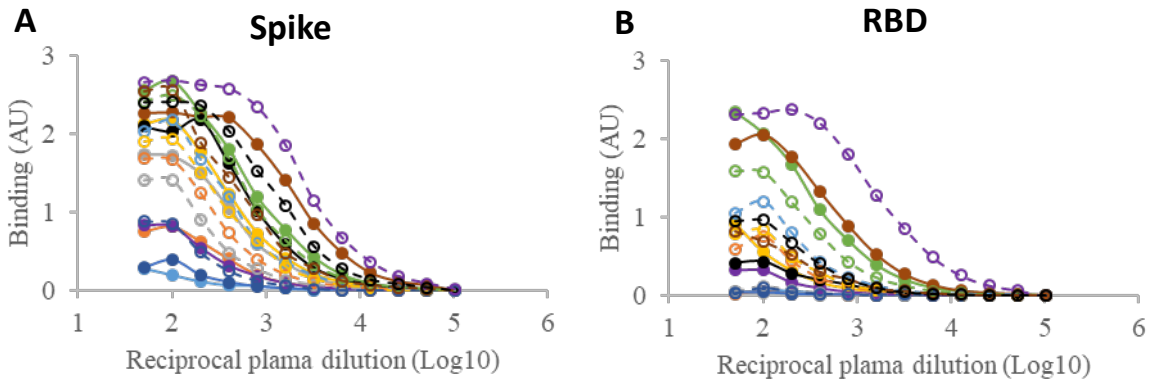

Figure 3.1 Plasma from donors with confirmed SARS-CoV-2 infection were tested for binding to SARS-CoV-2 spike (A) and RBD (B).

Neutralisation assays on Wuhan live virus were also performed, and as has been described previously, antibody titres varied between patients, and there was a strong correlation between the level of anti-S/RBD binding ability or neutralisation titre with disease severity[39] (Figure 3.2), although we cannot exclude the possibility that the age difference between the two groups also plays a role.

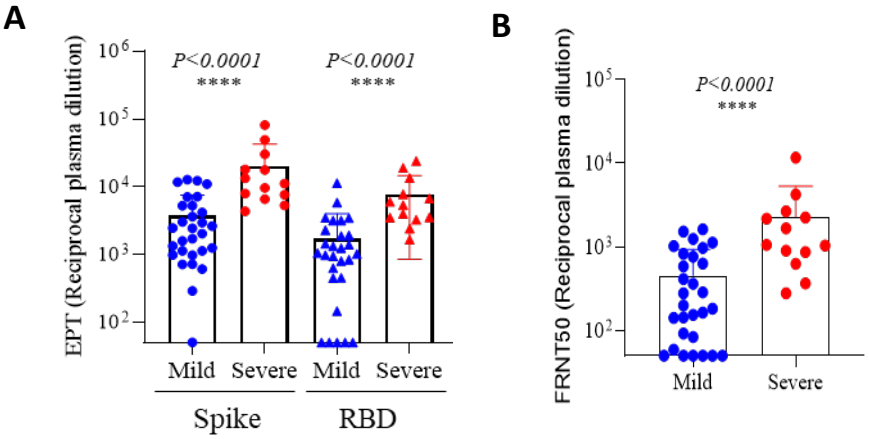

Figure 3.2 (A) Comparison of the binding titre against Spike and RBD in mild cases and severe cases measured by ELISA. (B) Neutralising titres to authentic live viruses. Data are representative of one experiment with 42 samples and presented as means ± S.E. The Mann-Whitney U test was used for the analysis and two-tailed P values were calculated.

To generate mAbs, two strategies were used. First, IgG-expressing B cells were sorted, and then divided into 4 cells per well in 384-well plates, cultured with IL-2, IL-21, and 3T3-msCD40L cells for 13-14 days, and supernatants were tested for reactivity to S protein; positive clones were identified by RT-PCR (Figure 3.3A). In the second strategy, B cells were stained with double-strep tagged S or 6 x His tagged RBD proteins, DY549 conjugated anti-tag antibodies were applied, and single positive cells were sorted and subjected to RT-PCR (Figure 3.3B). Cell recovery was higher in the severe COVID-19 cases (Figure 3.3C), and in total, we isolated mAbs from 16 patients (9 mild, 7 severe).

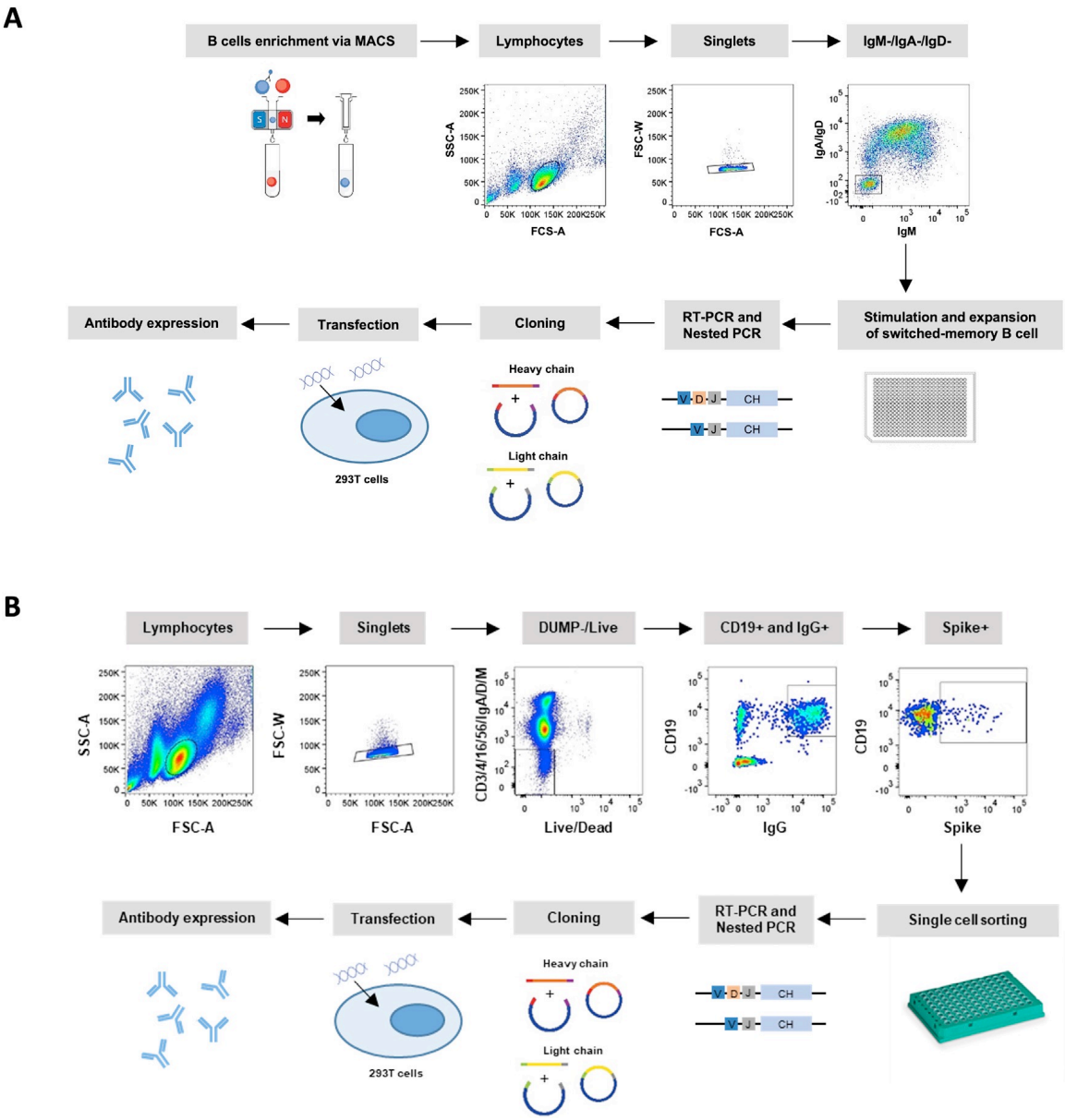
A
B cells enrichment via MACS
Lymphocytes
Singlets
IgM-/IgA-/IgD-
SSC-A
FCS-A
FSC-W
FCS-A
IgA/IgD
IgM
Stimulation and expansion of switched-memory B cell
RT-PCR and Nested PCR
Cloning
Transfection
Antibody expression
Heavy chain
Light chain
V-D-J-CH
V-J-CH
293T cells
B
Lymphocytes
Singlets
DUMP-/Live
CD19+ and IgG+
Spike+
SSC-A
FSC-A
FSC-W
FSC-A
CD3/4/16/56/IgA/D/M
Live/Dead
CD19
IgG
CD19
Spike
Single cell sorting
RT-PCR and Nested PCR
Cloning
Transfection
Antibody expression
Heavy chain
Light chain
V-D-J-CH
V-J-CH
293T cells
C
P<0.05
*
Frequency (%)
Mild
Severe

Figure 3.3 SARS-CoV-2 antibody isolation strategies. (A) IgG expressing B cells were isolated and cultured with IL-2, IL21 and 3T3-msCD40L cells for 13-14 days. Supernatants were harvested and tested for reactivity to spike protein by ELISA. (B) Antigen-specific single B cells were isolated using labelled recombinant spike or RBD proteins as baits. The IgG heavy and light chain variable genes from both strategies were amplified by nested PCR and cloned into expression vectors to produce full-length IgG1 antibodies. (C) Comparison of the frequency of spike-reactive IgG expressing B cells in mild cases and severe cases measured by FACS. Small horizontal lines indicate the median. Data are representative of one experiment with 16 samples. The Mann-Whitney U test was used for the analysis and two-tailed P values were calculated.

377 antibodies reacting to full-length S by ELISA were produced, which were further screened for reactivity to recombinant proteins S1 (34%), S2 (53%), RBD (21%), and NTD (11%), with the remaining 13% reactive to only full-length trimeric spike (Figure 3.4A). Analysis of antibody sequences revealed low levels of somatic mutation of germline sequences for both heavy (mean 4.11 ± 2.75 amino acids) and light chains (mean 4.10 ± 2.84 amino acids) (Figure 3.4B). In general, responses within and between individuals were highly polyclonal with diverse V-gene usage (Figure 3.4C).

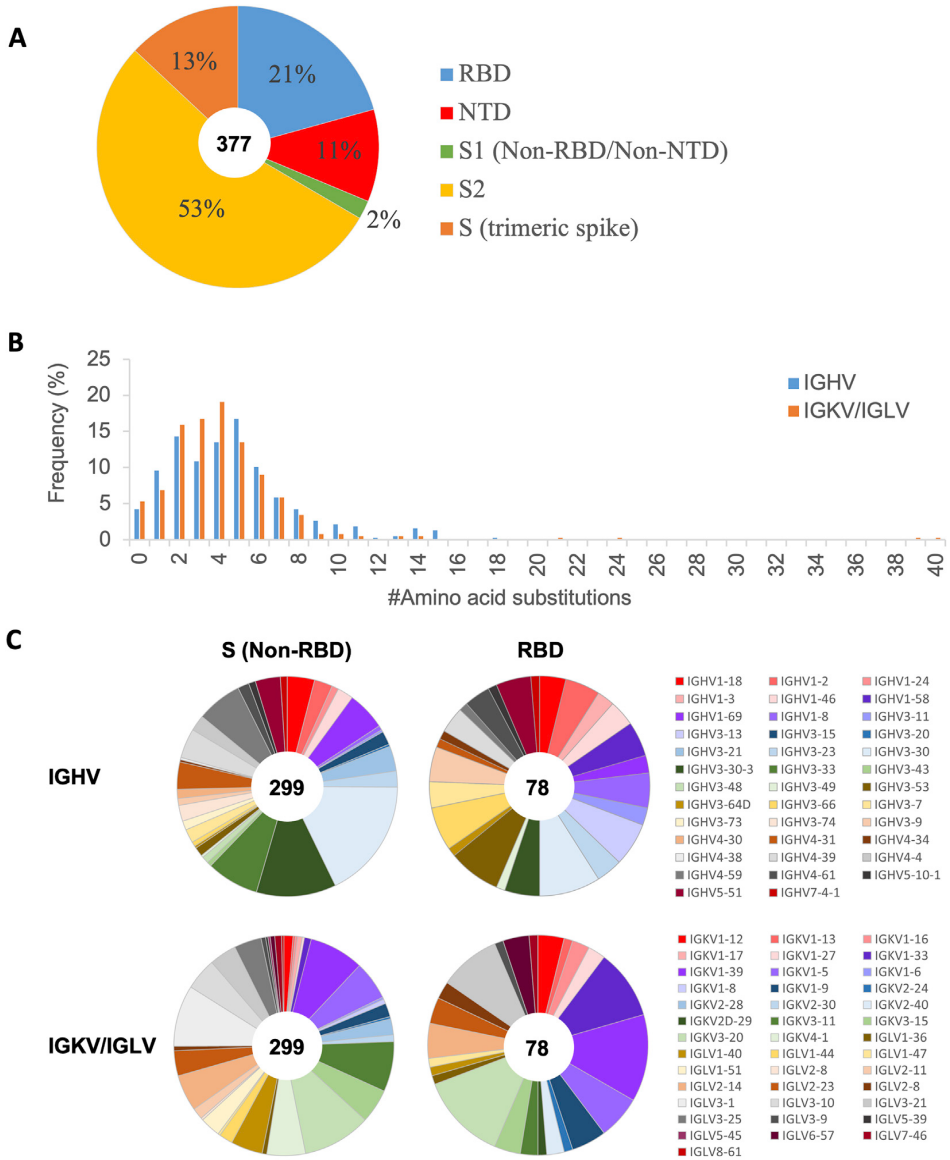

Figure 3.4 Specificity and sequence analysis of 377 early-pandemic mAbs. (A) Antibody specificity analysis against the NTD, RBD, S1 subunit (aa 16-685) and S2 subunit (aa 686-1213). Antibodies interacting with none of the subdomains, but only trimeric S were identified as trimeric spike. The number in the centres indicate the total number of tested antibodies. (B) Frequency of amino acid substitutions from germline in SARS-CoV-2-specific heavy and light chains (n=377). (C) Repertoire analysis of antibody heavy and light chains of anti-S (Non-RBD) and anti-RBD antibodies. The number in centre is the number of antibodies. Each slice represents a distinct clone and is proportional to the clone size.

3.2.2 Neutralisation activity of early-pandemic SARS-CoV-2 mAbs

We investigated the neutralising activity of all 377 mAbs using a focus reduction neutralisation assay (FRNT) on Vero cells. Only 5% of non-RBD mAbs showed neutralising activity (IC_{50}<10 µg/ml), while 60% of RBD-specific mAbs showed neutralising activity (Figure 3.5A), consistent with previous studies of SARS-CoV-1 and SARS-CoV-2[132].

In total, 19 out of 80 anti-RBD mAbs yielded IC_{50} levels of <0.1 µg/ml (Figure 3.5B), which we define as potent neutralisers. FRNT50 values for the selected mAbs are shown in Table 3.2.

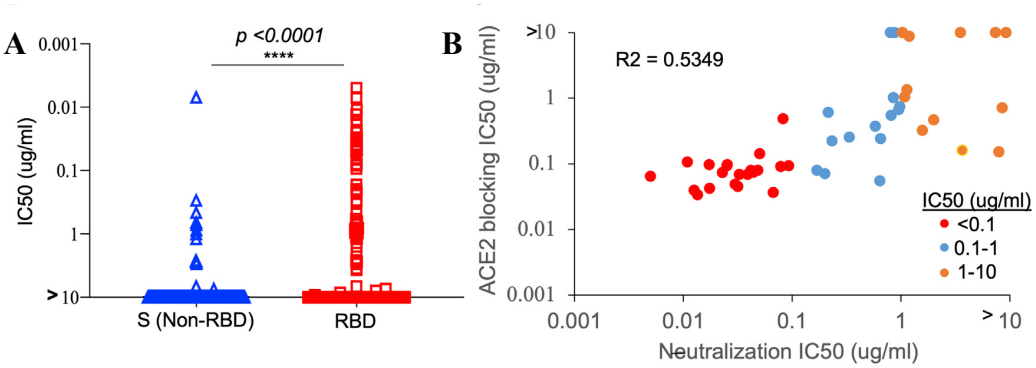

Figure 3.5 Characterisation of SARS-CoV-2-specific mAbs. (A) Comparison of neutralisation potencies (IC50) between anti-spike (non-RBD) and anti-RBD antibodies against authentic SARS-CoV-2 using focus reduction neutralisation test (FRNT). The Mann-Whitney U test was used for the analysis and two-tailed p values were calculated. (B) Correlation between SARS-CoV-2 neutralisation and RBD:ACE2 blocking by anti-RBD antibodies. Antibodies with IC50<0.1 µg/ml, 0.1-1 µg/ml, and 1-10 µg/ml are highlighted in red, blue, and orange, respectively.

Table 3.2 Neutralisation of selected antibodies against Victoria

Ab ID	Specificity	IC50 (µg/ml)*
40	RBD	0026 ± 0.007
55	RBD	0.095 ± 0.015
58	RBD	0.041 ± 0.003
88	RBD	0.033 ± 0.001
132	RBD	0.048 ± 0.000
150	RBD	0.012 ± 0.000
158	RBD	0.031 ± 0.004
159	NTD	0.011 ± 0.000
165	RBD	0.034 ± 0.004
170	RBD	0.025 ± 0.004
175	RBD	0.026 ± 0.000
222	RBD	0.019 ± 0.000
253	RBD	0.055 ± 0.008
269	RBD	0.030 ± 0.000
278	RBD	0.014 ± 0.007
281	RBD	0.005 ± 0.001
316	RBD	0.018 ± 0.007
318	RBD	0.029 ± 0.008
384	RBD	0.004 ± 0.001
398	RBD	0.091 ± 0.004

*Data are from 2 independent experiments, each with duplicate wells and the data are shown as mean ± s.e.m.

mAb159, which binds to the NTD, was one of the most potent inhibitory antibodies we obtained with an IC_{50} of 11 ng/ml.

We measured the ability of anti-RBD mAbs to block interaction with ACE2 using a competitive ELISA. For antibodies showing neutralisation, there was broad correlation

between neutralising potency and ACE2 blocking (Figure 3.5B), whereas NTD-binding mAb 159 did not block ACE2 binding.

3.2.3 Structural analysis of potent early-pandemic mAbs

To determine the epitopes of the neutralising antibodies, the pairwise competition between antibodies using biolayer interferometry (BLI) was conducted by Dr. Daming Zhou from the Division of Structural Biology, University of Oxford. Using 3 additional ("external") antibodies of known binding positions and one structure determined mAb in the present study, the binding position of the remaining 79 mAbs were determined. To facilitate interpretation of the results, we introduce a naming convention for the RBD by comparison with a human torso (Figure 3.6A). The predicted locations were classified into 5 groups using a clustering algorithm[133] (Figure 3.6B). Competition was strongest between the left shoulder and neck, although the neck and right shoulder groups also cross-compete strongly (Figure 3.6C).

The ACE2 binding site is shown in Figure 3.6D, and the binding location of the 80 mAbs are shown in Figure 3.6E. The neck cluster is the site of binding of a number of mAbs possessing the public IGVH3-53 V-region[74] and strongly overlaps the ACE2 binding site (Figure 3.6D and E). The left flank cluster includes previously determined structures EY6A, CR3022 and H014, all of which are reported to show neutralising activity, but do not compete with ACE2 binding. Some regions of the RBD are notable for the lack of antibody binding, like the right and left flank clusters (Figure 3.6E).

We also mapped neutralisation to antibody position on the RBD. As expected, there is good correlation between overlap with the ACE2 footprint and neutralisation. However, there were examples of non-neutralising antibodies that were good ACE2 blockers, and it is not clear why these antibodies performed poorly. There are also mechanisms of neutralisation beyond ACE2 blocking, for instance, 159 binds the NTD, remote from the ACE2 binding site. Interestingly, antibodies co-locating with known neutralising/protecting antibodies EY6A/H014 and S309[57,134,135] in the left and right flank clusters, respectively, didn't show significant neutralising ability in our assay.

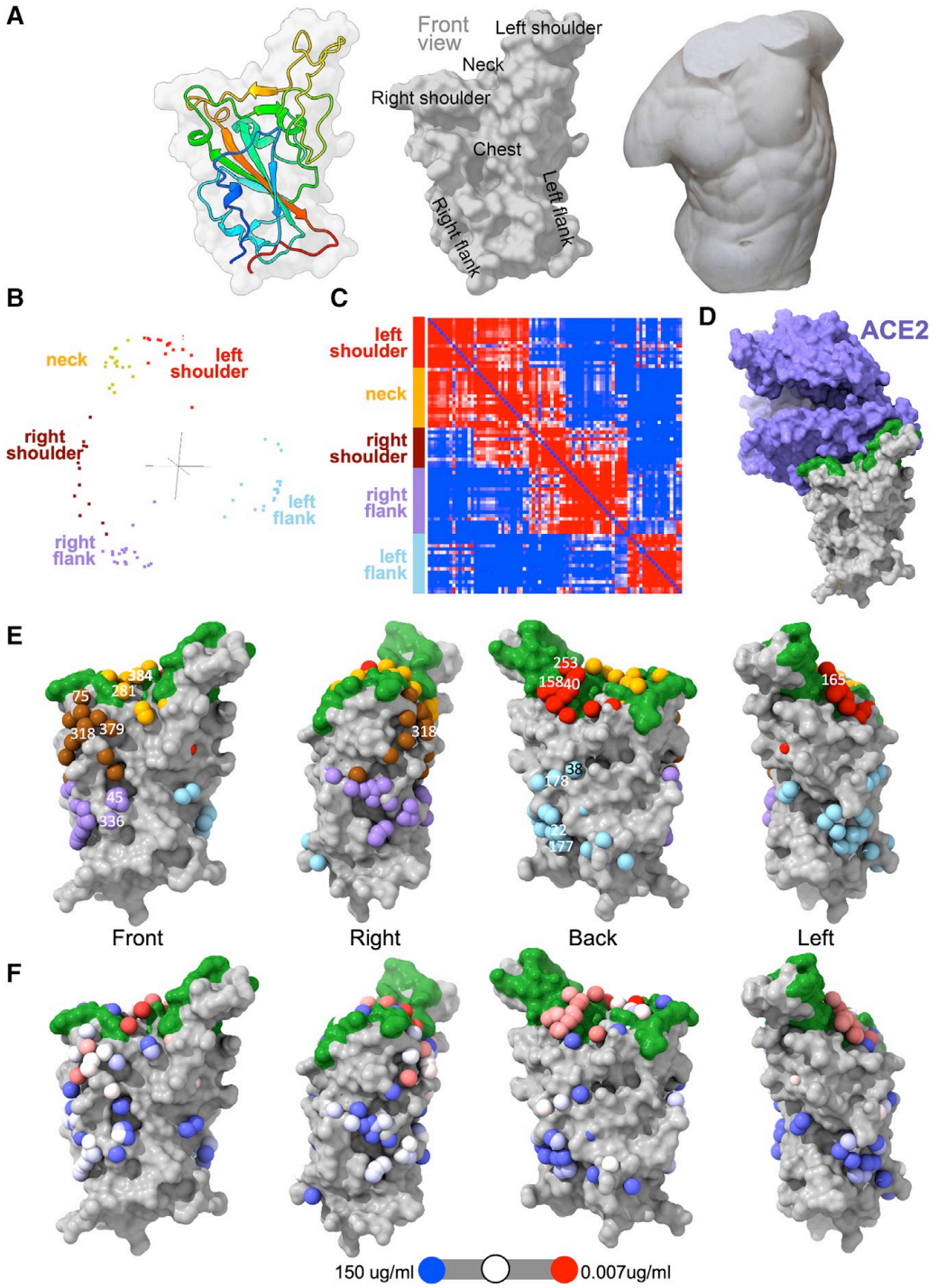

Figure 3.6 RBD anatomy and epitope definition based on mapping results. (A) Pale gray RBD surface with cartoon depiction of one monomer rainbow coloured from blue (N-terminus) to red (C terminus) alongside grey surface depiction of RBD labelled to correspond to the adjacent torso (Torso Gaddi, Wikipedia, CC BY-SA 3.0, modified in Adobe Photoshop) used by analogy to enable definition of epitopes. (B) Cluster maps showing the output of the mapping algorithm with each spot corresponding to a "located" antibody and colour-coded according to epitope. (C) BLI antibody data competition matrix (calculated values) output from cluster analysis showing the clustering into 5 epitopes. (D) RBD (gray)-ACE2 (purple) complex (PDB: 6M0J)[10]. RBD residues contacting ACE2 are shown in green. (E) Located antibodies mapped onto the RBD shown as a grey surface with the ACE2-binding site in green. The individual antibodies are depicted as spheres and colour coded as in (B). (F) As for (E), but antibodies are colour-coded according to their ability to neutralise. Experiments were performed by Dr. Daming Zhou, , and the figures were depicted by Dr Helen M. Ginn.

3.2.4 Public heavy-chain V-region usage

The potent neutralising mAbs we have identified frequently use public HC V-regions (shared by most people, compared to private, patient-specific responses). Thus 5 potent mAbs use IGHV3-53 (150, 158, 175, 222 and 269, bearing 3-10 non-silent mutations) (Figure 3.7). IGHV3 mAbs have been observed before[74,136-141]. Our competition data showed that these all bind at a similar site, which is at the back of the neck.

A second V-region that repeatedly confers potent (IC50<0.1 μg/ml) neutralisation is IGHV1-58 (mAbs 55, 165, 253, and 318). These have even fewer non-silent mutations (2-5) and longer HC CDR3s (12-16 residues). Three antibodies (55, 165, and 253), which have a disulphide bond in their CDR3 regions, compete with each other strongly, and map to the neck epitope, but do not compete with mAb318, which binds at the right shoulder as indicated by competition mapping (Figure 3.6E).

The final V-region with at least 2 potent neutralising mAbs is IGHV3-66, which was found a total of 5 times with 2 potent neutralisers (40 and 282). They strongly compete with each other on RBD binding.

Although IGHV3-30 is found in 11 RBD binders, no potent neutralising mAbs was found in this family. H3 lengths of IGHV3-30 vary from 12 to 20 residues, suggesting that they bind at different sites.

In summary, the major public V-regions used by potent antibodies generally target the neck epitope, but this is not true for weaker neutralisers (Figure 3.6E, F).

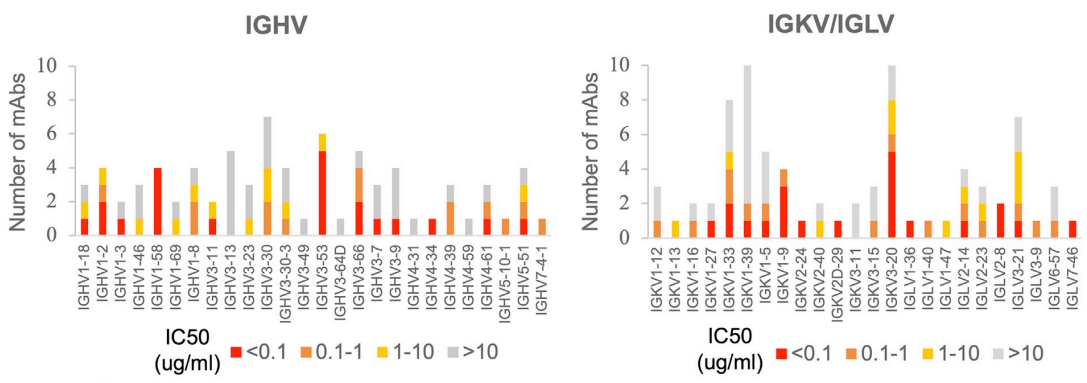

Figure 3.7 The distribution of IGHV, IGKV, and IGLV gene usage of anti-RBD mAbs. mAbs are grouped and coloured according to their neutralisation IC_{50} values.

3.2.5 Light-chain switch can increase neutralisation titre

For the three potent anti-RBD antibody clusters IGHV3-53, IGHV1-58, and IGHV3-66, which have more than 2 members in each cluster, we performed a mix and match experiment, where each IGHV was matched with all the IGLV within that cluster (Figure 3.8A). Antibody chimeras were expressed, and neutralisations were conducted and compared with the original mAb clone. We found a 10-fold increase in neutralisation titres when the heavy chain of mAb 253 (IGHV1-58, IGKV3-20) was combined with the light chain of either mAb 55 or 165, which have the same V-gene pairing (IGHV1-58, IGKV3-20) but a different J gene, having IGKJ1 in contrast of IGKJ2 in mAb 253 (Figure 3.8B).

A

	Heavy chain					Light chain				
mAb	**V-GENE**	**J-GENE**	**D-GENE**	**CDR3-IMGT length**	**AA JUNCTION**	**Light Chain**	**V-GENE**	**J-GENE**	**CDR3-IMGT length**	**AA JUNCTION**
253	1-58*01 F	3*02 F	2-2*01 F	16	CAAPHCNSTSCYDAFDIW	K	3-20*01 F	2*01 F	9	CQQYGSSPYTF
55	1-58*01 F	3*02 F	2-2*01 F	15	CAAPAC-GTSCSDAFDIW	K	3-20*01 F	1*01 F	9	CQQYGSSPWTF
165	1-58*01 F	3*02 F	2-15*01 F	16	CAAPHCIGGSCHDAFDIW	K	3-20*01 F	1*01 F	9	CQQYGSSPWTF

B

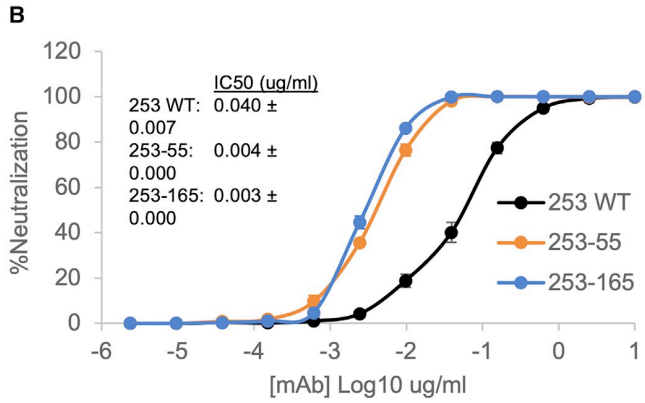

Figure 3.8 Heavy chain, light chain swapping. (A) Table of sequences of mAbs 253, 55, and 165. (B) Neutralisation activity of authentic SARS-CoV-2 by the original mAb253, chimera 253H55L, and chimera 253H165L (presented as IC50 values). Data are from 3 independent experiments, each with duplicate wells and the data are shown as mean ± s.e.m.

3.2.6 In vivo efficacy of potent early-pandemic mAbs

To determine the efficacy of our most potent neutralising human mAbs in vivo, Natasha M. Kafai, Adam L. Bailey, and Rita E. Chen of Washington University School of Medicine, USA, utilised the K18-hACE2 transgenic mouse model of SARS-CoV-2 pathogenesis, wherein human ACE2 expression is driven by an epithelial cell-specific, cytokeratin-18 gene

promoter[142,143]. In this model, SARS-CoV-2 infected animals develop severe pulmonary disease and high levels of viral infection in the lung that is accompanied by immune cell infiltration and tissue damage[143].

First, a single 250 µg (10 mg/kg) dose of mAbs 40 and 88 were administered as prophylaxis by intraperitoneal injection 1 day prior to intranasal (i.n.) challenge with 10^3 plaque-forming unit (PFU) of SARS-CoV-2. Passive transfer of mAb 40 or 88, but not an isotype control mAb (hE16), prevented SARS-CoV-2 infection caused weight loss (Figure 3.9A). In the lung homogenates of mAb 40- and 88- treated mice, no infectious virus was detected at 7 dpi, whereas substantial amounts were present in mice treated with the isotype control mAb (Figure 3.9B). Consistent with these results, viral RNA levels were reduced by ~10, 000- to 100,000-fold compared to control mAb (Figure 3.9C). In peripheral organs, including the spleen and brain, viral RNA levels were also reduced or undetectable in mAb 40- and 80- treated mice. Moreover, levels of viral RNA at 7dpi were significantly lower in the nasal washes of animals treated with mAbs 40 and 88 compared to the isotype control.

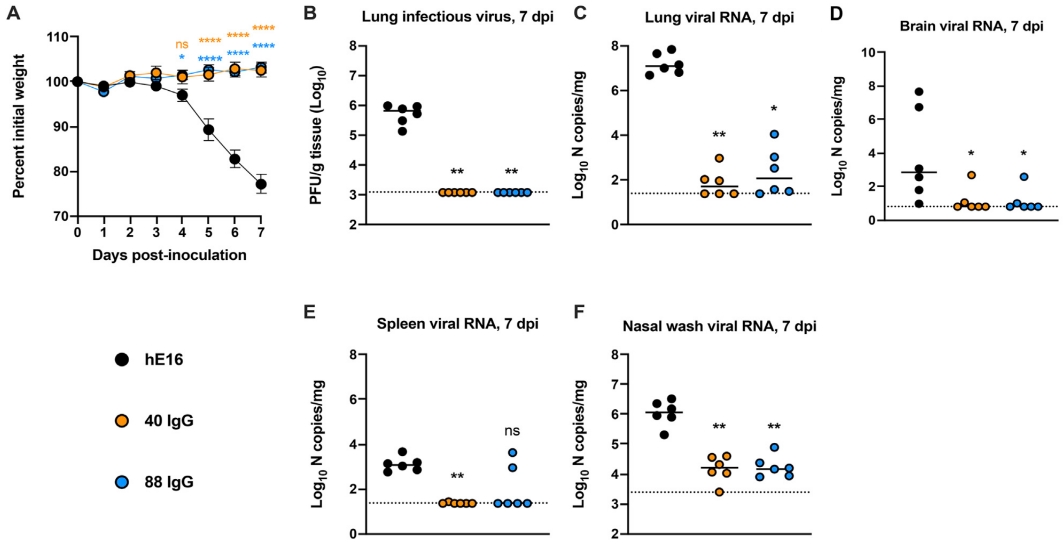

Figure 3.9 Prophylaxis with mAbs 40 and 88 protects against weight loss and decreases viral burden. (A-F) Seven to eight-week-old male and female K10-hACE2 transgenic mice were given a single 250 µg dose of the indicated mAbs by intraperitoneal injection. One day after injection, mice were inoculated by intranasal route with 10^3 PFU of SARS-CoV-2. (A) Weight change (mean ± S.E., n=6, two independent experiments: two-way ANOVA with Sidak's post test: ns, not significant, *p<0.05, ***p<0.0001; comparison is to the isotype control mAb treated group). At 7dpi tissues were harvested and viral burden was determined in the lung (B-C), brain (D), spleen (E) and nasal wash (F) by plaque assay (B) or RT-qPCR (C-F) assay (n=6 mice per group. Kruskal-Wallis test with Dunn's post-test: ns, not significant, *p<0.05, **p<0.01, ***p<0.001). Dotted lines indicate the limit of detection. The experiments were conducted by Natasha M. Kafai, Adam L. Bailey, and Rita E. Chen.

To further evaluate the in vivo potency of our mAbs, we assessed the therapeutic activities of a larger panel at 1 dpi with 10^3 PFU of SARS-CoV-2. Although varying degrees of

protection were observed for individual mAbs, weight loss was significantly reduced in mice treated with anti-SARS-CoV-2 mAbs (mAb 40, 88, 159, 384, and chimera 253H55L) at 6 and 7 dpi compared to the isotype control (hE16) (Figure 3.10A). There was barely infectious virus in the lungs of mice treated with the anti-SARS-CoV-2 mAbs, comparing to ~10^6 PFU/g of infectious virus in lung tissue of isotype control (Figure 3.10B). Lung viral RNA levels at 7 dpi were also reduced in animals treated with the mAbs 40, 159, 384, and 253H55L, while statistical significance was not achieved with mAb 88 despite a mean reduction of ~100-fold (Figure 3.10C). At the heart, spleen, and brain, all anti-SARS-CoV-2 mAbs showed protective activity, although mAbs 384 and 253H55L conferred the greatest reductions in viral RNA levels (Figure 3.10C-G). In nasal washes, mAbs 159 and 384 showed the best ability to reduce viral RNA levels (Figure 3.10F).

Collectively, these data demonstrate several mAbs in our panel can reduce infection in the upper airway, lower airway, and at distance sites when administered after infection.

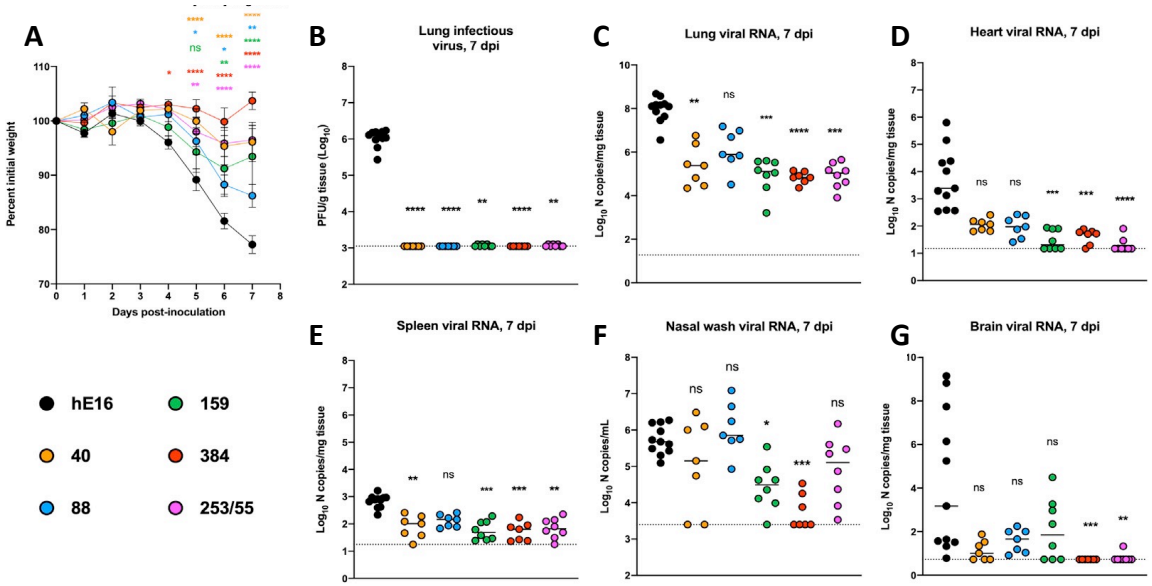

Figure 3.10 In vivo studies of mAb treatments. 7- to 8-week-old male and female K18-hACE2 transgenic mice were inoculated by an intranasal route with 10^3 PFU of SARS-CoV-2. At 1 dpi, mice were given a single 250 µg (10 mg/kg) dose of the indicated mAb by intraperitoneal injection. (A) Weight change (mean ± SEM; n = 5–10, two independent experiments: two-way ANOVA with Sidak's post-test: ns, not significant, *p < 0.05, **p < 0.01, ****p <0.0001; comparison to the isotype control mAb treated group). (B-G) At 7 dpi tissues were harvested and viral burden was determined in the lung (B and C), heart (D), spleen (E), nasal washes (F), and brain (G) by plaque (B) or qRT-PCR (C–G) assay (n = 7-11 mice per group; Kruskal-Wallis test with Dunn's post-test: ns, not significant, *p < 0.05, **p < 0.01, ***p < 0.001, ****p < 0.0001).Dotted lines indicate the limit of detection. The experiments were conducted by Natasha M. Kafai, Adam L. Bailey, and Rita E. Chen.

3.3 Discussion

Here, we isolated and measured the neutralisation ability of a set of 377 mAbs from a substantial cohort of patients infected by early pandemic COVID-19 and identified 80 of these bind the RBD. We have identified the binding sites of all 80 of them and defined five binding clusters or epitopes. By analogy with a human torso, four of these clusters form a continuous swathe running from the left shoulder to the neck, right shoulder, and down the right flank of the torso, whereas the fifth cluster forms a more discrete site toward the left flank. Among all 80 RBD mAbs, we identified 20 most potent (IC50<0.1 μg/ml) neutralising mAbs which all but one block receptor attachment to the neck. The single exception, mAb 159, binds the NTD and the mechanism of neutralisation is unclear.

There is a close association between potent neutralisers and public V-genes suggesting that vaccination responses should be strong[74,132]. Three public V-genes, IGHV3-53, IGHV1-58, and IGHV3-66, occurred at least twice in our set, which all focus around the neck cluster. By switching light chains within these sets, we found that function of one mAb (253) could improve by an order of magnitude by using an alternative light chain.

Furthermore, we show that the most potent neutralising mAbs we identified can protect in an animal model, when administered prophylactically or therapeutically. The competition mapping method suggests that a series of combinations of neutralising mAbs with non-overlapping epitopes that could create an immunotherapy with greater protection and resistance against mutations than a single mAb.

There is one highly potent anti-NTD neutralising mAb, 159, in the set of mAbs we isolated, while the mechanisms of neutralisation are not yet established here, and will be the subject of our further study. Meanwhile, highly potent ACE2 blockers map to two sites in the region of the neck and the left shoulder, residues E484-F486 bridge the epitopes and are accessible to Fabs binding. During the isolation and characterisation of these mAbs, two mutations among this region had been identified: F486L, which was associated with host-adaptation in mink[144], and E484K, which was found in Beta and Gamma variants. We would assess the impact of these mutations on the set of 20 potent neutralising mAbs. A characterisation of the polyclonal antibody response would give insight into the potential for vaccine escape.

CHAPTER 4 Immune evasion of SARS-CoV-2 variants Alpha, Beta, Gamma and Delta

4.1 Introduction

Since the emerge of SARS-CoV-2 in Wuhan in December 2019, it has spread globally at an unprecedented speed. By late 2020, there were several variant strains of SARS-CoV-2 emerging in different parts of the world. Alpha (B.1.1.7) was first reported in the UK from a sample obtained in October 2020, Beta (B.1.351) was identified in October 2020 in South Africa, and Gamma was detected in Brazil in December 2020, all were designated as variants of concern (VoC) by WHO. Later, in early 2021, another two variant viruses, Kappa (B.1.617.1) and Delta (B.1.617.2) were first reported in India and then spread globally in fast speed, with Delta causing particular concern in the United Kingdom, and designated a VoC in May 2021.

There are a large number of mutations in the genome of each variant, but due to the importance of the spike protein as a receptor binding protein, the mutations in the spike, especially RBD region, caused the most interest in terms of immune escape.

Alpha variant contains total of 9 changes in the spike protein relative to Wuhan: N501Y, A570D, D614G, P681H, T716I, S982A, D1119H, and deletions of residues 69-70 and 144, with N501Y being the only mutation in RBD region (Figure 4.1A).

Beta variant has 10 changes in spike protein relative to Wuhan sequence[145]: L18F, D80A, D215G, L242-244 deletion, R246I, K417N, E484K, N501Y, D614G, and A701V. It has three changes in the RBD, K417N, E484K, and N501Y, which shares N501Y mutation with Alpha variant (Figure 4.1B).

Gamma variant has 12 mutations in spike protein comparing to which in Wuhan strain: L18F, T20N, P26S, D138Y, R190S, K417T, E484K, N501Y, D614G, H655Y, T1027I, and V1176F. In the RBD region, it has three changes in RBD region, K417T, E484K, and N501Y, with K417T being the only different RBD mutations comparing with Beta variant, which is K417N mutation in this position (Figure 4.1C).

Delta variant occurred later than Alpha, Beta, and Gamma, with some new mutations in the RBD. Delta variant we tested here has 9 mutations: T19R, G142D, Δ156-157/R158G, A222V,

L452R, T478K, D614G, P681R, and D950N. In RBD region, L452R and T478K mutations had never occurred in any other variants before (Figure 4.1D).

There are many possible ways whereby a mutation in SARS-CoV-2 may give the virus a selective advantage; however, concentrating on mutations in S, there are two clear possibilities: increased efficiency of transmission and escape from neutralising mAbs[146]. Here, we measured and compared the binding affinity of RBD-ACE2 interaction for Wuhan, Alpha, Beta, Gamma, and Delta. Then we tested the neutralising ability of the set of 20 mAbs we isolated from patients infected presumably by early pandemic strains without RBD mutations (See Chapter 3), as well as 11 commercial mAbs developed by different companies. Moreover, we assessed the neutralising abilities of serum samples we obtained from infected patients or vaccinees against all four VoCs (Alpha, Beta, Gamma, and Delta) appeared at the early stage of the pandemic.

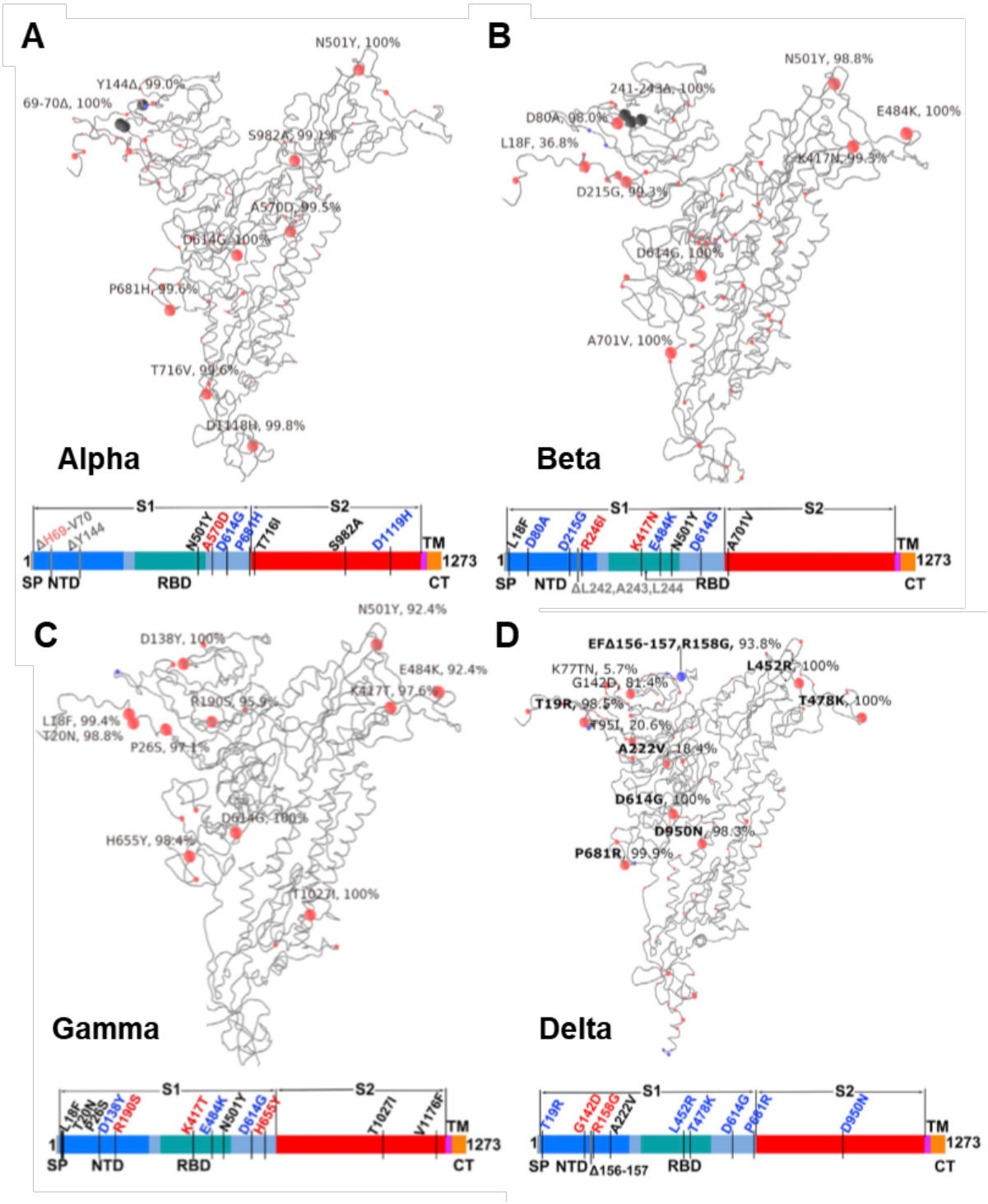

Figure 4.1 Mutation landscape of early major variants. (A-D) Schematic showing the locations of amino acid substitutions in Alpha (A), Beta (B), Gamma (C), and Delta (D) relative to Wuhan spike sequences. Point mutations are shown in red and deletions in dark grey. Under the structural cartoon is a linear representation of S with changes marked on. Where there is a charge change introduced by mutations, the change is coloured (red if the change makes the mutant more acidic/less basic and blue if the change makes the mutant more basic/less acidic). Figures were produced by Dr Jingshan Ren.

4.2 Results

4.2.1 The effects of RBD mutations on ACE2 affinity

To measure the impact of the RBD mutations of different variants having on ACE2 binding affinity, we expressed and purified RBDs of Alpha, Beta, Gamma, and Delta, and performed BLI assay between RBD and ACE2 protein. This assay was conducted by Dr. Daming Zhou.

Comparing RBD-ACE2 affinity of Alpha and Wuhan, we see a marked (7-fold) increase in binding affinity (WT RBD: 75.1 nM vs Alpha RBD: 10.7 nM), as reported previously[147] (Figure 4.2A-B).

The three mutations in Beta RBD, K417N, E484K, and N501Y, are situated within the ACE2 footprint, and in vitro evolution to optimise the affinity of ACE2 has suggested that they confer higher affinity for the receptor[147]. We investigated the kinetics of binding of soluble ACE2 to recombinant RBD by BLI. As expected, the affinity of Beta RBD is 19-fold higher than for the Victoria RBD and 2.7-fold higher than for Alpha[79] (Beta RBD: 4.0 nM) (Figure 4.2C).
n

The triple mutations in Gamma RBD, K417T, E484K, and N501Y are similar to those in Beta RBD, we expect a similar K_D value. Indeed, the KD for the Gamma RBD-ACE2 interaction is 4.8 nM (Figure 4.2D), showing that binding to Gama is essentially indistinguishable from Beta (4.0 nM).

We went on to analyse interactions of Delta RBD with ACE2. The results for ACE2 show that the Delta (Figure 4.2 E) double mutations (L452R and K478T) have a modest increase in affinity for ACE2 (57 nM) compared with Wuhan RBD (75 nM), which is surprising in the case of Delta considering the high transmissibility of the variant.

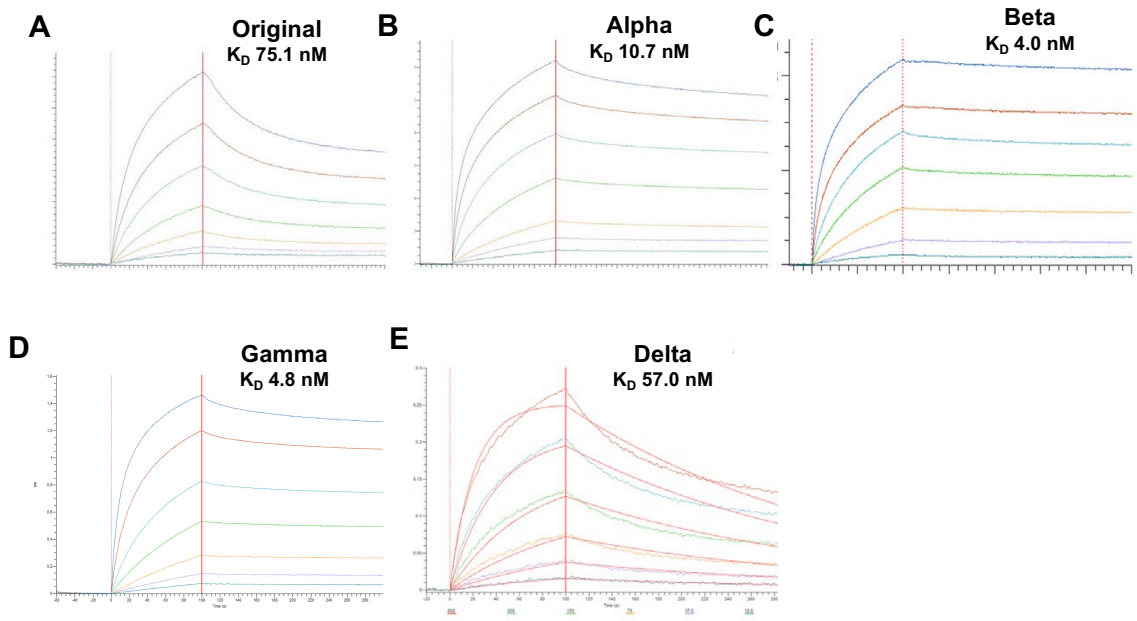

Figure 4.2 Interaction of RBDs of early major variants with ACE2. (A-F) BLI experiments showing binding of ACE2 to RBDs of Original SARS-CoV-2 (A), Alpha (B), Beta (C), Gamma (D), and Delta (E). Experimental data for the dilution series is shown in different colours and the models as red lines. Experiments were performed by Dr Daming Zhou.

4.2.2 Immune escape of Alpha, Beta, Gamma and Delta from early-pandemic mAbs

Using the set of 20 potent neutralising mAbs we isolated from patients infected with early strains of SARS-CoV-2 previously, before the emerging of Alpha variant[123], neutralisation against Alpha, Beta, Gamma and Delta authentic viruses was measured by FRNT compared to neutralisation against Victoria.

For some antibodies (40, 88, 222, 316, 384, 398), FRNT50 values were minimally affected by Alpha variant (<2-fold difference between Victoria and Alpha). However, for others there was a fall in the neutralisation titres for Alpha, particularly pronounced for mAb 269, where neutralisation was almost completely lost and mAb278, which failed to reach 100% neutralisation showing a maximum of only 78% (Figure 4.3A, Table 4.1). Considering all these antibodies are RBD mAbs, the effect of neutralisation is very likely caused by the single mutation in Alpha RBD region, N501Y.

The effects of Beta variant on mAb neutralisation were severe, 14 of 20 mAbs had >10-fold fall in neutralisation titres (40, 88, 132, 150, 158, 159, 170, 175, 269, 278, 281, 316, 384, 398), with most of these showing a complete knockout of activity (Figure 4.3A, Table 4.1). This is

in line with the key roles of K417, E484, and N501, in particular E484, in antibody recognition of the ACE2 interaction surface of the RBD. Interestingly, the single potent NTD-binding mAb included in these assays, mAb159, also showed a complete knockout of activity against Beta, which includes deletion of amino acids 242-244 in the NTD, part of the epitope for mAb 159.

Using the same set of 20 potent mAbs, we tested their neutralisations against Gamma. Compared to Victoria neutralisation by the mAbs was significantly impacted by Gamma, with 12 out of 20 mAbs showing >10-fold reduction in FRNT50 titre (88, 132, 158, 159, 170, 175, 269, 278, 281, 316, 384, 398), and a number showing complete knockout of activity (Figure 4.3A, Table 4.1). The results with Gamma showed a greater impact compared to Alpha but were, as expected, similar to those with Beta.

Neutralisation of Delta was also measured using an FRNT and compared with the Victoria viral isolate. Neutralisation of Delta was reduced more than 5-fold for 11 mAbs (58, 159, 165, 170, 175, 269, 278, 281, 316, 384, and 398), with neutralisation by NTD mAb 159 lost completely. Interestingly, mAb253 showed increased neutralisation of Delta.

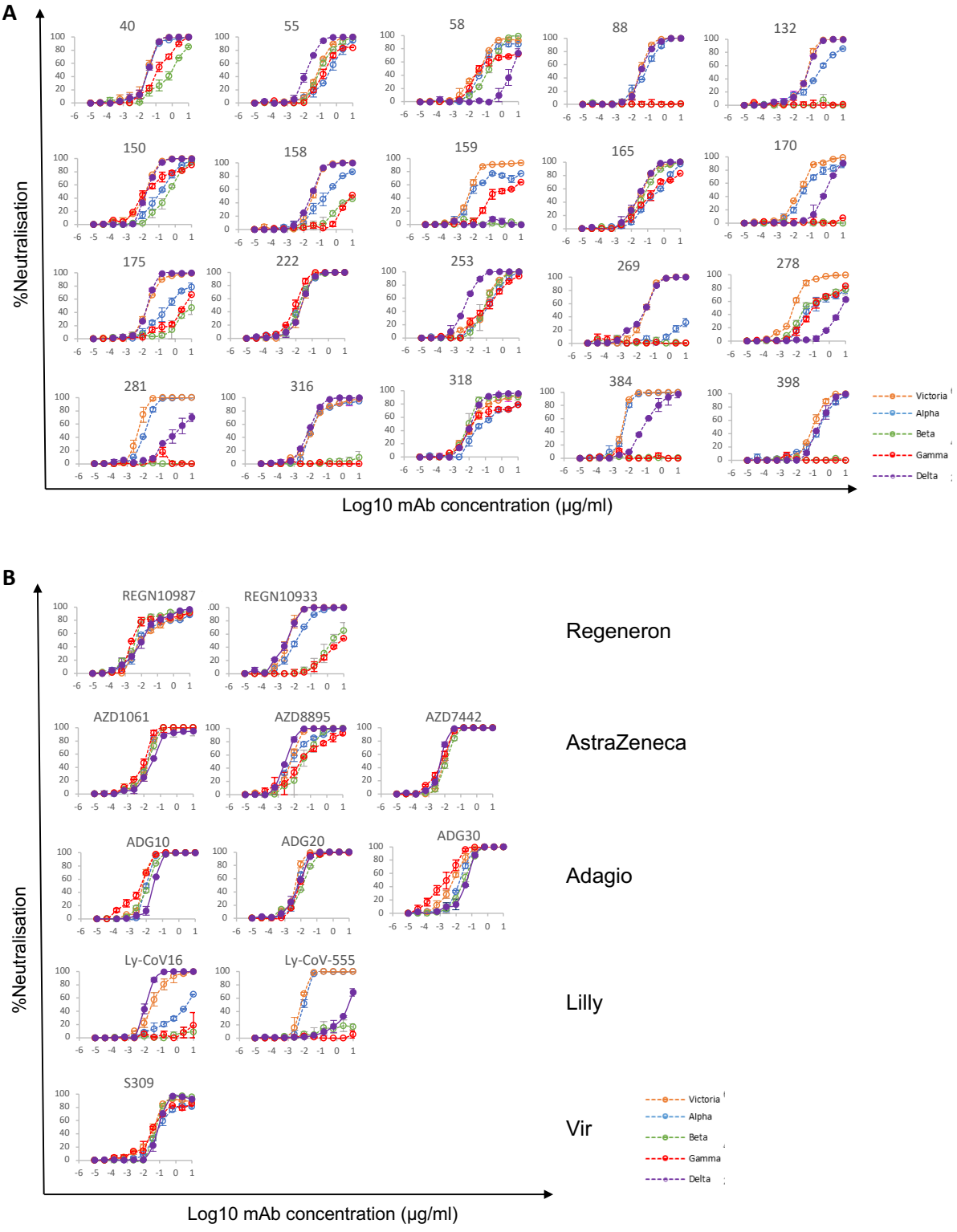

Figure 4.3 Neutralisation of Victoria, Alpha, Beta, and Gamma by 20 early-pandemic mAbs. (A) Neutralisation of Victoria, Alpha, Beta and Gamma by a panel of 20 potent human mAbs. (B)Neutralisation curves for mAbs in different stages of development for commercial use from Vir, Regeneron, AstraZeneca, Lily and Adagio. Neutralisation was measured by FRNT, two independent experiments were conducted for each mAb and data are shown as mean ± s.e.m.

Table 4.1 $FRNT_{50}$ of monoclonal mAbs neutralisation against authentic live viruses

Ab ID	$FRNT_{50}$ (μg/ml)*				
	Victoria	Alpha	Beta	Gamma	Delta
40	0.026 ± 0.007	0.035 ± 0.008	0.738 ± 0.311	0.153 ± 0.037	0.029 ± 0.010
55	0.095 ± 0.015	0.348 ± 0.044	0.127 ± 0.014	0.306 ± 0.046	0.016 ± 0.005
58	0.041 ± 0.003	0.116 ± 0.029	0.136 ± 0.010	0.236 ± 0.075	6.434 ± 2.623
88	0.033 ± 0.001	0.058 ± 0.008	>10	>10	0.039 ± 0.007
132	0.048 ± 0.000	0.337 ± 0.048	>10	>10	0.051 ± 0.013
150	0.012 ± 0.000	0.139 ± 0.019	0.350 ± 0.010	0.040 ± 0.003	0.020 ± 0.001
158	0.031 ± 0.004	0.254 ± 0.109	>10	>10	0.026 ± 0.002
159	0.011 ± 0.000	0.061 ± 0.020	>10	1.434 ± 0.804	>10
165	0.034 ± 0.004	0.212 ± 0.004	0.054 ± 0.013	0.241 ± 0.030	0.027 ± 0.006
170	0.025 ± 0.004	0.105 ± 0.050	>10	>10	0.841 ± 0.103
175	0.026 ± 0.000	0.575 ± 0.280	>10	3.881 ± 0.738	0.017 ± 0.003
222	0.019 ± 0.000	0.014 ± 0.002	0.017 ± 0.005	0.008 ± 0.003	0.018 ± 0.001
253	0.055 ± 0.008	0.126 ± 0.018	0.109 ± 0.055	0.137 ± 0.005	0.005 ± 0.001
269	0.030 ± 0.000	>10	>10	>10	0.021 ± 0.004
278	0.014 ± 0.007	0.370 ± 0.149	0.160 ± 0.018	0.245 ± 0.042	7.374 ± 1.397
281	0.005 ± 0.001	0.012 ± 0.000	>10	>10	1.494 ± 0.302
316	0.018 ± 0.007	0.024 ± 0.005	>10	>10	0.008 ± 0.001
318	0.029 ± 0.008	0.185 ± 0.037	0.019 ± 0.008	0.083 ± 0.032	0.018 ± 0.003
384	0.004 ± 0.001	0.005 ± 0.002	>10	>10	0.108 ± 0.035
398	0.091 ± 0.004	0.180 ± 0.001	>10	>10	0.237 ± 0.038
AZD1061	0.013 ± 0.003	0.012 ± 0.002	0.014 ± 0.002	0.007 ± 0.002	0.038 ± 0.006
AZD8895	0.005 ± 0.001	0.011 ± 0.002	0.046 ± 0.031	0.046 ± 0.016	0.003 ± 0.000
AZD7742	0.009 ± 0.000	0.007 ± 0.001	0.012 ± 0.001	0.006 ± 0.003	0.005 ± 0.000
REGN10987	0.032 ± 0.007	0.028 ± 0.003	0.007 ± 0.001	0.013 ± 0.002	0.017 ± 0.009
REGN10933	0.004 ± 0.002	0.014 ± 0.002	3.284 ± 2.014	6.177 ± 1.914	0.003 ± 0.001
ADG10	0.006 ± 0.000	0.010 ± 0.001	0.011 ± 0.001	0.003 ± 0.000	0.026 ± 0.005
ADG20	0.004 ± 0.001	0.006 ± 0.000	0.010 ± 0.001	0.009 ± 0.000	0.006 ± 0.001
ADG30	0.007 ± 0.002	0.016 ± 0.001	0.029 ± 0.003	0.002 ± 0.001	0.033 ± 0.007
LY-CoV555	0.006 ± 0.002	0.009 ± 0.000	>10	>10	8.311 ± 4.059
LY-CoV16	0.034 ± 0.007	3.225 ± 1.030	>10	>10	0.012 ± 0.002
S309	0.040 ± 0.005	0.078 ± 0.069	0.082 ± 0.002	0.076 ± 0.014	0.113 ± 0.028

*Data are from 2 independent experiments, each with duplicate wells and the data are shown as mean ± s.e.m.

4.2.3 Immune escape of Alpha, Beta and Gamma variants from commercial mAbs

A number of potent neutralising mAbs are being developed for clinical use either therapeutically or prophylactically, with several of them having been approved[148-150]. We

performed neutralisation assays against Victoria, Alpha, Beta, Gamma, and Delta using antibodies S309 Vir[56], AZD8895, AZD1061, and AZD7442 (a combination of AZD8895 and AZD1061) (AstraZeneca); REGN10987 and REGN10933 (Regeneron); LY-CoV555 and LY-CoV16 (Lilly); and ADG10, ADG20, and ADG30 (Adagio) (Figure 4.3B, Table 4.1).

Neutralisation of both Lilly antibodies was severely impacted, with LY-CoV16 and LY-CoV555 showing almost complete loss of neutralisation of Beta and Gamma, and LY-CoV16 also showing marked reduction in neutralisation of Alpha, while surprisingly showing a modest increase in neutralising Delta.

There was escape from neutralisation of Beta and Gamma by REGN10933, and a modest reduction in neutralisation of Beta and Gamma by AZD8895, while AZD1061 and AZD7442 showed equal neutralisation of all SARS-CoV-2 variants. Delta variant has no impact on neutralisation of REGN10987, REGN10933, AZD1061, AZD8895, and AZD7442.

The three Adagio antibodies neutralised all variants, with a modest reduction in neutralisation of Alpha Beta, and Gamma by ADG30. ADG10 also showed some level of decrease of neutralisation on Delta. Interestingly, ADG10 and ADG30 showed a slight increase of neutralisation of Gamma.

S309 Vir was largely unaffected, although the antibody failed to completely neutralise Alpha, Beta, and Gamma, conceivably reflecting incomplete glycosylation at N343, since the sugar interaction is key to binding of this antibody[56]. It also showed a greater reduction of neutralisation of Delta comparing with other early VoCs.

4.2.4 Immune escape of Alpha, Beta and Gamma variants from convalescent plasma

Convalescent plasma samples were collected from a cohort of volunteers who had suffered from SARS-CoV-2 infection, as evidenced by a positive diagnostic PCR test result, samples were obtained early in the pandemic before the emergence of Alpha, Beta, Gamma and Delta. Neutralisation of Victoria, Alpha, Beta, Gamma and Delta was assessed by FRNT on 34 convalescent samples (Figure 4.4A). The geometric mean neutralisation titres of Alpha were reduced 2.9-fold compared to Victoria ($p<0.0001$), and the reduction was similar to Gamma (3.1-fold) and Delta (2.7-fold), but considerably less than Beta (13.3-fold).

When using plasma from individuals infected with Alpha (Figure 4.4B), their neutralising ability against Victoria was actually better than Alpha, the homologous infecting lineage (0.5-fold), while more significant reductions in neutralisation was seen in Beta (2.6-fold). Gamma and Delta showed modest reduction (1.7-fold and 1.5-fold, respectively) when comparing with Alpha.

For Beta serum (Figure 4.4C), it had 1.9-fold reduction against Victoria compared with Beta, the homologous infecting lineage, 3.3-fold reduction on Alpha, and 2-fold reduction on Gamma. More significantly, neutralisation of Delta reduced 11.5-fold compared with Beta.

Gamma serum showed a similar pattern as Beta serum (Figure 4.4D). The reduction of neutralisation of Victoria, Alpha, and Beta were 3.9-, 4.1, and 2.2-fold, respectively, while neutralisation of Delta by Gamma serum dramatically reduced 11.3-fold.

Serum from donors infected by Alpha appears to give good protection against all variants of concern, whereas protection from Delta afforded by previous infection with Beta and Gamma is much more compromised.

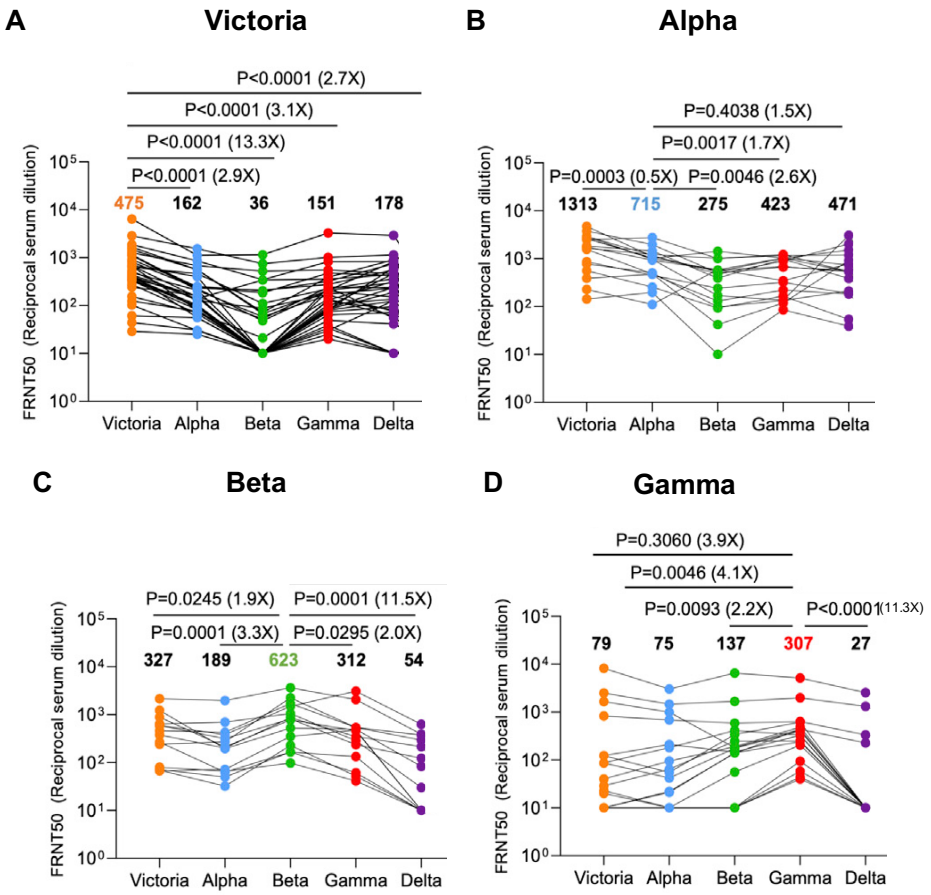

Figure 4.4 Neutralisation of Victoria, Alpha, Beta, Gamma, and Delta by convalescent plasma. Neutralisation titres for Victoria, Alpha, Beta, Gamma, and Delta live virus, measured by FRNT using (A) convalescent plasma (n=34) collected from volunteers 4-9 weeks following SARS-CoV-2 infection; all samples were collected before June 2020 and therefore represent infection before emergence of Alpha in the United Kingdom. Neutralisation was also measured using (B) Alpha convalescent plasma (n=18), (C) Beta convalescent plasma (n=14), and (D) Gamma convalescent plasma (n=17). Wilcoxon matched-pairs signed-rank test was used for the analysis, and two-tailed p values were calculated.

4.2.5 Protection from Alpha, Beta, Gamma, and Delta by vaccine serum

We also performed neutralisation assays on serum collected from individuals who had received either the BNT162b2 Pfizer-BioNTech or ChAdOx1 nCoV-19 Oxford-AstraZeneca vaccine (Figure 4.5). For the Pfizer-BioNTech vaccine, serum was collected 4-14 days after the second dose of vaccine administered 3 weeks after the first dose (n = 25). For the Oxford-AstraZeneca vaccine, serum was taken 14 or 28 days following the second dose, which was administered 8-14 weeks following the first dose (n = 25). Geometric mean neutralisation tires against Delta were reduced 2.5-fold ($p<0.0001$) relative to the Victoria virus for the Pfizer-BioNTech vaccine serum and 4.3-fold ($p<0.0001$) for the Oxford-AstraZeneca vaccine. The reductions were comparable with those seen with Alpha and Gamma, which were 3.3-fold and 2.6-fold reductions for the Pfizer-BioNTech vaccine serum and 2.3- and 2.9-fold reductions

for the Oxford-AstraZeneca vaccine serum. The reductions of neutralisation on Beta were more concerning, with 7.6-fold reduction for Pfizer-BioNTech vaccine serum and 9.1-fold reductions for the Oxford-AstraZeneca vaccine serum (Figure 4.5).

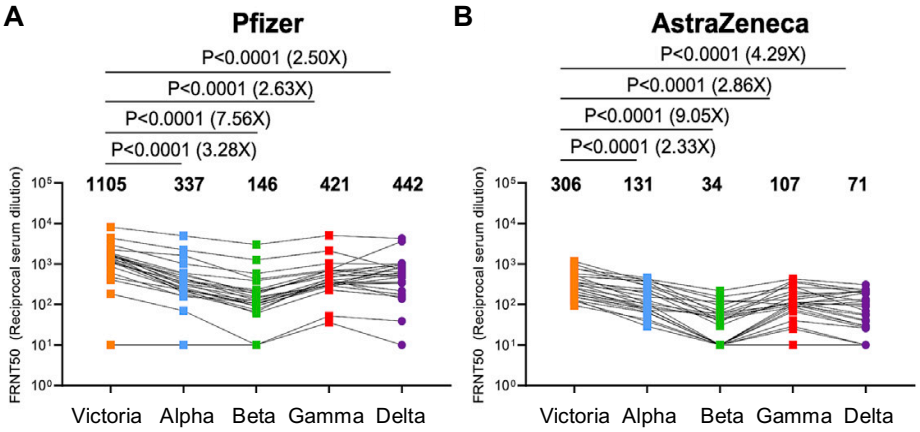

Figure 4.5 Neutralisation by vaccine serum. (A) FRNT50 titres of Pfizer-BioNTech serum (n = 25) against Victoria, Alpha, Beta, Gamma, and Delta live virus; (B) FRNT50 titres of Oxford-AstraZeneca serum (n = 25) against Victoria, Alpha, Beta, Gamma, and Delta live virus. Wilcoxon matched-pairs signed-rank test was used for the analysis, and two-tailed *p* values were calculated.

4.2.6 The antigenic landscape of Alpha, Beta, Gamma and Delta

Dr. Helen M. Ginn from Diamond Light Source Ltd developed a method related to antigenic cartography[151,152] to visualise and quantify the emerging antigenic landscape of SARS-CoV-2. The "antigenic distance" was defined by comparison of the log of dilution values for 50% neutralisation for all serum/virus strain pairs[22,23,79,123]. 113 sera from natural infection and vaccinations were used to compare against 7 virus strains, assembling a 113 x 7 matrix. Single value decomposition of the serum/virus strain pair matrix was carried out, producing weighted orthogonal vectors representing the axes of variation within the data and each strain was expressed as a vector in this new orthogonal basis. The largest axis of variation was largely identical for each strain, representing the positivity in common with all log dilution values. The 2nd, 3rd and 4th major axes were plotted using cluster4x[133] to show the separation between each virus strain in antigenic space. The result, using the somewhat incomplete set of data available from our studies, is shown in Figure 4.5. This provides a very simple view onto complex, sparse and noisy data and shows that the largest distance is between the Beta/Gamma lineages and Delta. Although Beta is roughly orthogonal to Delta, Gamma is essentially opposite Delta, reflecting the especially poor ability of Gamma serum to neutralise Delta. It also demonstrates that Alpha and Victoria are reasonably central to the distribution.

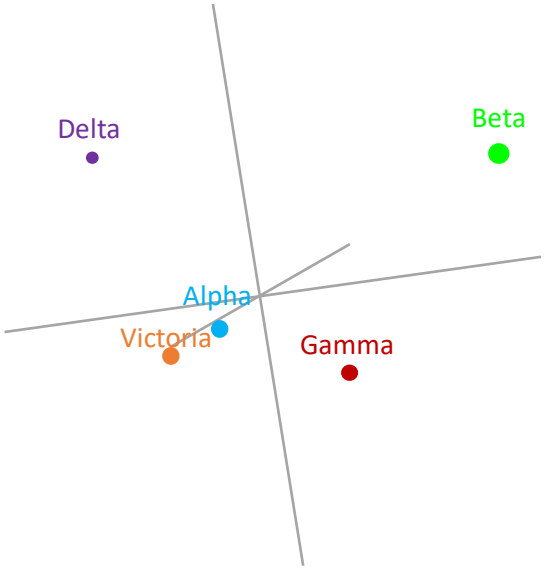

Figure 4.6 Map of variants in antigenic space. Figure show output of principal-component analysis converting serum/virus strain pair neutralisation capacities to antigenic space. Circle size denotes depth along the axis connecting the reader's nose to the origin. The model was devised by Dr. Helen M. Ginn.

4.3 Discussion

SARS-CoV-2 is under close genome surveillance in many parts of the world following its transfer from animals to humans. In the early stage of the pandemic, SARS-CoV-2 was under selective pressure to adapt to its new host, evade the immune system, bind to and infect host cells, and transmit to the next host. As more and more of the population develops immunity through natural infection or vaccination, the pressure for the virus to more effectively find an infectible host through increased transmissibility or evasion of the acquired immune response and causes reinfection is increases.

Because the S protein initiates binding to cell surface receptor ACE2, and it is the target of neutralising antibody responses, it undergoes many changes and evolves quickly. More importantly, mutations in and around the ACE2-interacting surface are the key mutations and have been found in all VoCs.

In this chapter, the affinities of RBDs of 4 major VoCs, Alpha, Beta, Gamma, and Delta with ACE2 were measured. The results showed remarkable increase in affinities of Alpha, Beta, and Gamma (7-, 19-, and 19-fold), while only a very modest increase (<2-fold) was found in Delta RBD. It is likely that Delta RBD mutations were selected by different pressure.

We also observed the reduction of neutralisation of a number of potent mAbs isolated from early pandemic convalescent serum samples against Alpha, and the majority of the mAbs suffered substantial reduction or knockout activity against Beta and Gamma, highlighting the importance of N501Y and E484K mutations in immune escape, in line with *in vitro* evolution experiments[153-155]. L452R and T478K in Delta variant also impact the neutralisation of some of the mAbs, but not to the extent of Beta and Gamma.

The loss of activity of some potent neutralising mAbs in the four major VoCs indicates that there is likely to be a reduction in neutralisation of VoCs by convalescent and vaccine sera. As we expected, there is modest reduction in Alpha, Gamma and Delta for the early pandemic convalescent sera and vaccine sera comparing with Victoria, but a much higher level of resistant to neutralisation in Beta (13.3-fold for the early pandemic convalescent sera, 7.6-fold for the Pfizer vaccine sera and 9.1-fold for the AstraZeneca vaccine sera). Because Beta and Gamma harbour similar mutations in the RBD region, the difference in reduction of neutralisation is likely to be caused by different mutations in the NTD of S. Beta S has a deletion at amino acid 241-243, which is close to the recognised NTD supersite of attack aa 245–264[76] and may confer its ability to escape neutralisation of anti-NTD mAbs.

More intriguingly, Delta shows a remarkable reduction of neutralisation by sera from people infected previously with Beta and Gamma, with 11.6-fold reduction by Beta serum and 11.3-fold reduction by Gamma serum. An explanation for the disparity in neutralisation of Delta by beta and Gamma serum may be because that the differences between the two viruses are additive. Thus, there are three RBD amino acid substitutions in Beta and Gamma compared with Wuhan RBD, but five compared with Delta (K417N/T, R452L, K478T, E484K, N501Y, the amino acid before the number represents the Delta RBD sequence). In addition, there are many changes in the NTD regions, meaning that more antibodies generated by Beta and Gamma infection will likely be ineffective against Delta.

To visualise and quantify the antigenic landscape of SARS-CoV-2, we defined a multidimensional antigenic space representing “antigenic distances” within the sero-complex and show that, even using the incomplete data available, projecting the principal components into a lower dimensional space allows visualisation of the antigenic relationship between the different lineages, confirming the qualitative assessment that the largest distance is between Delta and the Beta/Gamma lineages, with Gamma being anti-correlated with Delta. We suggest

that the virus closest to the centroid of the distribution of the antigenic differences might be a good candidate for a vaccine, which can produce the most effective responses against all identified variants.

In this study, we investigated the effect of RBD mutations in four early VoCs on the affinity of RBD-ACE2 binding and the immune escape. The reduced titre of convalescent serum and vaccine serum may lead to breakthrough infection. It should also be noted that the in vitro neutralisation assays described here are performed in the absence of complement or Fc receptor-bearing cells, which can mediate antibody-dependent cell-mediated cytotoxicity, meaning that there may be underestimation of the protection of immune serum. The assays do not measure the T cell response, which also contribute to protection of SARS-CoV-2 infection[156]. It will be interesting to see how antibodies in the sera of Beta/Gamma infected individuals recognise different epitopes, and reveal the influence of the each RBD mutation on the generation of neutralising mAbs.

CHAPTER 5 Generation and characterisation of Beta mAbs

5.1 Introduction

As we reported previously, the mutations found in Beta RBD (K417N, E484K, and N501Y) are located in or closely adjacent to the ACE2-interacting surface and increase the affinity of RBD-ACE2 interaction and disrupt the binding of neutralising mAbs. When compared with early pandemic strain, we have seen a reduced vaccine efficacy against Beta, shown as significant reduction of neutralisation titres to Beta using serum obtained from early pandemic infection patients or vaccinees[22]. The mutations in Beta RBD (K417N, E484K, and N501Y) disrupt the binding of a number of potent neutralising mAbs, including some antibodies being developed for clinical use[22].

We also observed a remarkable reduction of neutralisation on Delta by Beta infected patient serum, which indicates the antigenic distance between Beta and Delta strains[80]. To understand the antigenic landscape of Beta at an epitope level, and to find a potential candidate for clinical usage, we produced a substantial panel of mAbs isolated from memory B cells of convalescent Beta infection patient samples. We isolated 647 mAbs from 5 donors, and identified 27 potent neutralising mAbs (against Beta, FRNT50 < 100 ng/ml). Neutralisation assays were performed on a variety of live viruses, indicating that most mAbs showed restricted neutralisation of a set of strains. The majority of potent mAbs target the mutations present in the Beta RBD, principally E484K and N501Y, showing the small antigenic distance between Beta and Gamma. Only a small number of mAbs can neutralise Delta, highlighting the large antigenic distance between Beta and Delta[80].

5.2 Results

5.2.1 mAb generation from Beta infected patient samples

Blood samples from 18 volunteers in the UK, who had recovered 4-8 weeks after Beta infection were collected, and plasma and PBMC were isolated in the lab. Beta infection was confirmed by viral sequencing or was inferred to have suffered Beta infection as they became infected after being isolated following contact with a proven Beta-infected cases. ELISA binding assay against full-length Beta S protein and FRNT assays against Victoria and Beta

were performed, and 5 cases with the highest titres were selected for antibody isolation (Figure 5.1A and 5.1B). As expected, FRNT50 titres were higher on Beta than Victoria.

We used antigen-specific single cell sorting to isolate memory B cells as we reported previously. PBMC were stained with full-length double Strep tagged Beta S, and IgG^+ B cells binding Beta S were single cell sorted (Figure 5.1C and 5.1D). RT-PCR and Nested-PCR were conducted to recover IgVH and IgVL sequences, and heavy chain and light chain-expressing plasmids were created using a Gibson assembly reaction. Gibson assembly products were transfected into HEK-293T cells in 24-well plates, and supernatants were harvested and tested in neutralisation assays against Beta virus at a final concentration of 0.1-1 μg/ml. mAbs showing >90% neutralisation in the initial assay were selected for further study. In total, we isolated 674 mAb IgGs from the 5 samples, 22% among them bound to RBD epitopes, 78% bound to non-RBD epitopes, and 18% of the RBD-specific mAbs achieved >90% neutralisation (Figure 5.1E and 5.1F). We performed Spike-ACE2 binding inhibition assay for the 27 potent mAbs, most of which were able to block ACE2 binding to S, although there were exceptions, like Beta-43, Beta-49, Beta-50, and Beta-53 (Figure 5.1G).

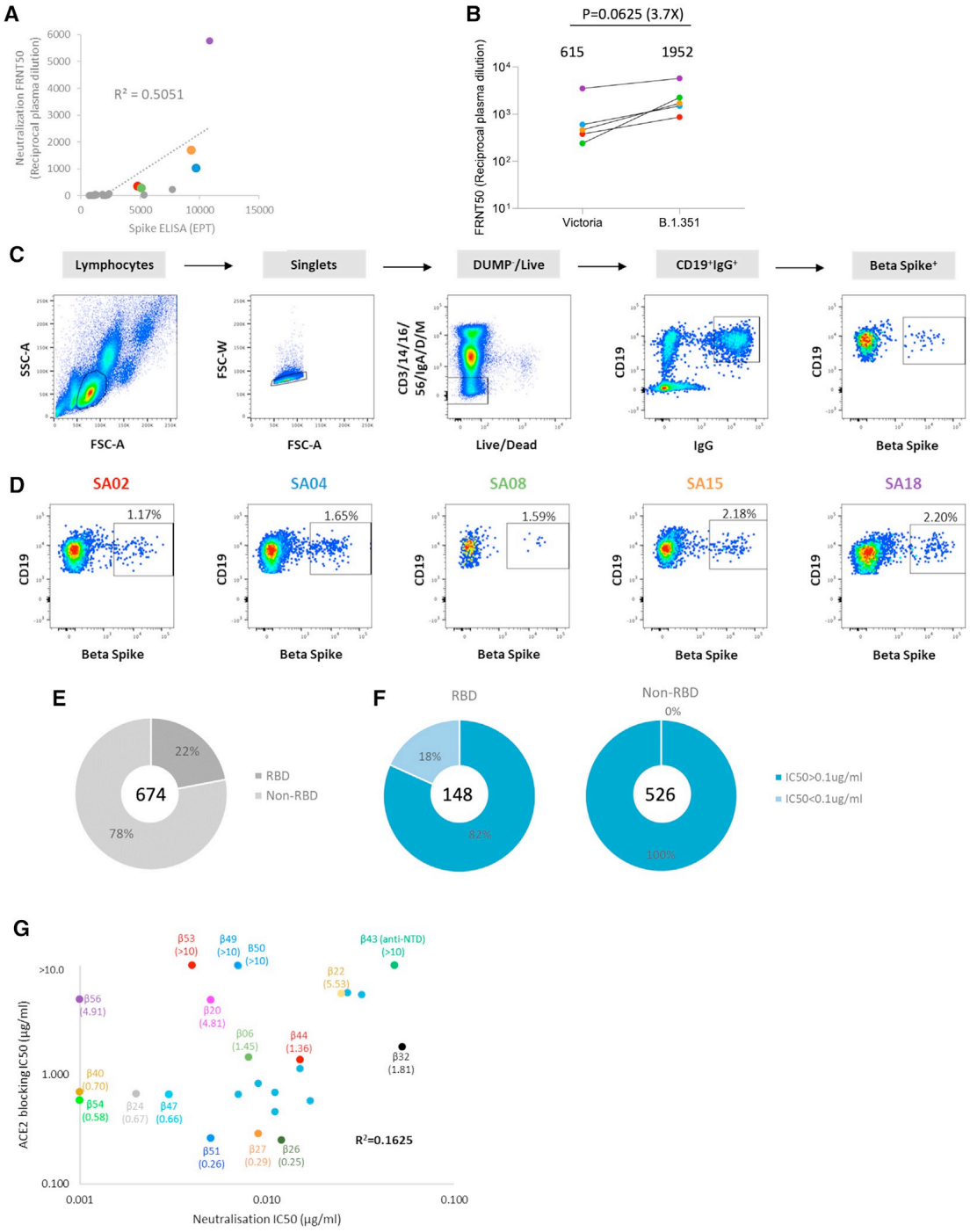

Figure 5.1 Isolation and characterisation of Beta mAbs. (A) Comparison of Beta SARS-CoV-2 neutralisation and S binding ELISA by convalescent plasma from confirmed Beta infected donors. (B) Neutralisation titres against Victoria and Beta strains for the 5 selected plasma samples, analysis used the Wilcoxon matched-pairs signed rank test and two-tailed p values were calculated; geometric means are indicated above each column. (C) Schematic of the Beta mAb isolation strategy. (D) Antigen-specific single B cells were isolated using labelled recombinant S protein as bait. The frequency of S-positive IgG^+ B cells was measured by FACS. (E) Epitope mapping of Beta SARS-CoV-2 specific mAbs against S and RBD were measured by ELISA. (F) FRNT50 test of anti-S (non-RBD) and anti-RBD mAbs against Beta live virus. (G) Comparison of IC50 values for ACE2-S blocking and FRNT50 titres for the 27 potent mAbs.

5.2.2 Cross-reactivity of Beta mAbs

Neutralisation assays using Beta mAbs were performed using the following authentic viruses with RBD mutations indicated in brackets: Victoria (an early pandemic strain), Alpha (N501Y), Beta (K417N, E484K, and N501Y), Gamma (K417T, E484K, and N501Y), Delta (L452R and T478K), Alpha+E484K (E484K and N501Y), and B.1.525 (E484K) (Figure 5.2A-5.2F; Table 5.1).

All mAbs can effectively neutralise Beta strains with FRNT50 as low as 1 ng/ml (Table 5.1). mAbs are varied on cross-reactivity between different variants, with some fully cross-neutralising mAbs such as Beta-27, -32, -47, -48, -49, -50, and -53 showing <10-fold difference between FRNT50s (Figure 2A). A big set of mAbs, including Beta-6, -10, -23, -24, -30, -40, -54, -55, and -56, showed good neutralisation against Alpha, Beta, Gamma, and Alpha+ variants, with either reduced neutralisation or completely knocked-out by Victoria, B.1.525 (E484K), and Delta (Figure 5.2B). We propose that the lack of neutralisation on these variants is due to the lack of N501Y mutation, and this mutation is the epitope for RBD recognition of this set of mAbs.

E484K mutation disrupts the binding of many potent mAbs we tested previously[22]. We inferred six mAbs to recognise Lys-484 due to the reduced activity to Alpha while regaining activity on Alpha+484K, which are Beta-26, -33, -34, -38, -45, and -51 (Figure 5.2C). Three mAbs, Beta-20, -22, and -29 showed maximum activity toward Beta and Gamma, but at least >5 fold, mostly >100-fold reduction on other variants, suggesting that they recognise an epitope related to the K417N/T changes in Beta and Gamma.

Four mAbs, Beta-26, -34, -44, and -51, showed selective loss of neutralisation to Delta (FRNT50 > 10 μg/ml). We propose that Beta-44 is vulnerable to L452R/T478K mutations, while Beta-26, -34, and -51 recognise an epitope composed of K484 + L452/T478 (Figure 5.2C and 5.2E). We also have a single potent NTD-specific mAb, Beta-43, which specifically neutralises Beta.

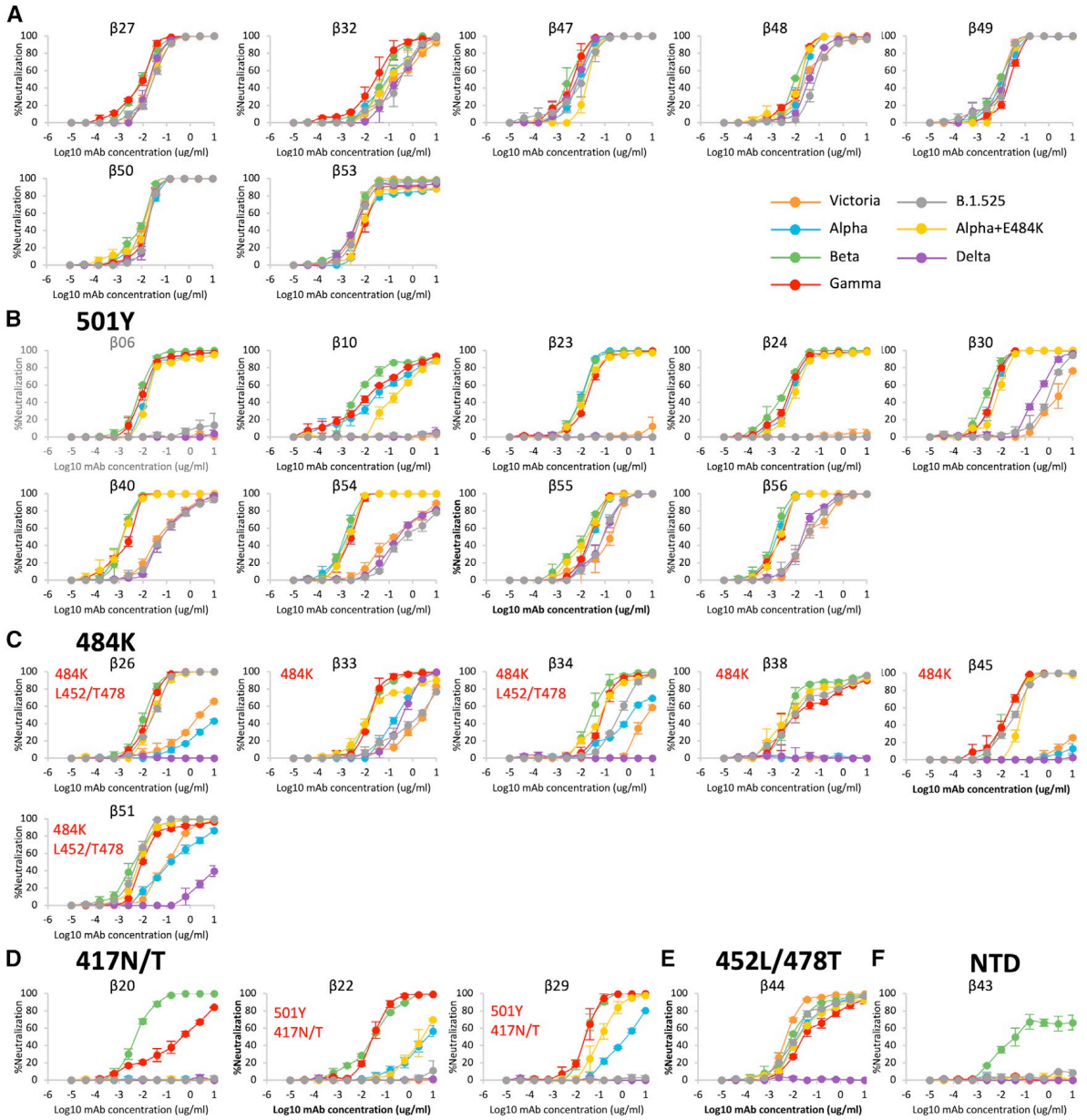

Figure 5.2 Cross-reactivity of Beta mAbs. Neutralisation assays performed against Victoria, Alpha (N501Y), Beta (K417N, E484K, and N501Y), Gamma (K417T, E484K, and N501Y), Delta (L452R and T478K), Alpha+E484K (E484K and N501Y), and B.1.525 (E484K) authentic viruses with 27 potent Beta mAbs. mAbs are grouped by the patterns of cross-reactivity between the viral variants, potential binding determinants are indicated for the mAbs that show differential neutralisation between isolates. Data are shown as mean ± SEM. (A) Fully cross-reactive mAbs, (B) N501Y-dependent mAbs, (C) E484K-dependent mAbs, (D) K417N/T-dependent mAbs, (E) L452R/T478K-dependent mAbs, and (F) an NTD-binding mAb.

Table 5.1 IC50 titres of 28 Beta SARS-CoV-2-specific human mAbs against live virus strains

mAbs	IC50 (ug/ml)*						
	Victoria	Alpha	Beta	Gamma	Alpha+E484K	B.1.525	Delta
β06	>10	0.024 ± 0.002	0.008 ± 0.002	0.015 ± 0.003	0.034 ± 0.003	>10	>10
β10	>10	0.064 ± 0.042	0.015 ± 0.000	0.025 ± 0.011	0.322 ± 0.071	>10	>10
β20	>10	>10	0.005 ± 0.001	0.345 ± 0.122	>10	>10	>10
β22	>10	6.580 ± 2.988	0.025 ± 0.004	0.030 ± 0.007	3.672 ± 1.538	>10	>10
β23	>10	0.009 ± 0.001	0.011 ± 0.001	0.020± 0.000	0.019 ± 0.002	>10	>10
β24	>10	0.007 ± 0.001	0.002 ± 0.001	0.005 ± 0.001	0.011 ± 0.003	>10	>10
β26	2.742 ± 0.208	>10	0.012 ± 0.003	0.016 ± 0.000	0.030 ± 0.009	0.025 ± 0.001	>10
β27	0.018 ± 0.002	0.018 ± 0.000	0.009 ± 0.000	0.006 ± 0.002	0.026 ± 0.002	0.025 ± 0.004	0.021 ± 0.004
β29	>10	1.372 ± 0.016	0.027 ± 0.003	0.023 ± 0.009	0.149 ± 0.065	>10	>10
β30	2.643 ± 0.880	0.004 ± 0.001	0.003 ± 0.001	0.004 ± 0.000	0.007 ± 0.002	0.966 ± 0.239	0.350 ± 0.035
β32	0.248 ± 0.003	0.119 ± 0.044	0.053 ± 0.025	0.027 ± 0.014	0.173 ± 0.097	0.257 ± 0.171	0.267 ± 0.068
β33	2.016 ± 0.051	0.234 ± 0.013	0.017 ± 0.003	0.017 ± 0.001	0.042 ± 0.014	1.359 ± 0.406	0.334 ± 0.005
β34	8.241 ± 1.067	1.466 ± 0.136	0.032 ± 0.010	0.092 ± 0.003	0.072 ± 0.002	0.387 ± 0.034	>10
β38	>10	>10	0.011 ± 0.003	0.043 ± 0.025	0.017 ± 0.010	0.021 ± 0.006	>10
β40	0.075 ± 0.005	0.001 ± 0.000	0.001 ± 0.000	0.001 ± 0.000	0.001 ± 0.001	0.118 ± 0.045	0.107 ± 0.031
β43	>10	>10	0.048 ± 0.024	>10	>10	>10	>10
β44	0.007 ± 0.002	0.028 ± 0.008	0.015 ± 0.008	0.071 ± 0.026	0.035 ± 0.005	0.019 ± 0.001	>10
β45	>10	>10	0.018 ± 0.003	0.015 ± 0.006	0.068 ± 0.010	0.027 ± 0.005	>10
β47	0.006 ± 0.001	0.008 ± 0.003	0.003 ± 0.001	0.004 ± 0.002	0.018 ± 0.003	0.010 ± 0.007	0.005 ± 0.000
β48	0.034 ± 0.011	0.020 ± 0.008	0.009 ± 0.001	0.011 ± 0.001	0.011 ± 0.001	0.087 ± 0.016	0.042 ± 0.016
β49	0.009 ± 0.000	0.011 ± 0.001	0.007 ± 0.000	0.019 ± 0.003	0.014 ± 0.002	0.008 ± 0.002	0.008 ± 0.003
β50	0.011 ± 0.000	0.014 ± 0.006	0.007 ± 0.001	0.015 ± 0.005	0.010 ± 0.002	0.018 ± 0.001	0.019 ± 0.005
β51	0.119 ± 0.008	0.242 ± 0.024	0.005 ± 0.000	0.019 ± 0.001	0.008 ± 0.003	0.005 ± 0.001	>10
β53	0.005 ± 0.000	0.032 ± 0.009	0.004 ± 0.000	0.017 ± 0.001	0.023 ± 0.009	0.008 ± 0.001	0.007 ± 0.000
β54	0.232 ± 0.092	0.002 ± 0.001	0.001 ± 0.000	0.002 ± 0.001	0.002 ± 0.000	0.834 ± 0.247	0.409 ± 0.071
β55	0.108 ± 0.069	0.028 ± 0.004	0.010 ± 0.003	0.022 ± 0.001	0.014 ± 0.003	0.075 ± 0.016	0.076 ± 0.020
β56	0.046 ± 0.013	0.001 ± 0.000	0.001 ± 0.000	0.002 ± 0.000	0.002 ± 0.000	0.034 ± 0.014	0.022 ± 0.002

*Data are from 2 independent experiments, each with duplicate wells and the data are shown as mean ± s.e.m.

5.2.3 Antibody gene usage

The IgVH and IgVL gene usages of the 27 potent Beta Abs are shown in Figure 5.3A with more detailed breakdown in Table 5.2. The 7 full cross-neutralising mAbs came from different IgVH families, apart from Beta-49 and -50, which were IgVH1-69. Beta-27 uses IgVH3-53, which is a public response to RBD, highly represented in mAbs isolated from individuals infected with early pandemic strains (5 out of 20 potent mAbs FRNT < 100 ng/ml in previous study[123]), but only occurred twice here. Similarly, another public gene family, IgVH1-58, was found in a number of potent mAbs isolated previously (4/20 in early pandemic mAbs), but only has one representative in this set (Beta-47).

Tyr-501-reactive mAbs were the most represented in all potent antibodies, with 11 out of 27. 6/11 of the Tyr-501-reactive mAbs used IgVH 4-39 (Beta-6, -10, -23, -40, -54, and -55), making IgVH4-39 a public antibody response following Beta infection. 6/27 IgVH 4-39 mAbs in Beta set, comparing with 0/20 in the potent mAbs generated from early pandemic cases (p=0.0241, two-proportion Z-test). The six Lys-484-reactive mAbs came from diverse IgVH backgrounds.

The 27 Beta mAbs show low levels of somatic hypermutations with median 7 changes in IgVH and IgVL (Figure 5.3B), which is consistent with the low level of hypermutation seen in early pandemic mAbs (median IgVH = 5, IgVL = 3)[123].

In summary, potent Beta mAbs show significant difference in their cross-neutralising ability against SARS-CoV-2 variants compared with neutralisation profile of early pandemic mAbs. The existence of E484K and N501Y mutations also differ the IgVH and IgVL usages of Beta mAbs with early pandemic mAbs. The domination of Tyr-501 and Lys-484 epitopes to the immune response leads to a number of mAbs failing to neutralise Victoria and Delta, which underscores the antigenic distance between these viruses and Beta[80]. Neutralisation of Delta is further impaired by a subset of mAbs that are sensitive to the RBD mutations in Delta, explaining why Beta and Delta occupy the most distant position on the antigenic landscape[80].

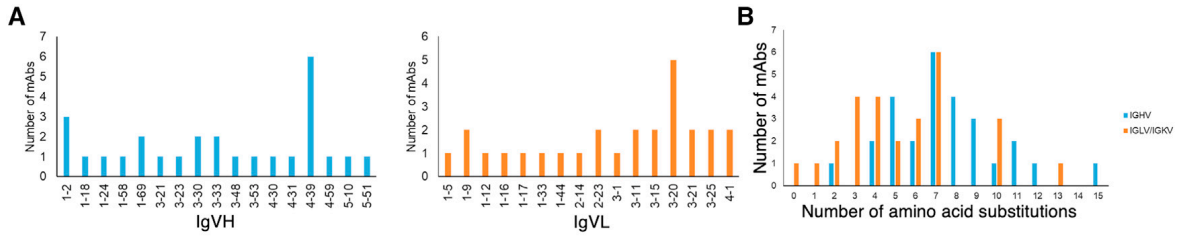

Figure 5.3 Gene usage analysis of Beta mAbs. (A) IgVH and IgVL gene usage and (B) amino acid substitutions in IgVH and IgVL of the 27 potent mAbs.

Table 5.2 Immunoglobulin heavy and light chain gene families of 27 Beta mAbs.

mAbs	Patient No.	Predicted contact residues	HC				LC			
			V-GENE	J-GENE	D-GENE	#Amino acid substitutions	K/λ	V-GENE	J-GENE	#Amino acid substitutions
β06	SA02	501Y	4-39*07	4*02	3-16*02	9	K	3-11*01	5*01	7
β10	SA02	501Y	4-39*07	5*02	3-16*01	5	K	1-9*01	5*01	2
β20	SA02	417N/T	3-33*08	6*03	5-18*01	7	K	3-20*01	4*01	3
β22	SA02	417N/T, 501Y	3-30*03 or 3-30*18 or 3-30-5*01	6*02	2-2*01	7	K	4-1*01	3*01	7
β23	SA02	501Y	4-39*07	4*02	3-10*01	5	λ	3-1*01	1*01	7
β24	SA02	501Y	4-30-4*08	5*02	2-2*01	8	λ	2-23*01 or 2-23*03	1*01	10
β26	SA04	484K, 452L/478T	4-59*01	3*02	2-15*01	8	λ	3-21*02	1*01	4
β27	SA04	Fully cross-neutralizing	3-53*04	6*02	3-3*01	7	K	3-20*01	4*01	7
β29	SA04	501Y, 417N/T	3-30*03 or 3-30*18 or 3-30-5*01	3*01	2-21*02	11	K	4-1*01	5*01	5
β30	SA15	501Y	1-2*02	5*02	4-11*01	8	K	1-17*01	3*01	4
β32	SA15	Fully cross-neutralizing	1-2*02	5*02	3-22*01	5	K	1-12*01 or 1-12*02 or 1D-12*02	1*01	1
β33	SA15	484K	1-2*02	6*02	3-16*01	6	λ	3-25*03	1*01	7
β34	SA02	484K, 452L/478T	3-48*04	3*02	1-14*01	7	K	3-11*01	4*01	5
β38	SA15	484K	5-51*03	6*02 or 6*03	1-26*01	4	λ	1-44*01	1*01	2
β40	SA15	501Y	4-39*01	5*02	2-15*01	6	λ	3-25*03	2*01 or 3*01	13
β43	SA15	Non-RBD	3-33*01 or 3-33*06	6*02	2-15*01	4	λ	3-21*04	1*01	6
β44	SA15	452L/478T	1-18*01	5*02	3-10*01	2	λ	2-23*01 or 2-23*03	3*02	3
β45	SA15	484K	3-23*04	6*02	2-2*01	15	K	1-33*01 F, or 1D-33*01	4*01	4
β47	SA18	Fully cross-neutralizing	1-58*03	3*02	2-2*01	9	K	3-20*01	3*01	6
β48	SA18	Fully cross-neutralizing	3-21*01	3*02	1-26*01	9	K	3-15*01	1*01	10
β49	SA18	Fully cross-neutralizing	1-69*01, or 1-69D*01	4*02	1-26*01	8	K	3-20*01	1*01	4
β50	SA18	Fully cross-neutralizing	1-69*01, or 1-69D*01	4*02	1-26*01	11	K	3-20*01	2*01	6
β51	SA18	484K, 452L/478T	1-24*01	4*02	6-19*01	5	K	1-16*02	5*01	3
β53	SA18	Fully cross-neutralizing	5-10-1*03	4*02	5-24*01	7	K	3-15*01	1*01	3
β54	SA18	501Y	4-39*01	5*02	6-19*01	10	K	1-9*01	4*01	0
β55	SA18	501Y	4-39*01 F	3*02	3-22*01	7	K	1-5*03	1*01	7
β56	SA18	501Y	4-31*06	4*02	6-6*01	12	λ	2-14*03	2*01 or 3*01	10

5.2.4 Quantitative dissection of differences in mAb responses

The neutralisation profile of the 27 potent Beta mAbs we isolated in this study appeared markedly different from the 20 potent mAbs we generated from convalescent samples infected by early pandemic strains. To qualify this, Helen M. Ginn from Diamond Light Source Ltd devised a neutralisation-correlation method, comparing the neutralisation results of mAbs against seven virus strains between all possible pairs of the 47 potent mAbs. The metric for the comparison was the correlation coefficient between the neutralisation results for the two mAbs. Displaying this as a heat matrix (Figure 5.4A) reveals clear differences between the early pandemic mAbs and Beta mAbs. Cluster analysis effectively separated the two sets (Figure 5.4B), demonstrating that the pattern of strain neutralisation is similar within but significantly different between the two sets ($p < 0.00001$ for the Mann-Whitney U test). Further cluster dissection of the Beta mAbs (Figure 5.4C) segregates them according to their specificities to the individual RBD mutations described in Figure 5.2.

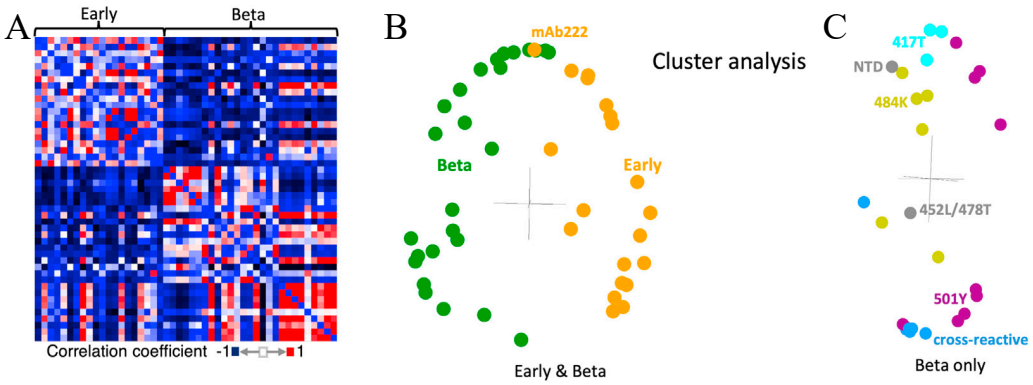

Figure 5.4 Computational analysis of the Beta mAbs. (A) Cross-correlation matrix showing agreement of neutralization titres for mAbs against seven variants of SARS-CoV-2. Every antibody is associated with a vector containing the residual neutralization titre after subtracting the mean for each variant and normalizing to a standard deviation of 1. (B) Major modes of variation after singular value decomposition of the matrix in (A). (C) Major modes of variation after singular value decomposition of a matrix similar to (B) but calculated for Beta mAbs and coloured according to their designation as a fully cross-reactive, 501Y-specific, 484K-specific, or 417T-specific mAbs. The experiments were conducted by Dr. Daming Zhou.

5.2.5 Potent mAbs protect against Beta infection in mice model

To test the therapeutic activity of Beta mAbs in vivo, a human ACE2 transgenic mouse model[142,143] was used by Natasha M. Kafai, Adam L. Bailey, and Rita E. Chen of Washington University School of Medicine as described in chapter *3.2.6*. Four Beta mAbs representing different epitope classes were selected to test on mouse model: Beta-20, which recognises K417N/T mutation and neutralises Beta potently and to a lesser extent Gamma; Beta-24, which recognise the N501Y mutation existing in Alpha, Beta, and Gamma; Beta-26, which is specific to the E484K mutation in Beta and Gamma; and Beta-27, which potently neutralises all variants.

Mice were inoculated with 10^3 FFU of Beta and a single 10 mg/kg does of mAb were administered via intraperitoneal injection at 24 hours post inoculation. All four Beta mAbs, but not an isotype control mAb (hE16), prevented weight loss over the 6 days following inoculation and reduced viral loads in the lung and brain but not in nasal wash (Figure 5.5A-D). These results demonstrated that all the Beta mAbs we tested here can efficiently protect host from severe infection and prevent systemic disease, but do not prevent viral infection in the upper respiratory tract.

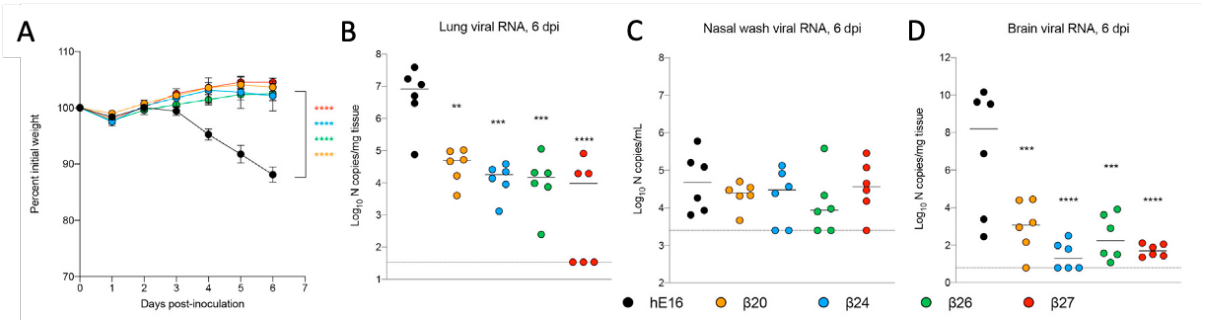

Figure 5.5 Therapeutic use of Beta mAb in K18-hACE2 mice. 8-week-old female K18-hACE2 transgenic mice were intranasally inoculated with 10^3 FFU of SARS-CoV-2 Beta strain. 24 hours after inoculation, mice were intraperitoneally injected with a single 10 mg/kg dose of the indicated mAb. Tissues were collected at 6dpi. (A) Weight change following Beta infection (mean ± SEM; n = 6 mice per group, two experiments; one-way ANOVA with Dunnett's test of area under the curve: ****p < 0.0001). Viral RNA levels in the lung (B), nasal wash (E), and brain (F) (lines indicate median; n = 6 mice per group, two experiments; one-way ANOVA with Dunnett's test with comparison to control mAb: **p < 0.01; ***p < 0.001, ****p < 0.0001. Dotted lines indicate the limit of detection of the assay). The experiments were conducted by Natasha M. Kafai, Adam L. Bailey, and Rita E. Chen.

5.2.6 Beta mAb epitope mapping using BLI

A matrix of pairwise BLI measurements on the potent Beta mAbs were acquired with some early pandemic mAbs of known binding sites by Dr. Daming Zhou. The mAbs do not segregate into epitopes, but cluster analysis shows that they nearly all fall in an arc, spanning the neck and shoulders of the RBD (Figure 5.6).

There is a good correlation between epitope prediction based on neutralisation results and the BLI data. For example, Beta-44, which is sensitive to L452R/T478K mutations, is perched adjacent to residue 478, while Beta-20, -22, and -29, which are suggested by neutralisation data to recognise an epitope related to residue 417, are tightly clustered atop this residue. Surprisingly, Beta-49 and Beta-50 showed very low affinity to Beta RBD, although they can tightly bound to full-length S, hence could not be mapped.

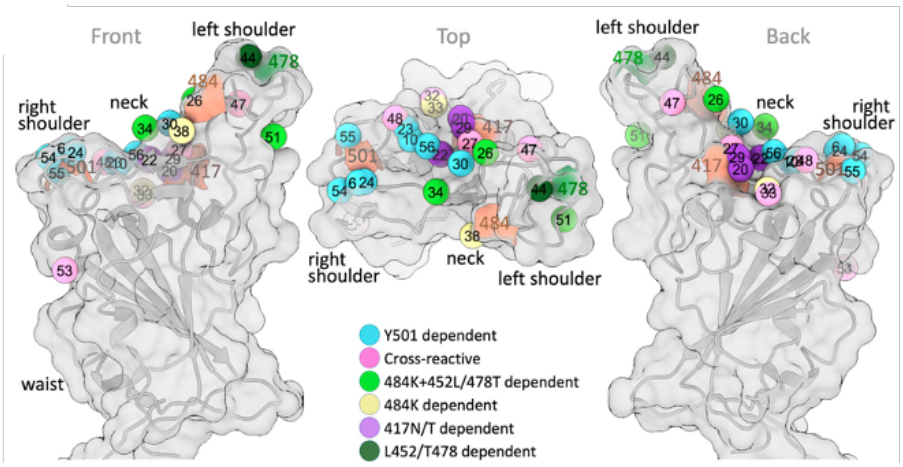

Figure 5.6 Mapping of the Beta mAbs based on BLI competition measurement. The mean positions of the mAbs are shown as spheres. Numbers match the antibody definitions in Table 5.1 with Beta omitted for clarity, coloured by one aspect of the serological properties. Anatomical terms related to the torso analogy[123]. The RBD is shown as a semi-transparent surface with cartoon embedded. The outer two are related by 180° rotation about the vertical axis, and the central view is related to the "front" view by a 90° rotation about the horizonal axis. The experiments were conducted by Dr. Daming Zhou and figures were depicted by Dr. Helen M. Ginn.

5.2.7 Two IgVH1-69 mAbs target a neutralising epitope conserved between SARS-CoV-1 and SARS-CoV-2

Beta-49 and -50 have very similar heavy chain and light chain sequences (Figure 5.7A), potently neutralise all strains of SARS-CoV-2 we tested here (Figure 5.2A), bound tightly to the full S trimer but only bound very weakly to the RBD and did not block binding of ACE2-Spike binding (Figure 5.1G and Figure 5.7B). Both mAbs belong to IgVH1-69 gene family, and Dr. Daming Zhou and Dr. Helen M.E. Duyvesteyn from Division of Structure Biology, University of Oxford, solved the crystal structures of Fab/RBD complexes and cryo-EM Fab/S complexes for both (Figure 5.7C and 5.7D).

The structures of Beta-49 and Beta-50 Fab/S (Figure 5.7D) shows both mAbs bound to the same site, despite the 19 amino acid differences in the variable domain of the heavy chain (VH) alone (Figure 5.7A and E). The epitope positions at the "waist" region of the RBD includes the N- and C- terminal junctions of the RBD and also harbours the N-linked glycan attached to residue 343 (Figure 5.7F). The cryo-EM image of Fab-S trimer complex shows all three RBDs in a "down" configuration (Figure 5.7D), with the heavy chain interacting with two different RBDs (Figure 5.7G). The presence of a secondary RBD epitope in the 1Fab:2RBD interaction, and fact that the primary epitope involves residues at the very ends of the soluble RBD construct likely explains the low affinity of Beta-49 and -50 to soluble monomeric RBD. The

residues comprising the primary (but not the secondary) epitope are conserved between SARS-CoV-1 and -2 (Figure 5.7J), and here we show that both mAbs bind to SARS-CoV-1 and SARS-CoV-2 S to a similar degree (Figure 5.7K). Finally we show that, Beta-49 and -50 potently neutralise SARS-CoV-1 pseudovirus (Figure 5.7L).

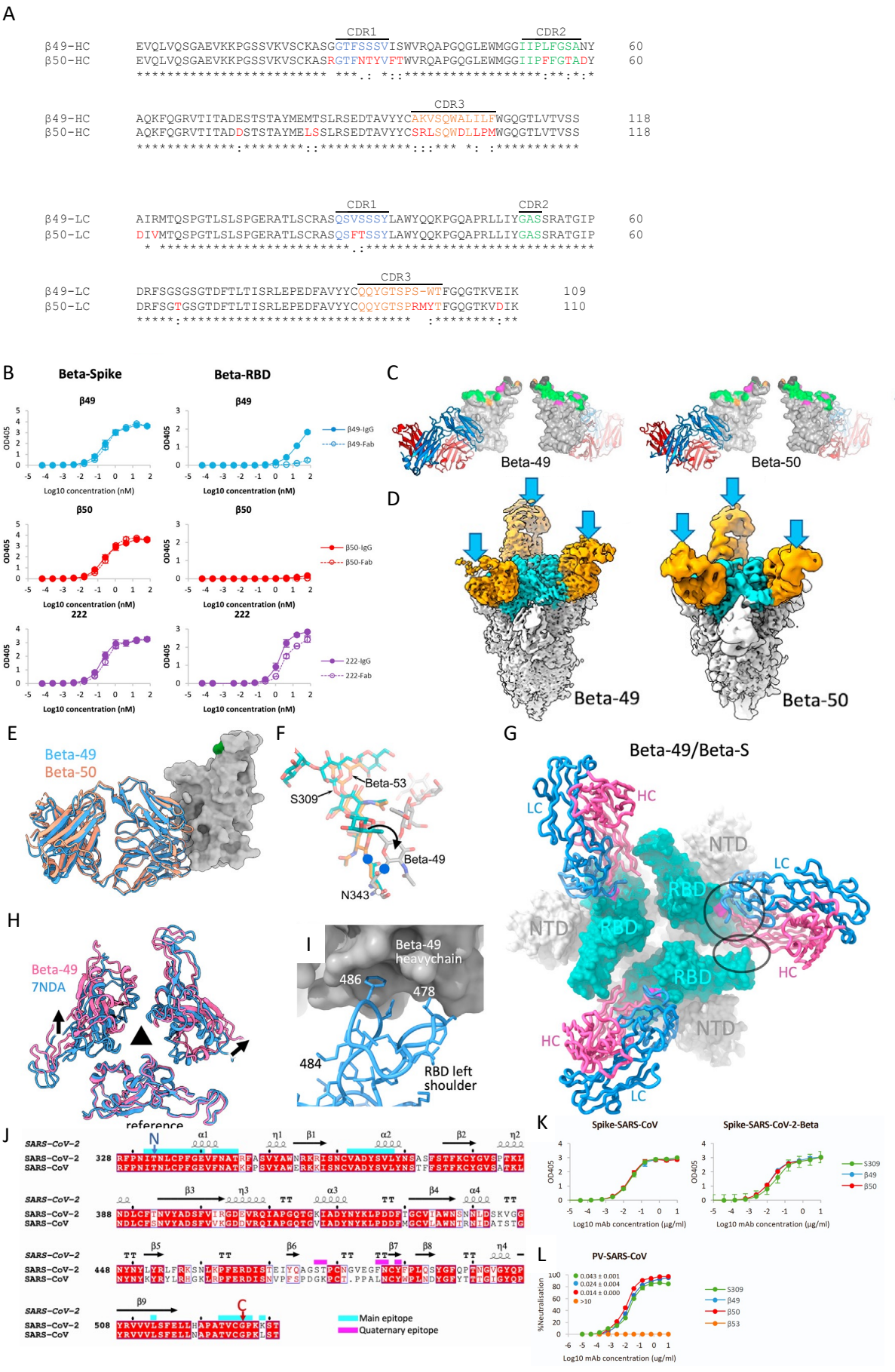
A
CDR1
CDR2
β49-HC EVQLVQSGAEVKKPGSSVKVSCKASGGTFSSSVISWVRQAPGQGLEWMGGIIPLFGSANY 60
β50-HC EVQLVQSGAEVKKPGSSVKVSCKASRGTFNTYVFTWVRQAPGQGLEWMGGIIPFFGTADY 60
CDR3
β49-HC AQKFQGRVTITADESTSTAYMEMTSLRSEDTAVYYCAKVSQWALILFWGQGTLVTVSS 118
β50-HC AQKFQGRVTITADDSTSTAYMELSSLRSEDTAVYYCSRLSQWDLLPMWGQGTLVTVSS 118
CDR1
CDR2
β49-LC AIRMTQSPGTLSLSPGERATLSCRASQSVSSSYLAWYQQKPGQAPRLLIYGASSRATGIP 60
β50-LC DIVMTQSPGTLSLSPGERATLSCRASQSFTSSYLAWYQQKPGQAPRLLIYGASSRATGIP 60
CDR3
β49-LC DRFSGSGSGTDFTLTISRLEPEDFAVYYCQQYGTSPS-WTFGQGTKVEIK 109
β50-LC DRFSGTGSGTDFTLTISRLEPEDFAVYYCQQYGTSPRMYTFGQGTKVDIK 110
B
Beta-Spike
Beta-RBD
β49
β50
222
OD405
Log10 concentration (nM)
β49-IgG
β49-Fab
β50-IgG
β50-Fab
222-IgG
222-Fab
C
Beta-49
Beta-50
D
Beta-49
Beta-50
E
Beta-49
Beta-50
F
Beta-53
S309
Beta-49
N343
G
Beta-49/Beta-S
HC
LC
NTD
RBD
H
Beta-49
7NDA
reference
I
Beta-49
heavychain
486
478
484
RBD left
shoulder
J
SARS-CoV-2
SARS-CoV
Main epitope
Quaternary epitope
K
Spike-SARS-CoV
Spike-SARS-CoV-2-Beta
Log10 mAb concentration (μg/ml)
S309
β49
β50
L
PV-SARS-CoV
%Neutralisation
0.043 ± 0.001
0.024 ± 0.004
0.014 ± 0.000
>10
Log10 mAb concentration (ug/ml)
S309
β49
β50
β53

Figure 5.7 Structural details of IgVH1-69 mAbs Beta 49 and Beta 50. (A) Alignment of amino acid sequences of heavy chains and light chains of Beta 49 and Beta 50. (B) Binding of Beta-49 and -50 Fab and IgG1 to Beta S trimer or Beta RBD measured by ELISA, early pandemic mAb 222 is used for comparison, data are shown as mean ± s.e.m. (C) Front and back views of Beta RBD/Beta-49 Fab and Beta RBD/Beta-50 Fab. Fabs are drawn as ribbons with HC red and LC blue, and RBDs as grey surfaces with ACE2 footprint in green, mutation sites of the Beta variant in magenta and Delta variant in orange. (D) Cryo-EM maps of Beta S complexes with Beta-49 and -50. The bound Fabs are orange, RBD domains cyan, and the rest of S grey. Arrows indicate the RBD orientations. (E) Binding model of Beta-49 (blue) and Beta-50 (salmon) to the RBD. (F) Overlay of N343 RBD glycan from the S309[56] (green), Beta-53 (yellow) and Beta-49 (grey) complexes, the side chain rotated into an unfavourable conformation in the latter. (G) Top view of the Beta-49 Fab/Beta S complex. S is shown as a surface (RBD cyan, position of glycan attachment to residue 343 magenta) while Beta-49 HC (dark pink) and LC (blue) are shown as cartoons. The HC contacts two RBDs, forming a primary (circle) and secondary (ellipse) epitope. (H) Top view of the RBDs in all RBD down S (PDB 7NDA) and in the Beta-49 bound state. The 3-fold axis of S is shown. One RBD is superposed (reference), arrows show the movement in the other RBDs induced on binding Beta-49. (I) Close up of the secondary epitope with some RBD residues marked. (J) Sequences of the RBD region for SARS-CoV-2 and SARS-CoV-1. The conserved major epitope is marked in cyan, N and C mark the ends of the natural sequence in the soluble RBD construct. Secondary structure in SARS-CoV-2 is marked above and sequence numbers are given for SARS-CoV-2. Drawn with ESPript[157]. (K) Cross-reactivity of Beta-49, and -50 with SARS-CoV and Beta S trimer measured by ELISA, comparison is made with mAb S309. (L) SARS-CoV pseudovirus neutralisation curves for mAb S309, Beta-49, -50, and -53. Figure C-I were made by Dr. Daming Zhou and Dr. Helen M.E. Duyvesteyn, and Figure J was depicted by Dr. Jingshan Ren.

5.3 Discussion

In this study, we presented a structural-based function analysis of potent mAbs isolated from Beta-infected patient samples. There is a significant shift in the neutralisation profile of the antibody response in Beta infection cases compared with infection with early pandemic strains (Figure 5.4), with most of the potent Beta mAbs repositioned to interact with the three RBD amino acid changes found in Beta, 3/27 at K417N, 6/27 at E484K, and especially N501Y, which has 11/27 mAbs[158]. This underlines the antigenic difference between Beta and the other VoCs tested here, including early pandemic strains. In the 27 mAbs, there are profound reductions in the neutralisation ability of Beta mAbs against Victoria, with 10/27 mAbs were knocked out, while the reductions are even more extreme with Delta (14/27 knocked out). Delta has 5 different amino acids in the RBD with Beta (K417, L452, T478, E484, and N501), while Beta and Gamma are more antigenically close, only one Beta mAb is knocked out by Gamma. These data are consistent with the neutralisation data using Beta and Gamma serum, which have remarkably reduced neutralisation ability against Delta[80].

A pair of potent cross-reactive mAbs (Beta-49 and -50) belong to the IgVH1-69 gene family and bind to the "waist" of the RBD, an epitope that is conserved in SARS-CoV (Figure 5.7 I) and are also capable of neutralising SARS-CoV pseudovirus. The possible mechanism of

neutralisation of the mAbs may be to lock the RBDs in an unusual “down and out” conformation.

Despite the skewed antibody response by the three mutations on the RBD after Beta infection, we also identified 7 cross-reactive mAbs which potently neutralise all variants tested, including Delta. But more mutations have been accumulating in the RBD region and more variants is coming. It will be interesting to see how these potent cross-reactive mAbs will perform on neutralising newly emerged variants.

CHAPTER 6 Potent cross-reactive antibodies following BA.1 breakthrough infection

6.1 Introduction

From late 2020 until mid-2021, four VoCs emerged in the world. Some caused large regional outbreaks, like Beta[22] and Gamma[23], while others dominated globally, like Alpha[79] and Delta[80]. All VoCs harbour mutations in their RBD region, which can serve two functions: first is to increase the affinity of the spikes binding on host cell surface receptor ACE2 and potentially increase their transmissibility, as observed for Alpha, Beta, and Gamma; second is to provide the variants with immune escape from serum induced by vaccination or previous infection. Escape from serum neutralisation is modest for Alpha, while more marked for Beta, Gamma, and Delta.

First reported to WHO on 24 November 2021 from South Africa (https://www.who.int/news/item/26-11-2021-classification-of-omicron-(b.1.1.529)-sars-cov-2-variant-of-concern), BA.1, which was given the name Omicron, spread around the world speedily and dominated in the UK by 17 December 2021 (https://assets.publishing.service.gov.uk/government/uploads/system/uploads/attachment_data/file/1042100/20211217_OS_Daily_Omicron_Overview.pdf). BA.1 contains an unprecedented 30 amino acid substitutions, 6 deletions and 3 insertions in the S gene, which likely lead to altered ACE2 affinity and loss of neutralisation by serum from vaccination or natural infection, and also reduce the neutralisation or completely knock out the mAbs we generated from early pandemic and Beta cases[81].

In February 2022, two sub-lineages of BA.1 were identified: BA.1.1 and BA.2 (https://www.who.int/publications/m/item/weekly-epidemiological-update-on-covid-19---1-february-2022). Compared to BA.1, BA.1.1 contains an additional R346K mutation in RBD, while BA.2 has 8 unique mutations in its S with 6 of them in RBD and lacks 13 mutations found in BA.1. BA.2 gradually replaced BA.1 and became the dominant strain in England (https://www.gov.uk/government/news/covid-19-variants-identified-in-the-uk-latest-updates). The new mutations occurred in BA.1.1 and BA.2 may cause breakthrough infections in vaccinated population and even in BA.1 infected population[128].

In this study, we investigated the neutralisation of BA.1 by serum samples collected from convalescents of early pandemic, Alpha, Beta, Gamma, and Delta infected patients with vaccinees who had received three doses of the Oxford/AstraZeneca (AZD1222) or the Pfizer BioNtech (BNT16b2) vaccines. We also tested the neutralising abilities of mAbs isolated from early pandemic and Beta infected convalescent samples.

545 mAbs were isolated from samples collected following vaccine breakthrough BA.1 infections and 28 most potent mAbs (IC50 < 100 ng/ml against BA.1) were identified and analysed in detail. In addition to BA.1, the immune escape ability of Omicron sublineages BA.1.1 and BA.2 were also studied to assess their risk of generating breakthrough infection.

6.2 Results

6.2.1 RBD of BA.1 compared with early VoCs

There are 30 amino acid substitutions in the S of BA.1, with a further 6 deletions and 3 insertions (Figure 6.1A and 6.1B). Ten of the mutations in BA.1 S were found previously in at least two lineages (D614G exists in all VoCs).

The Alpha variant has a single mutation, N501Y, in the RBD, which occupies the right shoulder and contributes to the ACE2 binding footprint[79] (Figure 6.1D). Beta has two more mutations in RBD: K417N and E484K, which are at the back of the neck and left shoulder, respectively and also part of the ACE2 footprint[22] (Figure 6.1E). Gamma has similar mutations with Beta: K417T, E484K, and N501Y[23]. Delta harbours two mutations in RBD: L452R in front of the neck, and T478K on the far side of the left shoulder, both fall just peripheral to the ACE2 binding footprint[80] (Figure 6.1F). All the variants have at least one RBD mutations in common with BA.1. There are 15 mutations in BA.1 RBD, nine of them are part of the ACE2 binding footprint: K417N, G446S, S477N, E484A, Q493R, G496S, Q498R, N501Y, Y505H, and N440K and T478K just peripheral (Figure 6.1B and 6.1C). Four mutations occur on the right flank: G339D, A371L, S373P, and S375F (Figure 6.1B), the last three of which are adjacent to a lipid-binding pocket[159]. When the pocket is occupied by lipid similar to linoleic acid, the S is in a rigid state where all RBDs are found in a locked-down configuration stabilised by lipid-bridged quaternary interactions between adjacent RBDs[160]. When the pocket is empty,

the RBD alternates between looser down and up conformations. It seems that loss of lipid potentially promotes RBD presentation to the target cells.

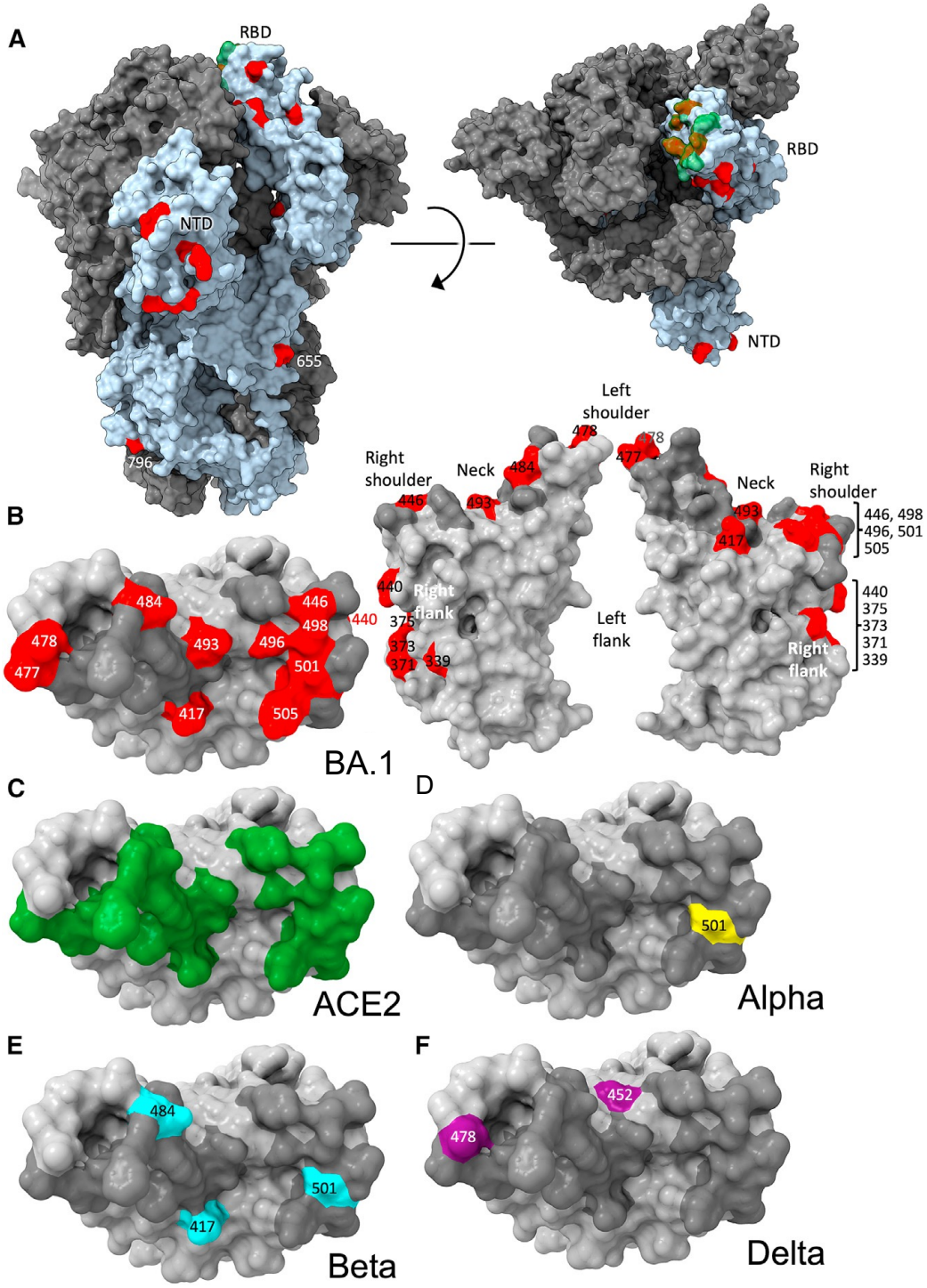

Figure 6.1 Distribution of BA.1 changes. (A) Trimeric S model depicted as a grey surface with one monomer highlighted in pale blue, ACE2 binding site in green and changes in Omicron shown in red, left side view, right top view. (B) RBD depicted as a grey surface with the ACE2 footprint in dark grey and changes in Omicron in red, left: top view, right: front and back views. Epitopes are labelled according to the torso analogy and mutations labelled. (C–F) Top view of RBD depicted as a grey surface with the following: (C) ACE2 binding site in green. (D) Alpha change in yellow, (E) Beta changes in cyan, and (F) Delta changes in purple. Figure produced using chimeraX[161] by Prof. David Stuart.

6.2.2 Neutralisation of BA.1 by vaccinated or convalescent serum

The collection of convalescent serum of early pandemic, Alpha, Beta, Gamma infection are described previously. Convalescent samples of Delta infection were collected 4-6 weeks after infection, n = 19, median day after infection is 38. Neutralisation assays were performed against BA.1 and compared with neutralisation titres of Victoria, Alpha, Beta, Gamma, and Delta (Figure 6.2 A-E).

Neutralisation titres on BA.1 were significantly reduced in all cases compared with either the early pandemic strain Victoria or the homologous strain causing infection, and in many cases, the immune serum failed to neutralise BA.1 at the lowest dilution rate (1:20). Compared with the homologous viruses, the neutralisation titres of sera for BA.1 were reduced 16.9-fold ($p < 0.0001$) for early pandemic, 18.4-fold ($p < 0.0001$) for Alpha, 22.5-fold ($p = 0.0001$) for Beta, 12.3-fold ($p < 0.0001$) for Gamma, and 25.9-fold ($p < 0.0001$) for Delta. This significant reduction of neutralisation titres on BA.1 indicates that previously infected individuals will have little protection from infection by BA.1.

Since the spread of Delta variant coincided with the vaccine campaign in the UK, we collected three different groups of Delta infection samples: Delta infection only (Figure 6.2E), Delta infection following vaccination (n = 9), and vaccination following Delta infection (n = 8) (Figure 6.2F). Using Delta + Vaccine sera, neutralisation assays were performed on early pandemic, Alpha, Beta, Gamma, Delta, and BA.1 authentic viruses. Compared with Delta-infection only sera, sera from cases who had received the vaccine before or after Delta infection show substantially higher neutralisation titres to all viruses tested, with Delta + vaccine sera showing an 8.0-fold ($p < 0.0001$) increase in the neutralisation of BA.1 compared to Delta-infection alone.

We also investigated the effect of the third dose of vaccination on neutralisation of BA.1. Sera from vaccinees who received three doses of AZD1222 (n = 41) and BNT162b2 (n = 20) were tested against Victoria, Delta, and Omicron. For AZD1222, the serum was obtained 28 days following the second and third doses (Figure 6.2G). For BNT162b2, the serum was obtained 28 days and 6 months after the second dose, immediately prior to the third dose, and 28 days following the third dose (Figure 6.2H).

At 28 days following the third dose, the neutralisation titres for BA.1 were boosted 2.7-fold ($p < 0.0001$) and 34.2-fold ($p < 0.0001$) following the third dose of ADZ1222 and BNT162b2, respectively, compared with 28 days following the second dose. It shows that the booster vaccines added considerable protection against BA.1 infection.

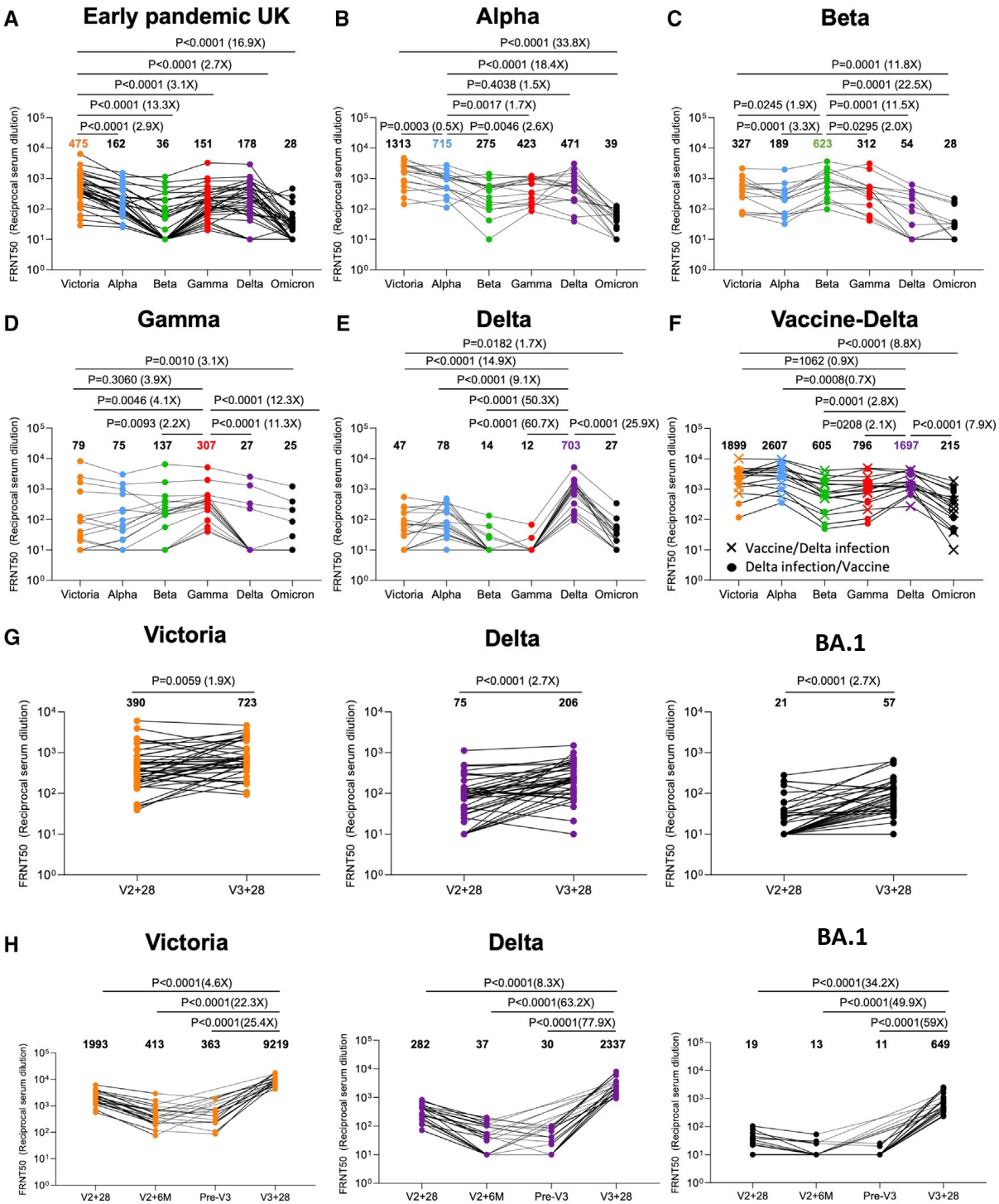

Figure 6.2 Neutralisation assays against BA.1. FRNT50 values for the indicated viruses using serum from convalescents previously infected by (A) early pandemic virus (n = 32), (B) Alpha (n = 18), (C) Beta (n = 14), (D) Gamma (n = 16), (E) Delta (n = 10), (F) Delta before vaccination or after vaccination (n = 17), or vaccinee serum samples before and after the third dose of (G) AZD1222 (n = 41), and (H) 4 weeks, 6 months after the second dose, before the third, and after the third dose of BNT162b2 (n = 20). Geometric mean titres are shown above each column. The Wilcoxon matched-pairs signed rank test was used for analysis, and two-tailed *p* values were calculated.

6.2.3 Neutralisation of BA.1 by early pandemic, Beta, and therapeutic mAbs

Previously we have identified 20 potent neutralising mAbs (FRNT50 < 100 ng/ml against homologous viruses) from early pandemic virus infected cases[123]. Neutralisation ability was tested against BA.1 and compared with early pandemic, Alpha, Beta, Gamma, and Delta strains. All 20 mAbs show reduced or failed neutralisation against BA.1, with 17/20 completely knocked out by BA.1 (FRNT50 > 10 μg/ml) and another three mAbs, mAb 58, 222, and 253, reduced 3.4- 12.6, and 19.3-fold, respectively, compared with Victoria (Figure 6.3A and Table 6.1). The binding sites of selected mAbs were mapped on the BA.1 RBD with mutations indicated (6.4A). As expected, there is a correlation between the position of the mutations and the sites of antibody binding, although the antibody centroids are more broadly spread across the RBD surface.

27 potent neutralising mAbs were isolated from Beta infected cases, and most of the mAbs target the three Beta RBD mutations, K417N, E484K, and N501Y, as we reported previously[127]. Neutralisation assays were performed on BA.1 and 17/27 Beta mAbs showed a complete loss of activity, some had substantial reductions in neutralisation titres, while Beta-22, -29, -40, -47, -53, -54, -55, and -56 were able to neutralise BA.1 with titres < 400 ng/ml (Figure 6.3B and Table 6.1).

There are five Beta mAbs cross-neutralise all Alpha, Beta, Gamma, and Delta variants. Of these, Beta-27, as with mAb 222, belongs to VH3-53 family that contacts Q493 and Y505, and shows reduced neutralisation against BA.1 (Figure 6.3B, 6.4B and Table 6.1). Beta-47 has contacts with S477 and Q493and reduced neutralisation of BA.1 (Figure 6.3B, 6.4B and Table 6.1). Beta-49 and -50, which are IGVH1-69 mAbs, bind to the right flank and are knocked out by BA.1 (Figure 6.3B, 6.4B and Table 6.1). They have direct contact with G339 on RBD and would clash with G339D. Similarly, Beta-53 also binds to the right flank and potentially clashes with G339D and G446S, causing >100-fold reduction in neutralisation of BA.1 compared with Beta (Figure 6.3B, 6.4B and Table 6.1).

We also assessed the neutralising abilities of various individual antibodies that have been licensed for use against BA.1. Their binding footprints are shown on BA.1 RBD which illustrates a strong correlation of binding to the positions of mutations in BA.1 (Figure 6.4C). Regeneron 10933 binds to the back of the left shoulder and 10987 to the right shoulder[162] (Figure 6.4C), and the activity of both is knocked out by BA.1 (Figure 6.3C and Table 6.1). S309[56,163] binds to the right flank, contacting G339 and N343 (glycan close to S371L, S373P, and S375F) (Figure 6.4C), and its neutralisation against BA.1 is only reduced 6.4-fold compared with Victoria (Figure 6.3C and Table 6.1). AZD8895 binds to the back of the left shoulder and its neutralising ability against BA.1 is reduced 230-fold compared with Victoria due to the contact with S477 and Q493 (Figure 6.3C, Figure 6.4C and Table 6.1). AZD1061 binds the front of the right shoulder is reduced 268-fold due to its contacts with G446 (Figure 6.3C, Figure 6.4C and Table 6.1). AZD7442, which is a combination of AZD8895 and AZD1061, is reduced 30.3-fold compared with Victoria (Figure 6.3C, Figure 6.4C and Table 6.1). The activity of LY-CoV016 and LY-CoV-555 are both knocked out by BA.1. LY-CoV016 is vulnerable to N501 and Y505 mutations, and LY-CoV555 is sensitive to E484 and Q493 mutations (Figure 6.3C, Figure 6.4C and Table 6.1). All three ADG mAbs, ADG10, 20 and 30 show considerable loss of activity against BA.1 (Figure 6.3C and Table 6.1).

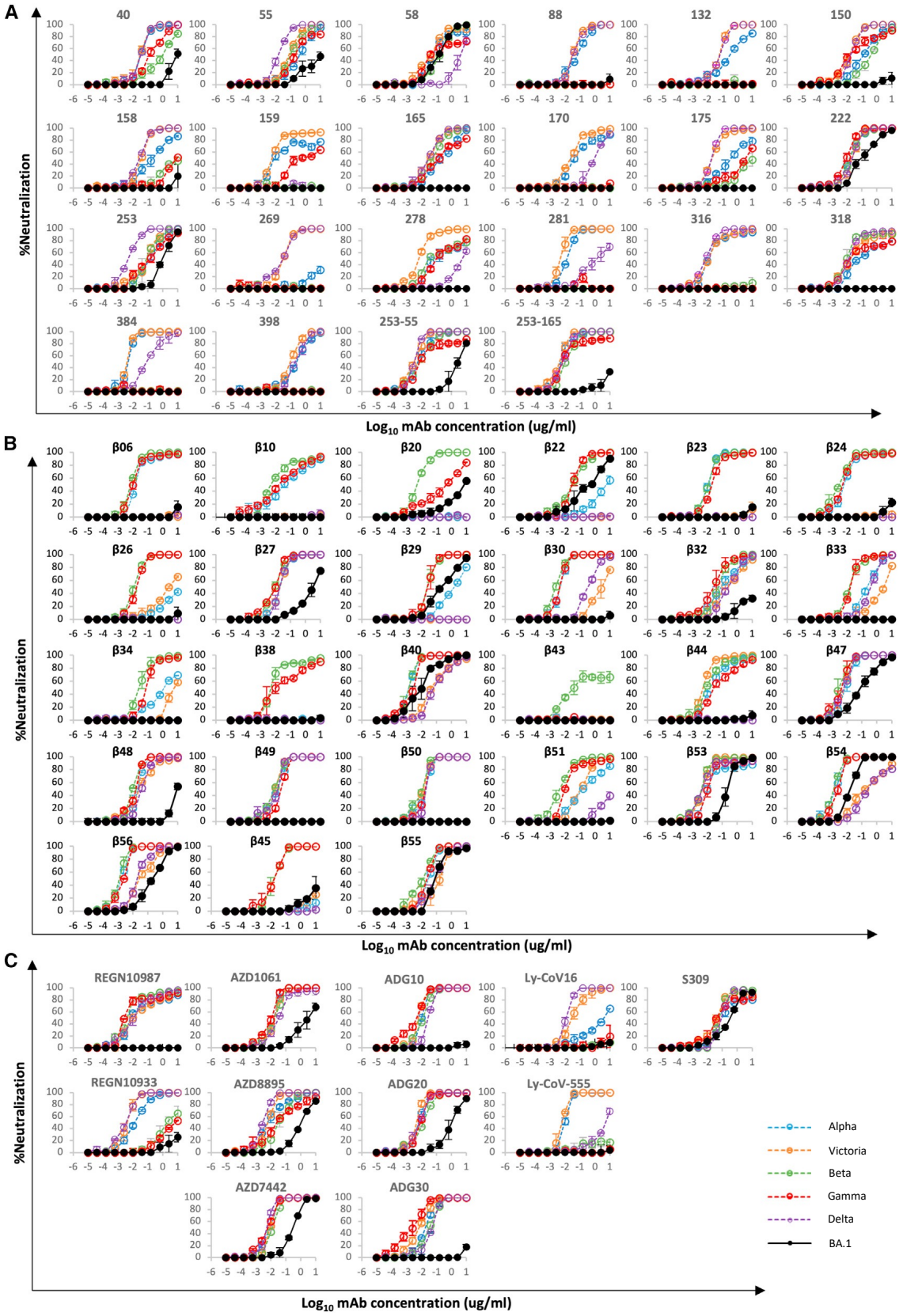

Figure 6.3 FRNT curves of mAb neutralise BA.1. FRNT curves for mAb from (A) early pandemic, (B) Beta infected cases and (C) commercial sources. BA.1 neutralisation is compared with Victoria, Alpha, Beta, Gamma, and Delta.

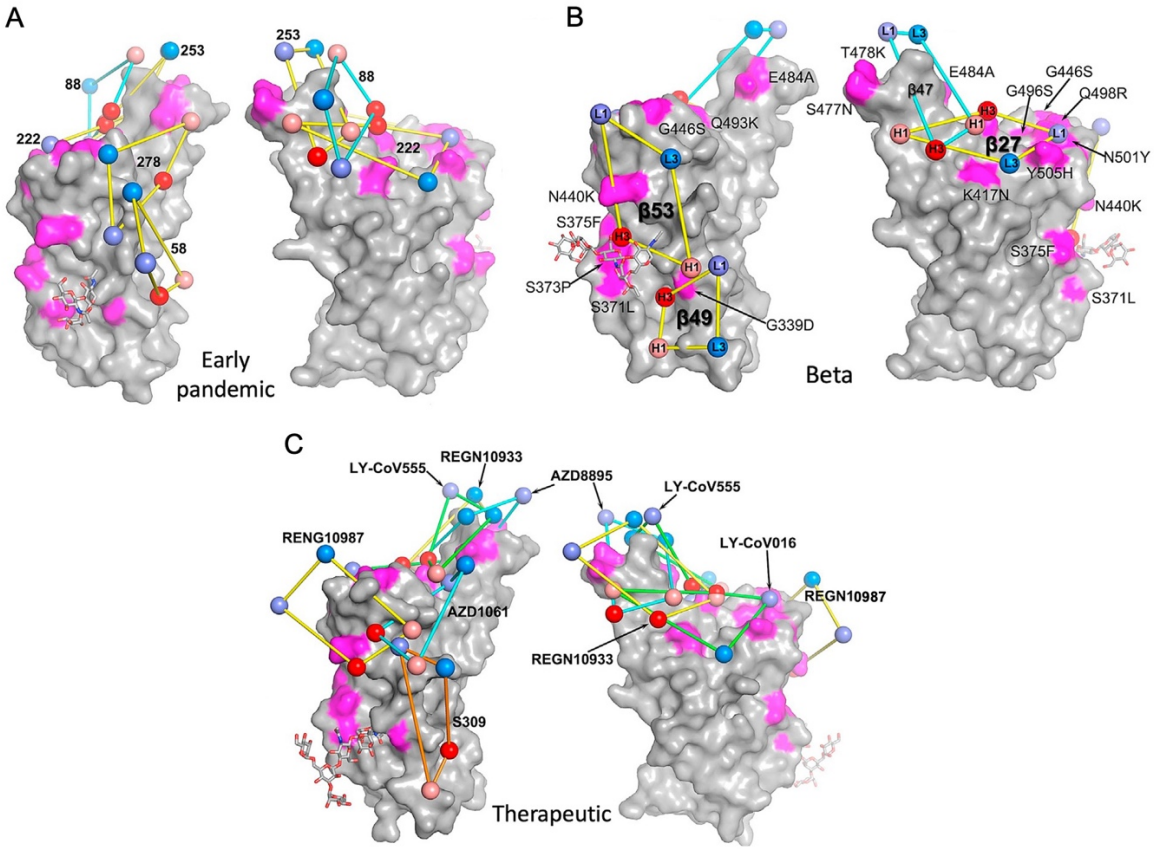

Figure 6.4 Relative antibody contact. (A) Outline footprints of a selection shown by quadrilaterals of early pandemic mAbs: 58, 88, 222, 253, and 278 are shown by balls representing the centroid of H3 (red), H1 (salmon), L3 (blue) and L1 (slate) loops joined by yellow or cyan sticks. (B) as for (A), showing a selection of Beta antibodies: 27, 47, 49, and 53. (C) As for (B) showing a selection of commercial antibodies: REGN10933, REGN10987, S309, AZD1061, AZD8895, LY-CoV555, and LY-CoV016. Pink colours represent the mutations on BA.1 RBD. The figures were depicted by Dr. Jingshan Ren from Division of Structural Biology, University of Oxford.

Table 6.1 FRNT50 of BA.1 by early pandemic, Beta and commercial mAbs.

mAb	IC50 (ug/ml)					
	Victoria	Alpha	Beta	Gamma	Delta	BA.1
40	0.026 ± 0.007	0.035 ± 0.008	0.738 ± 0.311	0.153 ± 0.037	0.029 ± 0.010	7.989 ± 2.011
55	0.095 ± 0.015	0.348 ± 0.044	0.127 ± 0.014	0.306 ± 0.046	0.016 ± 0.005	7.120 ± 2.880
58	0.041 ± 0.003	0.116 ± 0.029	0.136 ± 0.010	0.236 ± 0.075	6.434 ± 2.623	0.141 ± 0.063
88	0.033 ± 0.001	0.058 ± 0.008	>10	>10	0.039 ± 0.007	>10
132	0.048 ± 0.000	0.337 ± 0.048	>10	>10	0.051 ± 0.013	>10
150	0.012 ± 0.000	0.139 ± 0.019	0.350 ± 0.010	0.040 ± 0.003	0.020 ± 0.001	>10
158	0.031 ± 0.004	0.254 ± 0.109	>10	>10	0.026 ± 0.002	>10
159	0.011 ± 0.000	0.061 ± 0.020	>10	1.434 ± 0.804	>10	>10
165	0.034 ± 0.004	0.212 ± 0.004	0.054 ± 0.013	0.241 ± 0.030	0.027 ± 0.006	>10
170	0.025 ± 0.004	0.105 ± 0.050	>10	>10	0.841 ± 0.103	>10
175	0.026 ± 0.000	0.575 ± 0.280	>10	3.881 ± 0.738	0.017 ± 0.003	>10
222	0.019 ± 0.000	0.014 ± 0.002	0.017 ± 0.005	0.008 ± 0.003	0.018 ± 0.001	0.240 ± 0.122
253	0.055 ± 0.008	0.126 ± 0.018	0.109 ± 0.055	0.137 ± 0.005	0.005 ± 0.001	1.063 ± 0.367
269	0.030 ± 0.000	>10	>10	>10	0.021 ± 0.004	>10
278	0.014 ± 0.007	0.307 ± 0.149	0.160 ± 0.018	0.245 ± 0.042	7.374 ± 1.397	>10
281	0.005 ± 0.001	0.012 ± 0.000	>10	>10	1.494 ± 0.302	>10
316	0.018 ± 0.007	0.024 ± 0.005	>10	>10	0.008 ± 0.001	>10
318	0.029 ± 0.008	0.185 ± 0.037	0.019 ± 0.008	0.083 ± 0.032	0.018 ± 0.003	>10
384	0.004 ± 0.001	0.005 ± 0.002	>10	>10	0.108 ± 0.035	>10
398	0.091 ± 0.004	0.180 ± 0.001	>10	>10	0.237 ± 0.038	>10
253-55	0.003 ± 0.000	0.008 ± 0.002	0.009 ± 0.002	0.026 ± 0.006	0.003 ± 0.000	2.945 ± 1.283
253-165	0.003 ± 0.000	0.006 ± 0.000	0.013 ± 0.003	0.019 ± 0.000	0.007 ± 0.002	>10
β06	>10	0.024 ± 0.002	0.008 ± 0.002	0.015 ± 0.003	>10	>10
β10	>10	0.064 ± 0.042	0.015 ± 0.000	0.025 ± 0.011	>10	>10
β20	>10	>10	0.005 ± 0.001	0.345 ± 0.122	>10	7.518 ± 1.105
β22	>10	6.58 ± 2.988	0.025 ± 0.004	0.030 ± 0.007	>10	0.393 ± 0.234
β23	>10	0.009 ± 0.001	0.011 ± 0.001	0.020± 0.000	>10	>10
β24	>10	0.007 ± 0.001	0.002 ± 0.001	0.005 ± 0.001	>10	>10
β26	2.742 ± 0.208	>10	0.012 ± 0.003	0.016 ± 0.000	>10	>10
β27	0.018 ± 0.002	0.018 ± 0.000	0.009 ± 0.000	0.006 ± 0.002	0.021 ± 0.004	2.693 ± 0.741
β29	>10	1.372 ± 0.016	0.027 ± 0.003	0.023 ± 0.009	>10	0.261 ± 0.079
β30	2.643 ± 0.88	0.004 ± 0.001	0.003 ± 0.001	0.004 ± 0.000	0.350 ± 0.035	>10
β32	0.248 ± 0.003	0.119 ± 0.044	0.053 ± 0.025	0.027 ± 0.014	0.267 ± 0.068	>10
β33	2.016 ± 0.051	0.234 ± 0.013	0.017 ± 0.003	0.017 ± 0.001	0.334 ± 0.005	>10
β34	8.241 ± 1.067	1.466 ± 0.136	0.032 ± 0.010	0.092 ± 0.003	>10	>10
β38	>10	>10	0.011 ± 0.003	0.043 ± 0.025	>10	>10
β40	0.075 ± 0.005	0.001 ± 0.000	0.001 ± 0.000	0.001 ± 0.000	0.107 ± 0.031	0.012 ± 0.007
β43	>10	>10	0.048±0.024	>10	>10	>10
β44	0.007 ± 0.002	0.028 ± 0.008	0.015 ± 0.008	0.071 ± 0.026	>10	>10
β45	>10	>10	0.018 ± 0.003	0.015 ± 0.006	>10	9.947 ± 0.053
β47	0.006 ± 0.001	0.008 ± 0.003	0.003 ± 0.001	0.004 ± 0.002	0.005 ± 0.000	0.096 ± 0.011
β48	0.034 ± 0.011	0.020 ± 0.008	0.009 ± 0.001	0.011 ± 0.001	0.042 ± 0.016	8.362 ± 1.638
β49	0.009 ± 0.000	0.011 ± 0.001	0.007 ± 0.000	0.019 ± 0.003	0.008 ± 0.003	>10
β50	0.011 ± 0.000	0.014 ± 0.006	0.007 ± 0.001	0.015 ± 0.005	0.019 ± 0.005	>10
β51	0.119 ± 0.008	0.242 ± 0.024	0.005 ± 0.000	0.019 ± 0.001	>10	>10
β53	0.005 ± 0.000	0.032 ± 0.009	0.004 ± 0.000	0.017 ± 0.001	0.007 ± 0.000	0.266 ± 0.117
β54	0.232 ± 0.092	0.002 ± 0.001	0.001 ± 0.000	0.002 ± 0.001	0.409 ± 0.071	0.020 ± 0.011
β55	0.108 ± 0.069	0.028 ± 0.004	0.01 0± 0.003	0.022 ± 0.001	0.076 ± 0.020	0.109 ± 0.013
β56	0.046 ± 0.013	0.001 ± 0.000	0.001 ± 0.000	0.002 ± 0.000	0.022 ± 0.002	0.194 ± 0.056
AZD1061	0.013 ± 0.003	0.012 ± 0.002	0.014 ± 0.002	0.007 ± 0.002	0.038 ± 0.006	3.488 ± 2.085
AZD8895	0.005 ± 0.001	0.011 ± 0.002	0.046 ± 0.031	0.046 ± 0.016	0.003 ± 0.000	1.152 ± 0.170
AZD7442	0.009 ± 0.000	0.007 ± 0.001	0.012 ± 0.001	0.006 ± 0.003	0.005 ± 0.000	0.273 ± 0.062
REGN10987	0.032 ± 0.007	0.028 ± 0.003	0.007 ± 0.001	0.013 ± 0.002	0.017 ± 0.009	>10
REGN10933	0.004 ± 0.002	0.014 ± 0.002	3.284 ± 2.014	6.177 ± 1.914	0.003 ± 0.001	>10
ADG10	0.006 ± 0.000	0.010 ± 0.001	0.011 ± 0.001	0.003 ± 0.000	0.026 ± 0.005	>10
ADG20	0.004 ± 0.001	0.006 ± 0.000	0.010 ± 0.001	0.009 ± 0.000	0.006 ± 0.001	1.104 ± 0.509
ADG30	0.007 ± 0.002	0.016 ± 0.001	0.029 ± 0.003	0.002 ± 0.001	0.033 ± 0.007	>10
Ly-CoV-555	0.006 ± 0.002	0.009 ± 0.000	>10	>10	8.311 ± 4.059	>10
Ly-CoV16	0.034 ± 0.007	3.225 ± 1.030	>10	>10	0.012 ± 0.002	>10
S309	0.040 ± 0.005	0.078 ± 0.069	0.082 ± 0.002	0.076 ± 0.014	0.113 ± 0.028	0.256 ± 0.034

6.2.4 Antigenic cartography of BA.1

Dr. Helen M. Ginn used the neutralisation data we generated to place BA.1 on the antigenic map using a similar method developed for analysing the Victoria, Alpha, Beta, Gamma, and Delta previously. Individual viruses are modelled independently and allow for serum specific scaling of the responses. The result shows that the previous variants are placed in a planetary band around a central point, with Delta locating opposite to Beta and Gamma, while BA.1 is displaced a large distance out of this plane, almost on a line drawn from the central point perpendicular to the planetary band, demonstrating that BA.1 dramatically expands our view of the antigenic landscape of SARS-CoV-2 (Figure 6.5).

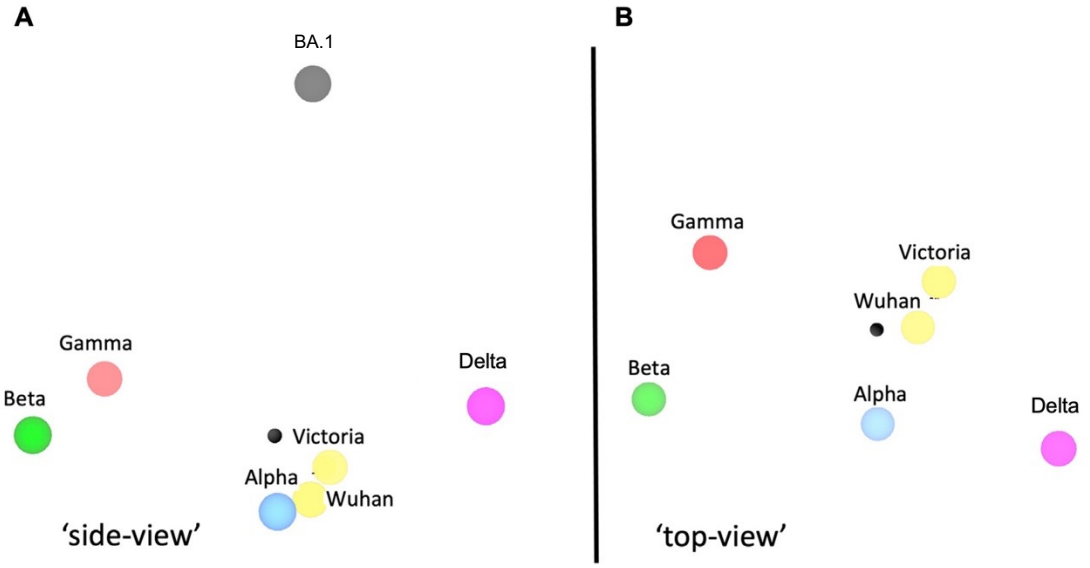

Figure 6.5 Antigenic landscape of SARS-CoV-2 varients. (A) A view of the three-dimensional antigenic map for variants tested. The distance between two points relates to the drop-off in neutralisation titres. (B) Same as (C) but rotated 90º, to look downward from BA.1. The model was devised by Dr. Helen M. Ginn.

6.2.5 Isolation of potent mAbs following BA.1 breakthrough infection

A panel of human monoclonal antibodies were isolated from convalescent volunteers who were infected by BA.1 (confirmed by sequencing) after receiving 2 doses of the Pfizer-BioNtech vaccine. We used a similar method as described previously for generation of early pandemic and Beta mAbs. Firstly, neutralisation assays were performed using BA.1 breakthrough serum samples against Victoria and BA.1 (Figure 6.6A). Five samples with the highest neutralising activity (FRNT50) against BA.1 were selected for single cell sorting.

B cells from five selected samples were stained with full-length BA.1 S trimer and single cell sorted by FACS (Figure 6.6B). Following RT-PCR and Nested-PCR, heavy chain and light chain sequences were ligated into expression vectors using Gibson reaction and transfected into 293T cells. Cultured supernatants after transfection were screened for reactivity to BA.1 and Wuhan S together with BA.1 RBD and NTD by ELISA. 1,122 cells were sorted in total and 545 mAbs were recovered.

Nearly all mAbs are cross-reactive to BA.1 and Wuhan S (Figure 6.6C). We also noticed a high proportion of RBD-reactive mAbs in this set of mAbs compared to the previous panel of mAbs from naïve cases infected by early pandemic strains: 56% compared to 21% (binomial two-population proportion test, $p < 0.0001$, $Z \sim 10$) (Figure 6.6D). It is also reported by others in another similar study on early pandemic samples that raw data on unsorted B-cells showed a similar proportion (23%) of RBD-reactive mAbs[164].

Neutralisation assays were performed and the 28 most potent mAbs were selected, with FRNT50 < 100 ng/ml against BA.1, and they were named as Omi-n due to the early naming strategy of the variant. All of them bound to the RBD, except for Omi-41 which is an anti-NTD mAb, and none cross-reacted with SARS-CoV-1 S by ELISA. Apart from Omi-30 and Omi-41, they block the interaction between RBD and ACE2 (Figure 6.6E).

Alignment of the heavy chains and light chains revealed that Omi-32 and Omi-33, which have five different amino acids, are clonally related (IGVH3-33). 30% (9/28) of the mAbs belong to the IGVH3-53 and related 3-66 gene families (Figure 6.6F, Table 6.2). These antibodies generally bind a site at the back of the neck of the RBD and block ACE2 binding[123]. They are the best-know public antibody response to SARS-CoV-2 infection[74], show a similar incidence (7/20) in potent early pandemic mAbs we isolated previously[123]. But the mAbs in the early pandemic set using IGVH3-53 and 3-66 are sensitive to the N501Y mutation, and even two antibodies from this family, mAb 222 and Beta-27, which resist to the N501Y change, show reduced neutralising ability to BA.1 (Figure 6.3A and 6.3B).

Around half of the gene families that we found in the early pandemic mAbs are also observed in BA.1 mAbs (Figure 6.6F). Out of 27 potent BA.1 mAbs, four mAbs belong to IGHV1-69 family, which are Omi-2, -24, -30, -31, -34, and -38. Although this family didn't appear in the

early pandemic set, it has been found in several potent mAbs isolated following natural infection or vaccination by others[165-167].

Compared with early pandemic mAbs, BA.1 mAbs show higher levels of somatic hypermutation in both heavy chains and light chains, with mean number of amino acid substitutions 9.00/6.00 for BA.1 mAbs and 4.55/4.25 for early pandemic set, respectively (Figure 6.6 G).

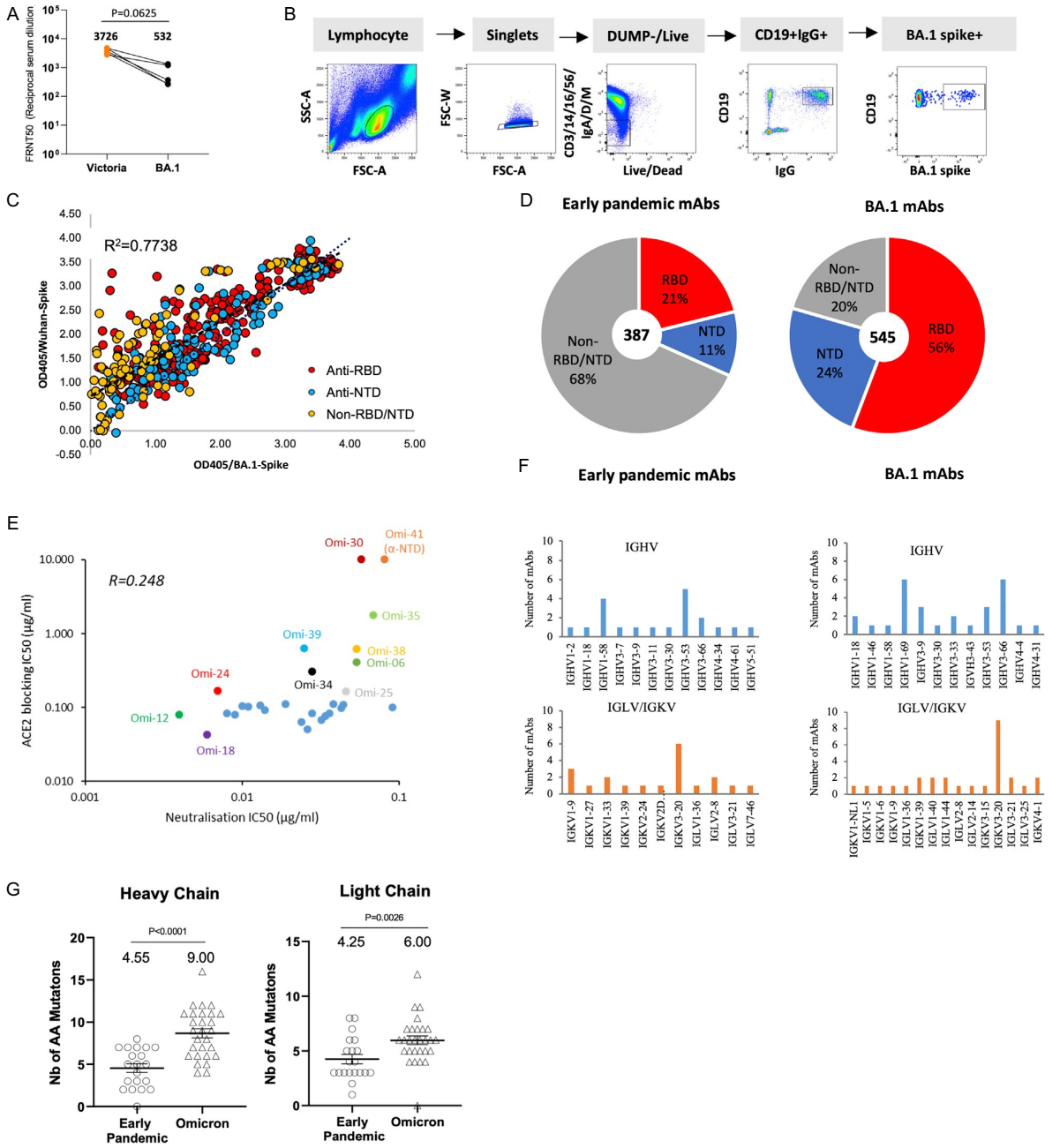

Figure 6.6 Generation of a panel of BA.1 mAbs. (A) FRNT50 titres against Victoria and BA.1 from donors to produce BA.1 mAbs. (B) Gate strategy for FACS sorting of B cells using full length BA.1 S.

(C) ELISA results of 525 mAbs isolated from BA.1 breakthrough cases comparing OD against Wuhan and BA.1 trimeric S, further mapping to RBD (red), NTD (blue) and non-RBD/NTD (orange) is indicated. (D) Proportion of RBD and NTD reactive mAbs in the BA.1 mAbs compared to the early pandemic set. (E) BA.1 mAbs block binding of ACE2 to BA.1 S trimer. (F) Heavy chain and light chain variable gene usages of BA.1 mAbs. (G) Somatic mutations in the potent BA.1 mAbs compared to the early pandemic set.

Table 6.2 Analysis of BA.1 mAbs heavy chain and light chain variable gene usage and mutation

mAbs	Patient No.	Heavy chain				Light chain			
		V-GENE	J-GENE	D-GENE	#Amino acid substitutions	K/λ	V-GENE	J-GENE	#Amino acid substitutions
Omi-02	07	1-69*01 , or 1-69D*01	2*01	2-21*02	7	K	3-20*01	5*01	5
Omi-03	07	3-53*01	4*02	1-26*01	5	K	3-20*01	2*01	0
Omi-06	07	4-4*07	3*02	3-16*02	4	K	1-39*01 , or 1D-39*01	4*01	12
Omi-08	07	1-46*01 , or 1-46*03	4*02	6-13*01	12	λ	1-40*02	1*01	4
Omi-09	07	3-30*01	3*02	4-17*01	6	λ	3-25*02	2*01 , or 3*01	4
Omi-12	08	1-58*02	3*02	2-2*01	12	K	3-20*01	1*01	9
Omi-16	09	3-66*02	4*02	2-15*01	9	K	3-20*01	2*01	7
Omi-17	09	3-66*02	4*02	6-19*01	7	K	3-20*01	2*01	6
Omi-18	09	3-53*01	6*02	4-11*01	11	λ	3-21*02	1*01	6
Omi-20	09	3-66*02	6*02	5-12*01	11	K	1-9*01	4*02	5
Omi-23	12	4-31*03	4*02	3-22*01	6	K	1-NL1*01	1*01	5
Omi-24	14	1-69*06	4*02	3-16*02	9	K	3-15*01	1*01	7
Omi-25	14	3-9*01	6*02	3-16*01	6	K	1-39*01 , or 1D-39*01	2*01	7
Omi-26	14	1-18*01	4*02	1-26*01	12	λ	1-36*01	3*02	4
Omi-27	14	3-66*01 , or 3-66*04	6*02	6-19*01	8	K	1-6*01	2*01	6
Omi-28	14	3-66*01 , or 3-66*04	4*02	3-16*01	4	K	3-20*01	1*01	9
Omi-29	14	3-53*04	6*02	2-15*01	11	λ	2-14*01 , or 2-14*03	3*02	6
Omi-30	14	1-69*06	6*02	2-15*01	10	λ	1-44*01	3*02	7
Omi-31	14	1-69*06	6*02	3-16*01	11	λ	1-44*01	3*02	6
Omi-32	08	3-33*01 , or 3-33*06	4*02	2-21*02	6	K	3-20*01	4*01	6
Omi-33	08	3-33*01 , or 3-33*06	4*02	2-21*02	10	K	3-20*01	4*01	4
Omi-34	09	1-69*06 , or 1-69*14	4*02	2-2*01	10	λ	1-40*01	1*01	6
Omi-35	09	3-9*01	6*02	2-2*02	5	λ	3-21*02	2*01 , or 3*01	7
Omi-36	09	3-66*02	4*02	2-15*01	9	K	3-20*01	2*01	5
Omi-38	15	1-69*09	3*01	1-26*01	16	K	1-5*01	5*01	10
Omi-39	07	3-43*01	6*03	2-2*01	8	K	4-1*01	3*01	6
Omi-41	08	1-18*04	4*02	3-9*01	11	K	4-1*01	2*02 ()	5
Omi-42	09	3-9*01	6*02	6-19*01	7	λ	2-8*01	2*01 , or 3*01 or 3*02	5

6.2.6 Broad neutralisation of VoC by potent BA.1 mAbs

Live virus neutralisation assays using BA.1 mAbs were performed on Alpha, Beta, Gamma, Delta, and BA.1. The FRNT50 against Victoria are < 100 ng/ml for all 28 potent mAbs (Figure 6.7, Table 6.3), the reason for this is perhaps because the antibodies have been derived from vaccine-induced memory B cells. There are 5 mAbs that neutralise BA.1 very potently, with FRNT50 titres < 10 ng/ml, and 17/28 mAbs are cross-reactive against all VoCs tested with < 10-fold difference in FRNT50 titres between all viruses (Figure 6.7, Table 6.3).

Omi-6, -24, -30, -31, -34, and -41 show reduced or absent activity against Delta, and four of them belong to the IGHV1-69 family, whose epitopes may be around L452R mutation (L452R is the unique mutation on Delta compared with BA.1). Omi-9 and -32 show reduce activity against Beta and Gamma, which suggest that they are sensitive to E484K mutation in these variants but resistant to the E484A change in BA.1 (Beta, Gamma, and BA.1 share N501Y

mutation, and Beta shares K417N with BA.1 while it is K417T in Gamma). Intriguingly, we observed an enhancement of BA.1 infection at a certain level of concentrations of Omi-38, which was not seen for other variants against Omi-38 (Figure 6.7).

We isolated 129 NTD-specific mAbs in total and only one antibody, Omi-41, showed FRNT50 < 100 ng/ml against BA.1. It also neutralises Victoria, Alpha, and Gamma, but not Beta and Delta, which may be due to the unique NTD changes in these variants (Figure .

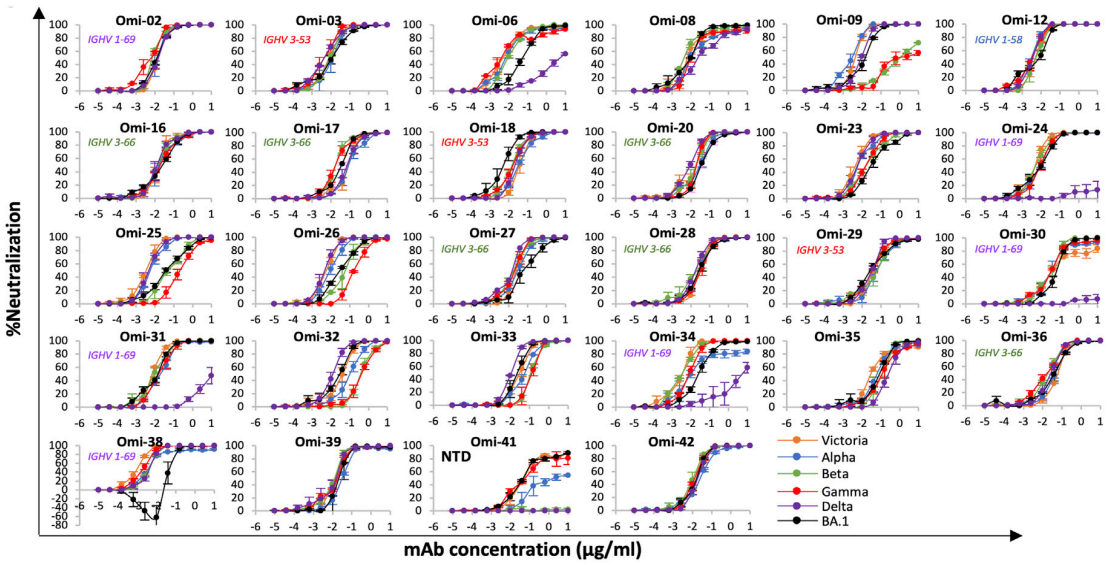

Figure 6.7 Live virus neutralisation curves of BA.1 mAbs against Victoria, Alpha, Beta, Gamma, Delta, and BA.1. Two independent experiments with duplicate were performed for each assay, and heavy chain variable gene usages are labelled to each antibody.

Table 6.3 FRNT50 of BA.1 mAbs against SARS-CoV-2 live virus.

mAbs	IC50 (μg/ml)					
	Victoria	Alpha	Beta	Gamma	Delta	BA.1
Omi-02	0.015 ± 0.001	0.014 ± 0.005	0.009 ± 0.000	0.004 ± 0.000	0.014 ± 0.003	0.013 ± 0.001
Omi-03	0.007 ± 0.000	0.012 ± 0.007	0.009 ± 0.001	0.004 ± 0.000	0.004 ± 0.000	0.009 ± 0.002
Omi-06	0.007 ± 0.001	0.011 ± 0.002	0.012 ± 0.000	0.010 ± 0.003	5.040 ± 0.747	0.054 ± 0.005
Omi-08	0.014 ± 0.007	0.022 ± 0.002	0.007 ± 0.000	0.024 ± 0.007	0.048 ± 0.012	0.008 ± 0.004
Omi-09	0.004 ± 0.001	0.002 ± 0.000	1.218 ± 0.324	2.373 ± 1.008	0.008 ± 0.002	0.011 ± 0.005
Omi-12	0.005 ± 0.000	0.003 ± 0.001	0.006 ± 0.001	0.003 ± 0.000	0.003 ± 0.000	0.004 ± 0.001
Omi-16	0.016 ± 0.002	0.022 ±0.009	0.018 ±0.004	0.022 ±0.007	0.016 ±0.002	0.019 ±0.003
Omi-17	0.066 ± 0.015	0.098 ±0.027	0.021 ±0.007	0.021 ±0.007	0.074 ±0.019	0.028 ±0.005
Omi-18	0.041 ± 0.005	0.038 ±0.008	0.018 ±0.006	0.016 ±0.004	0.025 ±0.000	0.006 ±0.003
Omi-20	0.012 ± 0.002	0.023 ±0.004	0.019 ±0.009	0.019 ±0.006	0.008 ±0.001	0.043 ±0.012
Omi-23	0.005 ± 0.002	0.009 ±0.004	0.020 ±0.005	0.018 ±0.006	0.006 ±0.002	0.044 ±0.013
Omi-24	0.005 ± 0.001	0.008 ±0.003	0.006 ±0.001	0.010 ±0.005	>10	0.007 ±0.001
Omi-25	0.003 ± 0.001	0.007 ±0.001	0.059 ±0.007	0.257 ±0.079	0.006 ±0.002	0.046 ±0.015
Omi-26	0.005 ± 0.000	0.010 ±0.003	0.055 ±0.020	0.214 ±0.046	0.005 ±0.001	0.034 ±0.000
Omi-27	0.026 ± 0.001	0.032 ±0.012	0.019 ±0.006	0.017 ±0.006	0.010 ±0.001	0.091 ±0.050
Omi-28	0.028 ± 0.004	0.028 ±0.001	0.019 ±0.010	0.033 ±0.008	0.018 ±0.002	0.032 ±0.009
Omi-29	0.044 ± 0.002	0.066 ±0.034	0.048 ±0.020	0.040 ±0.007	0.029 ±0.004	0.036 ±0.003
Omi-30	0.109 ± 0.035	0.043 ±0.016	0.028 ±0.009	0.038 ±0.004	>10	0.058 ±0.008
Omi-31	0.007 ± 0.001	0.020 ±0.003	0.011 ±0.005	0.017 ±0.006	>10	0.010 ±0.002
Omi-32	0.032 ± 0.016	0.102 ±0.041	0.460 ±0.092	0.430 ±0.012	0.012 ±0.002	0.024 ±0.011
Omi-33	0.028 ± 0.005	0.057 ± 0.017	0.136 ± 0.002	0.132 ± 0.037	0.011 ± 0.001	0.026 ± 0.008
Omi-34	0.003 ± 0.001	0.041 ±0.027	0.003 ±0.000	0.008 ±0.002	>10	0.028 ±0.009
Omi-35	0.057 ± 0.003	0.080 ±0.030	0.128 ±0.058	0.136 ±0.024	0.280 ±0.059	0.069 ±0.032
Omi-36	0.056 ± 0.008	0.047 ± 0.009	0.018 ± 0.001	0.015 ± 0.000	0.026 ± 0.003	0.038 ± 0.006
Omi-38	0.001 ± 0.000	0.009 ± 0.001	0.004 ± 0.000	0.002 ± 0.000	0.004 ± 0.001	0.054 ± 0.028
Omi-39	0.015 ± 0.006	0.039 ± 0.007	0.009 ± 0.000	0.014 ± 0.001	0.012 ± 0.007	0.025 ± 0.004
Omi-41	0.090 ± 0.013	2.262 ± 1.199	>10	0.126 ± 0.059	>10	0.081 ± 0.004
Omi-42	0.016 ± 0.003	0.024 ± 0.001	0.011 ± 0.004	0.013 ± 0.003	0.019 ± 0.001	0.014 ± 0.002

6.2.7 Mapping of RBD-specific potent BA.1 mAbs by using BLI competition measurement

As previously, Dr. Daming Zhou performed pairwise BLI competition measurements on the 27 potent RBD-specific BA.1 mAbs together with several early pandemic mAbs of known binding position. A map of binding epitopes was obtained with average positional error of 9 Å (Figure 6.8A). The mAbs segregate into two clusters, which are a subset of the epitopes observed for the early pandemic virus and distinct from the focus seen for Beta[123,127] (Figure 6.8A-D).

The first cluster includes the mAbs belonging to IGHV3-53 and IGHV3-66 antibody families and is toward the back of the neck/left shoulder, extending up to the top of the left shoulder. This region is a major binding epitope for potent neutralising mAbs in the early pandemic mAb set (Figure 6.8B and 6.8D). Omi-9, which shows reduced neutralisation of Beta and Gamma, is located close to residue 484, which is mutated from Glu to Lys in Beta/Gamma and to Ala in BA.1. The second cluster is on the right shoulder, which was seen in the full set

of early pandemic mAbs above the S309 site (Figure 6.8C) but not seen in the potent early pandemic mAb set (Figure 6.8D). This region is occupied by 5 of the 6 IGHV1-69 mAbs; the other one, Omi-2, lies within the neck/left shoulder cluster. Four IGHV1-69 mAbs Omi-24, -30, -31, and -34, which show reduced neutralisation of Delta, positions adjacent to residue 452, with is mutated in Delta from Leu to Arg. Omi-6, an IGHV4-4 mAb, also shows reduced Delta neutralisation and is placed to a similar position to the major cluster of IGHV1-69 antibodies.

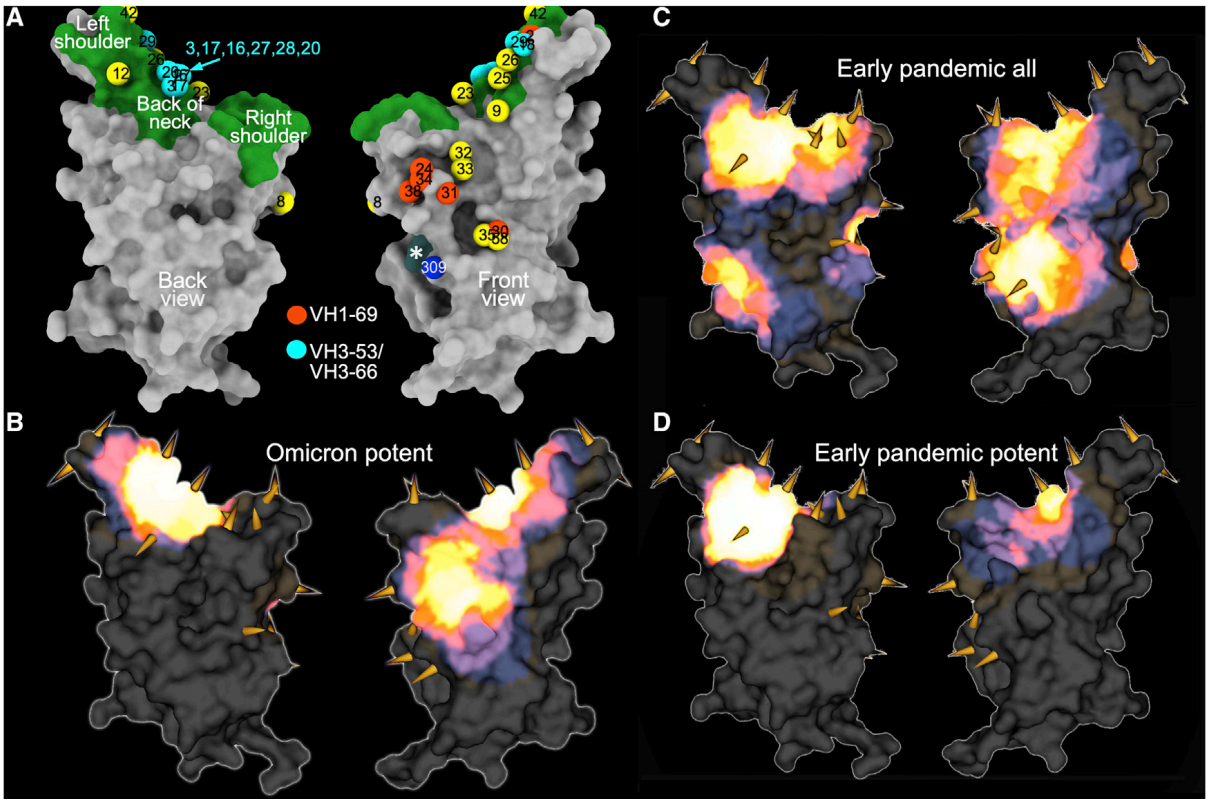

Figure 6.8 Mapping of BA.1 mAbs. (A) Mabscape antibody map (back and front views). Surface rendering of RBD in grey, ACE2 footprint in green, N343 glycan site in dark slate grey marked with *. Spheres locate BA.1 mAbs: IGHV3-53 in cyan, IGHV1-69 in red, the rest in yellow; in addition, S309 is shown in blue. (B) Heatmap of surface occupation of RBD by BA.1 mAbs (back and front views) by iron heat colours (black<blue<red<orange<yellow<white hot) according to the relative level of antibody contact, calculated for each surface vertex as the number of antibodies within a 10 Å radius. Mutations in BA.1 are shown by the spikes. (C) Heatmap as in (B) for the whole set of early pandemic mAbs. (D) Heatmap as in (C) for the potent neutralising mAbs from the early pandemic set. The analyses were done by Dr. Daming Zhou and figures were depicted by Dr. Helen M. Ginn.

6.2.8 Quantitative dissection of the BA.1 mAb responses

Dr. Helen M. Ginn applied the same neutralisation-correlation method we used for clustering early pandemic and Beta mAbs, which takes neutralisation results of mAbs against different variants, calculates correlation coefficients for all possible pairs of mAbs, and then cluster the mAbs[123]. Neutralisation data (Figure 6.9A) for early pandemic, Beta, and BA.1 mAbs showed

clear differences between the three sets (Figure 6.9B). BA.1 mAbs are distinctly separated with early pandemic set, presumably by selection and somatic mutations, and they are also largely distinguished from Beta antibodies. But there are some Beta mAbs, Beta-27, -40, -47, -48, -49, -50, -53, -54, and -56, share similarities with BA.1 mAbs. When analysing BA.1 mAbs separately (Figure 6.9C), five BA.1 mAbs are segregated due to their lack of neutralisation against Delta, which are Omi-06, -24, -30, -31, and -34).

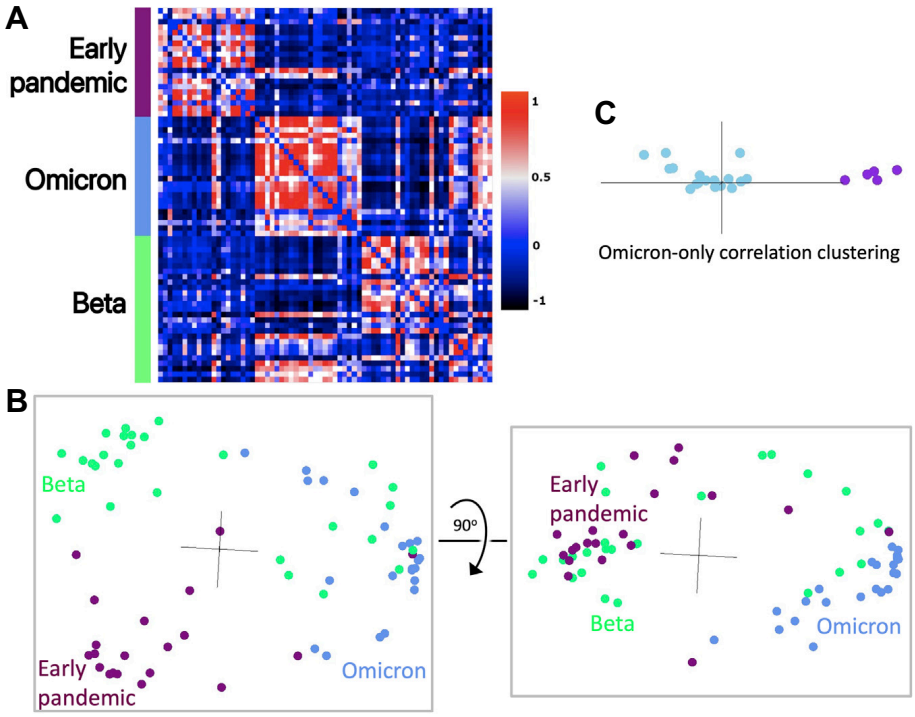

Figure 6.9 Correlation of neutralisation between antibodies from different responses. (A) Cross-correlation matrix between pairs of antibodies. Each pairwise value is the correlation coefficient between the normalised log neutralisation titres of the corresponding antibodies against a panel of SARS-CoV-2 (Victoria, Alpha, Beta, Gamma, Delta and BA.1). (B) Cluster4X principal component analysis of the cross-correlation matrix from two orthogonal views. (C) Principal component analysis on the sub-matrix of C consisting of only the BA.1 antibodies. Omi-6, -24, -30, -31, and -34 are shown in purple while the rest of the antibodies are shown in cyan. The model was devised by Dr. Helen M. Ginn.

6.3 Discussion

Omicron BA.1 strain was discovered in November 2021, and three weeks after its detection it had outnumbered Delta in the UK, due to its high transmissibility and ability to infected previously exposed or vaccinated individuals.

The density of the mutations in S protein of BA.1 is astonishing, and the NTD, RBD, and the furin cleavage site are mutation hotspots. Within RBD, the mutations are concentrated on the ACE2 interacting surface and the right flank.

The majority of potent neutralising mAbs bind to or in proximity to the ACE2 interacting surface (neck and shoulder epitopes) and block the interaction of ACE2 with S, therefore preventing virus from attaching to the host cell surface. But there are two other group of potent neutralising antibodies. The first group of mAbs bind on the area around N343 glycan (right flank epitope), with the example of Vir S309. Beta-49, -50, and -53 belong to this group, which bind distant from the ACE2 binding site, do not block ACE2-spike interaction, and destabilise the S-trimer as their possible mechanism of neutralisation. The other group is potent neutralising antibodies binding to the NTD supersite. The mechanism of this group of antibodies is still unknown. There are numerous mutations found at all three sites: the receptor binding site, the area proximate to N343 glycan, and NTD. These mutations lead to remarkable reduction of neutralisation for naturally immune or vaccine sera. This immune evasion indicates a driving force of the evolution of BA.1. But we also observed that following three doses of vaccine, the neutralisation titres against Victoria, Delta and BA.1 are all increased, especially with BNT162b2, in line with other studies[168,169], due to boosting effect of vaccination and the higher ability of BNT162b2 activating humoral immunity comparing with AZD1222.

For the majority of the antibodies that we isolated from early pandemic or Beta infection cases, the changes in interaction are so severe that their neutralising ability has been greatly impaired or completely lost. This observation is also true in the set of mAbs developed for clinical use, whose activities are mostly lost, AZ8895 and ADG20 are substantially compromised, while S309 still retain its neutralising ability with a modest reduction.

To find more potent neutralising antibodies against BA.1, we isolated 545 mAbs from BA.1 breakthrough infection convalescent samples and identified 28 mAbs that can potently neutralise BA.1. All these potent mAbs cross-neutralise Victoria, and many broadly neutralise other VoCs, which indicates that these responses may be recalled from memory B cells generated following vaccination, but this remains uncertain due to the lack of paired samples following vaccination but before BA.1 infection.

These potent neutralising mAbs can be segregated into two clusters based on their epitopes (Figure 6.8A and 6.8B): the first, at the neck/left shoulder, includes mAbs that bind at the back of the neck (e.g. IGHV3-53 mAbs), and those that bind more upright on the left shoulder (Omi-

09); the second cluster bind on the front of the right shoulder, which has been seen in the full set of our early pandemic mAbs but does not include any of the highly potent mAbs in that set. Although most of the BA.1 mAbs potently neutralise all variants tested here (Victoria, Alpha, Beta, Gamma, Delta, and BA.1), there are some mAbs showing reduced neutralisation against Beta/Gamma or Delta. In terms of heavy chain gene usage, the IGVH3-53 and IGVH3-66 families (9/27) are the most frequent public antibody response in the RBD-specific BA.1 mAbs, which is the same as in the early pandemic set. The second mostly used IGVH family is IGVH1-69 (6/27), which is also found in the set of Beta mAbs.

In summary, we have shown that BA.1 harbours a large number of mutations which lead to deceased neutralising titres of natural infection and vaccine sera, and substantially knockdown or knockout a panel of mAbs isolated from early pandemic and Beta infected samples. Third-dose boosters effectively induced a higher titre against Victoria, Delta, and BA.1. We isolated 28 potent BA.1-neutralising mAbs induced by BA.1 breakthrough infections, and most of them cross-neutralise Victoria, Alpha, Beta, Gamma, Delta, and BA.1. It suggests that there is still space available on the SARS-CoV-2 RBD for the binding of potent mAbs that can broadly neutralise all VoCs attributing to the plasticity of the public antibody responses through IGVH3-53/IGVH3-66 and IGVH1-58.

We observed that all the mutations in BA.1, except for S371L, require only one single-nucleotide change, which opened up the potential for two-nucleotide mutations and epistatic mutations to generate future variants.

CHAPTER 7 Immune escape of SARS-CoV-2 Omicron sublineages

7.1 Introduction

Since the emergence of SARS-CoV-2 in late 2019, it has caused more than 700 million confirmed cases and 7 million deaths globally. SARS-CoV-2 is an RNA virus, and its RNA polymerase is intrinsically error prone. It is estimated that one single-nucleotide change in SARS-CoV-2 RNA genome will be generated in an infected individual every day[170].

At the early stage of the pandemic, the immunity in the population towards SARS-CoV-2 was low, and spike mutations in RBD, like N501Y in Alpha which improves ACE2 affinity[79], were may have been selected for increased transmissibility[171], while others emerged on the background of strong population immunity conferred by vaccination or infection were likely driven by their ability to escape the neutralising antibody response. An extreme example is the occurrence of Omicron BA.1, which harbours 30 amino acid residue substitutions, 6 deletions and 3 insertions in its spike compared with ancestral spike sequence, producing a large antigenic distance with preceding strains. As we reported in the previous chapters, the mutations accumulated in the NTD and RBD of BA.1 spike led to huge decrease or knockout of neutralising abilities of sera from vaccinated or infected volunteers. As well, neutralising titres of several therapeutic antibodies were reduced or knocked out by mutations on BA.1 spike.

After spreading globally, Omicron developed at least 3 lineages in November 2021. The first wave of Omicron infection was caused by BA.1, followed by two Omicron sublineages, BA.1.1 and BA.2 in early 2022[172]. BA.2 dominated globally shortly after and continued to generate a succession of variants: first BA.2.12.1[173], followed by BA.4 and BA.5[82], and BA.5 became the globally dominant variant in June 2022. After the dominance of BA.5, several new trends were observed in the evolution of Omicron: firstly, the emergence of the second generation of BA.2 variants, including derivatives of BA.5, like BA.2.75, BJ.1, BS.1, BA.2.10.4, and BA.2.3.20[174]; secondly, antigenic drift, both observed in BA.5 and within the secondary generation of BA.2 sublineages, notably BQ.1 and BA.2.75[175]; finally, the recombination between two of these second-generation variants, for example BJ.1 and BM.1.1.1 have produced XBB. These Omicron sublineages are dominating globally right now, with XBB accounting for 80% of infections globally. Many of these variants show a large degree of convergent evolution at the

known antigenic residues in RBD, which may lead to escape from of antibody neutralisation and the protection afforded by vaccination or previous SARS-CoV-2 infection.

Here we report the mutations and antigenic characterisations of a series of Omicron sublineages, and their immune escape of the neutralisation by sera from individuals who were triple vaccinated or suffered from breakthrough infection. We also explored the neutralisation of the Omicron sublineage by the potent BA.1 mAbs we isolated previously, and found that the neutralisation of all but one BA.1 mAbs are severely hampered or completely knocked out by at least three Omicron sublineages. Finally, we tested a panel of therapeutic mAbs against the Omicron sublineages, and all lost their function against one or more variants.

7.2 Results

7.2.1 Emerging Omicron sub-lineages

Comparing with BA.1, BA.1.1 have an extra mutation, R346K, in its RBD (Table 1.1). BA.2 shares 21 amino acid changes with BA.1, but also has an additional 3 deletions and 7 substitutions; BA.1 has extra 6 amino acid deletions, 3 insertions, and 9 substitutions compared to BA.2 (Table 1.1). Some of the mutations in the RBD of BA.1, BA.1.1, and BA.2 have the potential to affect antibody binding and could affect neutralisation, particularly G446S and G496S in BA.1, D405N and R408S in BA.2, and the BA.1.1 additional R346K change.

At present, a number of variants within BA.2 and BA.5 branches are growing rapidly. Remarkably, there is a large degree of convergent evolution, particularly at antigenic positions in RBD, for example R346 (T, K), K444T (R), L452 (R, Q, M), N460 (K), F486 (V, S, P), F490 (S, V), Q493R (or reverse mutation), and S494 (P). These lineages include those from BA.4/5 branches which contain L452R, F486V, and the reverse mutation R493Q, such as BA.4.6 and BF.7(R346T), BQ.1 (K444T, N460K), and BQ.1.1 (R346T, K444T, N460K); from BA.2.75 branch which are characterised by G339H, G446S, N460K, and the reverse mutation R493Q, such as BA.2.75.2 (R346T, F486A) and BN.1 (R346T, K356T, F490A). There are also other second generation of BA.2 variants, for example BJ.1 (G339H, R346T, L368I, V445P, G446S, V483A, F490V), BA.2.10.4 (G446S, F486P, S494P, reverse mutation R493Q), BS.1 (R346T, L452R, N460K, G476S, reverse mutation R493Q), BA.2.3.20 (K444R, N450D,

L452M, N460K, E484R, reverse mutation R493Q), and XBB (R346T, L368I, V445P, G446S, N460K, F486S, F490S, reverse mutation R493Q), which is a recombinant variant of BJ.1 and BM.1.1.1 (Table 1.1). The distribution of the mutations on the surface of the RBD is shown in Figure 7.1.

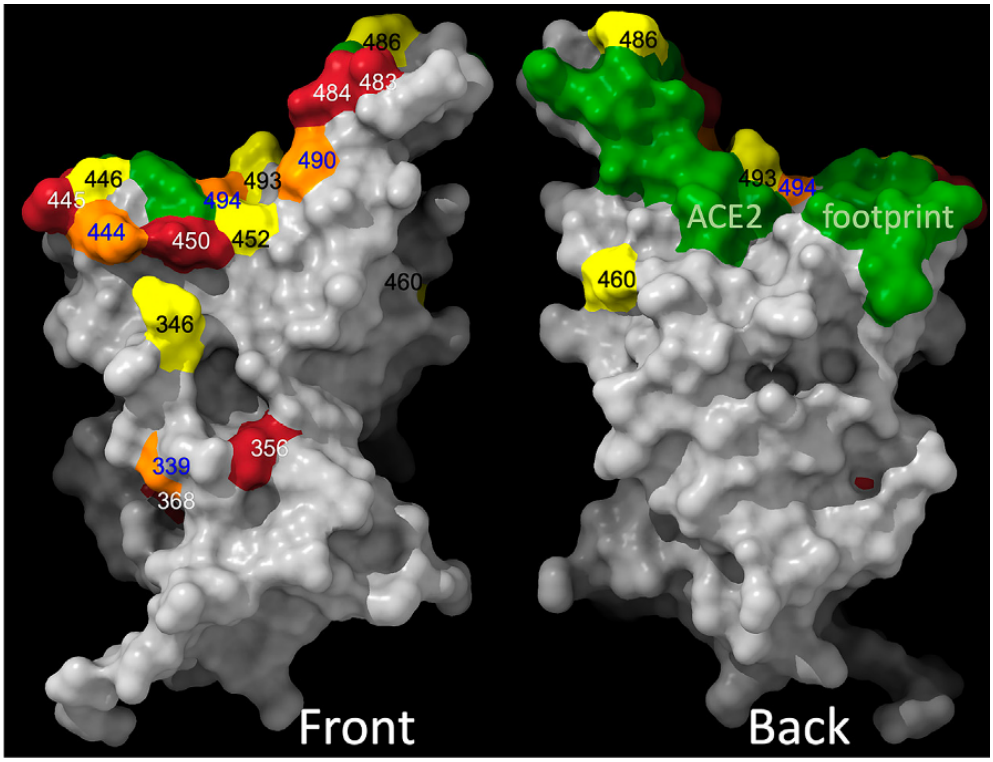

Figure 7.1 Amino acid changes in Omicron sublineages are shown on the RBD surface. The ACE2 footprint is shown in green. Colouring is according to the frequency count for the change in the various sub-variants, red represents low frequencies and yellow represents high frequencies. The figures were depicted by Prof. David I. Stuart.

7.2.2 Widespread escape from neutralisation by Omicron mAbs

Live virus of BA.1, BA.1.1, and BA.2 were isolated from patient swabs in our lab, and confirmed by Sanger sequencing. Firstly, we tested the neutralisation of the 27 potent antibodies we isolated from samples acquired after BA.1 breakthrough infection against the three live viruses (Figure 7.2A and Table 7.2). The NTD-specific mAb Omi-41 was omitted for the test due to the lack of neutralisation against BA.2 and its sublineages. Most of the mAbs show little difference between BA.1, BA.1.1, and BA.2. But there are some exceptions: BA.1.1 neutralisation was reduced 28-fold and 193-fold compared to BA.1 for Omi-6 and -32, respectively, and knocked out Omi-38 and -39; BA.2 neutralisation was reduced 189-, 79-, and 26-fold compared to BA.1 for Omi-8, -32, and -33, respectively.

To test the neutralisation of the panel of BA.1 mAbs against newly emerged BA.2 sublineages, we constructed a set of pseudoviruses expressing spike gene with the variant sequences and measured their resilience against BA.1 mAbs using BA.2 pseudovirus as comparison (Figure 7.2B and Table 7.2).

On BA.4, the activity of 9/27 was knocked out, and four antibodies, Omi-09, -12, -29, and -35 showed >5-fold reduction in the neutralisation titre of BA.4/5 compared with BA.2. All antibodies in IGHV1-69 family, except for Omi-38, failed to neutralize BA.4/5, due to their interaction with L452R mutation (or F486V mutation in the case of Omi-02). Omi-38 has interaction with the residue R346K indicated by its potent neutralisation against BA.1 and inactivity against BA.1.1, hence it retains the neutralisation against BA.4.

BA.2.75 particularly affected neutralisation of mAbs in IGHV3-53 and 3-66 family, with 3 mAbs completely knocked out (Omi-26, -29, and -36) and Omi-17, -20, -27, and -28 reduced 4-, 12-, 196-, and 17-fold, respectively. On the other hand, BA.2.75.2 showed a much broader impact on neutralisation of BA.1 mAbs with 20/27 losing their function completely, showing that BA.2.75.2 has evolved to evade antibody responses initiated by BA.1 infection.

BA.2.3.20, which has a number of mutations across the top of the shoulders, neck, and the back of the RBD (Figure 7.1), also caused a considerable disruption: neutralisation of 11/27 mAbs were knocked out by BA.2.3.20. For BJ.1, which has a different set of mutations across the top of the RBD, the activity of 11/27 mAbs were completely lost.

Finally, the activity of most mAbs was reduced or completely knocked out against BQ.1, BQ.1.1, BS.1, BN.1, XBB, and XBB.1, while some of the mAbs retained activity against BA.2.10.4. Only one antibody, Omi-42, was unusually unaffected by all variants. Omi-42 binds at the back of the left shoulder of the RBD (Figure 6.8A) in an area that has not been targeted by mutations in the set of BA.2 sublineages, perhaps because of the rarity of antibodies binding in this region.

Table 7.2 Heat map of IC50 neutralisation titres for the panel of BA.1 mAbs, related to Figure 7.2.

mAbs	WT virus								Psudo-virus															
	Victoria	Alpha	Beta	Gamma	Delta	BA.1	BA.1.1	BA.2	Victoria	BA.2	BA.2.12.1	BA.4/5	BA.4.6	BA.2.75	BA.2.75.2	BA.2.3.20	BJ.1	BF.7	BQ.1	BQ.1.1	BS.1	BA.2.10.4	BN.1	XBB	XBB.1
Omi-29 (3-53)	0.044	0.066	0.048	0.040	0.029	0.036	0.052	0.192	0.014	0.056	0.011	0.396	0.170	10.000	10.000	10.000	0.025	0.266	0.266	10.000	10.000	1.738	10.000	10.000	10.000
Omi-36 (3-66)	0.056	0.047	0.018	0.015	0.026	0.038	0.053	0.105	0.022	0.030	0.051	0.024	0.029	10.000	10.000	10.000	0.045	0.043	10.000	10.000	10.000	0.110	10.000	10.000	10.000
Omi-16 (3-66)	0.016	0.022	0.018	0.022	0.016	0.019	0.027	0.067	0.014	0.034	0.017	0.029	0.007	10.000	10.000	1.075	0.025	0.034	0.034	10.000	10.000	0.073	10.000	10.000	10.000
Omi-27 (3-66)	0.026	0.032	0.019	0.017	0.010	0.091	0.239	0.039	0.008	0.034	0.005	0.069	0.023	6.672	10.000	0.215	0.007	0.032	0.032	10.000	10.000	0.140	10.000	10.000	10.000
Omi-17 (3-66)	0.066	0.098	0.021	0.021	0.074	0.028	0.026	0.095	0.023	0.060	0.022	0.028	0.039	0.255	10.000	0.347	0.030	0.100	0.100	10.000	6.675	0.068	1.294	10.000	10.000
Omi-20 (3-66)	0.012	0.023	0.019	0.019	0.008	0.043	0.032	0.022	0.009	0.015	0.007	0.014	0.008	0.178	10.000	0.030	0.009	0.014	1.222	1.479	0.481	0.041	1.017	10.000	10.000
Omi-28 (3-66)	0.028	0.028	0.019	0.033	0.018	0.032	0.075	0.047	0.022	0.008	0.007	0.028	0.035	0.133	10.000	0.053	0.010	0.056	3.382	10.000	0.555	0.323	1.191	10.000	10.000
Omi-18 (3-53)	0.041	0.038	0.018	0.016	0.025	0.006	0.006	0.007	0.008	0.005	0.002	0.005	0.006	0.035	10.000	0.011	0.005	0.007	1.021	1.143	0.009	0.017	0.134	10.000	10.000
Omi-03 (3-53)	0.007	0.012	0.009	0.004	0.004	0.009	0.015	0.028	0.003	0.008	0.005	0.017	0.006	0.017	0.546	0.020	0.014	0.016	0.681	0.541	6.895	0.024	0.088	4.239	4.876
Omi-24 (1-69)	0.005	0.008	0.006	0.010	10.000	0.007	0.035	0.008	0.005	0.007	10.000	10.000	10.000	0.008	10.000	10.000	10.000	10.000	10.000	10.000	10.000	3.889	10.000	10.000	10.000
Omi-31 (1-69)	0.007	0.020	0.011	0.017	10.000	0.010	0.017	0.083	0.376	0.013	10.000	10.000	10.000	0.014	0.012	10.000	10.000	10.000	10.000	10.000	10.000	0.014	10.000	10.000	10.000
Omi-34 (1-69)	0.003	0.041	0.003	0.008	10.000	0.028	0.074	0.014	0.007	0.009	10.000	10.000	10.000	0.005	0.005	10.000	10.000	10.000	10.000	10.000	10.000	0.011	10.000	10.000	10.000
Omi-30 (1-69)	0.109	0.043	0.028	0.038	10.000	0.058	0.084	0.045	0.012	0.011	10.000	10.000	10.000	0.008	0.009	0.343	1.827	10.000	10.000	10.000	10.000	0.017	10.000	10.000	10.000
Omi-02 (1-69)	0.015	0.014	0.009	0.004	0.014	0.013	0.015	0.040	0.002	0.003	0.004	10.000	10.000	0.009	10.000	0.013	0.011	10.000	10.000	10.000	0.052	10.000	0.013	10.000	10.000
Omi-38 (1-69)	0.001	0.009	0.004	0.002	0.004	0.054	10.000	0.027	0.015	0.005	0.004	0.005	10.000	0.011	10.000	10.000	10.000	10.000	10.000	10.000	10.000	0.101	10.000	10.000	10.000
Omi-35 (3-9)	0.057	0.080	0.128	0.136	0.280	0.069	0.262	0.082	0.018	0.094	0.667	1.687	10.000	0.020	10.000	10.000	10.000	10.000	10.000	10.000	10.000	0.039	10.000	10.000	10.000
Omi-25 (3-9)	0.003	0.007	0.059	0.257	0.006	0.046	0.138	0.056	0.005	0.024	0.007	10.000	10.000	0.014	10.000	0.025	0.041	10.000	10.000	10.000	0.040	10.000	0.097	10.000	10.000
Omi-42 (3-9)	0.016	0.024	0.011	0.013	0.019	0.014	0.017	0.031	0.013	0.021	0.009	0.013	0.010	0.003	0.011	0.018	0.010	0.011	0.013	0.021	0.023	0.023	0.024	0.017	0.009
Omi-26 (1-18)	0.005	0.010	0.055	0.214	0.005	0.034	0.055	0.030	0.002	0.013	0.007	10.000	10.000	0.010	10.000	0.006	0.031	10.000	10.000	10.000	0.005	10.000	0.041	10.000	10.000
Omi-32 (3-33)	0.032	0.102	0.460	0.430	0.012	0.024	4.642	1.899	0.010	2.682	0.070	0.035	10.000	0.354	10.000	10.000	10.000	10.000	0.061	10.000	10.000	10.000	10.000	10.000	10.000
Omi-33 (3-33)	0.028	0.057	0.136	0.132	0.011	0.026	0.113	0.681	0.027	0.068	0.008	0.013	10.000	0.053	10.000	10.000	10.000	10.000	0.041	10.000	10.000	0.109	10.000	10.000	10.000
Omi-06 (4-4)	0.007	0.011	0.012	0.010	5.040	0.054	1.505	0.238	0.007	0.039	10.000	10.000	10.000	0.063	10.000	10.000	10.000	10.000	10.000	10.000	10.000	0.420	10.000	10.000	10.000
Omi-23 (4-31)	0.005	0.009	0.020	0.018	0.006	0.044	0.030	0.028	0.005	0.019	0.009	10.000	10.000	0.011	10.000	0.009	0.024	10.000	10.000	10.000	3.113	10.000	0.018	10.000	10.000
Omi-39 (3-43)	0.015	0.039	0.009	0.014	0.012	0.025	10.000	0.073	0.014	0.026	0.018	0.035	10.000	0.027	10.000	10.000	10.000	10.000	10.000	10.000	10.000	0.011	10.000	10.000	10.000
Omi-09 (3-30)	0.004	0.002	1.218	2.373	0.008	0.011	0.017	0.034	0.006	0.008	0.016	0.166	0.108	0.003	0.012	0.133	10.000	0.376	0.215	0.217	0.029	10.000	0.165	10.000	10.000
Omi-08 (1-46)	0.014	0.022	0.007	0.024	0.048	0.008	0.007	1.510	0.008	0.114	0.099	0.086	0.033	0.036	0.027	0.426	10.000	0.192	0.501	0.633	0.584	0.024	0.063	10.000	10.000
Omi-12 (1-58)	0.005	0.003	0.006	0.003	0.003	0.004	0.009	0.010	0.006	0.003	0.002	0.429	0.074	0.003	10.000	0.008	0.004	0.496	5.902	7.949	0.167	10.000	0.004	10.000	10.000

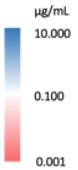

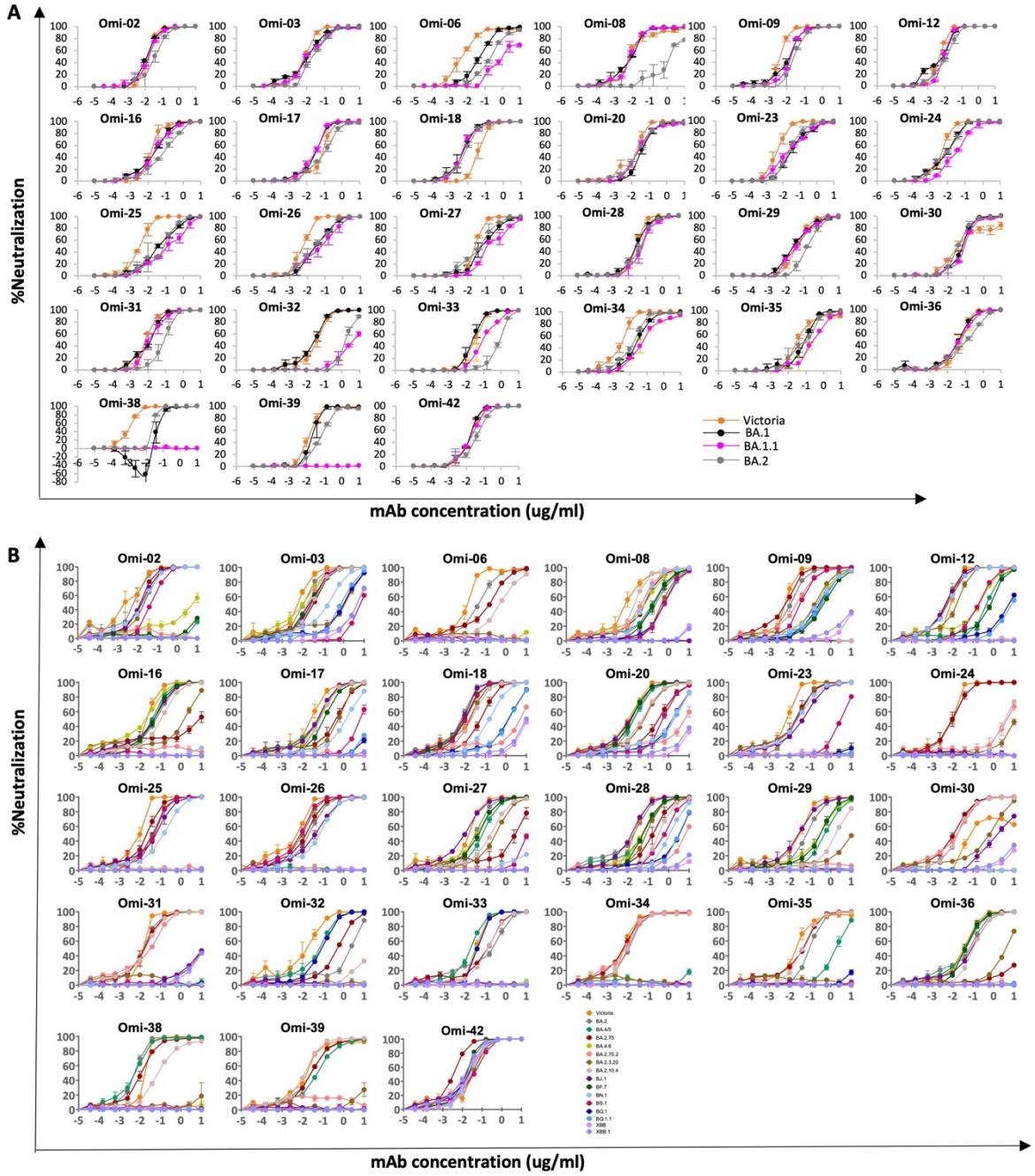

Figure 7.2 Neutralisation assays of BA.1 mAbs against Omicron sublineages. (A) Live virus neutralisation curves of BA.1 mAbs against Victoria, BA.1, BA.1.1, and BA.2 viruses. (B) Neutralisation curves of BA.1 mAbs using psudotyped lentivirus with the S gene of the indicated BA.2 sublineages.

7.2.3 Neutralisation of Omicron sub-lineages by therapeutic mAbs

A panel of mAbs developed for clinical use[162,163,176,177] were tested against the pseudo-typed viruses of BA.2 sublineages (Figure 7.3 and Table 7.3).

AZD8895, AZD1061, and AZD7442: AZD8895 and AZD1061 bind the back of the left shoulder and the front of the right shoulder, respectively (Figure 6.4). AZD1061 potently neutralises BA.2, BA.4/5, BA.2.75, and BA.2.10.4, although there is a 36-fold reduction on BA.2.10.4 compared with Victoria, while AZD8895 retained high neutralising ability against BA.2.75, BA.2.3.20, BJ.1 and BN.1. Both antibodies were failed to neutralise the other BA.2 sublineages, including a remarkable decrease of activity on BA.2 by AZD8895. AZD7442 is a cocktail antibody formed by AZD8895 and AZD1061, and it showed a combined profile of the two individual antibodies.

REGN10987 and REGN10933: REGN10933 binds the back of the left shoulder, and REGN10987 binds the right shoulder. Both antibodies suffered huge reduction of activities or completely knocked out by all BA.2 sublineages we tested here.

LY-CoV016, LY-CoV555 and LY-CoV1404: LY-CoV016 and LY-CoV555 completely lost their activity against BA.2 and all its sublineages due to their sensitivity to mutation N501Y and E484K, respectively. LY-CoV1404, on the other hand, was only inactive on BQ.1, BQ.1.1, BJ.1, XBB and XBB.1, probably due largely to the K444T mutation on BQ.1 and BQ.1.1, and V445P mutation on XBB and XBB.1.

ADG20: The function of ADG20 was knocked out by all BA.2 sublineages.

Vir-S309: S309 retains some level of activity across the Omicron lineages except BN.1. A glycan on spike protein attached to the residue 343 of the RBD is essential for S309 binding, and the combination of G339H, R346T, and K356T mutations in BN.1 severely interrupted the binding of S309.

Table 7.3 Heatmap of IC50 neutralisation titres of commercial mAbs.

	Pseudovirus Neutralisation														
	Victoria	BA.2	BA.4/5	BA.4.6	BA.2.75	BA.2.75.2	BA.2.3.20	BF.7	BQ.1	BQ.1.1	BJ.1	BS.1	BA.2.10.4	BN.1	XBB	XBB.1
AZD1061	0.002	0.008	0.015	10.000	0.021	10.000	10.000	10.000	10.000	10.000	10.000	10.000	0.072	10.000	10.000	10.000
AZD8895	0.001	1.333	10.000	10.000	0.008	10.000	0.007	10.000	10.000	10.000	0.085	10.000	10.000	0.024	10.000	10.000
AZD7442	0.001	0.008	0.065	10.000	0.017	10.000	0.026	10.000	10.000	10.000	0.228	10.000	0.098	0.068	10.000	10.000
REGN10987	0.002	0.616	10.000	10.000	10.000	10.000	10.000	3.925	10.000	10.000	10.000	10.000	10.000	10.000	10.000	10.000
REGN10933	0.001	10.000	10.000	10.000	10.000	10.000	8.624	10.000	10.000	10.000	10.000	10.000	10.000	1.954	10.000	10.000
ADG20	0.003	10.000	10.000	10.000	10.000	10.000	10.000	10.000	10.000	10.000	10.000	10.000	10.000	10.000	10.000	10.000
Ly-CoV555	0.002	10.000	10.000	10.000	10.000	10.000	10.000	10.000	10.000	10.000	10.000	10.000	10.000	10.000	10.000	10.000
Ly-CoV16	0.014	10.000	10.000	10.000	10.000	10.000	10.000	10.000	10.000	10.000	10.000	10.000	10.000	10.000	10.000	10.000
Ly-CoV1404	0.001	0.001	0.002	0.001	0.002	0.002	0.018	0.002	10.000	10.000	10.000	0.004	0.003	0.004	10.000	10.000
S309	0.079	0.638	0.689	1.029	0.202	0.465	0.977	0.801	0.662	0.751	0.839	2.696	0.410	10.000	0.455	0.142

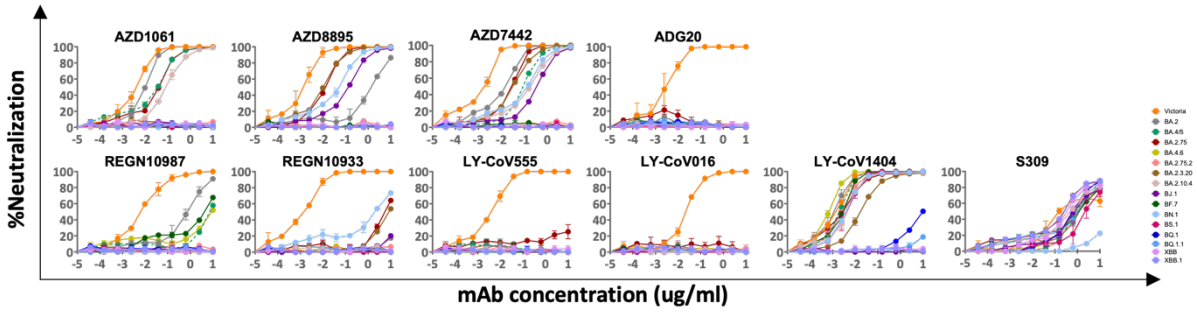

Figure 7.3 Neutralisation assays against pseudotyped lentivirus of the indicated BA.2 sublineages by commercial mAbs.

7.2.4 Severe knockdown of serum neutralisation titres

We tested neutralisation on serum samples collected 28 days following a third dose of Pfizer BNT162b2 vaccine and breakthrough cases infected by BA.1, BA.2 or BA.4/5 after the third dose of vaccine.

For serum collected 28 days post BNT162b vaccination, BA.2.75.2, XBB, and XBB.1 showed significant disruption on neutralisation with 16.6-, 20.5-, and 20.9-fold reduction, respectively, compared with BA.2 (Figure 7.4A). There was also large reduction in titres to BQ.1, BQ.1.1 and BA.2.3.20, 9.9-, 7.7-, and 11.3-fold, respectively, compared with BA.2. In contrast to BA.2.75.2, BA.2.75 only showed modest reduction compared with BA.2. The titres of BA.4.6, BJ.1 and BN.1 reduced 4.9-, 3.8-, and 3.9-fold, respectively, compared with BA.2, but less remarkable compared with BA.2.75.2, XBB, and XBB.1.

Next, we tested serum taken following BA.1, BA.2, or BA.4/5 infection; all were vaccine breakthrough infections except for one unvaccinated case of BA.4 infection (Figure 7.4B-D). In all cases, the later emerged Omicron lineages reduced the neutralisation titre of these infection serum compared with BA.2 and BA.4/5, but the reduction was generally to a lesser extent compared with those seen in BNT162b2 vaccine serum, likely due to the higher level of Omicron antibodies found in these serum samples. But we also observed that the reduction in neutralisation of XBB showed considerable escape from BA.1, BA.2 and BA.4/5 infection sera, with 22.1-, 44.8-, and 213-fold reduction in titres, respectively, compared with BA.2. BA.4/5 infection sera.

Overall, there were large reductions in neutralisation titres against most BA.2 sublineages, especially BA.2.75.2, BA.2.3.20, BQ.1, BQ.1.1, XBB and XBB.1, suggesting that they have been selected to escape pre-existing immunity to vaccines or earlier waves of SARS-CoV-2 infection, and they might become the dominant variants. Indeed, BQ.1/BQ.1.1 and XBB/XBB.1/XBB.1.5 have caused new waves of SARS-CoV-2 infection in several regions.

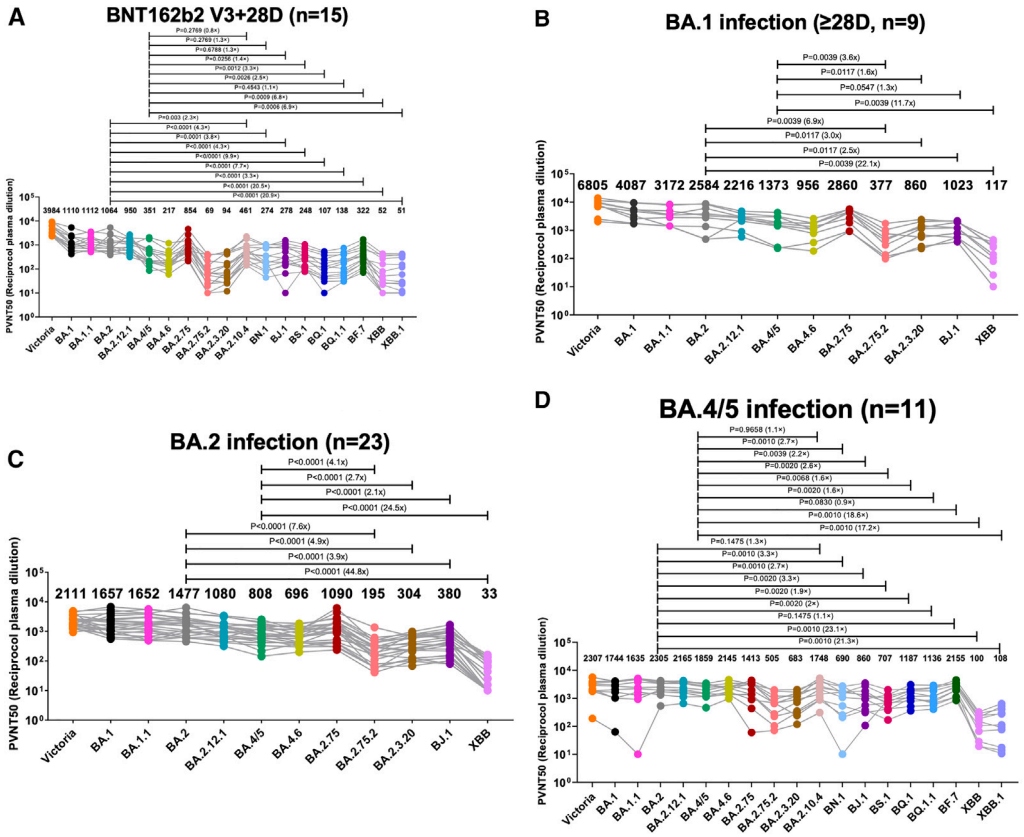

Figure 7.4 Serum neutralisation IC50 titres of pseudotyped lentivirus with the spike gene of the indicated BA.2 sublineages. (A) Serum obtained 28 days following the third dose of BNT162b2 vaccine (n = 15). (B-D) Serum taken 28-55 days (median 41.5 days) after PCR confirmed BA.1 breakthrough infection (n=9) (B), 12-43 days (median 29 days) following diagnosed breakthrough BA.2 infection (n = 23) (C), and 23-48 days (median 38 days) post PCR confirmed BA.4/5 infection (n = 11). The Wilcoxon matched-pairs signed rank test were used and two-tailed *p* values were calculated.

7.3 Discussion

In the early stage of the pandemic, RBD mutations existing in the variants prior to Omicron were in small numbers: 1 change in Alpha, 2 in Delta, and 3 in Beta and Gamma. The mutations in the RBD of these variants may have been selected by increased binding affinity with ACE2, although they also conferred the ability of immune escape to an extent. But the emergence and rapid spread of BA.1 in November 2021, with more than 39 amino acid changes in its spike

including 15 in RBD, astonished many in the field. The origin of this variant is assumed to be from a person with chronic infection and spread silently among population, but solid proof is still lacking.

Since the majority of the population have been either vaccinated or infected, it is likely that the evolution of variants in the SARS-CoV-2 Omicron family is now primarily driven by the pressure from immune response induced by vaccination and/or natural infection, with compensatory mutations to maintain or increase ACE2 affinity[81]. There has been a number of changes in the RBD of Omicron lineages to indicate convergent evolution. Many mutations are at the edge of the ACE2 binding footprint to knock out potent antibodies that block ACE2[10]. The RBD shows a high level of plasticity, able to accommodate wide-ranging changes while maintaining its binding affinity with ACE2. There are in total 29 residue mutations in RBD in all Omicron lineages compared with early-pandemic virus. This level of variations, focusing on the antigenic site and leading to remarkable immune escape, would conventionally lead to classify these variants into different serotypes[178]. The plasticity of the RBD at and around the small ACE2-bidning site means that rather than being a conserved antigenic site targeting by neutralising antibodies, it gives the virus the immense ability to throw off large parts of the antibody response through numerous mutations.

We have also observed here the failure to neutralise BA.2 sublineages by BA.1 mAbs and commercial mAbs, especially on BQ.1, BQ.1.1, BS.1, BN.1, XBB, and XBB.1. New approaches may be required to discover potent mAbs that bind at the conserved sites on spike that are not under immense selective pressure or have unique binding patterns that can circumvent the immune escape conferred by some residue changes. As observed in BA.1 mAbs, somatic mutation will probably be able to repair some antibodies.

CHAPTER 8 Generation of potent antibodies from BA.2 breakthrough cases

8.1 Introduction

Since the emergence of SARS-CoV-2 in late 2019, effective vaccines have been speedily developed, together with the increasing herd immunity from natural infection, greatly reduced the mortality from SARS-CoV-2 infection, although they are less efficient on preventing infection. These vaccines were all designed based on the spike proteins of the early-pandemic SARS-CoV-2 delivered in different ways[108,179].

Analysis of panels of S-specific mAbs by several laboratories has indicated that two domains of the S1 region of spike, NTD and RBD, are the main binding sites for potential neutralising mAbs. All known potent anti-NTD mAbs bind to an NTD supersite which do not block the interaction between ACE2 and S and the mechanism of this neutralisation is unknown. Most potent anti-RBD mAbs bind on or around the RBM, which is a 25 amino acid patch lying at the tip of the RBD to interact with ACE2 receptor. All commercial mAbs to date target the RBD, while potent anti-NTD mAbs are always SARS-CoV-2 variant specific due to the extensive mutation of the supersite between variants.

Following the detection and rapid spread of Omicron lineages, we have observed the loss of function on commercial antibodies against Omicron lineages and the significant reduction of titres on serum samples taken from vaccinated or infected volunteers[28]. These variants are likely to be selected by huge pressure of immune escape from antibodies induced by vaccination or previous infection, so it is vital to find effective antibodies that can potently neutralise all existing Omicron lineages while possibly resist to potential new variants emerging from near future.

In this study, we generated a set of mAbs from vaccinated volunteers who suffered breakthrough BA.2 infections. BLI were used to determine the binding area of the panel of BA.2 mAbs, and three distinctive binding patches were seen on RBD. This corresponds to a refocusing of the response, similar to that seen in BA.1. The positions of the binding sites strongly overlap with the mutations on the BA.2 sublineages.

8.2 Results

8.2.1 Antibody isolation from BA.2 infected cases

During the BA.2 wave in April 2022, 7 blood samples were obtained from volunteers >24 days (median 29 days) after PCR (n = 1) or lateral flow test (n = 6) confirmed SARS-CoV-2 infection, all triple vaccinated before infection. Three samples with the highest titres against BA.2 live virus were selected for mAb production, and single IgG-positive B cells were stained and sorted using BA.2 S trimer (Figure 8.1A). Following a reverse-transcript PCR and Nested-PCR, heavy chains and light chains were ligated into expression vectors using Gibson assembly. Gibson products were transient transfected into 293T cells, and the supernatants were collected and tested for reactivity to full-length BA.2 S or BA.2 RBD. As we observed in antibodies generated from BA.1 infection samples, a high proportion (67%) of mAbs are RBD-specific mAbs (Figure 8.1B). The neutralising ability of the supernatants were also tested against BA.2 authentic virus using FRNT, and from 672 sorted cells we recovered 383 antibodies, and 25 potent mAbs (FRNT50 < 100 ng/ml against BA.2) were selected for further characterisation.

We tested the ability of BA.2 mAbs to block the interaction between ACE2 with BA.2 S (Figure 8.1C). Seven BA.2 mAbs (BA.2-5, -13, -15, -21, -24, -34, and -36) had little or no ACE2 blocking ability.

Heavy chain and light chain gene usages were analysed for the set of mAbs, as shown in Figure 8.1D and Table 8.1. In the BA.2 mAbs, 10/25 mAbs belonged to IGHV1-69 family, a further expansion from that found in the set of BA.1 mAbs we generated previously (6/28). The public gene family IGHV3-53 and IGHV3-66 were less represented in the BA.2 mAbs (3/25) than in the BA.1 mAbs (9/28).

Somatic mutation in the BA.2 were analysed (Figure 8.1E). The numbers of somatic mutation in the two sets of mAbs were significantly greater than those in the early pandemic mAbs, but on the same level with each other and as well as BA.1 mAbs.

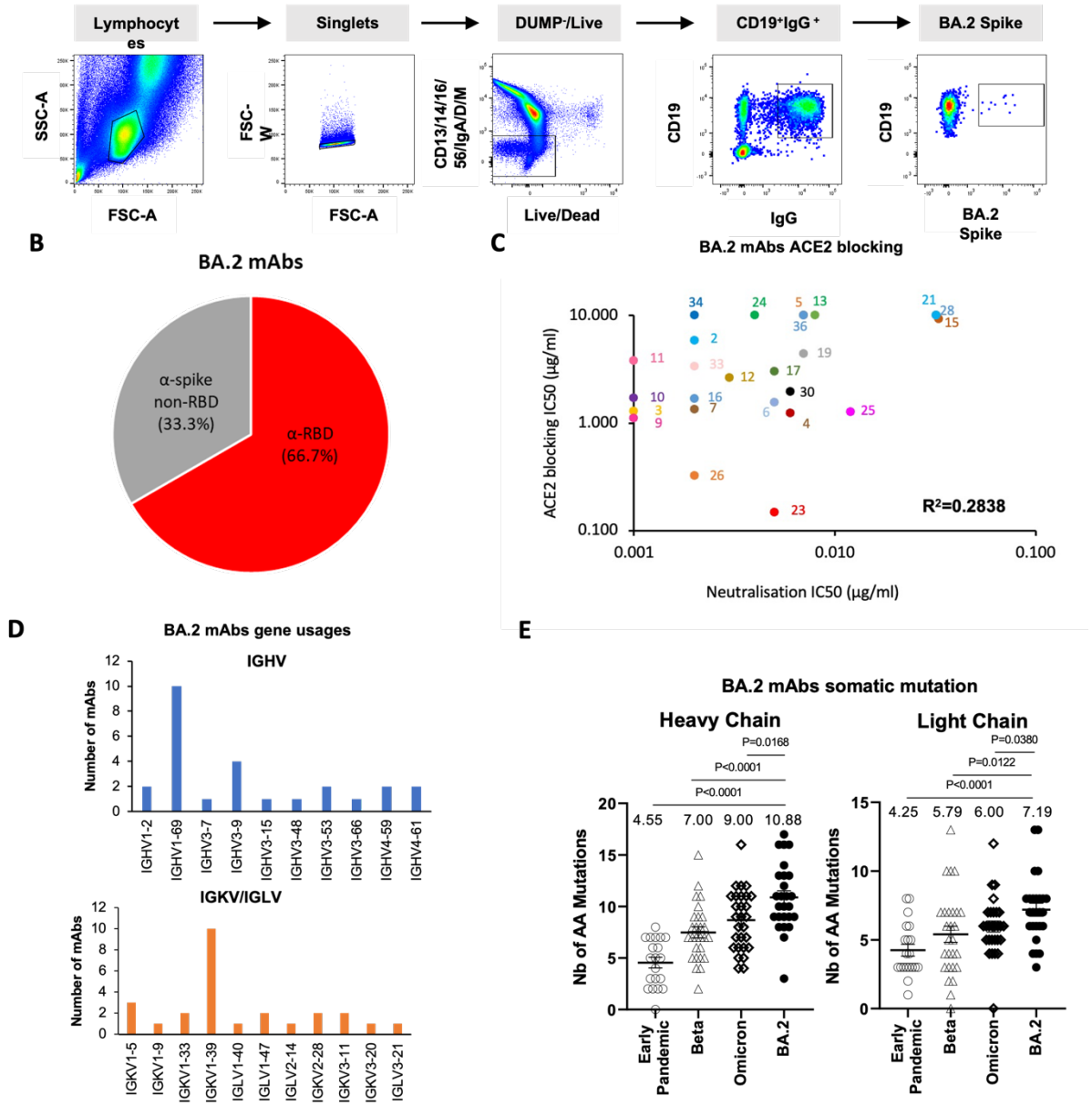

Figure 8.1 Generation of BA.2 and BA.4/5 mAbs. (A) Sorting of BA.2 S-specific B cells. (B) Proportion of RBD-specific mAbs in BA.2 mAbs. (C) The ability of BA.2 mAbs block interaction between ACE2 and BA.2 S. (D) Heavy chain and light chain gene usage in 25 potent BA.2 mAbs and 29 potent BA.4/5 mAbs. (E) Number of somatic mutations in BA.2 mAbs compared with previous sets of mAbs isolated from infections by early pandemic strain, Beta, and BA.1.

Table 8.1 Heavy chain and light chain gene usage of BA.2 mAbs.

Ab id.	Protein-Specific	Heavy Chain					Light Chain				
		V-GENE and allele	J-GENE and allele	D-GENE and allele	V-REGION Nb of AA changes	CDR3 length	Light Chain	V-GENE and allele	J-GENE and allele	V-REGION Nb of AA changes	CDR3 length
BA.2-02	RBD	1-69*01 F, or 1-69D*01 F	5*02 F	3-22*01 F	10	19	K	1-39*01 F, or 1D-39*01 F	4*01 F	7	9
BA.2-03	RBD	1-2*02 F	6*02 F	3-16*02 F	10	23	K	3-11*01 F	5*01 F	6	9
BA.2-04	RBD	3-53*02 F	6*02 F	3-9*01 F	11	11	K	1-9*01 F	5*01 F	8	10
BA.2-05	RBD	1-69*06 F, or 1-69*17 F	6*02 F	3-3*02 F	9	17	λ	1-47*01 F	3*02 F	10	11
BA.2-06	RBD	1-69*01 F, or 1-69D*01 F	4*02 F	3-22*01 F	8	20	K	1-39*01 F, or 1D-39*01 F	1*01 F	4	9
BA.2-07	RBD	1-69*01 F, or 1-69D*01 F	5*02 F	3-22*01 F	13	19	K	1-39*01 F, or 1D-39*01 F	4*01 F	8	9
BA.2-09	RBD	1-2*02 F	6*02 F	3-16*02 F	11	23	K	3-11*01 F	5*01 F	8	9
BA.2-10	RBD	3-9*01 F	3*02 F	3-22*01 F	7	18	K	1-39*01 F, or 1D-39*01 F	3*01 F	8	9
BA.2-11	RBD	1-69*01 F, or 1-69D*01 F	5*02 F	3-22*01 F	9	19	K	1-39*01 F, or 1D-39*01 F	4*01 F	5	9
BA.2-12	RBD	3-9*01 F	6*02 F	2-21*02 F	8	16	K	1-39*01 F, or 1D-39*01 F	2*01 F	13	9
BA.2-13	RBD	3-15*01 F	3*01 F	3-10*01 F	9	17	K	1-39*01 F, or 1D-39*01 F	4*01 F	4	8
BA.2-15	RBD	1-69*01 F, or 1-69D*01 F	4*02 F	3-22*01 F	10	20	K	1-39*01 F, or 1D-39*01 F	1*01 F	3	9
BA.2-16	RBD	1-69*01 F, or 1-69D*01 F	5*02 F	3-22*01 F	9	19	K	1-39*01 F, or 1D-39*01 F	4*01 F	7	9
BA.2-17	RBD	1-69*06 F	6*02 F	3-3*01 F	9	19	λ	2-14*01 F	2*01 F, or 3*01 F	8	11
BA.2-19	RBD	3-48*03 F	4*02 F	1-26*01 F	8	13	K	1-5*03 F	1*01 F	6	10
BA.2-21	RBD	3-9*01 F	4*02 F	5-24*01 ORF	11	16	λ	1-40*01 F	3*02 F	7	11
BA.2-23	RBD	3-53*04 F	6*02 F	1-26*01 F	12	13	K	1-33*01 F, or 1D-33*01 F	5*01 F	8	9
BA.2-24	RBD	1-69*09 F	4*02 F	3-22*01 F	13	16	K	1-39*01 F, or 1D-39*01 F	5*01 F	6	9
BA.2-25	RBD	4-59*01 F	4*02 F	5-12*01 F	16	16	K	2-28*01 F, or 2D-28*01 F	3*01 F	7	9
BA.2-26	RBD	3-66*01 F, or 3-66*04 F	5*01 F, or 5*02 F	2-15*01 F	16	10	K	1-33*01 F, or 1D-33*01 F	4*02 (F)	10	8
BA.2-28	RBD	3-9*01 F	6*02 F	6-6*01 F	14	19	λ	3-21*02 F	2*01 F, or 3*01 F	6	11
BA.2-30	RBD	4-59*03 F	4*02 F	5-12*01 F	13	16	K	2-28*01 F, or 2D-28*01 F	3*01 F	6	9
BA.2-33	RBD	4-61*11 (F)	5*02 F	2-15*01 F	16	14	λ	1-47*01 F	2*01 F, or 3*01 F	13	11
BA.2-34	RBD	1-69*09 F	4*02 F	2-21*02 F	11	12	K	1-5*01 F	1*01 F	4	8
BA.2-36	RBD	4-61*02 F, or 4-61*11 (F)	4*02 F	6-25*01 F	17	11	K	1-5*01 F	1*01 F, or 4*02 (F)	7	8

8.2.2 Neutralisation of SARS-CoV-2 variants by BA.2

To determine the neutralising abilities of potent BA.2 mAbs, pseudo-typed lentivirus neutralisation assays were used to test the antibodies against 34 variants seen throughout the pandemic with the emphasis on Omicron lineages (Table 8.2). All BA.2 mAbs were completely knocked out by at least one variant, with the exception of BA.2-07. BA.2-07 competently neutralises most of the variants we tested here, but showed severe knockdown of neutralisation of XBF, XBB.1.5, XBB.1.5.10, and XBB.1.16, with 1558-, 841-, 1029-, and 66.5-fold reduction compared to BA.2, respectively. The activities of 15/27, 18/27, 24/27, 24/27, and 23/27 BA.2 mAbs were completely knocked out by the most spreading variants, BQ.1, BQ.1.1, XBB, XBB.1, and XBB.1.5, respectively.

8.2.3 Epitope mapping of the BA.2 mAbs by BLI

As we did with previous sets of mAbs, Dr. Daming Zhou performed pairwised BLI competition measurements on the 25 potent RBD-specific BA.2 mAbs and some early pandemic and BA.1 mAbs with known binding locations. The binding sites of these antibodies are shown in Figure 8.2.

To understand the change of antibody responses following the evolution of SARS-CoV-2, the antibody binding sites for four sets of responses following the pandemic are shown on the RBD surface (Figure 8.3A and 8.3B). Heatmaps are also shown to display the concentration of antibodies across the RBD surface (Figure 8.3C and 8.3D).

The BA.2 mAbs segregate into 3 adjacent clusters, two of which (left shoulder and neck) are also hotspot for the binding of potent early pandemic mAbs. The third cluster, which binds on the right chest, was also found in the early pandemic mAbs but not in the potent mAb set. In contrast, the potent mAbs in early pandemic set and Beta set are clustered into three regions adjacent to the ACE2-binding site at the right shoulder, the neck, and the left shoulder. On the other hand, the binding sites of BA.1 mAbs are very similar to the three clusters found in the BA.2 mAb sets (Figure 8.3A and 8.3B).

Table 8.2 IC50 Heatmap of pseudoviral neutralisation titres of BA.2 mAbs

IC50 (μg/mL) Pseudoviruses neutralisation

mAbs	Victoria	Alpha	Beta	Gamma	Delta	BA.1	BA.1.1	BA.2	BA.2.12.1	BA.4/5	BA.4.6	BA.5.9	BA.2.75	BA.2.75.2	BA.2.3.20	BA.2.10.4	BJ.1	BF.7	BS.1	BN.1	BN.1.2.1	BQ.1	BQ.1.1	BQ.1.1+ A475V	CK.1	CA.3.1	CH.1.1	XBF	DS.1	XBB	XBB.1	XBB.1.5	XBB.1.5.10	XBB.1.16
BA.2-02	0.002	0.002	1.609	1.386	0.004	0.002	0.002	0.002	0.049	10.000	10.000	10.000	0.001	0.159	3.180	10.000	2.306	5.554	0.276	0.599	10.000	7.262	6.416	10.000	10.000	10.000	10.000	10.000	10.000	10.000	10.000	10.000	10.000	10.000
BA.2-03	0.003	0.003	1.243	0.079	0.004	0.002	0.002	0.001	0.001	0.015	0.036	0.028	0.004	0.829	10.000	10.000	0.910	0.013	0.007	0.404	0.281	0.058	0.027	0.086	0.069	1.479	1.122	10.000	10.000	10.000	10.000	10.000	10.000	10.000
BA.2-04	0.003	0.004	0.002	0.002	0.006	0.002	0.001	0.006	0.003	0.009	0.011	0.008	0.087	2.103	0.018	0.022	0.005	0.009	0.088	0.988	0.489	1.400	1.268	10.000	3.547	5.291	4.935	10.000	10.000	10.000	10.000	5.196	10.000	4.899
BA.2-05	0.001	0.004	0.006	0.005	0.929	0.030	0.012	0.007	0.108	10.000	10.000	10.000	0.015	0.040	10.000	0.040	10.000	10.000	10.000	10.000	10.000	10.000	10.000	10.000	10.000	10.000	10.000	10.000	10.000	10.000	10.000	10.000	10.000	10.000
BA.2-06	0.004	0.004	9.816	10.000	0.003	0.006	0.004	0.005	0.100	10.000	10.000	10.000	0.011	0.410	10.000	10.000	10.000	10.000	1.047	10.000	10.000	10.000	10.000	10.000	10.000	10.000	10.000	10.000	10.000	10.000	10.000	10.000	10.000	10.000
BA.2-07	0.003	0.002	0.001	0.001	0.004	0.001	0.0004	0.002	0.003	0.002	0.003	0.002	0.001	0.002	0.004	0.004	0.003	0.005	0.014	0.003	0.001	0.009	0.005	0.009	0.005	0.003	0.003	3.116	0.003	0.008	0.011	1.681	2.058	0.133
BA.2-09	0.007	0.005	10.000	10.000	0.003	0.003	0.003	0.001	0.001	0.558	0.774	1.064	0.004	10.000	10.000	10.000	1.722	0.283	0.004	2.183	5.606	0.802	0.288	2.665	1.524	10.000	10.000	10.000	10.000	10.000	10.000	10.000	10.000	10.000
BA.2-10	0.000	0.000	0.000	0.001	0.001	0.001	0.000	0.001	0.002	0.001	0.092	0.002	0.001	0.176	0.152	0.003	10.000	0.223	0.493	2.011	1.929	4.054	10.000	10.000	0.625	10.000	10.000	0.231	1.172	10.000	10.000	10.000	10.000	10.000
BA.2-11	0.004	0.002	0.690	0.086	0.003	0.002	0.002	0.001	0.019	10.000	10.000	10.000	0.003	0.040	10.000	10.000	0.084	10.000	0.070	0.165	10.000	10.000	10.000	10.000	10.000	10.000	10.000	10.000	10.000	10.000	10.000	10.000	10.000	10.000
BA.2-12	0.003	0.001	0.003	0.001	0.003	0.004	0.003	0.003	0.004	2.731	3.000	6.994	0.004	10.000	0.007	10.000	0.008	0.531	0.019	0.006	0.002	10.000	7.069	10.000	10.000	10.000	10.000	10.000	10.000	10.000	10.000	10.000	10.000	10.000
BA.2-13	0.012	0.020	0.003	0.003	0.024	0.006	0.474	0.008	0.005	0.007	4.595	5.414	0.018	10.000	10.000	0.009	10.000	0.341	4.698	10.000	10.000	0.013	10.000	10.000	0.019	10.000	4.141	10.000	10.000	10.000	10.000	10.000	10.000	10.000
BA.2-15	0.003	0.006	10.000	10.000	0.004	0.062	0.029	0.033	0.210	10.000	10.000	10.000	0.070	0.899	10.000	10.000	10.000	10.000	0.986	10.000	10.000	10.000	10.000	10.000	10.000	10.000	10.000	10.000	10.000	10.000	10.000	10.000	10.000	10.000
BA.2-16	0.006	0.007	0.155	0.105	0.003	0.003	0.003	0.002	0.011	10.000	10.000	10.000	0.004	0.016	1.112	4.104	0.068	10.000	0.036	0.197	9.710	10.000	10.000	10.000	10.000	3.157	2.299	10.000	10.000	4.566	4.604	10.000	10.000	10.000
BA.2-17	0.009	0.011	0.010	0.005	10.000	0.010	0.030	0.005	0.052	10.000	10.000	10.000	0.011	0.013	0.066	0.022	10.000	10.000	10.000	5.279	1.743	10.000	10.000	10.000	10.000	10.000	10.000	2.154	2.434	10.000	10.000	10.000	10.000	10.000
BA.2-19	0.004	0.003	0.003	0.003	0.003	0.006	0.005	0.007	0.009	10.000	10.000	10.000	0.005	10.000	0.009	10.000	0.022	10.000	0.925	0.018	0.008	10.000	10.000	10.000	10.000	10.000	10.000	10.000	10.000	10.000	10.000	10.000	10.000	10.000
BA.2-21	0.013	0.012	0.040	0.028	0.008	0.067	0.816	0.032	0.028	0.100	10.000	10.000	0.030	0.404	0.221	0.096	10.000	10.000	10.000	10.000	10.000	0.234	10.000	10.000	0.523	10.000	10.000	10.000	10.000	10.000	10.000	10.000	10.000	10.000
BA.2-23	0.012	0.008	0.002	0.003	0.009	0.005	0.005	0.005	0.006	0.005	0.004	0.002	0.211	0.199	0.120	0.008	0.012	0.003	0.095	5.012	2.118	0.654	0.749	10.000	1.237	0.604	0.519	0.763	2.656	0.915	0.667	0.261	8.764	0.253
BA.2-24	0.015	0.009	0.002	0.003	10.000	0.010	0.008	0.004	10.000	10.000	10.000	10.000	0.002	0.004	10.000	0.008	10.000	10.000	10.000	10.000	10.000	10.000	10.000	10.000	10.000	10.000	10.000	10.000	10.000	10.000	10.000	10.000	10.000	10.000
BA.2-25	0.007	0.005	0.002	0.005	0.011	0.050	0.034	0.012	0.011	0.034	0.361	0.787	0.031	0.251	10.000	10.000	10.000	0.220	0.408	10.000	10.000	10.000	10.000	10.000	10.000	10.000	10.000	10.000	10.000	10.000	10.000	10.000	10.000	10.000
BA.2-26	0.005	0.007	0.001	0.001	0.006	0.001	0.001	0.002	0.003	0.003	0.003	0.004	10.000	10.000	10.000	0.014	0.003	0.004	0.815	10.000	10.000	10.000	10.000	10.000	10.000	10.000	10.000	10.000	10.000	10.000	10.000	10.000	10.000	10.000
BA.2-28	0.034	0.010	0.020	0.034	0.007	0.043	0.023	0.032	0.016	0.133	10.000	10.000	0.032	1.517	0.767	0.054	10.000	10.000	10.000	10.000	10.000	2.553	10.000	10.000	4.713	10.000	10.000	10.000	10.000	10.000	10.000	10.000	10.000	10.000
BA.2-30	0.008	0.003	0.012	0.009	0.017	1.596	10.000	0.006	0.045	10.000	10.000	10.000	0.670	10.000	10.000	10.000	10.000	10.000	10.000	10.000	10.000	10.000	10.000	10.000	10.000	10.000	10.000	10.000	10.000	10.000	10.000	10.000	10.000	10.000
BA.2-33	0.004	0.003	0.001	0.005	0.008	0.003	0.002	0.002	0.003	10.000	10.000	10.000	0.002	10.000	0.012	0.691	0.003	2.099	0.007	0.005	0.001	10.000	10.000	10.000	10.000	10.000	10.000	10.000	10.000	10.000	10.000	7.002	10.000	6.842
BA.2-34	0.004	0.002	0.001	0.002	0.029	0.033	4.176	0.002	0.333	1.515	10.000	10.000	0.007	1.880	10.000	0.051	10.000	10.000	10.000	10.000	10.000	10.000	10.000	10.000	10.000	10.000	10.000	10.000	10.000	10.000	10.000	10.000	10.000	10.000
BA.2-36	0.005	0.002	0.001	0.004	0.001	0.007	0.466	0.007	0.010	0.064	10.000	10.000	0.014	1.315	10.000	0.026	10.000	10.000	10.000	10.000	10.000	10.000	10.000	10.000	10.000	10.000	10.000	10.000	10.000	10.000	10.000	10.000	10.000	10.000

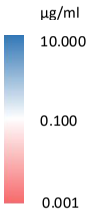

The right chest cluster, which is the most populous in BA.2 mAb set, has been identified in the BA.1 mAbs as a binding site for IGHV1-69 gene family antibodies. However, for BA.2 mAbs, only 4/10 IGHV1-69 mAbs bind here (BA.2-5, -17, -24, and -34) with 3/4 IGHV3-9 antibodies (-10, -21, and -28) (Figure 8.2). The second cluster is at the neck, which contains the remaining five IGHV1-69 BA.2 mAbs and matches one of the clusters of the BA.1 mAbs. The last cluster is at the left shoulder on the RBD, including the remaining IGHV3-9 antibodies, BA.2-12, and the three IGHV3-53/3-66 mAbs.

The relationship between the mutations in the BA.2 sublineages and the three BA.2 mAb hotspots indicates a strong correlation between them (Figure 8.3C and 8.3D). In summary, we saw that Omicron mAbs show a shift in focus of the antibody response, with BA.1 and BA.2 mAbs binding on similar areas, but BA.2 mAbs are more skewed from the early pandemic response.

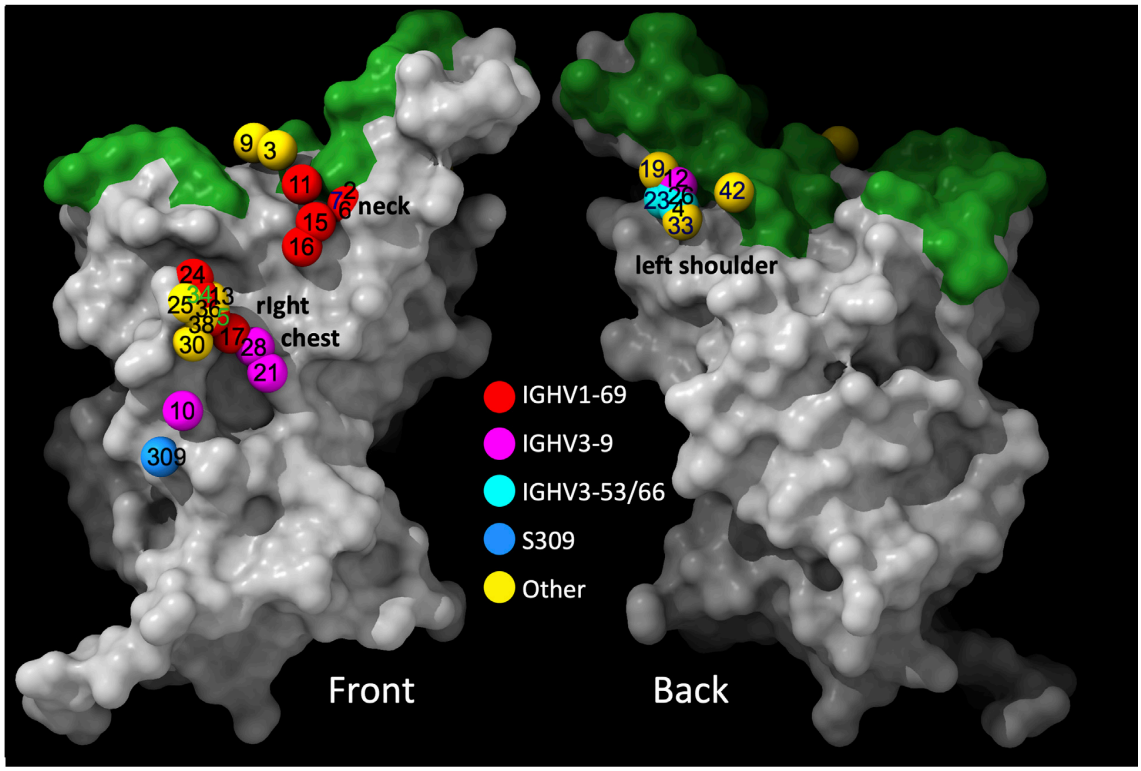

Figure 8.2 Result of BLI competition mapping of BA.2 mAbs**.** RBD surface representation with ACE-binding site in green and balls corresponding to centre of gravity of mapped potent BA.2 mAbs coloured according to variable gene usage. 42 in the figure represents Omi42 antibody isolated from BA.1 infected cases. The experiments were performed by Dr. Daming Zhou.

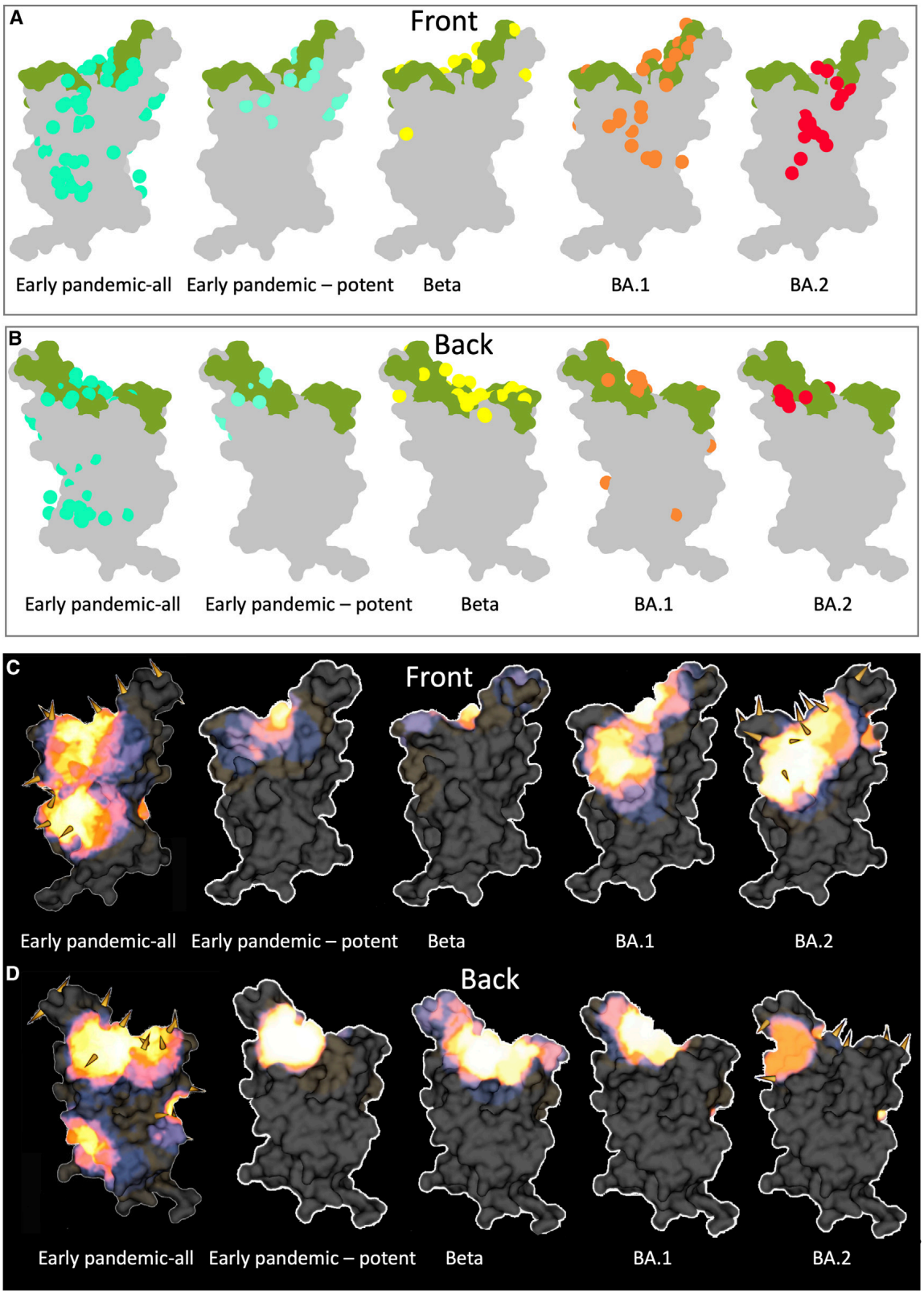

Figure 8.3 Comparison of mAb binding sites on RBD. (A and B) Front and back views of antibody maps from early pandemic, Beta, BA.1, and BA.2 antibody panels. Early pandemic-all represents the full panel of early pandemic mAbs, irrespective of their neutralising ability. All other panel show only potent mAbs (IC50 < 100 ng/ml). The RBDs are shown in grey with the ACE2 footprint in green. (C and D) Heatmaps of the binding sites on RBD of early pandemic, Beta, BA.1, and BA.2 panels by iron heat colours (black < blue < red < orange < yellow < white hot) according to the relative level of antibody contact. BA.1 mutations are shown as spikes. Figures were depicted by Dr. Helen M Ginn.

8.3 Discussion

Here we reported the isolation and analysis of a panel of potent mAbs from BA.2 infected convalescent samples, and find that the focus of potent mAbs has shifted from that observed in early pandemic responses to that in BA.1 mAbs. Two of the three regions clustered by BA.2 mAbs were seen in potent early pandemic antibodies, although mutations in Omicron families have knocked out most of the public responses, most obviously the gene families IGHV3-53/66. There is a third more extensive binding patch at the front of the RBD, which centres at the right chest and spans between the right flank and neck regions identified in the early-pandemic, non-neutralising mAbs. Unlike early pandemic mAbs binding on the right chest are generally weak neutralisers, a general feature of the BA.2 mAbs is that many of the potent BA.2 antibodies are much further from the ACE2-binding site and, as a result, are less strongly competitive with ACE2 than early-pandemic mAbs (Figure 8.1C). The mechanism of neutralisation is considered to be by disrupting the stability of spike or locking RBD to a 'down' conformation.

The changed pattern of potent antibody binding is likely due to the derivation of the BA.2 mAbs from responses induced by vaccination. In support of this, we found that the full set of BA.2 mAbs cross-react to ancestral strains (Victoria) and the fact that all donors were triple vaccinated. It is unclear whether the cross-reacting antibodies were fully matured before BA.2 infection or whether affinity maturation of lower affinity clones occurred in response to BA.2 infection. The set of mAbs may have been a mix of both, and the strong representation of weaker neutralising right chest mAbs that overlap these may have been matured to higher affinity and selected because this portion of the RBD has been subjected to less mutational change in BA.1 and BA.2.

The change away from antibodies binding more directly on the ACE2 footprint is highlighted by the substantial role in early responses played by public gene families such as IGHV3-53/66, IGHV1-69, IGHV3-9, and IGHV1-58. Almost all the BA.2 IGHV1-69 mAbs are knocked out by BA.4. Finally, the public response IGHV3-53/66 family of BA.2 mAbs are severely affected by the F486S mutation in BA.2.75.2, as are most of the IGHV3-53/66 members in the BA.1 mAbs.

In summary, the antibodies repopulated from the memory pool of repeated vaccination after BA.2 infection is likely to give a pressure for evolution of BA.2. It is revealing that the additional mutations in BA.2 sublineages described here target the regions used to bind 25 potent mAbs, causing all mAbs to be compromised for at least one variant.

CHAPTER 9 Discussion and prospect

Since the emergence of SARS-CoV-2 in late 2019, a great number of SARS-CoV-2 vaccines have been designed, produced, and administrated worldwide. All these vaccines are designed to induce antibodies response to the S protein, which is delivered in a variety of formats, such as DNA, mRNA, viral vector, protein, inactivated virus, VLP, and live attenuated vaccines[180]. Both vaccination and natural infection induce high levels of neutralising antibodies targeting S protein, which place S protein of the virus under immense selective pressure[181]. Indeed, Since the emergence of Alpha variant, within 4 years SARS-CoV-2 has concentrated remarkable mutational changes in the S gene. In late 2021 the emergence of Omicron marked a big leap of change, with profound drops in neutralisation titres in serum from vaccinees and from natural infection, leading to a global wave of infection and becoming the dominant variant in a matter of weeks[81,182]. Since then, Omicron has dominated and continued to evolve rapidly, BA.1 was replaced by BA.1.1 and BA.2[128] which were in turn replaced by BA.4/5[82], BA.4.6[183] and BF.7[184]. Since late 2022, an increasing number of BA.2 sub-variants have begun to cocirculate, with convergent evolution leading to the acquisition of subsets of common mutations in related variants[28]. In 2023, sub lineages related to XBB have been the dominant variants, although BA.2.86 has recently emerged, which has numerous mutations and likely evolved from BA.2 in a chronically infected immunosuppressed host[185].

Since the beginning of the pandemic, we have isolated, tested, and analysed panels of S-specific mAbs selected from PBMCs of patients infected by different SARS-CoV-2 variants before or after vaccination, which has led to considerable understanding of the antigenic landscape of S and sites of mAb binding[22,79-82]. Until now, two domains of the S1 region of S, NTD[78] and RBD[123,128,130] have been described as binding sites for most potent neutralising mAbs. All commercially developed mAbs to date target the RBD[162,176,186], while anti-NTD mAbs tend to be variant specific, due to extensive mutation of the supersite between variants.

Both the RBD and NTD are hot spots of mutation in SARS-CoV-2. RBD mutations can impart selective advantages to the virus, firstly some, for example the N501Y mutation found in the Alpha variant, increase the affinity to ACE2 and are believed to drive increased transmissibility[171]. Secondly, mutations in the RBD and NTD may lead to escape from neutralizing antibody responses[187]. Increasing herd immunity generates intense selective pressure on the virus to break through pre-existing immunity[82]. Evolution of S has therefore

been rapid with many mutations mapping closely to the sites of interaction of potent mAbs in the RBD and NTD[187]. The effects of these mutations have been profound, greatly lowering the neutralization titres of naturally infected or vaccinated serum and leading to the knock-out of activity of almost all mAb, including those developed for clinical use [162,186,188]. In the study presented here, one anti-RBD antibody, Omi42, stands out which targets a more conserved area on RBD and neutralises all variants tested so far (Table 7.2, Figure 7.2), and it is in phase III clinical trial at the moment. In the meantime, it is also meaningful to search for broadly neutralising mAbs targeting on more conserved areas of the S protein, such as SD1 or S2[189].

SD1 is a small domain present in the S1 subunit of spike, formed from residues 320-331 lying N-terminal to the RBD and 528-591, C-terminal to the RBD. Its sequence is conserved across SARS-CoV-2 variants, except for substitutions A570D in Alpha, T547K in Omicron BA.1, and E554K in BA.2.86. There have been several SD1-specific mAbs reported with broadly-neutralising abilities[189], and although the mechanism of their neutralisation is still unclear, there is an indication that the neutralisation of anti-SD1 mAbs may be through the inhibition of the S molecular rearrangement which is required for ACE2 attachment than blocking the interaction of S and ACE2 directly[189]. In general, anti-SD1 neutralising mAbs are still understudied.

Broadly-neutralising anti-S2 mAbs have been widely reported[46,190-195], and they mainly target two subdomains of S2: stem helix (SH) and fusion peptide (FP). mAbs specific to the SH region neutralise viruses by preventing S protein-mediated fusion of viral and cellular membrane and Fc effector function also plays a part[46]. Although anti-SH mAbs don't show as high neutralising ability as some of the highly potent RBD mAbs, most of them can neutralise all human beta-coronaviruses due to the conservativeness of this region. mAbs targeting FP subdomain were also isolated from patients recovering from COVID-19, and because S2 FPs are also highly conserved among all coronavirus genera, they showed an even broader neutralising spectrum than anti-SH mAbs, which extend to alpha-CoVs, beta-CoVs and even some gamma-CoVs and delta-CoVs. Synergetic effects can be found by using some anti-S2 mAbs together with anti-RBD mAbs[194]. Taken together, anti-S2 mAbs can guide the design of broadly-neutralising mAbs to highly variable SARS-CoV-2 variants and even other human Coronaviruses.

Considering the evolution of SARS-CoV-2, it is unavoidable that more mutations will be accumulated in NTD and RBD, hence antibodies targeting more conserved regions are urgently

needed. By using our antibody isolation platform, we can specifically sort memory B cells from PBMC of COVID-19 convalescent patients to generate large numbers of mAbs against more conserved areas, especially SD1 which is less studied than other regions on S. Through cryo-EM, binding epitopes of these mAbs could be discovered and may be able to suggest a vulnerable part on SD1 and the mechanism of neutralisation by anti-SD1 mAbs.

Here we have also built an antigenic map by analysing the immune escape ability of each SARS-CoV-2 variants against serum obtained from patients infected by different variants. This antigenic landscape shows the antigenic distance between SARS-CoV-2 variants, and sheds light on the selection of S proteins for constructing bivalent or even multivalent vaccines to generate antibodies effectively providing protection against more variants in the future.

Appendix

A.1. Primer sequences

Application	Name	Sequence 5' - 3'
Antibody PCR		
Heavy chain RT-PCR	5' L VH1	ACAGGTGCCCACTCCCAGGTGCAG
	5' L VH2	GACCATCCCTTCATCAGATCACC
	5' L VH3	AAGGTGTCCAGTGTGARGTGCAG
	5' L VH4/6	CCCAGATGGGTCCTGTCCCAGGTGCAG
	5' L VH5	CAAGGAGTCTGTTCCGAGGTGCAG
	5' L VH7	GGCAGCAGCAACAGCAGGTGCAGC
	3' Cγ CH1	GGAAGGTGTGCACGCCGCTGGTC
	3′ Cμ CH1	GGGAATTCTCACAGGAGACGA
Kappa chain RT-PCR	5' L VK1/2	ATGAGGSTCCCYGCTCAGCTGCTGG
	5' L VK3	CTCTTCCTCCTGCTACTCTGGCTCCCAG
	5' L VK4	ATTTCTCTGTTGCTCTGGATCTCTG
	3' CK 543	GTTTCTCGTAGTCTGCTTTGCTCA
Lambda chain RT-PCR	5' L Vλ1	GGTCCTGGGCCCAGTCTGTGCTG
	5' L Vλ2	GGTCCTGGGCCCCGTCTGCCCTG
	5' L Vλ3	GCTCTGTGACCTCCTATGAGCTG
	5' L Vλ4/5	GGTCTCTCTCSCAGCYTGTGCTG
	5' L Vλ6	GTTCTTGGGCCAATTTTATGCTG
	5' L Vλ7	GGTCCAATTCYCAGGCTGTGGTG
	5' L Vλ8	GAGTGGATTCTCAGACTGTGGTG
	3' Cλ	CACCAGTGTGGCCTTGTTGGCTTG
Heavy chain nested	FIn_AgeI_VH1	CATCCTTTTTCTAGTAGCAACTGCAACCGGTGTACATTCCCAGGTGCAGCTGGTGCAG
	FIn_AgeI_VH1_5	CATCCTTTTTCTAGTAGCAACTGCAACCGGTGTACATTCCGAGGTGCAGCTGGTGCAG
	FIn_AgeI_VH1–18	CATCCTTTTTCTAGTAGCAACTGCAACCGGTGTACATTCCCAGGTTCAGCTGGTGCAG
	FIn_AgeI_VH1–24	CATCCTTTTTCTAGTAGCAACTGCAACCGGTGTACATTCCCAGGTCCAGCTGGTACAG
	FIn_AgeI_VH2	CATCCTTTTTCTAGTAGCAACTGCAACCGGTGTACATTCCCAGATCACCTTGAAGGAG
	Fin_AgeI_VH3	CATCCTTTTTCTAGTAGCAACTGCAACCGGTGTACATTCTGAGGTGCAGCTGGTGGAG
	FIn_AgeI_VH3–9/30/33	CATCCTTTTTCTAGTAGCAACTGCAACCGGTGTACATTCCGAAGTGCAGCTGGTGGAG
	FIn_AgeI_VH3-23	CATCCTTTTTCTAGTAGCAACTGCAACCGGTGTACATTCCGAGGTGCAGCTGTTGGAG
	FIn_AgeI_VH3–33	CATCCTTTTTCTAGTAGCAACTGCAACCGGTGTACATTCCCAGGTGCAGCTGGTGGAG
	FIn_AgeI_VH4	CATCCTTTTTCTAGTAGCAACTGCAACCGGTGTACATTCCCAGGTGCAGCTGCAGGAG
	FIn_AgeI_VH4-34	CATCCTTTTTCTAGTAGCAACTGCAACCGGTGTACATTCCCAGGTGCAGCTACAGCAG
	FIn_AgeI_VH4–39	CATCCTTTTTCTAGTAGCAACTGCAACCGGTGTACATTCCCAGCTGCAGCTGCAGGAG
	FIn_AgeI_VH6–1	CATCCTTTTTCTAGTAGCAACTGCAACCGGTGTACATTCCCAGGTACAGCTGCAGCAG
	R_126KasI_IgCH134	TGTGCACGCCGCTGGTCAGGGCGCC

(Continued)

Application	Name	Sequence 5' - 3'
	R_126KasI_IgCH2	TGTGCACGCCGCTGGTCAGAGCGCC
	Rin_SalI_JH1_2_4_5	GAAGACCGATGGGCCCTTGGTCGACGCTGAGGAGACGGTGACCAG
	Rin_SalI_JH3	GAAGACCGATGGGCCCTTGGTCGACGCTGAAGAGACGGTGACCATTG
	Rin_SalI_JH6	GAAGACCGATGGGCCCTTGGTCGACGCTGAGGAGACGGTGACCGTG
Kappa chain nested	FIn_AgeI_VK1-5	CATCCTTTTTCTAGTAGCAACTGCAACCGGTGTACATTCCGACATCCAGATGAC CCAGTC
	FIn_AgeI_VK1-6	CATCCTTTTTCTAGTAGCAACTGCAACCGGTGTACATTCCGCCATCCAGATGAC CCAGTC
	FIn_AgeI_VK1-9	CATCCTTTTTCTAGTAGCAACTGCAACCGGTGTACATTCCGACATCCAGTTGAC CCAGTCT
	FIn_AgeI_VK1-13	CATCCTTTTTCTAGTAGCAACTGCAACCGGTGTACATTCCGCCATCCAGTTGAC CCAGTC
	FIn_AgeI_VK1D-8	CATCCTTTTTCTAGTAGCAACTGCAACCGGTGTACATTCCGTCATCTGGATGAC CCAGTC
	FIn_AgeI_VK1D-43	CATCCTTTTTCTAGTAGCAACTGCAACCGGTGTACATTCCGCCATCCGGATGAC CCAGTC
	FIn_AgeI_VK2-24	CATCCTTTTTCTAGTAGCAACTGCAACCGGTGTACATTCCGATATTGTGATGAC CCAGAC
	FIn_AgeI_VK2-30	CATCCTTTTTCTAGTAGCAACTGCAACCGGTGTACATTCCGATGTTGTGATGAC TCAGTC
	FIn_AgeI_VK2_4	CATCCTTTTTCTAGTAGCAACTGCAACCGGTGTACATTCCGAYATYGTGATGAC YCAGTC
	FIn_AgeI_VK3-11_20	CATCCTTTTTCTAGTAGCAACTGCAACCGGTGTACATTCCGAAATTGTGTTGAC RCAGTC
	FIn_AgeI_VK3-15	CATCCTTTTTCTAGTAGCAACTGCAACCGGTGTACATTCCGAAATAGTGATGAC GCAGTC
	Rin_BsiWI_JK1_2_4	GAAGACAGATGGTGCAGCCACCGTACGTTTGATYTCCACCTTGGTC
	Rin_BsiWI_JK3	GAAGACAGATGGTGCAGCCACCGTACGTTTGATATCCACTTTGGTC
	RIn_BsiWI_JK5	GAAGACAGATGGTGCAGCCACCGTACGTTTAATCTCCAGTCGTGTC
Lambda chain nested	FIn_AgeI_VL1	CATCCTTTTTCTAGTAGCAACTGCAACCGGTTCCTGGGCCCAGTCTGTGYTGAC KCAG
	FIn_AgeI_VL1-40	CATCCTTTTTCTAGTAGCAACTGCAACCGGTTCCTGGGCCCAGTCTGTCGTGAC GCAG
	FIn_AgeI_VL2	CATCCTTTTTCTAGTAGCAACTGCAACCGGTTCCTGGGCCCARTCTGCCCTGAC TCAG
	FIn_AgeI_VL3_10	CATCCTTTTTCTAGTAGCAACTGCAACCGGTTCCTGGGCCTCCTATGAGCTGAC WCAG
	FIn_AgeI_VL4_5_9	CATCCTTTTTCTAGTAGCAACTGCAACCGGTTCCTGGGCCCAGCCTGTGCTGAC TCAR
	FIn_AgeI_VL5-45	CATCCTTTTTCTAGTAGCAACTGCAACCGGTTCCTGGGCCCAGGCTGTGCTGAC TCAR
	FIn_AgeI_VL4-69	CATCCTTTTTCTAGTAGCAACTGCAACCGGTTCCTGGGCCCAGCTTGTGCTGAC TCAA
	FIn_AgeI_VL6-57	CATCCTTTTTCTAGTAGCAACTGCAACCGGTTCCTGGGCCAATTTTATGCTGAC TCAG
	FIn_AgeI_VL7_8	CATCCTTTTTCTAGTAGCAACTGCAACCGGTTCCTGGGCCCAGWCTGTGGTGAC YCAG
	Rin_XhoI_CL	CTTGTTGGCTTGAAGCTCCTCACTCGAGGGYGGGAACAGAGTG
Fab PCR		
Vector amplify	FIn_dbST_Hvec	CATCCACAGTTCGAGAAATAGGTGCGACGGCCGGCAAG
	Rin_CH1_SC_G1_TB	GTGGGACCAGGCACTACTTCCGCGTGGCACCAGACAAGATTTGGGCTCAACTCT CTTG
Tag amplify	Fin_CH1_SC_G1_TB	CAAGAGAGTTGAGCCCAAATCTTGTCTGGTGCCACGCGGAAGTAGTGCCTGGTC CCAC
	RIn_dbST_Hvec	CTTGCCGGCCGTCGCACCTATTTCTCGAACTGTGGATG

(Continued)

Application	Name	Sequence 5' - 3'
Virus sequencing		
Amplify primer	F_SARS2_AUS_SPIKE	CACGCGAACAAATAGATGGTTATGTCATGC
	R_SARS2_AUS_SPIKE	CACCCTTGGAGAGTGCTAGTTGCC
Sequencing primer	R_SARS2_AUS_S728	GCAAGTAAAGTTTGAAACCTAGTG
	F_SARS2_AUS_S619	CACACGCCTATTAATTTAGTGCG
	F_SARS2_AUS_S1426	GGTAGCACACCTTGTAATGGTG
	F_SARS2_AUS_S2230	GGTGATTCAACTGAATGCAGC
	R-SARS2_AUS_S_p64	GAGTAGCATCCTTGATTTCAC
RT primer	R_RT_SASR2_AUS_1	TTTTTTTTTTGTCATTCTCCTAAGAAGC
Pseudo-virus and soluble spike construction		
	pcDNA3-1_Tag_S_Eco_F	GCCACCCTCAGTTCGAGAAGTGAGAATTC
	pcDNA3-1_Bam_R	CTCTTGGTGGTCAGCAGGAACATGGATCC
	pcDNA3-1_Bam_F	GGATCCATGTTCCTGCTGACCACCAAGAG
	pcDNA3-1_Tag_S_Eco_R	GAATTCTCACTTCTCGAACTGAGGGTGGC
	SpikePV S247R_R	GCTGGCCCTGCACAGAAGATATCTTACACCAGGC
	SpikePV_Y453F_F	GCTCTTTCTGAACAGTCTGAACAGGTAATTGTAATTGCC
	SpikePV_Y453F_R	GGCAATTACAATTACCTGTTCAGACTGTTCAGAAAGAGC
	SpikePV_N439K_F	TTTCGAATCTAGATTCTTAGAGTTCCACGCGATCACG
	SpikePV_N439K_R	CGTGATCGCGTGGAACTCTAAGAATCTAGATTCGAAA
	SpikePV_S477N_F	CATTACACGGTGTGTTGCCGGCCTGGTAG
	SpikePV_S477N_R	CTACCAGGCCGGCAACACACCGTGTAATG
	SpikePV_F486L_F	GAGGGAAGTAGCAATTTAAGCCCTCCACGCCAT
	SpikePV_F486L_R	ATGGCGTGGAGGGCTTAAATTGCTACTTCCCTC
	SpikePV_G446V_F	GTACAGGTAATTGTAATTGCCTACAACTTTCGAATCTAGATTGTTA
	SpikePV_G446V_R	TAACAATCTAGATTCGAAAGTTGTAGGCAATTACAATTACCTGTAC
	SpikePV_A222V_F	CAGAGGCTCCAGGACGCTGAAGCCCTG
	SpikePV_A222V_R	CAGGGCTTCAGCGTCCTGGAGCCTCTG
	SS_A222V_R2	CAGAGGCTCCAGGACGCTGAAGCCCTG
	SS_A222V_F2	CAGGGCTTCAGCGTCCTGGAGCCTCTG
	SpikePV_S514F_F	GTGCAGCAGCTCGAAGAACAGCACCACCACTCTG
	SpikePV_S514F_R	CAGAGTGGTGGTGCTGTTCTTCGAGCTGCTGCAC
	SpikePV_E484A_F	GTAGCAATTGAAGCCCGCCACGCCATTACACGG
	SpikePV_E484A_R	CCGTGTAATGGCGTGGCGGGCTTCAATTGCTAC
	SpikePV D614G_F	CGGTGCAATTCACGCCCTGGTACAGCACG
	SpikePV D614G_R	CGTGCTGTACCAGGGCGTGAATTGCACCG
	SpikePV_delY144Y145_F	GACCCTTTCCTGGGTGTTCATAAGAACAACAAGAGC
	SpikePV_delY144Y145_R	GCTCTTGTTGTTCTTATGAACACCCAGGAAAGGGTC
	SpikePV_N501T_F	CCCACGCCAGTGGTAGGCTGGAAGCCG

(Continued)

Application	Name	Sequence 5' - 3'
	SpikePV_N501T_R	CGGCTTCCAGCCTACCACTGGCGTGGG
	SpikePV_delY144_R	GCTCTTGTTGTTCTTATGATAAACACCCAGGAAAGGGTC
	SpikePV_delY144_F	GACCCTTTCCTGGGTGTTTATCATAAGAACAACAAGAGC
	SpikePV_delY144_R_2	GCTCTTGTTGTTCTTATGATAAACACCCAGGAAAGGGTC
	SpikePV_delY144_F_2	GACCCTTTCCTGGGTGTTTATCATAAGAACAACAAGAGC
	SpikePV_A570D_R	CATCTGTGGTGTCGTCGATGTCTCTGCCG
	SpikePV_A570D_F	CGGCAGAGACATCGACGACACCACAGATG
	SpikePV_A570D_R_2	CATCTGTGGTGTCGTCGATGTCTCTGCCG
	SpikePV_A570D_F_2	CGGCAGAGACATCGACGACACCACAGATG
	SpikePV_P681H_R	GCTTCTGGCTCTTCTATGGCTATTGGTCTGGGT
	SpikePV_P681H_F	ACCCAGACCAATAGCCATAGAAGAGCCAGAAGC
	SS_P681H_GSAS_R	TGCTGGCGCTTCCATGGCTATTGGTCTGG
	SS_P681H_GSAS_F	CCAGACCAATAGCCATGGAAGCGCCAGCA
	SpikePV_N501Y_F	GTAGCCCACGCCATAGGTAGGCTGGAAGC
	SpikePV_N501Y_R	GCTTCCAGCCTACCTATGGCGTGGGCTAC
	AF_K417N_R	GTAATTGTAGTCGGCGATATTGCCGGTCTGCCCTG
	AF_K417N_F	CAGGGCAGACCGGCAATATCGCCGACTACAATTAC
	SpikePV_D1118H_R	GCTCACGAAGGTATTGTGGGTGGTGATGATCTGAG
	SpikePV_D1118H_F	CTCAGATCATCACCACCCACAATACCTTCGTGAGC
	AF_E484K_R	GTAGCAATTGAAGCCCTTCACGCCATTACACGGTG
	AF_E484K_F	CACCGTGTAATGGCGTGAAGGGCTTCAATTGCTAC
	AF_A701V_R	GGCCACGCTATTCTCGACGCCCAGGCTCATGGTG
	AF_A701V_F	CACCATGAGCCTGGGCGTCGAGAATAGCGTGGCC
	SpikePV_delH69V70_F	GGTTCCACGCCATCAGCGGCACCAATGG
	SpikePV_delH69V70_R	CCATTGGTGCCGCTGATGGCGTGGAACC
	AF_D215G_R	GAAGCCCTGAGGCAGGCCTCTCACCAGATTAAT
	AF_D215G_F	ATTAATCTGGTGAGAGGCCTGCCTCAGGGCTTC
	AF_L18F_R	CAGCTGGGTTCTGGTGGTGAAATTCACGCACTGGCTGCTC
	AF_L18F_F	GAGCAGCCAGTGCGTGAATTTCACCACCAGAACCCAGCTG
	SS_K417T_R	GTAGTCGGCGATCGTGCCGGTCTGCCC
	SS_K417T_F	GGGCAGACCGGCACGATCGCCGACTAC
	SS_681HGSAS_R2	GCTGGCCACGCTGCTGGCGCTTCCATGGC
	SS_681HGSAS_F2	GCCATGGAAGCGCCAGCAGCGTGGCCAGC
	SS_R190S_R	GATATTCTTGAACACGAACTCGCTCAGATTCTTGAAATTGCCC
	SS_R190S_F	GGGCAATTTCAAGAATCTGAGCGAGTTCGTGTTCAAGAATATC
	SS_D138Y_R	GATAATAAACACCCAGGAAAGGATAATTGCAGAACTGGAACTCGCAG
	SS_D138Y_F	CTGCGAGTTCCAGTTCTGCAATTATCCTTTCCTGGGTGTTTATTATC
	Spike_L452R_F	GGAGGCAATTACAATTACCGGTACAGACTGTTCAGAAAG

(Continued)

Application	Name	Sequence 5' - 3'
	Spike_L452R_R	CTTTCTGAACAGTCTGTACCGGTAATTGTAATTGCCTCC
	SS_S982A_PP_F	CTCAACGATATCCTGGCCAGACTGGACCCGCCAGAGGC
	SS_S982A_PP_R	GCCTCTGGCGGGTCCAGTCTGGCCAGGATATCGTTGAG
	SS_Q498R_R	CGCCATTGGTAGGCCGGAAGCCGTAGCTC
	SS_Q498R_F	GAGCTACGGCTTCCGGCCTACCAATGGCG
	PV_del242-244_F	CCAGATTCCAGACCCTGCACAGATCATATCTTACAC
	PV_del242-244_R	GTGTAAGATATGATCTGTGCAGGGTCTGGAATCTGG
	PV_in214ANRN215_F	CCATTAATCTGGTGAGAGCCAATAGAAATGACCTGCCTCAGGGC
	PV_in214ANRN215_R	GCCCTGAGGCAGGTCATTTCTATTGGCTCTCACCAGATTAATGG
	PV_del256-258_F	CTTACACCAGGCGATTCGTCAACCGCTGGAGCTGCG
	PV_del256-258_R	CGCAGCTCCAGCGGTTGACGAATCGCCTGGTGTAAG
	AF_D614G_R	CTCGGTGCAATTCACGCCCTGGTACAGCACGGC
	AF_D614G_F	GCCGTGCTGTACCAGGGCGTGAATTGCACCGAG
	P681R_GSAS_R	GCTGGCCACGCTGCTGGCGCTTCCACGGCTATTGGTCTG
	P681R_GSAS_F	CAGACCAATAGCCGTGGAAGCGCCAGCAGCGTGGCCAGC
	SpikePV_S982A_R	TCCACCTTGTCCAGTCTGGCCAGGATATCGTTGAGTAC
	SpikePV_S982A_F	GTACTCAACGATATCCTGGCCAGACTGGACAAGGTGGA
	SpikePV_T716I_R	CGCTGATGGTGAAATTGATAGGGATGGCGATGCTA
	SpikePV_T716I_F	TAGCATCGCCATCCCTATCAATTTCACCATCAGCG
	SS_H655Y_R	CTCGTAGCTATTATTCACATACTCGGCGCCGATCAGGC
	SS_H655Y_F	GCCTGATCGGCGCCGAGTATGTGAATAATAGCTACGAG
	SS_L18FT20NP26S_F	CAGCCAGTGCGTGAATTTCACCAACAGAACCCAGCTGCCTAGTGCCTACACCAA TAG
	SS_L18FT20NP26S_R	CTATTGGTGTAGGCACTAGGCAGCTGGGTTCTGTTGGTGAAATTCACGCACTGG CTG
	L452Q_R	CTTTCTGAACAGTCTGTACTGGTAATTGTAATTGCCTCC
	L452Q_F	GGAGGCAATTACAATTACCAGTACAGACTGTTCAGAAAG
	F_T478K	TACCAGGCCGGCAGCAAACCGTGTAATGG
	R_T478K	CCATTACACGGTTTGCTGCCGGCCTGGTA
	F_T732A	GAAATATTACCAGTCTCCATGGCCAAGACCAGCGTGG
	R_T732A	CCACGCTGGTCTTGGCCATGGAGACTGGTAATATTTC
	D80G_F	GCACCAAGAGATTCGGCAATCCTGTGCTGCC
	D80G_R	GGCAGCACAGGATTGCCGAATCTCTTGGTGC
	D253G_R	CCAACCGCTTGACGAACCGCCTGGTGTAAGATATG
	D253G_F	CATATCTTACACCAGGCGGTTCGTCAAGCGGTTGG
	L5F_R	CCAGAGGCAGCAGCACGAAGAACACGAACATGGTTC
	L5F_F	GAACCATGTTCGTGTTCTTCGTGCTGCTGCCTCTGG
	G669S_R	GCTGGCGCAGATGCTGGCGCCGATAGG
	G669S_F	CCTATCGGCGCCAGCATCTGCGCCAGC
	Q949R_R	GATTCACCACGTCCCGCAGCTTGCCCAGG
	Q949R_F	CCTGGGCAAGCTGCGGGACGTGGTGAATC

(Continued)

Application	Name	Sequence 5' - 3'
	N1187D_R	GATTCTTGGCCACTTCGTCGAGCCGATCAATTTCC
	N1187D_F	GGAAATTGATCGGCTCGACGAAGTGGCCAAGAATC
	G75V_T76I_R	GATTGTCGAATCTCTTGATGACATTGGTGCCGCTCACG
	G75V_T76I_F	CGTGAGCGGCACCAATGTCATCAAGAGATTCGACAATC
	V483A_R	CAATTGAAGCCCTCCGCGCCATTACACGGTG
	V483A_F	CACCGTGTAATGGCGCGGAGGGCTTCAATTG
	T859N_R	GTCAGCAGAGGAGGTAGTACATTCAAACCGTTAAACTTCTGG
	T859N_F	CCAGAAGTTTAACGGTTTGAATGTACTACCTCCTCTGCTGAC
	E1092K_R	GAACACGCCCTTTCTAGGGAAGTGGGCCTTG
	E1092K_F	CAAGGCCCACTTCCCTAGAAAGGGCGTGTTC
	V1176F_R	CCTTCTGGATATTCACGAAGCTGGCATTGATTCCCG
	V1176F_F	CGGGAATCAATGCCAGCTTCGTGAATATCCAGAAGG
	S12F_R	GATTCACGCACTGGCTGAACACCAGAGGCAGCAG
	S12F_F	CTGCTGCCTCTGGTGTTCAGCCAGTGCGTGAATC
	W152R_R	GAACTCGCTCTCCATCCTGCTCTTGTTGTTCTTATG
	W152R_F	CATAAGAACAACAAGAGCAGGATGGAGAGCGAGTTC
	V367F_R	GGCGCTATTGTACAGGAAGCTGTAGTCGGCCAC
	V367F_F	GTGGCCGACTACAGCTTCCTGTACAATAGCGCC
	Q613H_R	GGTGCAATTCACGTCATGGTACAGCACGGCC
	Q613H_F	GGCCGTGCTGTACCATGACGTGAATTGCACC
	A899S_R	CTGTAGGCCATCTGCATGCTGAAAGGGATTTGCAACGC
	A899S_F	GCGTTGCAAATCCCTTTCAGCATGCAGATGGCCTACAG
	G142V del144 _R	CTCTTGTTGTTCTTATGATAAACAACCAGGAAAGGGTCATTGCAGA
	G142V del144 _F	TCTGCAATGACCCTTTCCTGGTTGTTTATCATAAGAACAACAAGAG
	G142D_Del144_F	CTGCAATGACCCTTTCCTGGATGTTTATCATAAGAACAACAAGAGC
	G142D_Del144_R	GCTCTTGTTGTTCTTATGATAAACATCCAGGAAAGGGTCATTGCAG
	E1092K_H1101Y_R	CTGGGTCACGAACCAATAGGTGCCATTGCTCACGAACACGCCCTTTCTAGGGAA GTGGGCCTTG
	E1092K_H1101Y_F	CAAGGCCCACTTCCCTAGAAAGGGCGTGTTCGTGAGCAATGGCACCTATTGGTT CGTGACCCAG
	del246-252_D253N_F	CCCTGCTGGCCCTGCACAATTCGTCAAGCGGTTG
	del246-252_D253N_R	CAACCGCTTGACGAATTGTGCAGGGCCAGCAGGG
	I1130V_D1139H_F	GCAATTGCGACGTGGTGGTCGGGATAGTCAATAATACTGTCTACCACCCTCTGC AGCCTGAG
	I1130V_D1139H_R	CTCAGGCTGCAGAGGGTGGTAGACAGTATTATTGACTATCCCGACCACCACGTC GCAATTGC
	F490S_R	CGTAGCTCTGCAGAGGGCTGTAGCAATTGAAGCCC
	F490S_F	GGGCTTCAATTGCTACAGCCCTCTGCAGAGCTACG
	D80G_T95I_R	GATATTGCTCTTCTCGATGCTGGCGAAGTACACGCCGTCATTGAAAGGCAGCAC AGGATTGCCGAATCTCTTGGTGC
	D80G_T95I_F	GCACCAAGAGATTCGGCAATCCTGTGCTGCCTTTCAATGACGGCGTGTACTTCG CCAGCATCGAGAAGAGCAATATC
	AF_D80A_R	GGCAGCACAGGATTGGCGAATCTCTTGGTGC
	AF_D80A_F	GCACCAAGAGATTCGCCAATCCTGTGCTGCC

(Continued)

Application	Name	Sequence 5' - 3'
	D950H_R	CTGATTCACCACGTGCTGCAGCTTGCCCAG
	D950H_F	CTGGGCAAGCTGCAGCACGTGGTGAATCAG
	T76I_R	GATTGTCGAATCTCTTGATGCCATTGGTGCCGCTC
	T76I_F	GAGCGGCACCAATGGCATCAAGAGATTCGACAATC
	I1130V_R	GTATTATTGACTATCCCGACCACCACGTCGCAATTGC
	I1130V_F	GCAATTGCGACGTGGTGGTCGGGATAGTCAATAATAC
	D1139H_R	CTCAGGCTGCAGAGGGTGGTAGACAGTATTATTGAC
	D1139H_F	GTCAATAATACTGTCTACCACCCTCTGCAGCCTGAG
	Q957R_R	CAGGGTATTCAGGGCCCGGGCATTCTGATTCAC
	Q957R_F	GTGAATCAGAATGCCCGGGCCCTGAATACCCTG
	R346S_R	GTACACGCTGGCGAAGCTGGTGGCATTGAAC
	R346S_F	GTTCAATGCCACCAGCTTCGCCAGCGTGTAC
	D796H_R	GAAGCCGCCGAAGTGCTTGATCGGCGG
	D796H_F	CCGCCGATCAAGCACTTCGGCGGCTTC
	V1176F_N1187D_R	GATTCTTGGCCACTTCGTCGAGCCGATCAATTTCCTTCTGGATATTCACGAAGC TGGCATTGATTCC
	V1176F_N1187D_F	GGAATCAATGCCAGCTTCGTGAATATCCAGAAGGAAATTGATCGGCTCGACGAA GTGGCCAAGAATC
	Y144TY145SinsN_R	CCAGCTCTTGTTGTTCTTATGGTTACTAGTAACACCCAGGAAAGGGTCATTGCA G
	Y144TY145SinsN_F	CTGCAATGACCCTTTCCTGGGTGTTACTAGTAACCATAAGAACAACAAGAGCTG G
	Y144SY145N_R	GCTCTTGTTGTTCTTATGATTACTAACACCCAGGAAAGGGTCATTGCAG
	Y144SY145N_F	CTGCAATGACCCTTTCCTGGGTGTTAGTAATCATAAGAACAACAAGAGC
	G142D_Y145H_F	CTGCAATGACCCTTTCCTGGATGTTTATCATCATAAGAACAACAAGAGC
	G142D_Y145H_R	GCTCTTGTTGTTCTTATGATGATAAACATCCAGGAAAGGGTCATTGCAG
	Omi_P337I+G339D_F	CCTAATATCACCAATCTGTGCATTTTCGACGAGGTGTTCAATGC
	Omi_P337I+G339D_R	GCATTGAACACCTCGTCGAAAATGCACAGATTGGTGATATTAGG
	Omi_G339D+E340I_F	CACCAATCTGTGCCCTTTCGACATAGTGTTCAATGCCACCAGATTC
	Omi_G339D+E340I_R	GAATCTGGTGGCATTGAACACTATGTCGAAAGGGCACAGATTGGTG
	D405N_F	CTTCGTGATCAGAGGCAATGAGGTGAGACAGATCGCGCCAGGC
	D405N_R	GCCTGGCGCGATCTGTCTCACCTCATTGCCTCTGATCACGAAG
	Δ211/L212I_F	GCACACACCCATTATCGTGAGAGACCTGCCTCAGGGCTTC
	Δ211/L212I_R	AGGCAGGTCTCTCACGATAATGGGTGTGTGCTTGCTGTAG
	K356L_F	CGTGTACGCATGGAACCGCCTACGGATAAGCAATTGCGTGG
	K356L_R	CCACGCAATTGCTTATCCGTAGGCGGTTCCATGCGTACACG
	P337I_G339D_E340I_F.omi	TTCCCTAATATCACCAATCTGTGCATTTTCGACATAGTGTTCAATGCCACCAGA TTCGCC
	P337I_G339D_E340I_R.omi	GGCGAATCTGGTGGCATTGAACACTATGTCGAAAATGCACAGATTGGTGATATT AGGGAA
	P337I_G339D_E340I_F.2	CCAATCTGTGCATTTTCGACATAGTGTTCAATGCCACCAGATTCGCC
	P337I_G339D_E340I_R.2	CATTGAACACTATGTCGAAAATGCACAGATTGGTGATATTAGGGAATC
	T478K_E484K_F	AACCGTGTAATGGCGTGAAGGGCTTCAATTGCTAC
	T478K_E484K_R	GTAGCAATTGAAGCCCTTCACGCCATTACACGGTTTG

(Continued)

Application	Name	Sequence 5' - 3'
	G446S_L452R_F	CAATCTAGATTCGAAAGTTAGCGGCAATTACAATTACCGGTAC
	G446S_L452R_R	GTAATTGTAATTGCCGCTAACTTTCGAATCTAGATTGTTAGAG
	P337R_G339D_F	ATCACCAATCTGTGCCGTTTCGACGAGGTGTTC
	P337R_G339D_R	CCTCGTCGAAACGGCACAGATTGGTGATATTAG
	P337S_G339D_F	TCACCAATCTGTGCAGTTTCGACGAGGTGTTCAATG
	P337S_G339D_R	CACCTCGTCGAAACTGCACAGATTGGTGATATTAG
	P337M_G339D_F	CACCAATCTGTGCATGTTCGACGAGGTGTTCAATGCC
	P337M_G339D_R	CACCTCGTCGAACATGCACAGATTGGTGATATTAGG
	G339D_E340D_F	GTGCCCTTTCGACGATGTGTTCAATGCCACC
	G339D_E340D_R	GGTGGCATTGAACACATCGTCGAAAGGGCAC
	G339D_E340A_F	CTGTGCCCTTTCGACGCGGTGTTCAATGCCAC
	G339D_E340A_R	GTGGCATTGAACACCGCGTCGAAAGGGCACAG
	G339D_E340K_F	CAATCTGTGCCCTTTCGACAAGGTGTTCAATGCCAC
	G339D_E340K_R	GTGGCATTGAACACCTTGTCGAAAGGGCACAGATTG
	K356R_F	GTGTACGCATGGAACCGCAGGCGGATAAGCAATTG
	K356R_R	CAATTGCTTATCCGCCTGCGGTTCCATGCGTACAC
	E484A_F486V_F	GTAATGGCGTGGCCGGCGTCAATTGCTACTTCC
	E484A_F486V_R	GGAAGTAGCAATTGACGCCGGCCACGCCATTAC
	E484A_F486V_F_NEW	GTAATGGCGTGGCCGGCGTCAATTGCTACTTCC
	E484A_F486V_R_NEW	GGAAGTAGCAATTGACGCCGGCCACGCCATTAC
	H655Y_N658S_F_NEW	CGGCGCCGAGTACGTGAATAGTAGCTACGAGTG
	H655Y_N658S_R_NEW	CACTCGTAGCTACTATTCACGTACTCGGCGCCG
	H655Y_N658S_F_NEW	CGGCGCCGAGTACGTGAATAGTAGCTACGAGTG
	H655Y_N658S_R_NEW	CACTCGTAGCTACTATTCACGTACTCGGCGCCG
	T19I_del25-7_F_NEW	GAATCTGATCACCAGAACCCAGCTATACACCAATAGCTTCACCAGAG
	T19I_del25-7_R_NEW	CTCTGGTGAAGCTATTGGTGTATAGCTGGGTTCTGGTGATCAGATTC
	Q954H_F_NEW	CAGGACGTGGTGAATCACAATGCCCAGGCCCTG
	Q954H_R_NEW	CAGGGCCTGGGCATTGTGATTCACCACGTCCTG
	Delta_E406D_F	GACAGCTTCGTGATCAGAGGCGACGACGTGAGACAGATCGCGCCAGGG
	Delta_E406D_R	CCCTGGCGCGATCTGTCTCACGTCGTCGCCTCTGATCACGAAGCTGTC
	Delta_E406Q_F	GACAGCTTCGTGATCAGAGGCGACCAAGTGAGACAGATCGCGCCAGGG
	Delta_E406Q_R	CCCTGGCGCGATCTGTCTCACTTGGTCGCCTCTGATCACGAAGCTGTC
	Delta_L455F_F	GGCAATTACAATTACCGGTACAGATTCTTCAGAAAGAGCAATCTGAAGCC
	Delta_L455F_R	GGCTTCAGATTGCTCTTTCTGAAGAATCTGTACCGGTAATTGTAATTGCC
	Delta_L455S_F	GGCAATTACAATTACCGGTACAGAAGCTTCAGAAAGAGCAATCTGAAGCC
	Delta_L455S_R	GGCTTCAGATTGCTCTTTCTGAAGCTTCTGTACCGGTAATTGTAATTGCC
	Omi_K356T_F	GCCAGCGTGTACGCATGGAACCGCACCCGGATAAGCAATTGCGTGGCC
	Omi_K356T_R	GGCCACGCAATTGCTTATCCGGGTGCGGTTCCATGCGTACACGCTGGC
	Omi_R493Q_F	GGCTTCAATTGCTACTTCCCTCTGCAGAGCTACTCGTTCAGACCTACC

(Continued)

Application	Name	Sequence 5' - 3'
	Omi_R493Q_R	GGTAGGTCTGAACGAGTAGCTCTGCAGAGGGAAGTAGCAATTGAAGCC
	Omi_E340V_F	GCGTAGCTGAAACCGGCACCAATCTGTGCCCTTTCGACGTGGTGTTCAATGCCA CCAG
	Omi_E340V_R	CTGGTGGCATTGAACACCACGTCGAAAGGGCACAGATTGGTGCCGGTTTCAGCT ACGC
	F_E484A_V486D	GGCGTGGCCGGCGACAATTGCTACTTCC
	R_E484A_V486D	GGAAGTAGCAATTGTCGCCGGCCACGCC
	F_E484A_V486H	GTAATGGCGTGGCCGGCCACAATTGCTACTTCCC
	R_E484A_V486H	GGGAAGTAGCAATTGTGGCCGGCCACGCCATTAC
	F_E484A_V486R	GTAATGGCGTGGCCGGCCGCAATTGCTACTTCCC
	R_E484A_V486R	GGGAAGTAGCAATTGCGGCCGGCCACGCCATTAC
	F_E484A_V486G	GGCGTGGCCGGCGGCAATTGCTACTTCC
	R_E484A_V486G	GGAAGTAGCAATTGCCGCCGGCCACGCC
	F_S704L	GAGCCTGGGCGCCGAGAATCTAGTGGCCTACAGCAATAATAG
	R_S704L	CTATTATTGCTGTAGGCCACTAGATTCTCGGCGCCCAGGCTC
	F_E484A_F486Y	GTAATGGCGTGGCCGGCTATAATTGCTACTTCCCTCTG
	R_E484A_F486Y	CAGAGGGAAGTAGCAATTATAGCCGGCCACGCCATTAC
	F_E484A_F486W	GTAATGGCGTGGCCGGCTGGAATTGCTACTTCCCTC
	R_E484A_F486W	GAGGGAAGTAGCAATTCCAGCCGGCCACGCCATTAC
	F_K417N_D420Y	GCAGACCGGCAATATCGCCTATTACAATTACAAGCTGCCTG
	R_K417N_D420Y	CAGGCAGCTTGTAATTGTAATAGGCGATATTGCCGGTCTGC
	L452M_F	GTTGGAGGCAATTACAATTACATGTACAGACTGTTCAGAAAGA
	L452M_R	TCTTTCTGAACAGTCTGTACATGTAATTGTAATTGCCTCCAAC
	SS_Q498RN501Y_R	GCCCACGCCATAGGTAGGCCGGAAGCCGTAG
	SS_Q498RN501Y_F	CTACGGCTTCCGGCCTACCTATGGCGTGGGC
	A570C_R	CAGCATCTGTGGTGTCGCAGATGTCTCTGCCGAATTG
	A570C_F	CAATTCGGCAGAGACATCTGCGACACCACAGATGCTG
	Spike_V1176F_F	GATATTTCGGGAATCAATGCCAGCTTCGTGAATATCCAGAAGG
	Spike_V1176F_R	CAATTTCCTTCTGGATATTCACGAAGCTGGCATTGATTCCCGAAATATC
	AF_V382L_F	CACCTTCAAATGTTATGGTCTTTCGCCAACAAAGCTGAAT
	AF_V382L_R	ATTCAGCTTTGTTGGCGAAAGACCATAACATTTGAAGGTG
	S494P_F	CTACTTCCCTCTGCAGCCCTACGGCTTCCAGCC
	S494P_R	GGCTGGAAGCCGTAGGGCTGCAGAGGGAAGTAG
	BA.2_L455R_F	CAATTACAATTACCTGTACAGACGGTTCAGAAAGAGCAATCTGAAG
	BA.2_L455R_R	CTTCAGATTGCTCTTTCTGAACCGTCTGTACAGGTAATTGTAATTG
	BA.2_G416E_F	CGCCAGGGCAGACCGAGAATATCGCCGACTAC
	BA.2_G416E_R	GTAGTCGGCGATATTCTCGGTCTGCCCTGGCG
	BA.2_G416R_F	CCAGGGCAGACCCGCAATATCGCCG
	BA.2_G416R_R	CGGCGATATTGCGGGTCTGCCCTGG
	BA.2_G416Y_F	GATCGCGCCAGGGCAGACCTATAATATCGCCGACTACAATTAC
	BA.2_G416Y_R	GTAATTGTAGTCGGCGATATTATAGGTCTGCCCTGGCGCGATC

(Continued)

Application	Name	Sequence 5' - 3'
	BA.2_Y421R_F	CCGGCAATATCGCCGACCGCAATTACAAGCTGCCTG
	BA.2_Y421R_R	CAGGCAGCTTGTAATTGCGGTCGGCGATATTGCCGG
	BA.2_Y421W_F	CCGGCAATATCGCCGACTGGAATTACAAGCTGCCTGAC
	BA.2_Y421W_R	GTCAGGCAGCTTGTAATTCCAGTCGGCGATATTGCCGG
	BA.2_N487R_F	GTAATGGCGTGGCCGGCTTCAGGTGCTACTTCCCTC
	BA.2_N487R_R	GAGGGAAGTAGCACCTGAAGCCGGCCACGCCATTAC
	BA.2_N487W_F	GTAATGGCGTGGCCGGCTTCTGGTGCTACTTCCCTCTGAG
	BA.2_N487W-R	CTCAGAGGGAAGTAGCACCAGAAGCCGGCCACGCCATTAC
	BA.2_A475D_F	CCGAGATCTACCAGGACGGCAATAAACCGTG
	BA.2_A475D_R	CACGGTTTATTGCCGTCCTGGTAGATCTCGG
	BA.2_A475V_F	CCCGAGATCTACCAGGTCGGCAATAAACCGTG
	BA.2_A475V_R	CACGGTTTATTGCCGACCTGGTAGATCTCGGG
	BA.2_A475Y_F	CATCAGCACCGAGATCTACCAGTATGGCAATAAACCGTGTAATGGC
	BA.2_A475Y_R	GCCATTACACGGTTTATTGCCATACTGGTAGATCTCGGTGCTGATG
	BA.2_A475F_F	CAGCACCGAGATCTACCAGTTCGGCAATAAACCGTGTAATG
	BA.2_A475F_R	CATTACACGGTTTATTGCCGAACTGGTAGATCTCGGTGCTG
	BA.2_F486R_N487R_F	GCGTGGCCGGCCGCAGGTGCTACTTCCC
	BA.2_F486R_N487R_R	GGGAAGTAGCACCTGCGGCCGGCCACGC
	BA.2_F486R_N487W_F	GGCGTGGCCGGCCGCTGGTGCTACTTCCCTCTG
	BA.2_F486R_N487W_R	CAGAGGGAAGTAGCACCAGCGGCCGGCCACGCC
	BA.2_L455F_F	GCAATTACAATTACCTGTACAGATTCTTCAGAAAGAGCAATCTGAAGCC
	BA.2_L455F_R	GGCTTCAGATTGCTCTTTCTGAAGAATCTGTACAGGTAATTGTAATTGC
	T19I_F	CCAGTGCGTGAATCTGATCACCAGAACCCAGAGC
	T19I_R	CTGGGTTCTGGTGATCAGATTCACGCACTGG
	BA.2_G142D+M153I_F	CCTGGACGTTTATTATCATAAGAACAACAAGAGCTGGATAGAGAGCGAGTTC
	BA.2_G142D+M153I_R	GAACTCGCTCTCTATCCAGCTCTTGTTGTTCTTATGATAATAAACGTCCAGG
	BA.2_T299I_F	CCCTCTGAGCGAGATCAAGTGCACCCTGAAG
	BA.2_T299I_R	CTTCAGGGTGCACTTGATCTCGCTCAGAGGG
	BA.2_E484K_Q493_Q498R_F	CAATAAACCGTGTAATGGCGTGAAGGGCTTCAATTGCTACTTCCCTCTGCAGAGCTACGGCTTCAGAC
	BA.2_E484K_Q493_Q498R_R	GTCTGAAGCCGTAGCTCTGCAGAGGGAAGTAGCAATTGAAGCCCTTCACGCCATTACACGGTTTATTG
	BA.2_G1219C_F	GGTACATCTGGCTGTGCTTCATCGCCGGC
	BA.2_G1219C_R	GCCGGCGATGAAGCACAGCCAGATGTACC
	BA.4_V445P_G446S_F	CAAACTAGATTCGAGACCTAGCGGCAATTACGATTAC
	BA.4_V445P_G446S_R	GTAATCGTAATTGCCGCTAGGTCTCGAATCTAGTTT
BA.4_V483A_A484R_F486S_F490V_S494P_F		CCGTGTAATGGCGCGCGCGGCAGCAATTGCTACGTCCCTCTGCAGCCCTACGGCTTCCGGC
BA.4_V483A_A484R_F486S_F490V_S494P_R		GCCGGAAGCCGTAGGGCTGCAGAGGGACGTAGCAATTGCTGCCGCGCGCGCCATTACACGG
	K444T_N460K_F	CTAGATTCGACGGTTGGAGGCAATTACAATTACCGGTACAGACTGTTCAGAAAGAGCAAGCTGAAGCC
	K444T_N460K_R	GGCTTCAGCTTGCTCTTTCTGAACAGTCTGTACCGGTAATTGTAATTGCCTCCAACCGTCGAATCTAG

(Continued)

Application	Name	Sequence 5' - 3'
	R444T_M452R_F	CTCTAACAAACTAGATTCGACGCCTAGCGGCAATTACGATTACAGGTACAGACTGTTCAGAAAG
	R444T_M452R_R	CTTTCTGAACAGTCTGTACCTGTAATCGTAATTGCCGCTAGGCGTCGAATCTAGTTTGTTAGAG
	F486P_R393Q_S494P_F	GGCGTGGCCGGCCCCAATTGCTACTTCCCTCTGCAACCCTACGGCTTCAGACC
	F486P_R393Q_S494P_R	GGTCTGAAGCCGTAGGGTTGCAGAGGGAAGTAGCAATTGGGGCCGGCCACGCC
	S486F_F490S_F	GGCGTGGCCGGCTTCAATTGCTACAGCCCTCTGCAGAG
	S486F_F490S_R	CTCTGCAGAGGGCTGTAGCAATTGAAGCCGGCCACGCC
	G476S_F	GATCTACCAGGCCAGCAATAAACCGTG
	G476S_R	CACGGTTTATTGCTGGCCTGGTAGATC
	A348S_A352V_K356T_F	GCCACCACGTTCAGCAGCGTGTACGTATGGAACCGCACGCGGATAAGCAATTG
	A348S_A352V_K356T_R	CAATTGCTTATCCGCGTGCGGTTCCATACGTACACGCTGCTGAACGTGGTGGC
R403K_R408G_I410V_K417S_F		GCTTCGTGATCAAAGGCAATGAGGTGGGCCAGGTCGCGCCAGGGCAGACCGGCAGTATCGCCGACTAC
R403K_R408G_I410V_K417S_R		GTAGTCGGCGATACTGCCGGTCTGCCCTGGCGCGACCTGGCCCACCTCATTGCCTTTGATCACGAAGC
K444T_V445S_N450D_L452R_F456L_F		CAAACTAGATTCGACGAGTAGCGGCAATTACGATTACCGGTACAGACTGTTAAGAAAGAGCAAGC
K444T_V445S_N450D_L452R_F456L_R		GCTTGCTCTTTCTTAACAGTCTGTACCGGTAATCGTAATTGCCGCTACTCGTCGAATCTAGTTTG
	P463S_F	GAGCAAGCTGAAGAGTTTCGAGAGAGAC
	P463S_R	GTCTCTCTCGAAACTCTTCAGCTTGCTC
T470N_A475V_G476S_T478R_P479L_V484F_E484R_F		GAGACATCAGCAACGAGATCTACCAGGTCAGCAATAGACTGTGTAATGGCTTCCGCGGCCCCAATTG
T470N_A475V_G476S_T478R_P479L_V484F_E484R_R		CAATTGGGGCCGCGGAAGCCATTACACAGTCTATTGCTGACCTGGTAGATCTCGTTGCTGATGTCTC
	S494P_F	CAGCCCTCTGCAGCCCTACGGCTTCCGGCC
	S494P_R	GGCCGGAAGCCGTAGGGCTGCAGAGGGCTG
	S514F_P521S_F	GTGGTGGTGCTGTTCTTCGAGCTGCTGCACGCTAGCGCTACCGTGTG
	S514F_P521S_R	CACACGGTAGCGCTAGCGTGCAGCAGCTCGAAGAACAGCACCACCAC

A.2. Antibody expression vectors

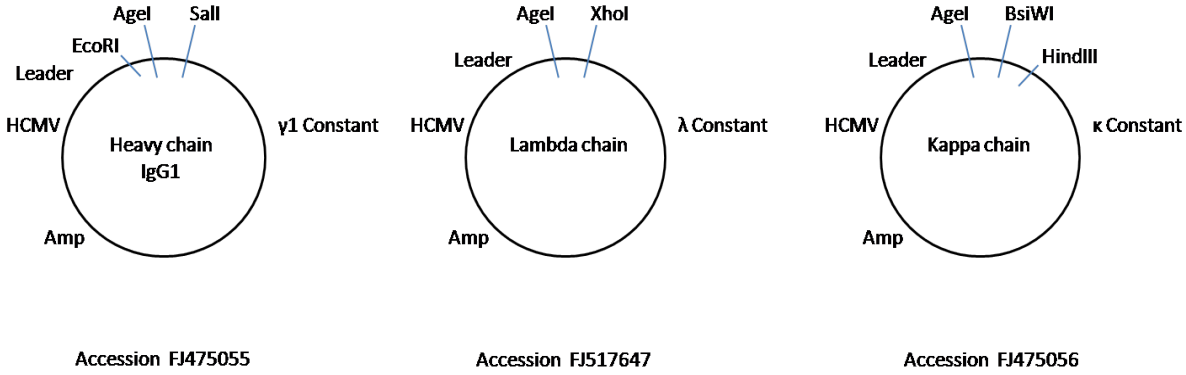

Accession FJ475055 Accession FJ517647 Accession FJ475056

A.3. Vector map pcDNA3.1(+)

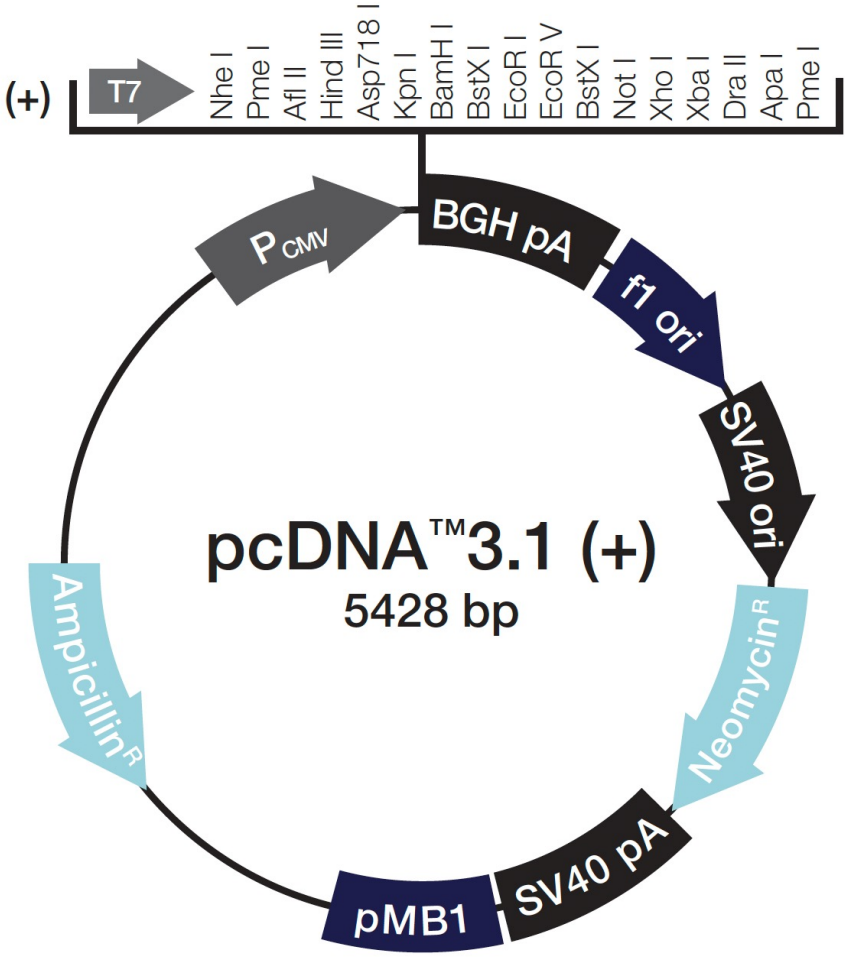

A.4. pHLSec

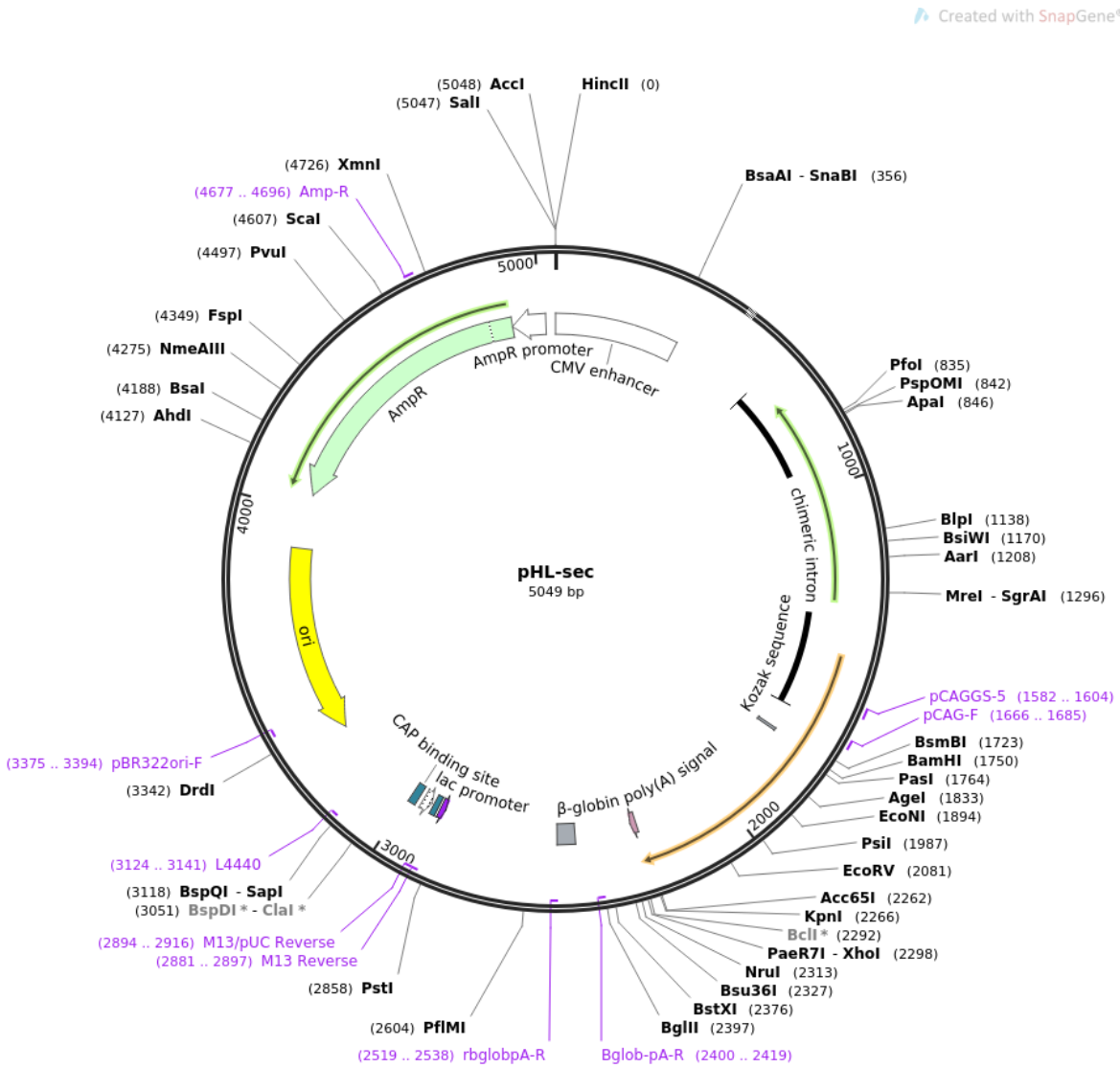
Created with SnapGene®
pHL-sec
5049 bp
(5048) AccI
(5047) SalI
HincII (0)
BsaAI - SnaBI (356)
PfoI (835)
PspOMI (842)
ApaI (846)
BlpI (1138)
BsiWI (1170)
AarI (1208)
MreI - SgrAI (1296)
pCAGGS-5 (1582 .. 1604)
pCAG-F (1666 .. 1685)
BsmBI (1723)
BamHI (1750)
PasI (1764)
AgeI (1833)
EcoNI (1894)
PsiI (1987)
EcoRV (2081)
Acc65I (2262)
KpnI (2266)
BclI * (2292)
PaeR7I - XhoI (2298)
NruI (2313)
Bsu36I (2327)
BstXI (2376)
BglII (2397)
Bglob-pA-R (2400 .. 2419)
(2519 .. 2538) rbglobpA-R
(2604) PflMI
(2858) PstI
(2881 .. 2897) M13 Reverse
(2894 .. 2916) M13/pUC Reverse
(3051) BspDI * - ClaI *
(3118) BspQI - SapI
(3124 .. 3141) L4440
(3342) DrdI
(3375 .. 3394) pBR322ori-F
(4127) AhdI
(4188) BsaI
(4275) NmeAIII
(4349) FspI
(4497) PvuI
(4607) ScaI
(4677 .. 4696) Amp-R
(4726) XmnI
5000
1000
2000
3000
4000
AmpR promoter
CMV enhancer
AmpR
chimeric intron
Kozak sequence
β-globin poly(A) signal
CAP binding site
lac promoter
ori

Publications during DPhil

2023

1. **Liu, C**.[#], Zhou, D.[#], Dijokaite-Guraliuc, A.[#], Supasa, P.[#], Duyvesteyn, H.M., Ginn, H.M., Selvaraj, M., Mentzer, A.J., Das, R., and de Silva, T. I., *et al.* (2023). The emerging BA.2.86 Omicron sub-lineage balances antibody escape and ACE2 affinity. **Cell**, submitted.
2. **Liu, C**.[#], Das, R. [#], Dijokaite-Guraliuc, A.[#], Zhou, D.[#], Mentzer, A.J., Supasa, P., Selvaraj, M., Duyvesteyn, H.M., Ritter, T. G., and Temperton, N., *et al.* (2023). Emerging variants develop total escape from potent monoclonal antibodies induced by BA.4/5 infection. **Cell Reports**, submitted.
3. Zhou, D.[#], Supasa, P.[#], **Liu, C**.[#], Dijokaite-Guraliuc, A.[#], Duyvesteyn, H.M. [#], Selvaraj, M., Mentzer, A.J., Das, R., Dejnirattisai, W., and Temperton, N., *et al.* (2023). The SARS-CoV-2 neutralizing antibody response to SD1 and its evasion by BA.2.86. **Nature Immunology**, in revision.
4. Hornsby, H. [#], Nicols , A.R. [#], Longet, S. [#], **Liu, C**. [#], Tomic, A., Angyal, A., Kronsteriner, B., Tyerman, J.K., Tipton, T., Zhang P., *et al*. (2023). Omicron infection following vaccination enhances a broad spectrum of immune responses dependent on infection history. **Nature communications**, 14:5065.
5. Ragonnet-Cronin, M. [#], Nutalai, R.#, Huo J. [#], Dijokaite-Guraliuc, A.[#], Das, R., Tuekprakhon, A., Supasa, P., **Liu, C**., Selvaraj, M., and Groves, N., *et al*. (2023). Generation of SARS-CoV-2 escape mutations by monoclonal antibody therapy. **Nature communications**, 14:3334.
6. Dijokaite-Guraliuc, A.[#], Das, R.[#], Zhou, D.[#], Ginn, H.M.[#], Mentzer, A.J.[#], **Liu, C**.[#], Duyvesteyn, H.M., Huo, J., Nutalai, R., *et al*. (2023). Rapid escape of new SARS-CoV-2 Omicron variants from BA.2 directed antibody responses. **Cell Reports** 112271.

2022

1. **Liu, C**.[#], Zhou, D.[#], Nutalai, R.[#], Duyvesteyn, H.M.[#], Tuekprakhon, A.[#], Ginn, H.M.[#], Dejnirattisai, W.[#], Supasa, P.[#], Mentzer, A.J.[#], and Wang, B., *et al.* (2022). The antibody response to SARS-CoV-2 Beta underscores the antigenic distance to other variants. **Cell host & microbe** *30*, 53-68. e12.
2. Huo, J.[#], Dijokaite-Guraliuc, A.[#], **Liu, C**.[#], Zhou, D., Ginn, H.M., Das, R., Supasa, P., Selvaraj, M., Nutalai, R., and Tuekprakhon, A., *et al.* (2022). A delicate balance

between antibody evasion and ACE2 affinity for Omicron BA. 2.75. **Cell Reports**, 111903.

3. Dejnirattisai, W.[#], Huo, J.[#], Zhou, D.[#], Zahradník, J.[#], Supasa, P.[#], **Liu, C**.[#], Duyvesteyn, H.M., Ginn, H.M., Mentzer, A.J., and Tuekprakhon, A., *et al*. (2022). SARS-CoV-2 Omicron-B. 1.1. 529 leads to widespread escape from neutralizing antibody responses. **Cell** *185*, 467-484. e415.
4. Nutalai, R., Zhou, D.[#], Tuekprakhon, A.[#], Ginn, H.M.[#], Supasa, P.[#], **Liu, C**.[#], Huo, J.[#], Mentzer, A.J.[#], Duyvesteyn, H.M., and Dijokaite-Guraliuc, A. *et al*. (2022). Potent cross-reactive antibodies following Omicron breakthrough in vaccinees. **Cell** *185*, 2116-2131. e2118.
5. Dejnirattisai, W.[#], Shaw, R.H.[#], Supasa, P.[#], **Liu, C**., Stuart, A.S., Pollard, A.J., Liu, X., Lambe, T., Crook, D., and Stuart, D.I., *et al*. (2022). Reduced neutralisation of SARS-CoV-2 omicron B. 1.1. 529 variant by post-immunisation serum. **The Lancet** *399*, 234-236.
6. Tuekprakhon, A.[#], Nutalai, R.[#], Dijokaite-Guraliuc, A.[#], Zhou, D.[#], Ginn, H.M., Selvaraj, M., **Liu, C**., Mentzer, A.J., Supasa, P., and Duyvesteyn, H.M., *et al*. (2022). Antibody escape of SARS-CoV-2 Omicron BA. 4 and BA. 5 from vaccine and BA. 1 serum. **Cell** *185*, 2422-2433. e2413.
7. Dijokaite-Guraliuc, A., Das, R., Nutalai, R., Zhou, D., Mentzer, A.J., **Liu, C**., Supasa, P., Dunachie, S.J., Lambe, T., and Fry, E.E., *et al*. (2022). Antigenic characterization of SARS-CoV-2 Omicron subvariant BA. 4.6. **Cell Discovery** *8*, 127.

2021

1. **Liu, C**.[#], Ginn, H.M.[#], Dejnirattisai, W.[#], Supasa, P.[#], Wang, B.[#], Tuekprakhon, A.[#], Nutalai, R.[#], Zhou, D.[#], Mentzer, A.J.[#], and Zhao, Y., *et al*. (2021). Reduced neutralization of SARS-CoV-2 B. 1.617 by vaccine and convalescent serum. **Cell** *184*, 4220-4236. e4213.
2. Zhou, D.[#], Dejnirattisai, W.[#], Supasa, P.[#], **Liu, C**.[#], Mentzer, A.J.[#], Ginn, H.M., Zhao, Y., Duyvesteyn, H.M., Tuekprakhon, A., and Nutalai, R., *et al*. (2021). Evidence of escape of SARS-CoV-2 variant B. 1.351 from natural and vaccine-induced sera. **Cell** *184*, 2348-2361. e2346.
3. Supasa, P.[#], Zhou, D.[#], Dejnirattisai, W.[#], **Liu, C**.[#], Mentzer, A.J.[#], Ginn, H.M., Zhao, Y., Duyvesteyn, H.M., Nutalai, R., and Tuekprakhon, A., *et al*. (2021). Reduced neutralization of SARS-CoV-2 B. 1.1. 7 variant by convalescent and vaccine sera. **Cell** *184*, 2201-2211. e2207.

4. Dejnirattisai, W.[#], Zhou, D.[#], Supasa, P.[#], **Liu, C**.[#], Mentzer, A.J.[#], Ginn, H.M., Zhao, Y., Duyvesteyn, H.M., Tuekprakhon, A., and Nutalai, R., *et al*. (2021). Antibody evasion by the P. 1 strain of SARS-CoV-2. **Cell** *184*, 2939-2954. e2939.
5. Dejnirattisai, W.[#], Zhou, D.[#], Ginn, H.M.[#], Duyvesteyn, H.M.[#], Supasa, P., Case, J.B., Zhao, Y., Walter, T.S., Mentzer, A.J., and **Liu, C**. *et al*. (2021). The antigenic anatomy of SARS-CoV-2 receptor binding domain. **Cell** *184*, 2183-2220. e22.
6. Yang, B., **Liu, C**., Pan, X., Fu, W., Fan, Z., Jin, Y., Bai, F., Cheng, Z., and Wu, W. (2021). Identification of novel phoP-phoQ regulated genes that contribute to polymyxin B tolerance in Pseudomonas aeruginosa. **Microorganisms** *9*, 344.

2020

1. Peng, Y.[#], Mentzer, A.J.[#], Liu, G.[#], Yao, X.[#], Yin, Z.[#], Dong, D.[#], Dejnirattisai, W.[#], Rostron, T., Supasa, P., and **Liu, C**., *et al*. (2020). Broad and strong memory CD4+ and CD8+ T cells induced by SARS-CoV-2 in UK convalescent individuals following COVID-19. **Nature immunology** 21, 1336-1345.
2. Xia, Y., Weng, Y., Xu, C., Wang, D., Pan, X., Tian, Z., Xia, B., Li, H., Chen, R., and **Liu, C**., *et al*. (2020). Endoribonuclease YbeY is essential for RNA processing and virulence in Pseudomonas aeruginosa. **MBio** *11*, e00659-00620.

Patents

IPs OUI 18353 COVID-19 antibodies;
IPs OUI 20169 COVID-19 antibodies (4);
IPs OUI 20238 Anti-NP antibodies for COVID-19 Lateral Flow Test;
IPs OUI 20550 COVID-19 antibodies (Omicron original);
IPs OUI 20551 COVID-19 antibodies (Omicron Beta);
IPs OUI 20601 Omicron antibodies (New);
IPs OUI 21281 COVID19 antibodies BA.2;
IPs OUI 21584 COVID19 antibodies BA.4/5;
IPs OUI 22029 COVID19 antibodies SD-1.

References

1 Organisation, W. H. https://covid19.who.int. *WHO*

2 Lu, R. *et al.* Genomic characterisation and epidemiology of 2019 novel coronavirus: implications for virus origins and receptor binding. *Lancet* **395**, 565-574 (2020). https://doi.org:10.1016/S0140-6736(20)30251-8

3 Cui, J., Li, F. & Shi, Z. L. Origin and evolution of pathogenic coronaviruses. *Nat Rev Microbiol* **17**, 181-192 (2019). https://doi.org:10.1038/s41579-018-0118-9

4 Shannon, A. *et al.* Rapid incorporation of Favipiravir by the fast and permissive viral RNA polymerase complex results in SARS-CoV-2 lethal mutagenesis. *Nat Commun* **11**, 4682 (2020). https://doi.org:10.1038/s41467-020-18463-z

5 Lin, S. *et al.* Crystal structure of SARS-CoV-2 nsp10 bound to nsp14-ExoN domain reveals an exoribonuclease with both structural and functional integrity. *Nucleic Acids Res* **49**, 5382-5392 (2021). https://doi.org:10.1093/nar/gkab320

6 Fung, T. S. & Liu, D. X. Human Coronavirus: Host-Pathogen Interaction. *Annu Rev Microbiol* **73**, 529-557 (2019). https://doi.org:10.1146/annurev-micro-020518-115759

7 de Wit, E., van Doremalen, N., Falzarano, D. & Munster, V. J. SARS and MERS: recent insights into emerging coronaviruses. *Nat Rev Microbiol* **14**, 523-534 (2016). https://doi.org:10.1038/nrmicro.2016.81

8 Chen, Y., Liu, Q. & Guo, D. Emerging coronaviruses: Genome structure, replication, and pathogenesis. *J Med Virol* **92**, 2249 (2020). https://doi.org:10.1002/jmv.26234

9 Yang, H. & Rao, Z. Structural biology of SARS-CoV-2 and implications for therapeutic development. *Nat Rev Microbiol* **19**, 685-700 (2021). https://doi.org:10.1038/s41579-021-00630-8

10 Lan, J. *et al.* Structure of the SARS-CoV-2 spike receptor-binding domain bound to the ACE2 receptor. *Nature* **581**, 215-220 (2020). https://doi.org:10.1038/s41586-020-2180-5

11 Shang, J. *et al.* Structural basis of receptor recognition by SARS-CoV-2. *Nature* **581**, 221-224 (2020). https://doi.org:10.1038/s41586-020-2179-y

12 Burton, D. R. Antiviral neutralizing antibodies: from in vitro to in vivo activity. *Nat Rev Immunol*, 1-15 (2023). https://doi.org:10.1038/s41577-023-00858-w

13 Wrapp, D. *et al.* Cryo-EM structure of the 2019-nCoV spike in the prefusion conformation. *Science* **367**, 1260-1263 (2020). https://doi.org:10.1126/science.abb2507

14 Koch, J. *et al.* TMPRSS2 expression dictates the entry route used by SARS-CoV-2 to infect host cells. *EMBO J* **40**, e107821 (2021). https://doi.org:10.15252/embj.2021107821

15 Jackson, C. B., Farzan, M., Chen, B. & Choe, H. Mechanisms of SARS-CoV-2 entry into cells. *Nat Rev Mol Cell Biol* **23**, 3-20 (2022). https://doi.org:10.1038/s41580-021-00418-x

16 Meng, B. *et al.* Altered TMPRSS2 usage by SARS-CoV-2 Omicron impacts infectivity and fusogenicity. *Nature* **603**, 706-714 (2022). https://doi.org:10.1038/s41586-022-04474-x

17 Robson, F. *et al.* Coronavirus RNA Proofreading: Molecular Basis and Therapeutic Targeting. *Mol Cell* **80**, 1136-1138 (2020). https://doi.org:10.1016/j.molcel.2020.11.048

18 Yurkovetskiy, L. *et al.* Structural and Functional Analysis of the D614G SARS-CoV-2 Spike Protein Variant. *Cell* **183**, 739-751 e738 (2020). https://doi.org:10.1016/j.cell.2020.09.032

19 Rambaut, A. *et al.* A dynamic nomenclature proposal for SARS-CoV-2 lineages to assist genomic epidemiology. *Nat Microbiol* **5**, 1403-1407 (2020). https://doi.org:10.1038/s41564-020-0770-5

20 Tegally, H. *et al.* Detection of a SARS-CoV-2 variant of concern in South Africa. *Nature* **592**, 438-443 (2021). https://doi.org:10.1038/s41586-021-03402-9

21 Faria, N. R. *et al.* Genomics and epidemiology of the P.1 SARS-CoV-2 lineage in Manaus, Brazil. *Science* **372**, 815-821 (2021). https://doi.org:10.1126/science.abh2644

22 Zhou, D. *et al.* Evidence of escape of SARS-CoV-2 variant B.1.351 from natural and vaccine-induced sera. *Cell* **184**, 2348-2361 e2346 (2021). https://doi.org:10.1016/j.cell.2021.02.037

23 Dejnirattisai, W. *et al.* Antibody evasion by the P.1 strain of SARS-CoV-2. *Cell* **184**, 2939-2954 e2939 (2021). https://doi.org:10.1016/j.cell.2021.03.055

24 Dhar, M. S. *et al.* Genomic characterization and epidemiology of an emerging SARS-CoV-2 variant in Delhi, India. *Science* **374**, 995-999 (2021). https://doi.org:10.1126/science.abj9932

25 Bolze, A. *et al.* SARS-CoV-2 variant Delta rapidly displaced variant Alpha in the United States and led to higher viral loads. *Cell Rep Med* **3**, 100564 (2022). https://doi.org:10.1016/j.xcrm.2022.100564

26 Viana, R. *et al.* Rapid epidemic expansion of the SARS-CoV-2 Omicron variant in southern Africa. *Nature* **603**, 679-686 (2022). https://doi.org:10.1038/s41586-022-04411-y

27 Rahimi, F. & Bezmin Abadi, A. T. The Omicron subvariant BA.2: Birth of a new challenge during the COVID-19 pandemic. *Int J Surg* **99**, 106261 (2022). https://doi.org:10.1016/j.ijsu.2022.106261

28 Dijokaite-Guraliuc, A. *et al.* Rapid escape of new SARS-CoV-2 Omicron variants from BA.2-directed antibody responses. *Cell Rep* **42**, 112271 (2023). https://doi.org:10.1016/j.celrep.2023.112271

29 Tamura, T. *et al.* Virological characteristics of the SARS-CoV-2 XBB variant derived from recombination of two Omicron subvariants. *Nat Commun* **14**, 2800 (2023). https://doi.org:10.1038/s41467-023-38435-3

30 Uriu, K. *et al.* Enhanced transmissibility, infectivity, and immune resistance of the SARS-CoV-2 omicron XBB.1.5 variant. *Lancet Infect Dis* **23**, 280-281 (2023). https://doi.org:10.1016/S1473-3099(23)00051-8

31 Yamasoba, D. *et al.* Virological characteristics of the SARS-CoV-2 omicron XBB.1.16 variant. *Lancet Infect Dis* **23**, 655-656 (2023). https://doi.org:10.1016/S1473-3099(23)00278-5

32 Elsner, R. A. & Shlomchik, M. J. Germinal Center and Extrafollicular B Cell Responses in Vaccination, Immunity, and Autoimmunity. *Immunity* **53**, 1136-1150 (2020). https://doi.org:10.1016/j.immuni.2020.11.006

33 Lam, J. H., Smith, F. L. & Baumgarth, N. B Cell Activation and Response Regulation During Viral Infections. *Viral Immunol* **33**, 294-306 (2020). https://doi.org:10.1089/vim.2019.0207

34 Palm, A. E. & Henry, C. Remembrance of Things Past: Long-Term B Cell Memory After Infection and Vaccination. *Front Immunol* **10**, 1787 (2019). https://doi.org:10.3389/fimmu.2019.01787

35 Long, Q. X. *et al.* Antibody responses to SARS-CoV-2 in patients with COVID-19. *Nat Med* **26**, 845-848 (2020). https://doi.org:10.1038/s41591-020-0897-1

36 Piccoli, L. *et al.* Mapping Neutralizing and Immunodominant Sites on the SARS-CoV-2 Spike Receptor-Binding Domain by Structure-Guided High-Resolution Serology. *Cell* **183**, 1024-1042 e1021 (2020). https://doi.org:10.1016/j.cell.2020.09.037

37 Suthar, M. S. *et al.* Rapid Generation of Neutralizing Antibody Responses in COVID-19 Patients. *Cell Rep Med* **1**, 100040 (2020). https://doi.org:10.1016/j.xcrm.2020.100040

38 Robbiani, D. F. *et al.* Convergent Antibody Responses to SARS-CoV-2 Infection in Convalescent Individuals. *bioRxiv* (2020). https://doi.org:10.1101/2020.05.13.092619

39 Chen, X. *et al.* Disease severity dictates SARS-CoV-2-specific neutralizing antibody responses in COVID-19. *Signal Transduct Target Ther* **5**, 180 (2020). https://doi.org:10.1038/s41392-020-00301-9

40 Dan, J. M. *et al.* Immunological memory to SARS-CoV-2 assessed for up to 8 months after infection. *Science* **371** (2021). https://doi.org:10.1126/science.abf4063

41 Wajnberg, A. *et al.* Robust neutralizing antibodies to SARS-CoV-2 infection persist for months. *Science* **370**, 1227-1230 (2020). https://doi.org:10.1126/science.abd7728

42 Seow, J. *et al.* Longitudinal observation and decline of neutralizing antibody responses in the three months following SARS-CoV-2 infection in humans. *Nat Microbiol* **5**, 1598-1607 (2020). https://doi.org:10.1038/s41564-020-00813-8

43 Wang, K. *et al.* Longitudinal Dynamics of the Neutralizing Antibody Response to Severe Acute Respiratory Syndrome Coronavirus 2 (SARS-CoV-2) Infection. *Clin Infect Dis* **73**, e531-e539 (2021). https://doi.org:10.1093/cid/ciaa1143

44 Muecksch, F. *et al.* Longitudinal Serological Analysis and Neutralizing Antibody Levels in Coronavirus Disease 2019 Convalescent Patients. *J Infect Dis* **223**, 389-398 (2021). https://doi.org:10.1093/infdis/jiaa659

45 Stamatatos, L. *et al.* mRNA vaccination boosts cross-variant neutralizing antibodies elicited by SARS-CoV-2 infection. *Science* **372**, 1413-1418 (2021). https://doi.org:10.1126/science.abg9175

46 Pinto, D. *et al.* Broad betacoronavirus neutralization by a stem helix-specific human antibody. *Science* **373**, 1109-1116 (2021). https://doi.org:10.1126/science.abj3321

47 Song, G. *et al.* Cross-reactive serum and memory B-cell responses to spike protein in SARS-CoV-2 and endemic coronavirus infection. *Nat Commun* **12**, 2938 (2021). https://doi.org:10.1038/s41467-021-23074-3

48 Qi, H., Liu, B., Wang, X. & Zhang, L. The humoral response and antibodies against SARS-CoV-2 infection. *Nat Immunol* **23**, 1008-1020 (2022). https://doi.org:10.1038/s41590-022-01248-5

49 Isho, B. *et al.* Persistence of serum and saliva antibody responses to SARS-CoV-2 spike antigens in COVID-19 patients. *Sci Immunol* **5** (2020). https://doi.org:10.1126/sciimmunol.abe5511

50 Cervia, C. *et al.* Systemic and mucosal antibody responses specific to SARS-CoV-2 during mild versus severe COVID-19. *J Allergy Clin Immunol* **147**, 545-557 e549 (2021). https://doi.org:10.1016/j.jaci.2020.10.040

51 Sterlin, D. *et al.* IgA dominates the early neutralizing antibody response to SARS-CoV-2. *Sci Transl Med* **13** (2021). https://doi.org:10.1126/scitranslmed.abd2223

52 Froberg, J. *et al.* SARS-CoV-2 mucosal antibody development and persistence and their relation to viral load and COVID-19 symptoms. *Nature Communications* **12** (2021). https://doi.org:ARTN 562110.1038/s41467-021-25949-x

53 Hu, B., Guo, H., Zhou, P. & Shi, Z. L. Characteristics of SARS-CoV-2 and COVID-19. *Nat Rev Microbiol* **19**, 141-154 (2021). https://doi.org:10.1038/s41579-020-00459-7

54 Dugan, H. L. *et al.* Profiling B cell immunodominance after SARS-CoV-2 infection reveals antibody evolution to non-neutralizing viral targets. *Immunity* **54**, 1290-1303 e1297 (2021). https://doi.org:10.1016/j.immuni.2021.05.001

55 Che, X. Y. *et al.* Antigenic cross-reactivity between severe acute respiratory syndrome-associated coronavirus and human coronaviruses 229E and OC43. *Journal of Infectious Diseases* **191**, 2033-2037 (2005). https://doi.org:Doi 10.1086/430355

56 Pinto, D. *et al.* Cross-neutralization of SARS-CoV-2 by a human monoclonal SARS-CoV antibody. *Nature* **583**, 290-295 (2020). https://doi.org:10.1038/s41586-020-2349-y

57 Huo, J. *et al.* Neutralization of SARS-CoV-2 by Destruction of the Prefusion Spike. *Cell Host Microbe* **28**, 497 (2020). https://doi.org:10.1016/j.chom.2020.07.002

58 Zhu, Y. *et al.* Cross-reactive neutralization of SARS-CoV-2 by serum antibodies from recovered SARS patients and immunized animals. *Sci Adv* **6** (2020). https://doi.org:10.1126/sciadv.abc9999

59 Anderson, E. M. *et al.* Seasonal human coronavirus antibodies are boosted upon SARS-CoV-2 infection but not associated with protection. *Cell* **184**, 1858-+ (2021). https://doi.org:10.1016/j.cell.2021.02.010

60 Majdoubi, A. *et al.* A majority of uninfected adults show preexisting antibody reactivity against SARS-CoV-2. *Jci Insight* **6** (2021). https://doi.org:ARTNe14631610.1172/jci.insight.146316

61 Tso, F. Y. *et al.* High prevalence of pre-existing serological cross-reactivity against severe acute respiratory syndrome coronavirus-2 (SARS-CoV-2) in sub-Saharan Africa. *Int J Infect Dis* **102**, 577-583 (2021). https://doi.org:10.1016/j.ijid.2020.10.104

62 Wang, C. *et al.* A conserved immunogenic and vulnerable site on the coronavirus spike protein delineated by cross-reactive monoclonal antibodies. *Nat Commun* **12**, 1715 (2021). https://doi.org:10.1038/s41467-021-21968-w

63 Guo, L. *et al.* Cross-reactive antibody against human coronavirus OC43 spike protein correlates with disease severity in COVID-19 patients: a retrospective study. *Emerg Microbes Infect* **10**, 664-676 (2021). https://doi.org:10.1080/22221751.2021.1905488

64 Hansen, K. E., Arnason, J. & Bridges, A. J. Autoantibodies and common viral illnesses. *Semin Arthritis Rheum* **27**, 263-271 (1998). https://doi.org:10.1016/s0049-0172(98)80047-4

65 Ng, K. W. *et al.* Preexisting and de novo humoral immunity to SARS-CoV-2 in humans. *Science* **370**, 1339-1343 (2020). https://doi.org:10.1126/science.abe1107

66 Rivera-Correa, J. & Rodriguez, A. Divergent Roles of Antiself Antibodies during Infection. *Trends Immunol* **39**, 515-522 (2018). https://doi.org:10.1016/j.it.2018.04.003

67 Bastard, P. *et al.* Autoantibodies against type I IFNs in patients with life-threatening COVID-19. *Science* **370** (2020). https://doi.org:10.1126/science.abd4585

68 Bastard, P. *et al.* Autoantibodies neutralizing type I IFNs are present in ~4% of uninfected individuals over 70 years old and account for ~20% of COVID-19 deaths. *Sci Immunol* **6** (2021). https://doi.org:10.1126/sciimmunol.abl4340

69 Gigli, G. L. *et al.* HLA and immunological features of SARS-CoV-2-induced Guillain-Barre syndrome. *Neurol Sci* **41**, 3391-3394 (2020). https://doi.org:10.1007/s10072-020-04787-7

70 Finsterer, J., Scorza, F. A. & Fiorini, A. C. SARS-CoV-2-associated Guillain-Barre syndrome in 62 patients. *Eur J Neurol* **28**, e10-e12 (2021). https://doi.org:10.1111/ene.14544

71 Bonometti, R. *et al.* The first case of systemic lupus erythematosus (SLE) triggered by COVID-19 infection. *Eur Rev Med Pharmacol Sci* **24**, 9695-9697 (2020). https://doi.org:10.26355/eurrev_202009_23060

72 Patil, N. R., Herc, E. S. & Girgis, M. Cold Agglutinin Disease and Autoimmune Hemolytic Anemia with Pulmonary Embolism as a Presentation of COVID-19 Infection. *Hematol Oncol Stem Cell Ther* **15**, 213-216 (2022). https://doi.org:10.1016/j.hemonc.2020.06.005

73 Ge, J. W. *et al.* Antibody neutralization of SARS-CoV-2 through ACE2 receptor mimicry. *Nature Communications* **12** (2021). https://doi.org:ARTN 25010.1038/s41467-020-20501-9

74 Yuan, M. *et al.* Structural basis of a shared antibody response to SARS-CoV-2. *Science* **369**, 1119-1123 (2020). https://doi.org:10.1126/science.abd2321

75 Zhou, T. Q. *et al.* Structural basis for potent antibody neutralization of SARS-CoV-2 variants including B.1.1.529. *Science* **376**, 369-+ (2022). https://doi.org:ARTNeabn889710.1126/science.abn8897

76 McCallum, M. *et al.* N-terminal domain antigenic mapping reveals a site of vulnerability for SARS-CoV-2. *Cell* **184**, 2332-2347 e2316 (2021). https://doi.org:10.1016/j.cell.2021.03.028

77 Suryadevara, N. *et al.* Neutralizing and protective human monoclonal antibodies recognizing the N-terminal domain of the SARS-CoV-2 spike protein. *Cell* **184**, 2316-2331 e2315 (2021). https://doi.org:10.1016/j.cell.2021.03.029

78 Cerutti, G. *et al.* Potent SARS-CoV-2 neutralizing antibodies directed against spike N-terminal domain target a single supersite. *Cell Host Microbe* **29**, 819-833 e817 (2021). https://doi.org:10.1016/j.chom.2021.03.005

79 Supasa, P. *et al.* Reduced neutralization of SARS-CoV-2 B.1.1.7 variant by convalescent and vaccine sera. *Cell* **184**, 2201-2211 e2207 (2021). https://doi.org:10.1016/j.cell.2021.02.033

80 Liu, C. *et al.* Reduced neutralization of SARS-CoV-2 B.1.617 by vaccine and convalescent serum. *Cell* **184**, 4220-+ (2021). https://doi.org:10.1016/j.cell.2021.06.020

81 Dejnirattisai, W. *et al.* SARS-CoV-2 Omicron-B.1.1.529 leads to widespread escape from neutralizing antibody responses. *Cell* **185**, 467-484 e415 (2022). https://doi.org:10.1016/j.cell.2021.12.046

82 Tuekprakhon, A. *et al.* Antibody escape of SARS-CoV-2 Omicron BA.4 and BA.5 from vaccine and BA.1 serum. *Cell* **185**, 2422-2433 e2413 (2022). https://doi.org:10.1016/j.cell.2022.06.005

83 Halstead, S. B., Chow, J. S. & Marchette, N. J. Immunological enhancement of dengue virus replication. *Nat New Biol* **243**, 24-26 (1973).

84 Slon Campos, J. L., Mongkolsapaya, J. & Screaton, G. R. The immune response against flaviviruses. *Nat Immunol* **19**, 1189-1198 (2018). https://doi.org:10.1038/s41590-018-0210-3

85 Liu, Y. *et al.* An infectivity-enhancing site on the SARS-CoV-2 spike protein targeted by antibodies. *Cell* **184**, 3452-3466 e3418 (2021). https://doi.org:10.1016/j.cell.2021.05.032

86 Li, D. *et al.* In vitro and in vivo functions of SARS-CoV-2 infection-enhancing and neutralizing antibodies. *Cell* **184**, 4203-4219 e4232 (2021). https://doi.org:10.1016/j.cell.2021.06.021

87 Dai, L. & Gao, G. F. Viral targets for vaccines against COVID-19. *Nat Rev Immunol* **21**, 73-82 (2021). https://doi.org:10.1038/s41577-020-00480-0

88 Tian, J. H. *et al.* SARS-CoV-2 spike glycoprotein vaccine candidate NVX-CoV2373 immunogenicity in baboons and protection in mice. *Nat Commun* **12**, 372 (2021). https://doi.org:10.1038/s41467-020-20653-8

89 Yang, J. *et al.* A vaccine targeting the RBD of the S protein of SARS-CoV-2 induces protective immunity. *Nature* **586**, 572-577 (2020). https://doi.org:10.1038/s41586-020-2599-8

90 Sadoff, J. *et al.* Interim Results of a Phase 1-2a Trial of Ad26.COV2.S Covid-19 Vaccine. *N Engl J Med* **384**, 1824-1835 (2021). https://doi.org:10.1056/NEJMoa2034201

91 Krammer, F. SARS-CoV-2 vaccines in development. *Nature* **586**, 516-527 (2020). https://doi.org:10.1038/s41586-020-2798-3

92 Pan, C., Yue, H., Zhu, L., Ma, G. H. & Wang, H. L. Prophylactic vaccine delivery systems against epidemic infectious diseases. *Adv Drug Deliv Rev* **176**, 113867 (2021). https://doi.org:10.1016/j.addr.2021.113867

93 Li, M. *et al.* The nano delivery systems and applications of mRNA. *Eur J Med Chem* **227**, 113910 (2022). https://doi.org:10.1016/j.ejmech.2021.113910

94 Corbett, K. S. *et al.* Evaluation of the mRNA-1273 Vaccine against SARS-CoV-2 in Nonhuman Primates. *N Engl J Med* **383**, 1544-1555 (2020). https://doi.org:10.1056/NEJMoa2024671

95 Vogel, A. B. *et al.* BNT162b vaccines protect rhesus macaques from SARS-CoV-2. *Nature* **592**, 283-289 (2021). https://doi.org:10.1038/s41586-021-03275-y

96 Turner, J. S. *et al.* SARS-CoV-2 mRNA vaccines induce persistent human germinal centre responses. *Nature* **596**, 109-113 (2021). https://doi.org:10.1038/s41586-021-03738-2

97 Goel, R. R. *et al.* Distinct antibody and memory B cell responses in SARS-CoV-2 naive and recovered individuals following mRNA vaccination. *Sci Immunol* **6** (2021). https://doi.org:10.1126/sciimmunol.abi6950

98 Smith, T. R. F. *et al.* Immunogenicity of a DNA vaccine candidate for COVID-19. *Nat Commun* **11**, 2601 (2020). https://doi.org:10.1038/s41467-020-16505-0

99 Brocato, R. L. *et al.* Protective efficacy of a SARS-CoV-2 DNA vaccine in wild-type and immunosuppressed Syrian hamsters. *NPJ Vaccines* **6**, 16 (2021). https://doi.org:10.1038/s41541-020-00279-z

100 Karpinski, T. M., Ozarowski, M., Seremak-Mrozikiewicz, A., Wolski, H. & Wlodkowic, D. The 2020 race towards SARS-CoV-2 specific vaccines. *Theranostics* **11**, 1690-1702 (2021). https://doi.org:10.7150/thno.53691

101 Creech, C. B., Walker, S. C. & Samuels, R. J. SARS-CoV-2 Vaccines. *JAMA* **325**, 1318-1320 (2021). https://doi.org:10.1001/jama.2021.3199

102 Gao, Q. *et al.* Development of an inactivated vaccine candidate for SARS-CoV-2. *Science* **369**, 77-81 (2020). https://doi.org:10.1126/science.abc1932

103 Zhu, F. C. *et al.* Safety, tolerability, and immunogenicity of a recombinant adenovirus type-5 vectored COVID-19 vaccine: a dose-escalation, open-label, non-randomised, first-in-human trial. *Lancet* **395**, 1845-1854 (2020). https://doi.org:10.1016/S0140-6736(20)31208-3

104 van Doremalen, N. *et al.* ChAdOx1 nCoV-19 vaccine prevents SARS-CoV-2 pneumonia in rhesus macaques. *Nature* **586**, 578-582 (2020). https://doi.org:10.1038/s41586-020-2608-y

105 Logunov, D. Y. *et al.* Safety and immunogenicity of an rAd26 and rAd5 vector-based heterologous prime-boost COVID-19 vaccine in two formulations: two open, non-randomised phase 1/2 studies from Russia. *Lancet* **396**, 887-897 (2020). https://doi.org:10.1016/S0140-6736(20)31866-3

106 Li, H. *et al.* Enhanced protective immunity against SARS-CoV-2 elicited by a VSV vector expressing a chimeric spike protein. *Signal Transduct Target Ther* **6**, 389 (2021). https://doi.org:10.1038/s41392-021-00797-9

107 Stephenson, K. E. *et al.* Immunogenicity of the Ad26.COV2.S Vaccine for COVID-19. *JAMA* **325**, 1535-1544 (2021). https://doi.org:10.1001/jama.2021.3645

108 Folegatti, P. M. *et al.* Safety and immunogenicity of the ChAdOx1 nCoV-19 vaccine against SARS-CoV-2: a preliminary report of a phase 1/2, single-blind, randomised controlled trial. *Lancet* **396**, 467-478 (2020). https://doi.org:10.1016/S0140-6736(20)31604-4

109 Pardi, N. & Weissman, D. Development of vaccines and antivirals for combating viral pandemics. *Nat Biomed Eng* **4**, 1128-1133 (2020). https://doi.org:10.1038/s41551-020-00658-w

110 Yamamoto, M., Tajiri, K., Ayuzawa, S. & Ieda, M. Pathological findings of clinically suspected myocarditis temporally associated with COVID-19 vaccination. *Eur J Heart Fail* **24**, 1132-1138 (2022). https://doi.org:10.1002/ejhf.2523

111 Tan, T. K. *et al.* A COVID-19 vaccine candidate using SpyCatcher multimerization of the SARS-CoV-2 spike protein receptor-binding domain induces potent neutralising antibody responses. *Nat Commun* **12**, 542 (2021). https://doi.org:10.1038/s41467-020-20654-7

112 Ward, B. J. *et al.* Phase 1 randomized trial of a plant-derived virus-like particle vaccine for COVID-19. *Nat Med* **27**, 1071-1078 (2021). https://doi.org:10.1038/s41591-021-01370-1

113 Talon, J. *et al.* Influenza A and B viruses expressing altered NS1 proteins: A vaccine approach. *Proc Natl Acad Sci U S A* **97**, 4309-4314 (2000). https://doi.org:10.1073/pnas.070525997

114 Broadbent, A. J. *et al.* Evaluation of the attenuation, immunogenicity, and efficacy of a live virus vaccine generated by codon-pair bias de-optimization of the 2009 pandemic H1N1 influenza virus, in ferrets. *Vaccine* **34**, 563-570 (2016). https://doi.org:10.1016/j.vaccine.2015.11.054

115 Wang, Y. *et al.* Scalable live-attenuated SARS-CoV-2 vaccine candidate demonstrates preclinical safety and efficacy. *Proc Natl Acad Sci U S A* **118** (2021). https://doi.org:10.1073/pnas.2102775118

116 Trimpert, J. *et al.* Development of safe and highly protective live-attenuated SARS-CoV-2 vaccine candidates by genome recoding. *Cell Rep* **36**, 109493 (2021). https://doi.org:10.1016/j.celrep.2021.109493

117 Sahin, U. *et al.* COVID-19 vaccine BNT162b1 elicits human antibody and T(H)1 T cell responses. *Nature* **586**, 594-599 (2020). https://doi.org:10.1038/s41586-020-2814-7

118 Frater, J. *et al.* Safety and immunogenicity of the ChAdOx1 nCoV-19 (AZD1222) vaccine against SARS-CoV-2 in HIV infection: a single-arm substudy of a phase 2/3 clinical trial. *Lancet HIV* **8**, e474-e485 (2021). https://doi.org:10.1016/S2352-3018(21)00103-X

119 Jackson, L. A. *et al.* An mRNA Vaccine against SARS-CoV-2 - Preliminary Report. *N Engl J Med* **383**, 1920-1931 (2020). https://doi.org:10.1056/NEJMoa2022483

120 Cox, R. J. & Brokstad, K. A. Not just antibodies: B cells and T cells mediate immunity to COVID-19. *Nat Rev Immunol* **20**, 581-582 (2020). https://doi.org:10.1038/s41577-020-00436-4

121 Lederer, K. *et al.* SARS-CoV-2 mRNA Vaccines Foster Potent Antigen-Specific Germinal Center Responses Associated with Neutralizing Antibody Generation. *Immunity* **53**, 1281-1295 e1285 (2020). https://doi.org:10.1016/j.immuni.2020.11.009

122 Nguyen-Contant, P. *et al.* S Protein-Reactive IgG and Memory B Cell Production after Human SARS-CoV-2 Infection Includes Broad Reactivity to the S2 Subunit. *mBio* **11** (2020). https://doi.org:10.1128/mBio.01991-20

123 Dejnirattisai, W. *et al.* The antigenic anatomy of SARS-CoV-2 receptor binding domain. *Cell* **184**, 2183-2200 e2122 (2021). https://doi.org:10.1016/j.cell.2021.02.032

124 Caly, L. *et al.* Isolation and rapid sharing of the 2019 novel coronavirus (SARS-CoV-2) from the first patient diagnosed with COVID-19 in Australia. *Med J Aust* **212**, 459-462 (2020). https://doi.org:10.5694/mja2.50569

125 Mukherjee, S. *et al.* Enhancing dengue virus maturation using a stable furin over-expressing cell line. *Virology* **497**, 33-40 (2016). https://doi.org:10.1016/j.virol.2016.06.022

126 Gibson, D. G. *et al.* Enzymatic assembly of DNA molecules up to several hundred kilobases. *Nat Methods* **6**, 343-345 (2009). https://doi.org:10.1038/nmeth.1318

127 Liu, C. *et al.* The antibody response to SARS-CoV-2 Beta underscores the antigenic distance to other variants. *Cell Host Microbe* **30**, 53-68 e12 (2022). https://doi.org:10.1016/j.chom.2021.11.013

128 Nutalai, R. *et al.* Potent cross-reactive antibodies following Omicron breakthrough in vaccinees. *Cell* **185**, 2116-2131 e2118 (2022). https://doi.org:10.1016/j.cell.2022.05.014

129 Walls, A. C. *et al.* Structure, Function, and Antigenicity of the SARS-CoV-2 Spike Glycoprotein. *Cell* **183**, 1735 (2020). https://doi.org:10.1016/j.cell.2020.11.032

130 Zost, S. J. *et al.* Potently neutralizing and protective human antibodies against SARS-CoV-2. *Nature* **584**, 443-449 (2020). https://doi.org:10.1038/s41586-020-2548-6

131 Liu, L. *et al.* Potent neutralizing antibodies against multiple epitopes on SARS-CoV-2 spike. *Nature* **584**, 450-456 (2020). https://doi.org:10.1038/s41586-020-2571-7

132 Barnes, C. O. *et al.* Structures of Human Antibodies Bound to SARS-CoV-2 Spike Reveal Common Epitopes and Recurrent Features of Antibodies. *Cell* **182**, 828-+ (2020). https://doi.org:10.1016/j.cell.2020.06.025

133 Ginn, H. M. Pre-clustering data sets using cluster4x improves the signal-to-noise ratio of high-throughput crystallography drug-screening analysis. *Acta Crystallogr D Struct Biol* **76**, 1134-1144 (2020). https://doi.org:10.1107/S2059798320012619

134 Zhou, D. *et al.* Structural basis for the neutralization of SARS-CoV-2 by an antibody from a convalescent patient. *Nat Struct Mol Biol* **27**, 950-958 (2020). https://doi.org:10.1038/s41594-020-0480-y

135 Lv, Z. *et al.* Structural basis for neutralization of SARS-CoV-2 and SARS-CoV by a potent therapeutic antibody. *Science* **369**, 1505-1509 (2020). https://doi.org:10.1126/science.abc5881

136 Wu, N. C. *et al.* An Alternative Binding Mode of IGHV3-53 Antibodies to the SARS-CoV-2 Receptor Binding Domain. *Cell Rep* **33**, 108274 (2020). https://doi.org:10.1016/j.celrep.2020.108274

137 Wu, Y. *et al.* A noncompeting pair of human neutralizing antibodies block COVID-19 virus binding to its receptor ACE2. *Science* **368**, 1274-1278 (2020). https://doi.org:10.1126/science.abc2241

138 Shi, R. *et al.* A human neutralizing antibody targets the receptor-binding site of SARS-CoV-2. *Nature* **584**, 120-124 (2020). https://doi.org:10.1038/s41586-020-2381-y

139 Hurlburt, N. K. *et al.* Structural basis for potent neutralization of SARS-CoV-2 and role of antibody affinity maturation. *Nat Commun* **11**, 5413 (2020). https://doi.org:10.1038/s41467-020-19231-9

140 Du, S. *et al.* Structurally Resolved SARS-CoV-2 Antibody Shows High Efficacy in Severely Infected Hamsters and Provides a Potent Cocktail Pairing Strategy. *Cell* **183**, 1013-+ (2020). https://doi.org:10.1016/j.cell.2020.09.035

141 Clark, S. A. *et al.* Molecular basis for a germline-biased neutralizing antibody response to SARS-CoV-2. *bioRxiv* (2020). https://doi.org:10.1101/2020.11.13.381533

142 McCray, P. B., Jr. *et al.* Lethal infection of K18-hACE2 mice infected with severe acute respiratory syndrome coronavirus. *J Virol* **81**, 813-821 (2007). https://doi.org:10.1128/JVI.02012-06

143 Winkler, E. S. *et al.* SARS-CoV-2 infection of human ACE2-transgenic mice causes severe lung inflammation and impaired function. *Nat Immunol* **21**, 1327-1335 (2020). https://doi.org:10.1038/s41590-020-0778-2

144 Tan, C. C. S. *et al.* Transmission of SARS-CoV-2 from humans to animals and potential host adaptation. *Nat Commun* **13**, 2988 (2022). https://doi.org:10.1038/s41467-022-30698-6

145 Tegally, H. *et al.* Sixteen novel lineages of SARS-CoV-2 in South Africa. *Nat Med* **27**, 440-446 (2021). https://doi.org:10.1038/s41591-021-01255-3

146 Volz, E. *et al.* Evaluating the Effects of SARS-CoV-2 Spike Mutation D614G on Transmissibility and Pathogenicity. *Cell* **184**, 64-75 e11 (2021). https://doi.org:10.1016/j.cell.2020.11.020

147 Zahradnik, J. *et al.* SARS-CoV-2 variant prediction and antiviral drug design are enabled by RBD in vitro evolution. *Nat Microbiol* **6**, 1188-1198 (2021). https://doi.org:10.1038/s41564-021-00954-4

148 Ku, Z. *et al.* Author Correction: Molecular determinants and mechanism for antibody cocktail preventing SARS-CoV-2 escape. *Nat Commun* **12**, 4177 (2021). https://doi.org:10.1038/s41467-021-24440-x

149 Baum, A. *et al.* Antibody cocktail to SARS-CoV-2 spike protein prevents rapid mutational escape seen with individual antibodies. *Science* **369**, 1014-+ (2020). https://doi.org:10.1126/science.abd0831

150 Kemp, S. A. *et al.* SARS-CoV-2 evolution during treatment of chronic infection. *Nature* **592**, 277-282 (2021). https://doi.org:10.1038/s41586-021-03291-y

151 Smith, D. J. *et al.* Mapping the antigenic and genetic evolution of influenza virus. *Science* **305**, 371-376 (2004). https://doi.org:10.1126/science.1097211

152 Fonville, J. M. *et al.* Antibody landscapes after influenza virus infection or vaccination. *Science* **346**, 996-1000 (2014). https://doi.org:10.1126/science.1256427

153 Starr, T. N. *et al.* Deep Mutational Scanning of SARS-CoV-2 Receptor Binding Domain Reveals Constraints on Folding and ACE2 Binding. *Cell* **182**, 1295-1310 e1220 (2020). https://doi.org:10.1016/j.cell.2020.08.012

154 Andreano, E. *et al.* SARS-CoV-2 escape from a highly neutralizing COVID-19 convalescent plasma. *Proc Natl Acad Sci U S A* **118** (2021). https://doi.org:10.1073/pnas.2103154118

155 Greaney, A. J. *et al.* Complete Mapping of Mutations to the SARS-CoV-2 Spike Receptor-Binding Domain that Escape Antibody Recognition. *Cell Host Microbe* **29**, 44-57 e49 (2021). https://doi.org:10.1016/j.chom.2020.11.007

156 Peng, Y. *et al.* Broad and strong memory CD4(+) and CD8(+) T cells induced by SARS-CoV-2 in UK convalescent individuals following COVID-19. *Nat Immunol* **21**, 1336-1345 (2020). https://doi.org:10.1038/s41590-020-0782-6

157 Gouet, P., Courcelle, E., Stuart, D. I. & Metoz, F. ESPript: analysis of multiple sequence alignments in PostScript. *Bioinformatics* **15**, 305-308 (1999). https://doi.org:10.1093/bioinformatics/15.4.305

158 Greaney, A. J. *et al.* Mapping mutations to the SARS-CoV-2 RBD that escape binding by different classes of antibodies. *Nature Communications* **12** (2021). https://doi.org:ARTN 419610.1038/s41467-021-24435-8

159 Toelzer, C. *et al.* Free fatty acid binding pocket in the locked structure of SARS-CoV-2 spike protein. *Science* **370**, 725-730 (2020). https://doi.org:10.1126/science.abd3255

160 Ke, Z. *et al.* Structures and distributions of SARS-CoV-2 spike proteins on intact virions. *Nature* **588**, 498-502 (2020). https://doi.org:10.1038/s41586-020-2665-2

161 Pettersen, E. F. *et al.* UCSF ChimeraX: Structure visualization for researchers, educators, and developers. *Protein Sci* **30**, 70-82 (2021). https://doi.org:10.1002/pro.3943

162 Weinreich, D. M. *et al.* REGN-COV2, a Neutralizing Antibody Cocktail, in Outpatients with Covid-19. *N Engl J Med* **384**, 238-251 (2021). https://doi.org:10.1056/NEJMoa2035002

163 Sun, Y. & Ho, M. Emerging antibody-based therapeutics against SARS-CoV-2 during the global pandemic. *Antib Ther* **3**, 246-256 (2020). https://doi.org:10.1093/abt/tbaa025

164 Zost, S. J. *et al.* Rapid isolation and profiling of a diverse panel of human monoclonal antibodies targeting the SARS-CoV-2 spike protein. *Nat Med* **26**, 1422-1427 (2020). https://doi.org:10.1038/s41591-020-0998-x

165 Wang, Z. *et al.* mRNA vaccine-elicited antibodies to SARS-CoV-2 and circulating variants. *Nature* **592**, 616-622 (2021). https://doi.org:10.1038/s41586-021-03324-6

166 Andreano, E. *et al.* Hybrid immunity improves B cells and antibodies against SARS-CoV-2 variants. *Nature* **600**, 530-535 (2021). https://doi.org:10.1038/s41586-021-04117-7

167 Cho, A. *et al.* Anti-SARS-CoV-2 receptor-binding domain antibody evolution after mRNA vaccination. *Nature* **600**, 517-522 (2021). https://doi.org:10.1038/s41586-021-04060-7

168 Roltgen, K. *et al.* Immune imprinting, breadth of variant recognition, and germinal center response in human SARS-CoV-2 infection and vaccination. *Cell* **185**, 1025-1040 e1014 (2022). https://doi.org:10.1016/j.cell.2022.01.018

169 Muecksch, F. *et al.* Increased memory B cell potency and breadth after a SARS-CoV-2 mRNA boost. *Nature* **607**, 128-134 (2022). https://doi.org:10.1038/s41586-022-04778-y

170 Sender, R. *et al.* The total number and mass of SARS-CoV-2 virions. *Proc Natl Acad Sci U S A* **118** (2021). https://doi.org:10.1073/pnas.2024815118

171 Liu, Y. *et al.* The N501Y spike substitution enhances SARS-CoV-2 infection and transmission. *Nature* **602**, 294-299 (2022). https://doi.org:10.1038/s41586-021-04245-0

172 Xia, S., Wang, L., Zhu, Y., Lu, L. & Jiang, S. Origin, virological features, immune evasion and intervention of SARS-CoV-2 Omicron sublineages. *Signal Transduct Target Ther* **7**, 241 (2022). https://doi.org:10.1038/s41392-022-01105-9

173 Huo, J. *et al.* Humoral responses against SARS-CoV-2 Omicron BA.2.11, BA.2.12.1 and BA.2.13 from vaccine and BA.1 serum. *Cell Discov* **8**, 119 (2022). https://doi.org:10.1038/s41421-022-00482-3

174 van der Straten, K. *et al.* Antigenic cartography using sera from sequence-confirmed SARS-CoV-2 variants of concern infections reveals antigenic divergence of Omicron. *Immunity* **55**, 1725-1731 e1724 (2022). https://doi.org:10.1016/j.immuni.2022.07.018

175 Huo, J. *et al.* A delicate balance between antibody evasion and ACE2 affinity for Omicron BA.2.75. *Cell Rep* **42**, 111903 (2023). https://doi.org:10.1016/j.celrep.2022.111903

176 Dong, J. *et al.* Genetic and structural basis for SARS-CoV-2 variant neutralization by a two-antibody cocktail. *Nat Microbiol* **6**, 1233-1244 (2021). https://doi.org:10.1038/s41564-021-00972-2

177 Yuan, M. *et al.* A broad and potent neutralization epitope in SARS-related coronaviruses. *Proc Natl Acad Sci U S A* **119**, e2205784119 (2022). https://doi.org:10.1073/pnas.2205784119

178 Simon-Loriere, E. & Schwartz, O. Towards SARS-CoV-2 serotypes? *Nat Rev Microbiol* **20**, 187-188 (2022). https://doi.org:10.1038/s41579-022-00708-x

179 Angyal, A. *et al.* T-cell and antibody responses to first BNT162b2 vaccine dose in previously infected and SARS-CoV-2-naive UK health-care workers: a multicentre prospective cohort study. *Lancet Microbe* **3**, e21-e31 (2022). https://doi.org:10.1016/S2666-5247(21)00275-5

180 Li, M. *et al.* COVID-19 vaccine development: milestones, lessons and prospects. *Signal Transduct Target Ther* **7**, 146 (2022). https://doi.org:10.1038/s41392-022-00996-y

181 Carabelli, A. M. *et al.* SARS-CoV-2 variant biology: immune escape, transmission and fitness. *Nat Rev Microbiol* **21**, 162-177 (2023). https://doi.org:10.1038/s41579-022-00841-7

182 Dejnirattisai, W. *et al.* Reduced neutralisation of SARS-CoV-2 omicron B.1.1.529 variant by post-immunisation serum. *Lancet* **399**, 234-236 (2022). https://doi.org:10.1016/S0140-6736(21)02844-0

183 Dijokaite-Guraliuc, A. *et al.* Antigenic characterization of SARS-CoV-2 Omicron subvariant BA.4.6. *Cell Discov* **8**, 127 (2022). https://doi.org:10.1038/s41421-022-00493-0

184 Qu, P. *et al.* Enhanced neutralization resistance of SARS-CoV-2 Omicron subvariants BQ.1, BQ.1.1, BA.4.6, BF.7, and BA.2.75.2. *Cell Host Microbe* **31**, 9-17 e13 (2023). https://doi.org:10.1016/j.chom.2022.11.012

185 Roemer, C. *et al.* SARS-CoV-2 evolution in the Omicron era. *Nat Microbiol* **8**, 1952-1959 (2023). https://doi.org:10.1038/s41564-023-01504-w

186 Westendorf, K. *et al.* LY-CoV1404 (bebtelovimab) potently neutralizes SARS-CoV-2 variants. *Cell Rep* **39**, 110812 (2022). https://doi.org:10.1016/j.celrep.2022.110812

187 Greaney, A. J. *et al.* Mapping mutations to the SARS-CoV-2 RBD that escape binding by different classes of antibodies. *Nat Commun* **12**, 4196 (2021). https://doi.org:10.1038/s41467-021-24435-8

188 Mahase, E. Covid-19: AstraZeneca says its antibody drug AZD7442 is effective for preventing and reducing severe illness. *BMJ* **375**, n2860 (2021). https://doi.org:10.1136/bmj.n2860

189 Bianchini, F. *et al.* Human neutralizing antibodies to cold linear epitopes and subdomain 1 of the SARS-CoV-2 spike glycoprotein. *Science Immunology* **8** (2023). https://doi.org:ARTN eade095810.1126/sciimmunol.ade0958

190 Pinto, D. *et al.* Broad betacoronavirus neutralization by a stem helix-specific human antibody. *Science* **373**, 1109-1115 (2021). https://doi.org:10.1126/science.abj3321

191 Jennewein, M. F. *et al.* Isolation and characterization of cross-neutralizing coronavirus antibodies from COVID-19+subjects. *Cell Reports* **36** (2021). https://doi.org:ARTN 10935310.1016/j.celrep.2021.109353

192 Low, J. S. *et al.* ACE2-binding exposes the SARS-CoV-2 fusion peptide to broadly neutralizing coronavirus antibodies. *Science* **377**, 735-741 (2022). https://doi.org:10.1126/science.abq2679

193 Dacon, C. *et al.* Broadly neutralizing antibodies target the coronavirus fusion peptide. *Science* **377**, 728-+ (2022). https://doi.org:10.1126/science.abq3773

194 Sun, X. Y. *et al.* Neutralization mechanism of a human antibody with pan-coronavirus reactivity including SARS-CoV-2. *Nature Microbiology* **7**, 1063-+ (2022). https://doi.org:10.1038/s41564-022-01155-3

195 Zhou, P. P. *et al.* A human antibody reveals a conserved site on beta-coronavirus spike proteins and confers protection against SARS-CoV-2 infection. *Science Translational Medicine* **14** (2022). https://doi.org:ARTN eabi9215 10.1126/scitranslmed.abi9215